ANALYTICAL AND EXPERIMENTAL INVESTIGATIONS OF THE COLLAPSE LOAD CHARACTERISTICS OF THIN WALLED STRUCTURAL FORMS UNDER COMPRESSIVE LOAD ACTIONS.

A Thesis

Presented To The University Of Glasgow

For The Degree Of

Doctor of Philosophy.

Iftikharul Haq Qureshi,

B.Sc.,(Mech.Eng.) Pb., A.R.C.S.T.,

August, 1960.

INDEX.

ABSTRACT.

The advent of thin walled structural compression members high-lighted the reservoir of strength which exists beyond the initiation of a state of elastic instability in thin flat rectangular plates loaded in lengthwise compression. The evaluation of this post-critical strength generally called "maximum" strength has been attempted on a variety of semi-empirical bases and in a few cases on purely theoretical grounds.

The thesis presents a theoretical treatment for the maximum strength of flat plates, developed by the author, using the concepts of the classical large deflection theory of plates and the deformation theory of plasticity. A variety of unloaded edge conditions ranging from free through elastically fixed to built-in conditions and their symmetrical and unsymmetrical combinations are considered. This theory, developed for single plates is then applied by the introduction of appropriate assumptions to the assessment of the maximum strength of structural sections regarded as an assembly of such plates. Computations connected with the theory were programmed and carried out by the author on a "DEUGE" digital computer.

To check the results of the theory an extensive experimental programme covering the measurements of strains and deformations corresponding to the initiation of instability and progress to collapse was carried out. In connection with the experimental programme an original application of the Moire fringe technique was developed

by the author for the determination of deflection variations.

Following an introductory review of the relevant published literature, the subject matter of the thesis is divided into six Sections.

Section 1 presents the derivation of the basic large deflection equations by minimization of the energy integral effected by the use of Euler's equations, and a procedure for the approximate solution of the large deflection equation by Galerkin's method. This energy approach to the problem considered, and the generalisation of Euler's equations for two variables with higher derivatives put forward in this thesis is, to the author's knowledge, original.

In Section2 the approximate solutions of the large deflection equations and the results of elastic critical loads obtained thereby for two general cases of plates are presented. These are then compared with other available published results obtained by classical methods. The comparisons show excellent agreement.

Section 3 presents an analytical method for the maximum load carried by compressed plates, based on the application of the deformation theory of plasticity to the plates analysed by means of the large deflection concept. The application of this method of analysis to the evaluation of the maximum load for plates with free/and/or elastically supported unloaded edges is to the author's knowledge presented here for the first time.

In Section 4 the results obtained for single plates have been applied to evaluate the local instability and maximum stresses for box sections, lipped channels and plain channels.

The experimental work performed is presented in Section 5. This covers tests in uniform compression of plain and lipped channel, square tube and equal angle sections. In addition to the results of the actual tests, the various auxiliary techniques such as an original application of the Moire fringe method are fully described.

The mechanical properties inclusive of tensile and compressive yield, Young's Modulus E at zero and varying mean stress, have been evaluated for all the specimens used and are presented in full.

Section 6 contains the comparison of the theoretical and experimental results with a relevant critical discussion.

The main test concludes with a Summary indicating that generally good agreement has been obtained between the theory and the experiments, establishing the former as a rational and reliable analysis for the maximum strength in compression of single-plates and structural sections.

This is followed by 7 Appendices and an extensive Bibliography. The Appendices contain those details of the theoretical and experimental investigations which have been considered too bulky for inclusion in the main test.

DEFINITION OF SYMBOLS.

The following symbols are used throughout the text. Any additional symbols are defined where they first appear:

x, y, z	Rectangular co-ordinates.
u, v, w	Components of displacements in x, y and z directions.
N_x, N_y	Normal forces per unit length in the middle plane of the plate in the x and y directions.
N_{xy}	Shearing force in direction of y-axis per unit length of section of a plate perpendicular to x-axis.
M_x, M_y	Bending moments per unit length of sections of a plate perpendicular to the x- and y- axes respectively.
M_{xy}	Twisting moment per unit length of a section of a plate perpendicular to x- axis.
Q_{xz}, Q_{yz}	Shearing forces parallel to the z axis per unit length of sections of a plate perpendicular to x- and y- axes respectively.
E	Modulus of elasticity in tension and compression.
ν	Poisson's ratio.
a, b, h	Length, width and thickness of a plate.

$D = \frac{E h^3}{12(1-\nu^2)}$ ———— Flexural rigidity of a plate.

m ———— Number of sinusoidal half waves.

σ ———— Direct stress.

τ ———— Shearing stress.

ϵ ———— Direct strain.

γ ———— Shearing strain.

F ———— Airy's Stress Function.

$\sigma_{x_{crit}}$ ———— Critical buckling stress parallel to x - axis.

$\sigma_{x_{max}}$ ———— Maximum stress parallel to x - axis.

σ_{Yield} ———— Yield point stress.

The Sections, Sub-sections and equations have been numbered in accordance with the decimal system of referencing. In this the first figure denotes the main Section, the second Subsection and the subsequent figures give the appropriate equation number. For example 4.010 should be read as Section 4, Subsection 0, equation 10.

Throughout the text numbers shown in square brackets denote the appropriate reference listed in the Bibliography.

INTRODUCTORY REVIEW.

INTRODUCTORY REVIEW.

Development in structural and Aircraft Engineering has led to widespread use of plate elements in a very large number of applications and in consequence much research has been stimulated on the buckling of plates. Considerable basic progress has been made during the past twenty years in this field of engineering as far as the buckling strength of thin walled construction is concerned. It is well known that longitudinally compressed thin walled constructions have a considerable capacity of carrying loads many times larger than the loads initiating elastic buckling [1,2,3,28]. This has given rise to the use of maximum or collapse load rather than the buckling load as the basis of design. In turn this has led to the study of plate collapse problems (as opposed to those of elastic instability) which are generally too complex for rigorous mathematical analysis: To date only the relatively simple case of a simply supported and free edge plate has been satisfactory treated theoretically [4]. However semi-empirical treatments exist [5 - 9, 28] which at present are being used as the basis of design specifications in this country and abroad. This review is confined mainly to investigations conducted since and during the Second World War dealing with the collapse behaviour of single flat plates. Buckling and collapse strength of composite structural forms has also been reviewed.

SIMPLY SUPPORTED FLANGE

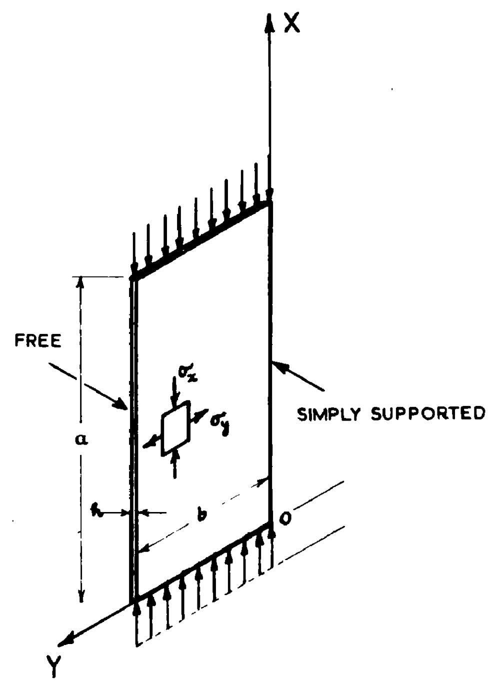

Fig.(1)

The relevant investigations are briefly reviewed under two main headings:

Analytical Investigations.

Experimental Investigations and their

Comparison with Analytical Investigations.

Also, since the collapse load of plate elements is directly associated with large finite deformations, the introductory review culminates in a short description of the development of large deflection theory for flat rectangular plates.

ANALYTICAL INVESTIGATIONS:

Collapse or Maximum Strength of Flat Plates:

An exact theoretical analysis of maximum strength would have to take into account large deflections and the inelastic behaviour of the material, both of which introduce non-linearities: making the problem very difficult to tackle. In the following available theoretical analyses on collapse or maximum strength of flat plates are briefly reviewed.

From the standpoint of theoretical analysis a hinged flange (i.e. a plate simply supported along the loaded edges, simply supported along one unloaded edge and free along the other: Fig.(1)) is the simplest element. In 1950 E.Z. Stowell [4] succeeded in deriving the collapse strength of such a plate. His analysis has served in many cases as a starting point from which semi-empirical methods have been devised to treat the collapse of elements. The cases considered empirically are generally more complex to analyse theoretically and therefore in the following Stowell's method of analysis has been reviewed in relative detail. Stowell computes the maximum load by making use of the deformation theory of plasticity in combination with the large deflection theory for such a plate. The fundamental hypothesis in the finite deflection analysis assumed by Stowell is that at any section across the plate there is no curvature in the direction normal to the applied load; this implies that there is no bending in this direction. This hypothesis enabled him to avoid the formalised plate treatment of the problem.

For infinitesimal rotations the differential equation of equilibrium for a column under the action of compressive stress σ_x has been shown by Wagner [10] to be:

$$\left(GJ - \sigma_x I_p\right)\frac{d\theta}{dx} - E\,C_{BT}\frac{d^3\theta}{dx^3} = 0 \quad \text{------------------ I.1}$$

where: θ is the angle of twist.

$GJ\frac{d\theta}{dx}$ is the St. Venant component of internal resisting torque.

$\sigma_x I_p \frac{d\theta}{dx}$ is the component of internal torque due to the application of compressive force.

$-EC_{BT}\frac{d^3\theta}{dx^3}$ is the component of internal resisting torque due to bending of the column as it twists.

Stowell amends the differential equation I.1 to include the effects of changes in the middle surface strains, which appear at finite values of the rotation θ, and obtains:

$$\left(GJ - \sigma_x I_p\right)\frac{d\theta}{dx} - E C_{BT}\frac{d^3\theta}{dx^3} + \frac{2}{15} E b^2 I_p \left(\frac{d\theta}{dx}\right)^3 = 0 \text{ ------ I.2}$$

where

$$\left.\begin{aligned} J &= \frac{bh^3}{3} \\ I_p &= \frac{b^3 h}{3} \\ C_{BT} &= \frac{b^3 h^3}{36} \\ G &= \frac{E}{2(1+\nu)} \end{aligned}\right] \text{ ---------------------- I.3}$$

Substituting from I.3 in I.2 and taking

$$\gamma_b = b\frac{d\theta}{dx}$$

$$\xi_x = \frac{x}{h}$$

$$\bar{m}^2 = 12\left\{\epsilon_{av.} - \frac{(h/b)^2}{2(1+\nu)}\right\}$$

he simplifies the differential equation to:

$$\frac{d^2\gamma_b^2}{d\xi_x^2} + \bar{m}^2\gamma_b - \frac{8}{5}\gamma_b^3 = 0 \text{ -------------------- I.4}$$

By solving this equation Stowell computes the

the various strain components and reduces them to forms depending on the parameter which specifies the amount of twist.

Since in this analysis he assumed $\sigma_y = 0$ (see Fig. (1)) therefore the fundamental deformation theory of plasticity relation for increasing load:

$$\sigma_i = E_{sec} \epsilon_i$$

where $\epsilon_i \equiv$ strain intensity $= \frac{2}{\sqrt{3}} \sqrt{\epsilon_x^2 + \epsilon_y^2 + \epsilon_x \epsilon_y + \gamma^2/4}$

and $\sigma_i \equiv$ stress intensity $= \sqrt{\sigma_x^2 + \sigma_y^2 - \sigma_x \sigma_y + 3\tau^2}$

reduces to

$$\sqrt{\sigma_x^2 + 3\tau^2} = E_{sec} \sqrt{\epsilon_x^2 + \gamma^2/3} \quad \text{------------------------} \quad \mathrm{I.5}$$

with the compatible relations:

$$\left.\begin{aligned} \sigma_x &= E_{sec}\,\epsilon_x \\ \tau &= E_{sec}\,\frac{\gamma}{3} \end{aligned}\right] \quad \text{------------------------} \quad \mathrm{I.6}$$

By assigning values to the twist parameter the strain components ϵ_x and γ at any point are computed and hence the strain intensity ϵ_i completely determined. From the stress strain curve of the material, the value of stress intensity σ_i and modulus E_{sec} is obtained corresponding to the value of ϵ_i and the stress σ_x is then computed by the relation I.6. The average value of σ_x across the width of the flange

$$\sigma_{av.} = \frac{1}{b} \int_0^b \sigma_x \, dy$$

is then determined for various values of the twist

STOWELLS THEORY

SIMPLY SUPPORTED FLANGE

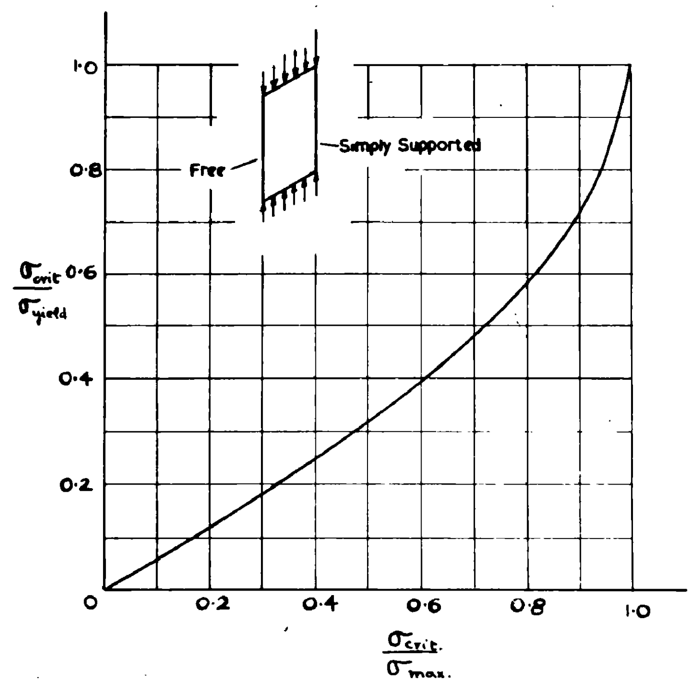

Fig. (2)

parameter giving a maximum $\sigma_{max.}$ for a certain value. Stowell's analysis indicates that the maximum load occurs just as the edge stress at the supported unloaded edge reaches a maximum. Therefore a significant physical fact which was brought to light by this analysis is that the edge stress is intimately associated with collapse and collapse occurs when the value of σ_i at the edge reaches a value approximately equal to compressive yield strength.

Stowell plots results obtained in this manner for Aluminium Alloy 24S-T4 flange in a non dimensional form of $\sigma_{crit}/\sigma_{max}$ against $\sigma_{crit}/\sigma_{yield}$ (Fig.(2)).

A number of theoretical analysis have also been concerned with the post buckling load carrying capacity of flat plates loaded in one direction and supported along all edges. With one recent exception [29] such analyses are based on purely elastic considerations and therefore yield relatively important information only on a limited range of post buckling behaviour. The important problem of collapse requires the incorporation of plasticity theory into the large deflection ananysis. Mayer's and Budiansky [29] introduced the plasticity effects and treated the case of a simply supported plate using variational principles. Assuming the average compressive stress at a strain of 0.01 for 2024-T3 alloy plate as an indication of collapse, Mayer's and Budiansky computed the maximum loads for plates that buckle elastically at 0.3, 0.4, 0.5 and 0.6 of the compressive yield strength. The results of this analysis are shown in Fig.(3).

MAYERS & BUDIANSKY THEORY

SIMPLY SUPPORTED PLATES

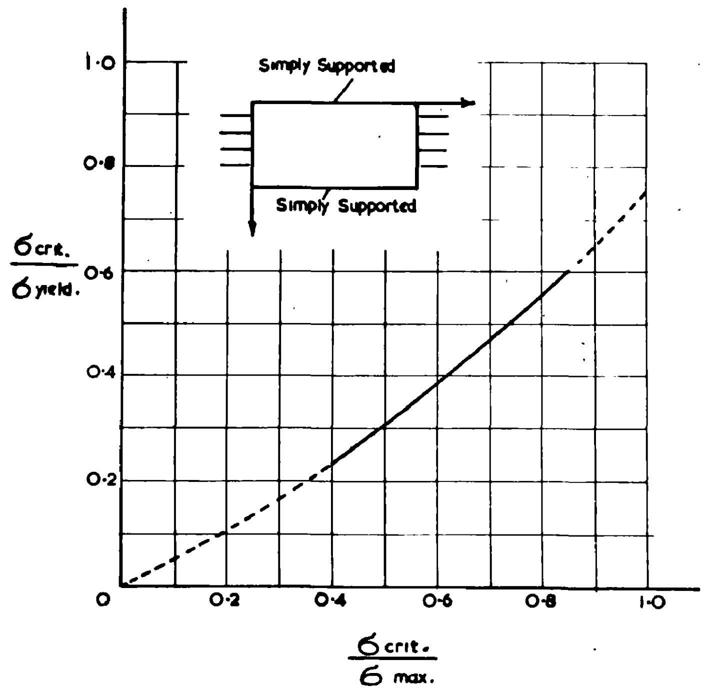

Fig. (3)

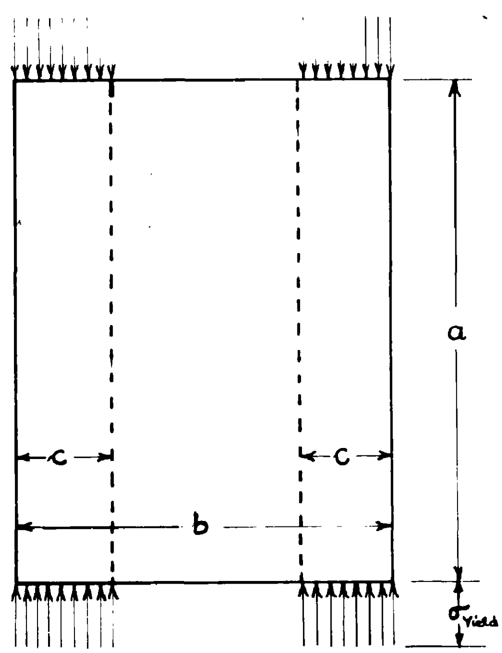

Fig. (4)

An approximate analysis based on the load carrying capacity of purely elastic plates after buckling is also available. This approximate analysis was first carried out by <u>Theodor Von Karmen</u>[2] and summarised by <u>S.P. Timoshenko</u>[1]. Von Karmen assumes that the entire compressive load is carried by two strips, along the two unloaded supported edges, of width $2c$, while the central buckled strip of breadth $(b-2c)$ is free from stress. Disregarding the middle portion of the plate the two strips are handled as a long plate of width $2c$ (Fig.(4)).
It is assumed that the maximum load is reached when the uniform critical stress σ_{crit} for such a plate becomes equal to the yield stress σ_{yield} of the material.

This results in the relation:

$$\sigma_{crit} = \frac{K\pi^2 E h^2}{12(1-\nu^2)4c^2} = \sigma_{yield} \quad \text{I.7}$$

(where K is a constant depending upon the plate dimensions and the support conditions) giving:

$$c = \frac{\pi h\sqrt{KE}}{\sqrt{48(1-\nu^2)\sigma_{yield}}}$$

The maximum stress referred to the actual portions of the plate is then:

$$\sigma_{max} = \frac{2c\,\sigma_{yield}}{b} = \frac{\pi h\sqrt{EK\sigma_{yield}}}{b\sqrt{12(1-\nu^2)}} \quad \text{I.8}$$

In the case of a plate with one unloaded edge supported, the same analysis holds but in this case there is one strip of equivalent width c carrying the load and

$$c = \frac{\pi h \sqrt{KE}}{\sqrt{12(1-\nu^2)\,\sigma_{Yield}}}$$

The relationship resulting from this analysis can be written in the form:

$$\frac{\sigma_{crit}}{\sigma_{max}} = \sqrt{\frac{\sigma_{crit}}{\sigma_{Yield}}} \qquad \text{------------------------------} \quad \text{I.9}$$

More elaborate investigations by Marguerre and Levy [11,12] again assuming that the maximum load is reached when the critical stress carried by the longitudinal edge strip of combined width $\ell \times b$ becomes equal to the yield stress and further assuming that the stress in the strip of width $(1-\ell)b$ remains equal to the elastic buckling value gives the relationship:

$$\frac{\sigma_{crit}}{\sigma_{max}} = \frac{\sigma_{crit}/\sigma_{Yield}}{\ell + (1-\ell)\,\sigma_{crit}/\sigma_{Yield}} \qquad \text{------------------------} \quad \text{I.10}$$

where

$$\ell = \frac{\pi h \sqrt{KE}}{b\sqrt{12(1-\nu^2)\,\sigma_{Yield}}}.$$

A large number of semi-empirical treatments of maximum strength of flat plates are summarised in [28] and are based on the fact that collapse is closely associated with the highest attainable value of edge stress which in turn is a function of the stress intensity σ_i at the edge. The varying boundary conditions along the unloaded edges vary the value of σ_i and may be expected to result in variations in the maximum strength. Therefore in these semi-empirical treatments the effect of boundary conditions along the unloaded edges on the maximum strength has been carefully considered.

Local Instability of Composite Structural Sections:

A composite structural section can be regarded as an assembly of plates, and thus the results obtained for single plates can be utilized to obtain the buckling loads in local instability of structural sections if the boundary conditions for the plates at the connected edges are determined.

In 1924 Bleich[30] first attempted to determine the buckling stresses of plate assemblies in the form of rectangular box sections. He assumed in his analysis the plates with the larger width to thickness ratio as being the buckling plates and the others as the supporting plates. Later, Melan[31] evaluated the buckling stresses for I sections by taking into account the flexural stiffnesses of the flanges which were taken as the supporting plates, and neglecting their torsional stiffness. This method of analysis was later developed by Timoshenko[1] for the case of a T section. In his analysis he takes into account the torsional stiffness of the supporting flange.

Chwalla[32] extended Melan's theory and included torsional stiffness effects of the flanges of I sections in determining the buckling stresses. A year later an approximate treatment of plain channel sections was carried out by Parr[33]. Lundquist [34, 35] and Stowell [36] also worked out local instability stresses for various open and closed structural sections. Using a more direct approach to the problem Chilver [37] evaluated the buckling stresses of open sections, of general form. His method consists in writing down separately the equations for various plate components and solving them simultaneously by the method of determinents. Harvey[18] gave a complete analysis for concentrically loaded plane and lipped channels. Harvey evaluated the elastic edge restraints at the connecting edges and utilized the single plate results to evaluate the local instability of these sections.

Kroll[38,39] prepared tables for evaluating the stiffness of elastic restraint provided between the plates of built-up sections, and charts of factor K where $\sigma_{crit} = \dfrac{K\pi^2 E \cdot h^2}{12(1-\nu^2)\, b^2}$ for various stiffness values for various types of plates. These charts in addition to the tables can be used, to evaluate the critical stress for a particular structural section if it is assumed that the stiffness of elastic edge restraint is constant.

Maximum Strength Of Composite Structural Sections:

Earlier attempts[40] to determine maximum strength of short structural sections under compressive loads were based on the buckling behaviour of the elements. In these analyses, the collapse load was taken as the sum of the buckling loads of each of the component plates.

Based on the fact that flat plates carry loads considerably larger than the buckling load, later methods of evaluating maximum strength of structural sections were refined. Needham[41] has recently proposed a method of analysis for formed structural sections. In this method, the maximum load of structural sections is obtained by summing the collapse loads of each of the component plates. The method is based on the argument that in cold formed sections there is a considerable increase in the compressive yield properties in the corners depending upon the radius of the rounded corner.

A large number of semi-empirical treatments for various structural sections exist. For Aluminium and Magnesium alloy structural sections the semi-empirical treatments are summarised by Gerard[28]. Other empirical analyses for steel structures are presented in [7], [9], [13]. The results of some of these treatments are shown in plotted forms in the part on Experimental Investigations.

EXPERIMENTAL INVESTIGATIONS AND COMPARISON WITH ANALYTICAL RESULTS:

In most of the experimental investigations; confined mainly to Aluminium alloy and steel structures, tests have been performed with particular attention to critical load and maximum load values. As a result there is lack of information on the complete strain and deformation characteristics of thin plate components of structural sections.

Tests carried out on cruciforms and square tubes provide data for single plates rather than for sections composed of plates. In effect the cruciform is composed of four simply supported ~ free plates and the

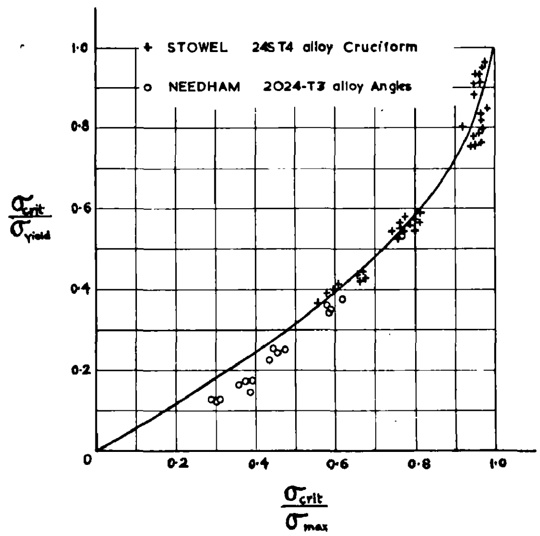

Fig.(5)

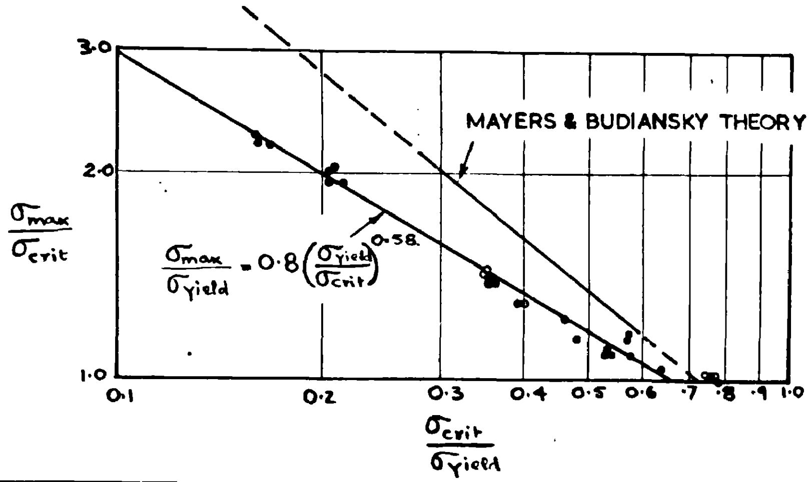

Fig.(6)

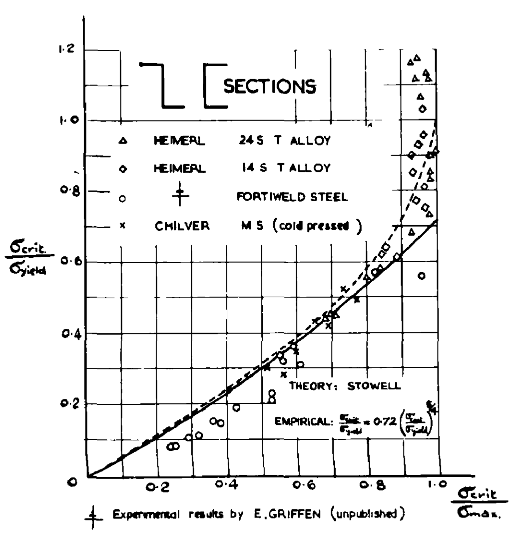

Fig.(7)

square tube is an integral assembly of four plates, simply supported on all edges. A considerable proportion of the experimental work carried out has been confined to these forms. The test results for cruciform sections obtained by Stowell[4] and for angle sections by Needham[41] with theoretical curve, obtained by Stowell are shown in Fig.(5). The departure of the angle sections from the theory for simply supported flanges may be attributed to the warping of the unloaded simply supported edge in the plane of the flange. However in the cruciform section the edge remains straight due to symmetry and test results are in good agreement with the theory.

Results of tests on square tubes and simply supported plates by Anderson and Anderson, Botman, Besseling [42,43,44] are shown in Fig.(6). In Fig.(6) are also shown by lines the theoretical results of Mayers and Budiansky [29] and one empirical treatment [28].

The strength of steel channel struts was first studied experimentally by Winter [8]. Extensive experimental work has since been conducted on I , ⅂L and channel sections to check theoretical results and to derive empirical relations. Test data on extruded equal flange ⅂L, channel and I sections of various aluminium and magnesium alloy obtained by Heimerl [24] and Shuette [45] is shown plotted in Fig.(7) with the empirical relation derived by Heimerl. Also shown in this figure by the dotted curve is the theoretically

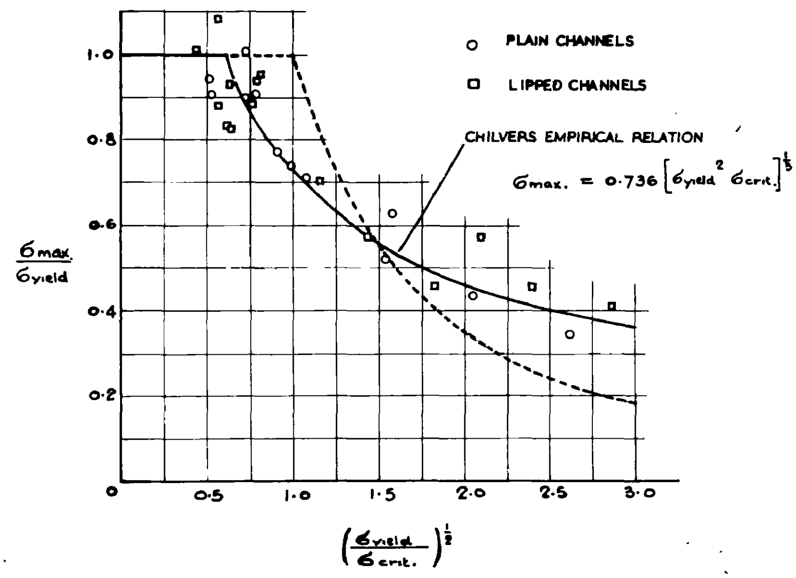
PLAIN CHANNELS
LIPPED CHANNELS
CHILVERS EMPIRICAL RELATION
$\sigma_{max.} = 0.736 \left[\sigma_{yield}^{2}\,\sigma_{crit.}\right]^{\frac{1}{3}}$
$\frac{\sigma_{max}}{\sigma_{yield}}$
$\left(\frac{\sigma_{yield}}{\sigma_{crit.}}\right)^{\frac{1}{2}}$
1.0
0.8
0.6
0.4
0.2
0
0.5
1.0
1.5
2.0
2.5
3.0

Fig. (8)

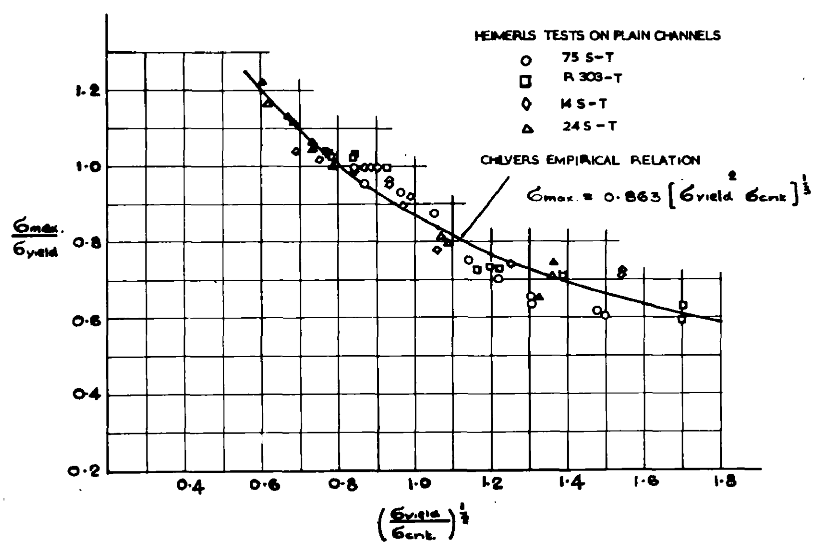
HEIMERLS TESTS ON PLAIN CHANNELS
75 S-T
R 303-T
14 S-T
24 S-T
CHILVERS EMPIRICAL RELATION
$\sigma_{max.} = 0.863 \left[\sigma_{yield}^{2}\,\sigma_{crit.}\right]^{\frac{1}{3}}$
$\frac{\sigma_{max.}}{\sigma_{yield}}$
$\left(\frac{\sigma_{yield}}{\sigma_{crit.}}\right)^{\frac{1}{2}}$
1.2
1.0
0.8
0.6
0.4
0.2
0.4
0.6
0.8
1.0
1.2
1.4
1.6
1.8

Fig. (9)

derived relationship for a simply supported flange.

Chilver [37] carried out tests on cold formed steel and light alloy plain and lipped channels under concentric loads. The experimental results and empirical relationships as given by Chilver are shown in Fig.(8) and (9). The dotted curve shown is the Von Karmen relationship for plates supported along all edges.

Kenedi, Shearer Smith and Fahmy [9] worked out various semi-empirical relations as a basis of design from a large number of tests on cold rolled plain and lipped channel sections and angle sections.

DEVELOPMENT OF LARGE DEFLECTION THEORY.

Lagrange in 1811 [14,15] developed the differential equation for bending of thin plates:

$$\nabla^4 w = \frac{\partial^4 w}{\partial x^4} + 2\frac{\partial^4 w}{\partial x^2 \partial y^2} + \frac{\partial^4 w}{\partial y^4} = \frac{q}{D} \quad \text{------------------ I.11}$$

where q is the lateral load intensity and w is lateral deflection.

In deriving this equation he assumed that the deflection w is small compared to the thickness of the plate which implies that the middle plane of the plate remains unstrained. Later Lagrange's equation was modified [1] for the case of a plate subjected to direct forces N_x, N_y and N_{xy} in the plane of the plate by considering q to consist of the lateral components of the middle plane forces. This yields:

$$\nabla^4 w = \frac{h}{D}\left[N_x \frac{\partial^2 w}{\partial x^2} + N_y \frac{\partial^2 w}{\partial y^2} + 2N_{xy}\frac{\partial^2 w}{\partial x^2 \partial y^2}\right] \quad \text{------------ I.12}$$

If it is assumed in the problem of bending of a plate subjected to direct forces in the plane of the plate, that the deflections are large compared to the thickness of the plate, then it is no longer rational to assume that the strains in the middle plane of the plate remain unchanged during bending. This problem of bending of plates acted upon by direct forces and taking into account effects due to large deflection was first generalized by <u>Von Karmen</u> [1,16]. In his analysis he assumes that the equation I.12 for the deflection form holds in this case also if the direct forces N_x, N_y and N_{xy} are considered to consist of the applied forces and the effect due to straining of the middle plane. These forces are then determined from the compatibility condition of the stress strain system present. Making use of Airy's Stress function F this analysis yields two equations:

$$\nabla^4 w = \frac{h}{D}\left[\frac{\partial^2 F}{\partial y^2}\cdot\frac{\partial^2 w}{\partial x^2} + \frac{\partial^2 F}{\partial x^2}\cdot\frac{\partial^2 w}{\partial y^2} - 2\frac{\partial^2 F}{\partial x \partial y}\,\frac{\partial^2 w}{\partial x \partial y}\right] \quad \text{I.13}$$

$$\nabla^4 F = E\left[\left(\frac{\partial^2 w}{\partial x \partial y}\right)^2 - \frac{\partial^2 w}{\partial x^2}\cdot\frac{\partial^2 w}{\partial y^2}\right] \quad \text{I.14}$$

which when solved simultaneously for w and F give the solution of the large deflection problem.

CONTENTS.

SECTION 1.

BASIC LARGE DEFLECTION PLATE EQUATIONS AND METHOD OF SOLUTION.

SECTION 2.

ELASTIC CRITICAL LOAD EVALUATION

SECTION 3.

POST CRITICAL LOAD CARRYING CAPACITY.

SECTION 4.

APPLICATION OF SINGLE PLATE RESULTS TO

COMPOSITE FORMS.

SECTION 5.

EXPERIMENTAL INVESTIGATIONS.

Test/

SECTION 6.

ANALYSIS AND DISCUSSION OF RESULTS.

APPENDICES.

SECTION. 1

BASIC LARGE DEFLECTION PLATE EQUATIONS AND METHOD OF SOLUTION.

BASIC LARGE DEFLECTION PLATE EQUATIONS AND METHOD OF SOLUTION.

In published literature it is possibly more customary to derive the governing equations of a particular problem from the consideration of the appropriate compatibility conditions of the stress and strain systems present. In a number of instances the approach tends to become laborious and relatively inapplicable. In such cases the minimum energy theorems may be utilised to give a relatively more direct route to the derivation of the basic differential equations.

The theoretical work presented in this section utilises this energy approach to derive the characteristic equations of flat plates subjected to direct force actions in the plane of the plate. The problem is generalised through taking account of middle plane strains in the plate due to the bending actions which arise, thus treating the problem as one of "large" lateral deflections. The process outlined, establishes the total strain energy of the loaded plate; the energy contents due to the direct actions, the bending actions and the middle plane effects due to bending being clearly differentiated. Minimisation of the energy integral is then effected by the use of Euler's Equations, culminating in a procedure for the solution of the differential equations, utilising Galerkin's Method. The application of the energy approach to the problem considered,

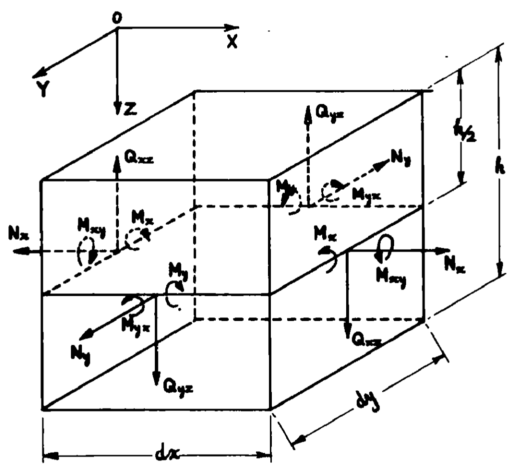

Fig.(10)

together with the generalisation of Euler's equations for two variables with higher derivatives, presented in this section, is to the author's knowledge, not available in the published literature.

1.0 STRAIN ENERGY INTEGRALS.

Consider a flat rectangular plate subjected to bending action and external forces in the plane of the plate, giving rise to "large" lateral deflections w and to the internal actions indicated on an element $dx\,dy\,h$ shown in Fig.(10)

Assuming that the vertical shearing forces Q_{xz} and Q_{yz} have negligible effect on the curvatures of the plate and therefore the strain energy due to these forces is negligible, the strain energy due to bending actions alone, accumulated in the element is equal to the work done by the moments $M_x dy$ and $M_y dx$ and by the twisting moments $M_{xy}\,dy$ and $M_{yx}\,dx$.

Since, $-\partial^2 w/\partial x^2$ represents approximately the curvature of the plate in the xz plane, the angle corresponding to $M_x dy$ is $-\frac{\partial^2 w}{\partial x^2}.dx$ and the work done by this moment is

$$-\frac{1}{2} M_x \frac{\partial^2 w}{\partial x^2} dx\,dy.$$

Similarly, the work done by the moment $M_y\,dx$ is:

$$-\frac{1}{2} M_y \frac{\partial^2 w}{\partial y^2} dx\,dy$$

Again, since the angle of twist corresponding to the twisting moment $M_{xy}\,dy$ is $\frac{\partial^2 w}{\partial x \partial y} dx$, the work done is:

$$\frac{1}{2} M_{xy} \frac{\partial^2 w}{\partial x \partial y} dx\,dy$$

Similarly, the work done by the twisting moment $M_{yx}\,dx$ is:

$$\frac{1}{2} M_{yx} \frac{\partial^2 w}{\partial x \partial y} dx\,dy$$

Assuming Hooke's Law to apply:

$$\left.\begin{aligned} M_x &= -D\left(\frac{\partial^2 w}{\partial x^2} + \nu \frac{\partial^2 w}{\partial y^2}\right) \\ M_y &= -D\left(\frac{\partial^2 w}{\partial y^2} + \nu \frac{\partial^2 w}{\partial x^2}\right) \\ M_{xy} &= -M_{yx} = D(1-\nu)\frac{\partial^2 w}{\partial x \partial y} \end{aligned}\right] \quad \text{———} \quad 1.01$$

and the total strain energy due to bending actions in the element becomes:

$$dV = \frac{1}{2} D\left[\left(\frac{\partial^2 w}{\partial x^2}\right)^2 + \left(\frac{\partial^2 w}{\partial y^2}\right)^2 + 2\nu \frac{\partial^2 w}{\partial x^2} \cdot \frac{\partial^2 w}{\partial y^2}\right] dx \cdot dy$$
$$+ D(1-\nu)\left(\frac{\partial^2 w}{\partial x \partial y}\right)^2 dx\,dy.$$

therefore the strain energy of bending of the entire region R of the plate is:

$$V = \frac{1}{2} D \iint_R \left[\left(\frac{\partial^2 w}{\partial x^2}\right)^2 + \left(\frac{\partial^2 w}{\partial y^2}\right)^2 + 2\nu \frac{\partial^2 w}{\partial x^2} \cdot \frac{\partial^2 w}{\partial y^2} + 2(1-\nu)\left(\frac{\partial^2 w}{\partial x \partial y}\right)^2\right] dx\,dy$$

OR

$$V_B = \frac{1}{2} D \iint_R \left[\left(\frac{\partial^2 w}{\partial x^2} + \frac{\partial^2 w}{\partial y^2} \right)^2 - 2(1-\nu) \left\{ \frac{\partial^2 w}{\partial x^2} \cdot \frac{\partial^2 w}{\partial y^2} - \left(\frac{\partial^2 w}{\partial x \partial y} \right)^2 \right\} \right] dx\, dy \qquad 1.02$$

To establish the expression for the strain energy content corresponding to the forces acting in the middle plane of the plate, it is assumed that these forces are applied first to the unbent plate.

Assuming that the forces N_x, N_y and N_{xy} are known at all points of the plate, the corresponding components of the middle plane strains according to Hooke's Law are given by:

$$\left.\begin{aligned} \epsilon_{x_1} &= \frac{1}{hE}\left(N_x - \nu N_y\right) \\ \epsilon_{y_1} &= \frac{1}{hE}\left(N_y - \nu N_x\right) \\ \gamma_{xy_1} &= \frac{2(1+\nu)}{hE} N_{xy} \end{aligned}\right] \qquad 1.03$$

Therefore the strain energy V_{s_1} due to the forces acting in the middle plane of the unbent plate is:

$$V_{s_1} = \frac{1}{2} \iint_R \left[N_x \epsilon_{x_1} + N_y \epsilon_{y_1} + N_{xy} \gamma_{xy_1} \right] dx\, dy.$$

$$= \frac{1}{2hE} \iint_R \left[N_x^2 + N_y^2 - 2\nu N_x N_y + 2(1+\nu) N_{xy}^2 \right] dx\, dy. \qquad 1.04$$

Now, when the plate is bent, additional strains are produced in the middle plane. The change in energy produced due to these additional strains in association with the already present finite forces N_x, N_y and N_{xy} is not negligible.

If u, v and w are the components of displacement of a point in the middle plane, the total strain components of the plate after it has been bent are given by:

$$\epsilon_x = \frac{\partial u}{\partial x} + \frac{1}{2}\left(\frac{\partial w}{\partial x}\right)^2$$

$$\epsilon_y = \frac{\partial v}{\partial x} + \frac{1}{2}\left(\frac{\partial w}{\partial y}\right)^2$$

$$\gamma_{xy} = \frac{\partial u}{\partial y} + \frac{\partial v}{\partial x} + \frac{\partial w}{\partial x} \cdot \frac{\partial w}{\partial y} .$$

Therefore, the components of additional strain in the middle plane, due to the deflection or bending of the plate becomes:

$$\left.\begin{aligned}
\epsilon_{x_2} &= \frac{\partial u}{\partial x} + \frac{1}{2}\left(\frac{\partial w}{\partial x}\right)^2 - \epsilon_{x_0} \\
\epsilon_{y_2} &= \frac{\partial v}{\partial y} + \frac{1}{2}\left(\frac{\partial w}{\partial y}\right)^2 - \epsilon_{y_0} \\
\gamma_{xy_2} &= \frac{\partial u}{\partial y} + \frac{\partial v}{\partial x} + \frac{\partial w}{\partial x} \cdot \frac{\partial w}{\partial y} - \gamma_{xy_0}
\end{aligned}\right] \text{———} 1.05$$

where ϵ_{x_1}, ϵ_{y_1} and γ_{xy_1} are given by the relations 1.03

Considering ϵ_{x_2}, ϵ_{y_2} and γ_{xy_2} etc., to be small in comparison with ϵ_{x_1}, ϵ_{y_1} and γ_{xy_1}, it is rational to assume that the forces N_x, N_y and N_{xy} remain constant during bending.

Hence, the additional strain energy V_{s_2} of the plate due to strains produced in the middle plane is:

$$\begin{aligned} V_{s_2} &= \iint_R \left(N_x \epsilon_{x_2} + N_y \epsilon_{y_2} + N_{xy}\gamma_{xy_2}\right) dx\,dy \\ &= \iint_R \left[N_x \frac{\partial u}{\partial x} + N_y \frac{\partial v}{\partial y} + N_{xy}\left(\frac{\partial u}{\partial y} + \frac{\partial v}{\partial x}\right)\right] dx\,dy \\ &+ \frac{1}{2}\iint_R \left[N_x\left(\frac{\partial w}{\partial x}\right)^2 + N_y\left(\frac{\partial w}{\partial y}\right)^2 + 2N_{xy}\frac{\partial w}{\partial x}\cdot\frac{\partial w}{\partial y}\right] dx\,dy \\ &- \iint_R \left(N_x \epsilon_{x_1} + N_y \epsilon_{y_1} + N_{xy}\gamma_{xy_1}\right) dx\,dy. \end{aligned}$$

Substitution in the last integral from 1.03 gives:

$$\begin{aligned} V_{s_2} &= \iint_R \left[N_x \frac{\partial u}{\partial x} + N_y \frac{\partial v}{\partial y} + N_{xy}\left(\frac{\partial u}{\partial y} + \frac{\partial v}{\partial x}\right)\right] dx\,dy \\ &+ \frac{1}{2}\iint_R \left[N_x\left(\frac{\partial w}{\partial x}\right)^2 + N_y\left(\frac{\partial w}{\partial y}\right)^2 + 2N_{xy}\frac{\partial w}{\partial x}\cdot\frac{\partial w}{\partial y}\right] dx\,dy. \\ &- \frac{1}{hE}\iint_R \left[N_x^2 + N_y^2 - 2\nu N_x N_y + 2(1+\nu)N_{xy}^2\right] dx\,dy. \end{aligned} \qquad 1.06$$

Now, the total strain energy of the plate is the sum of the strain energy content due to the forces acting in the middle plane of the unbent plate, the energy of bending and the additional strain energy of the plate associated with strains produced in the middle plane due to bending.

i.e. $V = V_{S_1} + V_B + V_{S_2}$.

$$\therefore \; V = \frac{1}{2hE}\iint_R \left[N_x^2 + N_y^2 - 2\nu N_x N_y + 2(1+\nu) N_{xy}^2\right] dx\,dy$$

$$+ \frac{D}{2}\iint_R \left[\left(\frac{\partial^2 w}{\partial x^2} + \frac{\partial^2 w}{\partial y^2}\right)^2 - 2(1-\nu)\left\{\frac{\partial^2 w}{\partial x^2}\cdot\frac{\partial^2 w}{\partial y^2} - \left(\frac{\partial^2 w}{\partial x \partial y}\right)^2\right\}\right] dx\,dy.$$

$$+ \iint_R \left[N_x \frac{\partial u}{\partial x} + N_y \frac{\partial v}{\partial y} + N_{xy}\left(\frac{\partial u}{\partial y} + \frac{\partial v}{\partial x}\right)\right] dx\,dy$$

$$+ \iint_R \left[N_x \left(\frac{\partial w}{\partial x}\right)^2 + N_y \left(\frac{\partial w}{\partial y}\right)^2 + 2 N_{xy} \frac{\partial w}{\partial x}\cdot\frac{\partial w}{\partial y}\right] dx\,dy$$

$$- \frac{1}{hE}\iint_R \left[N_x^2 + N_y^2 - 2\nu N\;N + 2(1+\nu) N_{xy}^2\right] dx\,dy$$

Introducing Airy's Stress Function F, such that:

$$\left.\begin{aligned} N_x &= h\frac{\partial^2 F}{\partial y^2} \\ N_y &= h\frac{\partial^2 F}{\partial x^2} \\ N_{xy} &= -h\frac{\partial^2 F}{\partial x \partial y} \end{aligned}\right] \qquad 1.07$$

the total strain energy of the plate becomes:

$$V = \frac{D}{2}\iint_R \left[\left(\frac{\partial^2 w}{\partial x^2}+\frac{\partial^2 w}{\partial y^2}\right)^2 - 2(1-\nu)\left\{\frac{\partial^2 w}{\partial x^2}\cdot\frac{\partial^2 w}{\partial y^2} - \left(\frac{\partial^2 w}{\partial x \partial y}\right)^2\right\}\right] dx\,dy$$

$$+h\iint_R \left[\frac{\partial^2 F}{\partial y^2}\cdot\frac{\partial u}{\partial x} + \frac{\partial^2 F}{\partial x^2}\cdot\frac{\partial v}{\partial y} - \frac{\partial^2 F}{\partial x \partial y}\left(\frac{\partial u}{\partial y}+\frac{\partial v}{\partial x}\right)\right] dx\,dy.$$

$$-\frac{1}{2E}\iint_R \left[\left(\frac{\partial^2 F}{\partial y^2}\right)^2 + \left(\frac{\partial^2 F}{\partial x^2}\right)^2 - 2\nu\frac{\partial^2 F}{\partial y^2}\cdot\frac{\partial^2 F}{\partial x^2} + 2(1+\nu)\left(\frac{\partial^2 F}{\partial x \partial y}\right)^2\right] dx\,dy$$

$$+\frac{h}{2}\iint_R \left[\frac{\partial^2 F}{\partial y^2}\left(\frac{\partial w}{\partial x}\right)^2 + \frac{\partial^2 F}{\partial x^2}\left(\frac{\partial w}{\partial y}\right)^2 - 2\frac{\partial^2 F}{\partial x \partial y}\cdot\frac{\partial w}{\partial x}\cdot\frac{\partial w}{\partial y}\right] dx\,dy \qquad 1.08$$

1.1 DERIVATION OF THE BASIC EQUATIONS FROM THE ENERGY INTEGRALS.

Since the expression for strain energy V does not contain derivatives higher than second order, the forms of Euler's Equations generalised for two variables (See Appendix 1) reduce to:

$$\phi_F - \frac{\partial}{\partial x}\phi_{F_x} - \frac{\partial}{\partial y}\phi_{F_y} + \frac{\partial^2}{\partial x^2}\phi_{F_{xx}} + \frac{\partial^2}{\partial y^2}\phi_{F_{yy}} + \frac{\partial^2}{\partial x \partial y}\phi_{F_{xy}} = 0 \qquad 1.11$$

$$\phi_w - \frac{\partial}{\partial x}\phi_{w_x} - \frac{\partial}{\partial y}\phi_{w_y} + \frac{\partial^2}{\partial x^2}\phi_{w_{xx}} + \frac{\partial^2}{\partial y^2}\phi_{w_{yy}} + \frac{\partial^2}{\partial x \partial y}\phi_{w_{xy}} = 0 \qquad 1.12$$

Noting that ϕ denotes the integrand

and $\phi_w = \frac{\partial \phi}{\partial w}$, $\phi_{F_{xy}} = \frac{\partial \phi}{\partial(\partial^2 F/\partial x \partial y)}$ and $\phi_{w_{yy}} = \frac{\partial \phi}{\partial(\partial^2 w/\partial y^2)}$ etc., the

application of equations 1.11 to the energy integrals 1.08

gives:

$$\frac{\partial^2}{\partial y^2} \cdot \frac{\partial u}{\partial x} + \frac{\partial^2}{\partial x^2} \cdot \frac{\partial v}{\partial y} - \frac{\partial^2}{\partial x \partial y}\left(\frac{\partial u}{\partial y} + \frac{\partial v}{\partial x}\right) + \frac{1}{2}\frac{\partial^2}{\partial y^2}\left(\frac{\partial w}{\partial x}\right)^2$$

$$+ \frac{1}{2}\frac{\partial^2}{\partial x^2}\left(\frac{\partial w}{\partial y}\right)^2 - \frac{\partial^2}{\partial x \partial y} \cdot \frac{\partial w}{\partial x} \cdot \frac{\partial w}{\partial y} - \frac{1}{E}\left(\frac{\partial^2}{\partial y^2} \cdot \frac{\partial^2 F}{\partial y^2} + \right.$$

$$\frac{\partial^2}{\partial x^2} \cdot \frac{\partial^2 F}{\partial x^2} - \frac{\partial^2}{\partial x^2} \nu . \frac{\partial^2 F}{\partial y^2} - \frac{\partial^2}{\partial y^2} \nu . \frac{\partial^2 F}{\partial y^2} + \frac{\partial^2}{\partial x \partial y} . 2 . \frac{\partial^2 F}{\partial x \partial y} +$$

$$\left. \frac{\partial^2}{\partial x \partial y} . 2\nu . \frac{\partial^2 F}{\partial x \partial y}\right) = 0 \qquad \text{———} \quad 1.13$$

Now, since

$$\frac{1}{2}\frac{\partial^2}{\partial y^2}\left(\frac{\partial w}{\partial x}\right)^2 = \left(\frac{\partial^2 w}{\partial x \partial y}\right)^2 + \frac{\partial w}{\partial x} \cdot \frac{\partial^3 w}{\partial y^2 \partial x}.$$

$$\frac{1}{2}\frac{\partial^2}{\partial x^2}\left(\frac{\partial w}{\partial y}\right)^2 = \left(\frac{\partial^2 w}{\partial x \partial y}\right)^2 + \frac{\partial w}{\partial y} \cdot \frac{\partial^3 w}{\partial y \partial x^2}.$$

and $$\frac{\partial^2}{\partial x \partial y} \cdot \frac{\partial w}{\partial x} \cdot \frac{\partial w}{\partial y} = \left(\frac{\partial^2 w}{\partial x \partial y}\right)^2 + \frac{\partial w}{\partial x} \cdot \frac{\partial^3 w}{\partial y^2 \partial x} + \frac{\partial w}{\partial y} \cdot \frac{\partial^3 w}{\partial y \partial x^2} + \frac{\partial^2 w}{\partial x^2} \cdot \frac{\partial^2 w}{\partial y^2}.$$

therefore 1.13 becomes:

$$\left(\frac{\partial^2 w}{\partial x \partial y}\right)^2 - \frac{\partial^2 w}{\partial x^2} \cdot \frac{\partial^2 w}{\partial y^2} - \frac{1}{E}\left(\frac{\partial^4 F}{\partial y^4} + 2 \cdot \frac{\partial^4 F}{\partial x^2 \partial y^2} + \frac{\partial^4 F}{\partial x^4}\right) = 0$$

or

$$\frac{\partial^4 F}{\partial y^4} + 2 \cdot \frac{\partial^4 F}{\partial x^2 \partial y^2} + \frac{\partial^4 F}{\partial x^4} = E\left[\left(\frac{\partial^2 w}{\partial x \partial y}\right)^2 - \frac{\partial^2 w}{\partial x^2} \cdot \frac{\partial^2 w}{\partial y^2}\right] \quad \text{——— 1.14}$$

Similarly, the application of equation 1.12 gives:

$$\frac{h}{2}\left(-2 \frac{\partial^2 F}{\partial y^2} \cdot \frac{\partial}{\partial x} \cdot \frac{\partial w}{\partial x} - 2 \frac{\partial^2 F}{\partial x^2} \cdot \frac{\partial}{\partial y} \cdot \frac{\partial w}{\partial y} + 2 \frac{\partial^2 F}{\partial x \partial y} \cdot \frac{\partial}{\partial x} \cdot \frac{\partial w}{\partial y}\right.$$

$$\left. + 2 \frac{\partial^2 F}{\partial x \partial y} \cdot \frac{\partial}{\partial y} \cdot \frac{\partial w}{\partial x}\right) + \frac{D}{2}\left[2 \frac{\partial^2}{\partial x^2} \cdot \frac{\partial^2 w}{\partial x^2} + 2 \frac{\partial^2}{\partial y^2} \cdot \frac{\partial^2 w}{\partial y^2}\right.$$

$$+ 2 \frac{\partial^2}{\partial x^2} \cdot \frac{\partial^2 w}{\partial y^2} + 2 \frac{\partial^2}{\partial y^2} \cdot \frac{\partial^2 w}{\partial x^2} - 2(1-\nu)\left\{\frac{\partial^2}{\partial x^2} \cdot \frac{\partial^2 w}{\partial y^2}\right.$$

$$\left.\left. + \frac{\partial^2}{\partial y^2} \cdot \frac{\partial^2 w}{\partial x^2} - 2 \frac{\partial^2}{\partial x \partial y} \cdot \frac{\partial^2 w}{\partial x \partial y}\right\}\right] = 0$$

or

$$\frac{\partial^4 w}{\partial x^4} + 2 \frac{\partial^4 w}{\partial x^2 \partial y^2} + \frac{\partial^4 w}{\partial y^4} = \frac{h}{D}\left(\frac{\partial^2 F}{\partial y^2} \cdot \frac{\partial^2 w}{\partial x^2} + \frac{\partial^2 F}{\partial x^2} \cdot \frac{\partial^2 w}{\partial y^2} - 2 \frac{\partial^2 F}{\partial x \partial y} \cdot \frac{\partial^2 w}{\partial x \partial y}\right)$$

——— 1.15

Thus, utilising the Euler's equations the minimum energy condition is reduced to the solution of equations 1.14 and 1.15. These equations are the Von Karman differential equations for "large" deflection of plates.

1.2 APPROXIMATE METHOD OF SOLUTION.

At present, to the best of author's knowledge, there are no methods available for the rigorous mathematical solution of the large deflection plate equations. From the applied point of view it is of great importance to have a solution predicting the actual physical behaviour of a particular case considered. Thus the rigorous solutions are important from this aspect as long as the fundamental assumptions involved and the boundary conditions considered in the analysis are in agreement with the practical aspects of the problem. Approximate methods become particularly valuable, if such rigorous solutions are intractable. Again, approximate methods should be such that all significant boundary conditions are taken into account in the solution. It is important at the same time that the deductions from the approximate solutions should be able to predict the actual behaviour adequately. This may be tested by comparison of the analytical result obtained with that of experiments reproducing the conditions investigated.

In the following an approximate method based on Galerkin's theorem [17] is presented. This method is considered of particular value in applied investigations because of its simplicity.

1.3 GALERKIN'S METHOD.

It was seen that the problem of minimizing the general strain energy integral,

$$I = \iint_R \phi\left(x, y, w, w_x, w_y, w_{xx}, w_{yy}, w_{xy}, \ldots\ldots\ldots, F, F_x, F_y, F_{xx}, F_{yy}, F_{xy}, \ldots\ldots\ldots\right) dx\,dy.$$

by imposing the arbitrary variation $\delta\eta(x,y)$ and $\delta\psi(x,y)$ in w and F respectively, led to the equations (See page Appendix 1):

$$\iint_R L(w)\eta\,dx\,dy = 0 \qquad \text{———— 1.31}$$

and

$$\iint_R L(F)\psi\,dx\,dy = 0 \qquad \text{———— 1.32}$$

where

$$L(w) = \phi_w - \frac{\partial\phi_{w_x}}{\partial x} - \frac{\partial\phi_{w_y}}{\partial y} + \frac{\partial^2\phi_{w_{xx}}}{\partial x^2} + \frac{\partial^2\phi_{w_{yy}}}{\partial y^2} + \frac{\partial^2\phi_{w_{xy}}}{\partial x\partial y} \mp \cdots\cdots = 0 \qquad \text{———— 1.33}$$

and

$$L(F) = \phi_F - \frac{\partial\phi_{F_x}}{\partial x} - \frac{\partial\phi_{F_y}}{\partial y} + \frac{\partial^2\phi_{F_{xx}}}{\partial x^2} + \frac{\partial^2\phi_{F_{yy}}}{\partial y^2} + \frac{\partial^2\phi_{F_{xy}}}{\partial x\partial y} \mp \cdots\cdots = 0 \qquad \text{———— 1.34}$$

are the Euler's equations which reduce to the differential equations for a particular problem, and η and ψ are arbitrary functions of (x, y) which, together with their partial derivatives satisfy homogeneous essential conditions on the boundary C of the region R (Appendix I).

Let w^* and F^* be approximate solutions of the problem such that:

$$w^* = \sum_{s=1}^{t} \alpha_s w_s \qquad \text{———— 1.35}$$

$$F^* = \sum_{s=1}^{t} \beta_s F_s \qquad \text{———— 1.36}$$

where the independent functions w_s and F_s each satisfy the respective boundary conditions imposed on the exact solutions and α_s and β_s are unknown constants.

In general, a particular variation δw^* in w^* can be substituted for the arbitrary variation $\varepsilon\eta^*(x,y)$. Similarly δF^* can be used to replace $\varepsilon\psi^*(x,y)$. Now from 1.35 and 1.36

$$\delta w^* = \sum_{s=1}^{t} \frac{\partial w^*}{\partial \alpha_s} \cdot \delta\alpha_s$$

$$\delta F^* = \sum_{s=1}^{t} \frac{\partial F^*}{\partial \beta_s} \cdot \delta\beta_s$$

By substitution, the left hand sides of equations 1.31 and 1.32 become:

$$\iint_R L(w^*) \sum_{s=1}^{s=t} \frac{\partial w^*}{\partial \alpha_s} \delta\alpha_s \, dx\, dy \quad \text{and} \quad \iint_R L(F^*) \sum_{s=1}^{s=t} \frac{\partial F^*}{\partial \beta_s} \delta\beta_s \, dx\, dy$$

Equations 1.33 and 1.34 are associated with the exact solutions w and F, therefore when the approximate solutions w^* and F^* are substituted for w and F, the equation 1.33 and 1.34 will no longer be satisfied and will result in:

$L(w^*) = \Omega(x,y)$ where $\Omega(x,y) \neq 0$ and $L(F^*) = \lambda(x,y)$ where $\lambda(x,y) \neq 0$

If $\Omega(x,y)$ and $\lambda(x,y)$, called the error functions, are sufficiently small then w^* and F^* (which it is to be remembered satisfy the boundary conditions exactly) can be regarded as satisfactory approximate solutions. Thus the problem reduces to selecting α_s and β_s so as to minimize the error functions.

A reasonable minimizing technique was suggested by Galerkin as follows: Let the true solutions w and F be represented by the series $w = \sum_{s=1}^{\infty} \alpha_s w_s$ and $F = \sum_{s=1}^{\infty} \beta_s F_s$ with suitable properties and suppose that $L(w^*) \to L(w)$ and $L(F^*) \to L(F)$ as $t \to \infty$.

Also assume that the arbitrary functions $\eta(x, y)$ and $\psi(x, y)$ can be represented in the series $\eta = \sum_{s=1}^{\infty} c_s w_s$ and $\psi = \sum_{s=1}^{\infty} d_s F_s$ where c_s and d_s are arbitrary constants. Then (noting that $\delta\alpha_s$ and $\delta\beta_s$ are variations in arbitrary constants and therefore are not zero),

$$\iint_R L(w^*) \sum_{s=1}^{t} \frac{\partial w^*}{\partial \alpha_s}\, dx\, dy = 0 \quad \text{as} \quad t \to \infty \qquad \text{1.38}$$

and $$\iint_R L(F^*) \sum_{s=1}^{t} \frac{\partial F^*}{\partial \beta_s}\, dx\, dy = 0 \quad \text{as} \quad t \to \infty \qquad \text{1.39}$$

demand that equations 1.31 and 1.32 be satisfied respectively. (Note that $\frac{\partial w^*}{\partial \alpha_s} = w_s$ and $\frac{\partial F^*}{\partial \beta_s} = F_s$).

Now since equations 1.31 and 1.32 lead to 1.33 and 1.34, it can be stated that the conditions 1.38 and 1.39 are equivalent, respectively to equations $L(w) = 0$ and $L(F) = 0$ as $t \to \infty$. This argument depends, of course, on the proper behaviour and selection of the series involved.

Now for a true solution the error functions vanish identically (equations: 1.33 and 1.34). For an approximate solution with a restricted number t

of parameters the best that can be done is to adjust the constants α_s and β_s so that $\Omega(x,y)$ and $\lambda(x,y)$ stay close to zero throughout the region.

The foregoing argument led Galerkin to suggest for the error function $L(w^*)$ and $L(F^*)$ a set of conditions:

$$\left.\begin{aligned}\iint_R L(w^*)\sum_{s=1}^{t}\frac{\partial w^*}{\partial \alpha_s}\,dx\,dy &= 0\\ \iint_R L(F^*)\sum_{s=1}^{t}\frac{\partial F^*}{\partial \beta_s}\,dx\,dy &= 0\end{aligned}\right] \quad 1.310$$

Yielding a set of t equations for the determination of the constants α_s etc., and β_s etc., giving the approximate solutions $w^*(x,y)$ and $F^*(x,y)$.

Thus Galerkin's Method consists of assuming an approximate series with unknown constants, for the governing functions; each term of the series satisfying all of the significant boundary conditions. These approximate functions are substituted into the differential equations, multiplied each time by their partial derivatives with respect to the unknown constants and equations of the type 1.310 formed. Solution of these equations simultaneously determines the unknown constants and hence the approximate solutions.

The justification of the Galerkin's method has also been approached by the consideration of the method of "Least mean Square Error." [26].

It is clear that the labour involved in obtaining approximate solutions by Galerkin's Method rises rapidly as the number t of the independent functions increases. Hence, for determining a particular mode of a problem, it is advantageous to employ a small number of functions which are known to resemble the required mode. Thus the choice of the functions should be guided by the greatest possible knowledge of analogous problems.

It has been shown both in this thesis and in References [26] and [27] that if the functions are well chosen excellent approximations can be obtained by the use of a 'very' small number of functions.

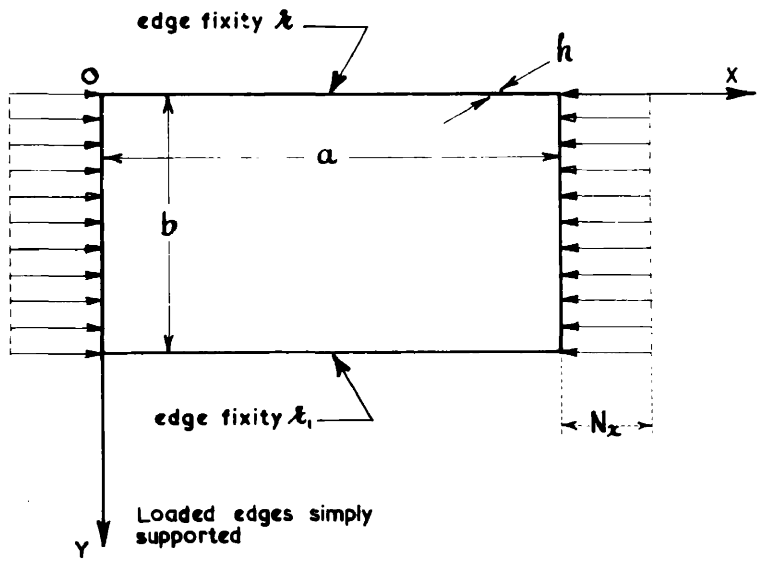
edge fixity k
h
O
X
a
b
edge fixity k_1
N_x
Loaded edges simply supported
Y

Fig. (11)

1.4 FORMULATION OF APPROXIMATE FORMS FOR STRESS FUNCTION F AND DEFLECTION w IN SELECTED CASES.

It is clear that the first essential requirement for the approximate solution of the large deflection equations for different cases of rectangular plates subjected to lengthwise compressive actions, is the formulation of approximate forms of F and w. In the following, two general cases of rectangular plates are considered and from their relevant boundary conditions, the approximate forms of F and w are derived. Only one unknown constant in each series is considered in the present analysis for simplicity; the procedure indicated however being equally applicable to series with more than one constant.

<u>Case (a)</u> Flat Rectangular Plate Uniformly Compressed Along Two Opposite Simply Supported Edges And Having Equal Or Un-equal Edge Fixities Along The Other Two Edges.

Fig.(11) shows such a plate, the compressive action is uniform along $x = 0$ and $x = a$: the simply supported edges, and is denoted by N_x force per unit length. The elastic coefficient of edge fixity (Moment per unit slope per unit length) for the edge $y = 0$ is denoted by k and for the edge $y = b$ by k_1.

Stress Function F :

The stress function F must satisfy all of the following boundary conditions:

$\sigma_y = \frac{\partial^2 F}{\partial x^2} = 0$ at $y=0$ and $y=b$

$\frac{\partial^2 F}{\partial y^2} = N_x/h$ at $x=0$ and $x=a$

and $\tau_{xy} = -\frac{\partial^2 F}{\partial x \partial y} = 0$ at $x=0, x=a, y=0$ and $y=b$.

The general form of the stress function which satisfies all these boundary conditions, as formulated in Appendix 2 page is:

$$F = \frac{N_x y^2}{2h} + \rho\left(\frac{x^2}{a^2} - \frac{x}{a}\right)^2\left(\frac{y^2}{b^2} - \frac{y}{b}\right)^2$$

where ρ may be a constant, a function of x and/or a function of y.

It is rational to assume that σ_x distribution is symmetrical when $k = k_1$ and unsymmetrical when $k \neq k_1$. Thus the problem reduces to selecting ρ in such a way that $\left|\partial^2 F/\partial y^2\right|$ distribution across any section parallel to the y - axis is symmetrical for $k = k_1$ and unsymmetrical for $k \neq k_1$.

To avoid the manipulative difficulty introduced by the permitted variations of k and k_1 from zero to infinity a function γ is taken such that when k and k_1 vary from zero to infinity γ assumes the values between -1 and +1; thus

$$\gamma = \sin\left(\frac{\mu-1}{\mu+1}\right)\frac{\pi}{2}$$

where $\mu = \frac{kb+1}{k_1 b+1}$

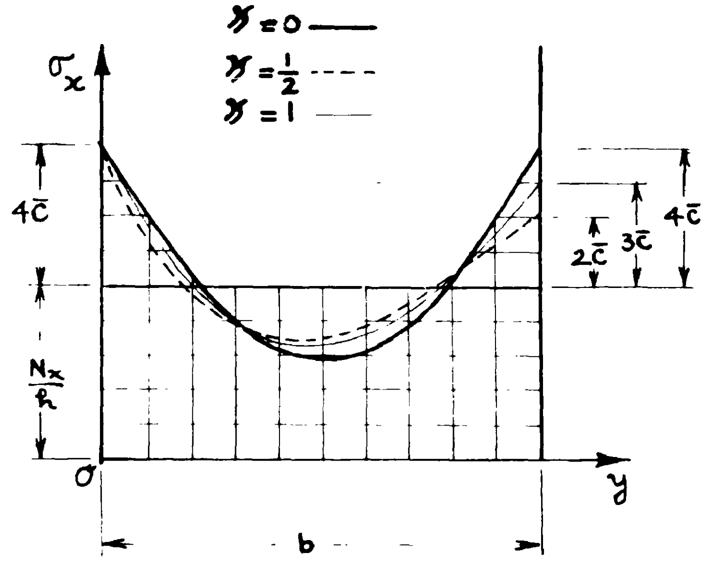

Fig.(12)

Again, since for equal numerical values of γ with opposite signs the two cases are mirror images of each other, the problem can be simplified by imposing the condition that k is always equal to or greater than k_1, in which case γ varies from zero to +1.

γ is then introduced in the function ρ as follows:

$$\rho = \left(2 - \frac{\gamma y}{b}\right)\beta$$

where β is an arbitrary constant.

It is seen that ρ is a constant for $\gamma = 0$ $(k = k_1)$ and gives a symmetrical σ_x distribution. For any other value of γ $(k \neq k_1)$ it gives an unsymmetrical σ_x distribution with respect to the centre line of the plate.

The stress function then becomes:

$$F = \frac{N_x y^2}{2k} + \beta\left(\frac{x^2}{a^2} - \frac{x}{a}\right)^2\left(\frac{y^2}{b^2} - \frac{y}{b}\right)^2\left(2 - \frac{\gamma y}{b}\right)$$

or

$$F = \frac{N_x y^2}{2k} + \beta\left(\frac{x^2}{a^2} - \frac{x}{a}\right)^2\left(\frac{-\gamma y^5}{b^5} + \frac{S y^4}{b^4} + \frac{T y^3}{b^3} + \frac{2y^2}{b^2}\right) \quad 1.41a$$

where $S = (2 + 2\gamma)$

and $T = (-\gamma - 4)$

The various σ_x distributions at $x = a/2$ for different values of γ are shown in Fig. (12).

Deflection Form w.

In deriving the deflection form of the plate, the form is presumed to be a sine wave in the x - direction;

the sides $x = 0$ and $x = a$ being simply supported. In the y - direction a simple analogy is used to formulate the deflection form. The details of this are shown in Appendix 2 page . This method gives the deflection as:

$$w = \alpha \sin \frac{m\pi x}{a} \left(\frac{y^4}{24 b^3} - \frac{A_1 y^3}{6 b^2} + \frac{B_1 y^2}{b} + \frac{C_1 y}{3} \right) \text{———} 1.42a$$

which satisfies all of the following boundary conditions:

$$\left.\begin{aligned} & w = 0 \\ & \frac{\partial^2 w}{\partial x^2} + \nu \frac{\partial^2 w}{\partial y^2} = 0 \end{aligned}\right] \quad \text{At } x = 0 \text{ and } x = a$$

$$\left.\begin{aligned} & w = 0 \\ & \frac{\partial^2 w}{\partial y^2} - k \frac{\partial w}{\partial y} = 0 \end{aligned}\right] \quad \text{At } y = 0$$

$$\left.\begin{aligned} & w = 0 \\ & \frac{\partial^2 w}{\partial y^2} + k_1 \frac{\partial w}{\partial y} = 0 \end{aligned}\right] \quad \text{At } y = b$$

A_1, B_1 and C_1 are constants and are given by:

$$\left.\begin{aligned} & A_1 = \frac{1}{2} + \frac{\bar{\phi}}{b^2} - \frac{\bar{q}}{b^2} \\ & B_1 = \frac{\bar{\phi}}{2 b^2} \end{aligned}\right] \text{———} 1.43a$$

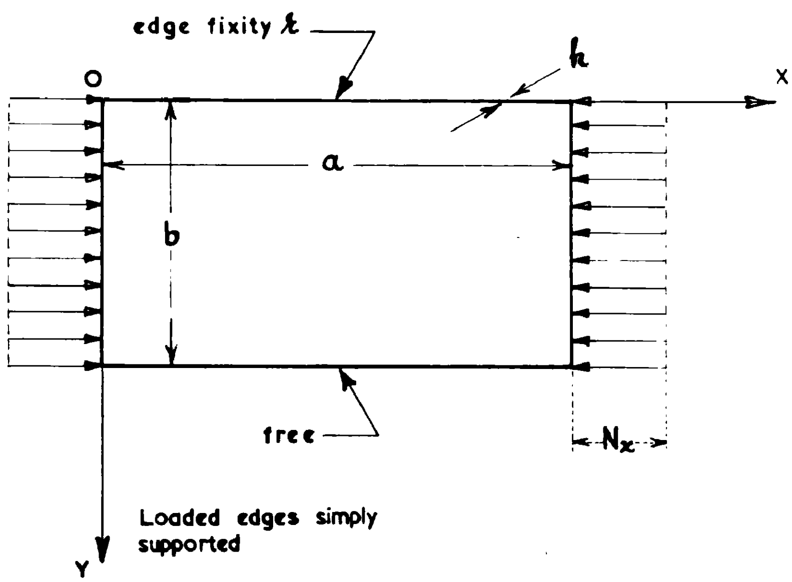

Fig. (13)

$$C_1 = \frac{1}{8} - \frac{\bar{p}}{b^2} - \frac{\bar{q}}{2b^2}$$

where a and b are the plate dimensions in the x and y directions respectively and

$$\bar{q} = \frac{6r_1 b^4 + r r_1 b^5}{144b + 48r_1 b^2 + 48rb^2 + 12rr_1 b^3}$$

$$\bar{p} = \frac{rb^3}{24 + 8rb} - \bar{q}\,\frac{rb}{6 + 2rb} \qquad \text{1.44a}$$

α is an arbitrary constant, and m is the number of half sine waves.

<u>Case (b)</u> Flat Rectangular Plate Uniformly Compressed Along Two Opposite Simply Supported Edges Elastically Fixed Along One Edge And Free Along The Other.

The plate shown in Fig.(13) has uniform compressive load N_x per unit length applied along the simply supported edges $x = 0$ and $x = a$. The edge $y = 0$ is elastically fixed: the coefficient of edge fixity being r, and the edge $y = b$ is free.

Stress Function F:

Proceeding in a manner similar to that for Case (a), the stress function as shown in Appendix 2 page is obtained as:

$$F = \frac{N_x y^2}{2h} + \beta\left(\frac{x^2}{a^2} - \frac{x}{a}\right)^2\left(\frac{y^2}{b^2} - \frac{y^4}{2b^4} - \frac{1}{2}\right) \qquad \text{1.41b}$$

DISTRIBUTION OF STRESS

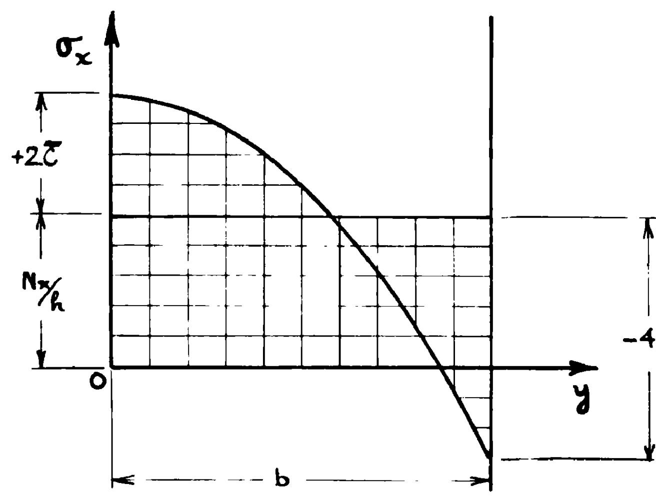

Fig. (14)

where β is a constant.

The stress function satisfies the following boundary conditions considered significant:

$$\sigma_y = \frac{\partial^2 F}{\partial x^2} = 0 \qquad \text{at} \quad y = b$$

$$\sigma_x = \frac{\partial^2 F}{\partial y^2} = \frac{N_x}{h} \qquad \text{at } x = 0 \text{ and } x = a.$$

and $\tau_{xy} = -\dfrac{\partial^2 F}{\partial x \partial y} = 0$ at $y = 0,\ y = b,\ x = 0$ and $x = a$

The distribution of σ_x along the section is shown in Fig. (14).

Deflection Form w :

In this case, also, it is assumed that the deflection form in the x- direction is a sine wave, while in the y-direction its formulation on lines somewhat different from the previous case is shown in Appendix II page .

The deflection form then becomes:

$$w = \alpha \sin \frac{m\pi x}{a}\left[\frac{A_2 y^4}{b^3} + \frac{B_2 y^3}{b^2} + \frac{r b y^2}{2(rb+2)b} + \frac{y}{(rb+2)}\right] \quad \text{1.42b}$$

where A_2 and B_2 are obtained from (See Appendix):

$$12A_2 + 6B_2 + \frac{rb}{(rb+2)} = \nu \frac{m^2\pi^2 b^2}{a^2}\left[A_2 + B_2 + \frac{rb}{2(rb+2)} + \frac{1}{(rb+2)}\right] \quad \text{1.43b}$$

and

$$24A_2 + 6B_2 = (2-\nu)\frac{m^2\pi^2 b^2}{a^2}\left[4A_2 + 3B_2 + \frac{rb}{(rb+2)} + \frac{1}{(rb+2)}\right] \quad \text{1.44b}$$

for any particular values of ν the Poisson's ratio, m the number of half sine waves a and b the plate dimensions and r the coefficient of edge fixity.

The deflection form satisfies all the following boundary conditions:

$$\left.\begin{aligned} & w = 0 \\ & \frac{\partial^2 w}{\partial x^2} + \nu \frac{\partial^2 w}{\partial y^2} = 0 \end{aligned}\right] \quad \text{At } x = 0 \text{ and } x = a$$

$$\left.\begin{aligned} & w = 0 \\ & \frac{\partial^2 w}{\partial y^2} - r \frac{\partial w}{\partial y} = 0 \end{aligned}\right] \quad \text{At } y = 0$$

$$\left.\begin{aligned} & \frac{\partial^2 w}{\partial y^2} + \nu \frac{\partial^2 w}{\partial x^2} = 0 \\ & \frac{\partial^3 w}{\partial y^3} + (2-\nu) \frac{\partial^3 w}{\partial x^2 \partial y} = 0 \end{aligned}\right] \quad \text{At } y = b$$

SECTION 2

ELASTIC CRITICAL LOAD EVALUATION

ELASTIC CRITICAL LOAD EVALUATION.

2.0 ELASTIC CRITICAL LOAD.

In calculating the load applied in the middle plane of the plate which will produce elastic instability, i.e. the critical load, it is assumed that initially the plate is perfectly flat. If the uniform compressive load applied to the plate is less than its critical, the plate remains perfectly flat and undergoes only an axial compression. This implies that the flat form of equilibrium is stable, i.e. if a lateral load is applied to the plate producing a small deflection, this deflection disappears when the lateral force is removed and the plate becomes flat again. However, if the applied compressive load is gradually increased, a condition is reached when the straight form of equilibrium ceases to be stable and a slight lateral load produces a deflection which does not disappear when the lateral force is removed. The critical load is thus defined as the smallest axial load which will maintain a deviation from the flat form of equilibrium, or conversely, the largest axial load which the plate may support in its initially flat configuration and which produces in the plate only acial compression.

Although, for the calculation of critical load, it is sufficient to solve the differential equation for the deflection form 1.15; approximate solutions, using Galerkin's Method, of both the large deflection plate equations 1.14 and 1.15 have been included, in the following, for their later use in the evaluation of post buckling maximum loads.

Case (a) Flat Rectangular Plate Uniformly Compressed Along Two Opposite Simply Supported Sides and Having Equal or Un-equal Elastic Fixities, Along The Other Two Sides.

The stress function and the deflection form, satisfying their relevant boundary conditions, for this case are given by equations 1.41 a and 1.42a respectively. To complete the approximate solution, β and α the unknown constants, will now be determined.

Applying Galerkin's Method to the large deflection plate equations 1.14 and 1.15, the following equations result:

$$\int_0^b\int_0^a\left[\frac{\partial^4 F}{\partial x^4}+2\frac{\partial^4 F}{\partial x^2\partial y^2}+\frac{\partial^4 F}{\partial y^4}-E\left(\frac{\partial^2 w}{\partial x\partial y}\right)^2+E\frac{\partial^2 w}{\partial x^2}\cdot\frac{\partial^2 w}{\partial y^2}\right]\frac{\partial F}{\partial\beta}\,dx\,dy=0 \qquad \text{2.01a}$$

$$\int_0^b\int_0^a\left[\frac{\partial^4 w}{\partial x^4}+2\frac{\partial^4 w}{\partial x^2\partial y^2}+\frac{\partial^4 w}{\partial y^4}-\frac{h}{D}\left(\frac{\partial^2 F}{\partial x^2}\frac{\partial^2 w}{\partial y^2}+\frac{\partial^2 F}{\partial y^2}\frac{\partial^2 w}{\partial x^2}-2\frac{\partial^2 F}{\partial x\partial y}\frac{\partial^2 w}{\partial x\partial y}\right)\right]\frac{\partial w}{\partial\alpha}\,dx\,dy=0 \qquad \text{2.02a}$$

Substituting the expressions for w and F in equations 2.01a and 2.02a and integrating, the following two simultaneous algebraic equations in β and α are obtained:

$$\frac{\beta}{b^2}\left[\frac{4b^3}{5a^3}\left\{\frac{\mathcal{R}^2}{11}-\frac{S\mathcal{R}}{5}+\frac{1}{9}\left(S^2-2T\mathcal{R}\right)+\frac{1}{8}\left(2ST-4\mathcal{R}\right)+\frac{1}{7}\left(4S+T^2\right)\right.\right.$$

$$\left.+\frac{2T}{3}+\frac{4}{5}\right\}-\frac{4b}{105a}\left\{\frac{20\mathcal{R}^2}{9}-4S\mathcal{R}+\frac{1}{7}\left(12S^2-26T\mathcal{R}\right)+\right.$$

$$\left.\frac{1}{6}\left(18ST-44\right)+\frac{1}{5}\left(28S+6T^2\right)+4T+\frac{8}{3}\right\}+\frac{a}{630b}\left\{\frac{120\mathcal{R}^2}{7}-24S\mathcal{R}\right.$$

$$\left.\left.+\frac{1}{5}\left(24S^2-120T\mathcal{R}\right)+6\left(ST-10\mathcal{R}\right)+16S\right\}\right]+\alpha^2E\,\frac{b}{a}\left(\frac{3}{4m^2\pi^2}-\frac{m^2\pi^2}{60}\right)$$

$$\left[-\frac{\mathcal{R}}{432}+\frac{1}{11}\left(\frac{S}{36}+\frac{A_1\mathcal{R}}{6}\right)+\frac{1}{10}\left(-\frac{2B_1\mathcal{R}}{3}-\frac{A_1^2\mathcal{R}}{4}-\frac{A_1S}{6}+\frac{T}{36}\right)\right.$$

$$+\frac{1}{9}\left(-\frac{C_1\mathcal{R}}{9}+2A_1B_1\mathcal{R}+\frac{2B_1S}{3}+\frac{A_1^2S}{4}-\frac{A_1T}{6}+\frac{1}{18}\right)+\frac{1}{8}\left(-4B_1^2\mathcal{R}\right.$$

$$\left.+\frac{A_1C_1\mathcal{R}}{3}+\frac{C_1S}{9}-2A_1B_1S+\frac{2B_1T}{3}+\frac{A_1^2T}{4}-\frac{A_1}{3}\right)+\frac{1}{7}\left(-\frac{4B_1C_1\mathcal{R}}{3}\right.$$

$$\left.+4B_1^2S-\frac{A_1C_1S}{3}+\frac{C_1T}{9}-2A_1B_1T+\frac{4B_1}{3}+\frac{A^2}{2}\right)+\frac{1}{6}\left(-\frac{C_1^2\mathcal{R}}{9}\right.$$

$$\left.+\frac{4B_1C_1S}{3}+4B_1^2T-\frac{A_1C_1T}{3}+\frac{2C_1}{9}-4A_1B_1\right)+\frac{1}{5}\left(\frac{C_1^2S}{9}+\right.$$

$$\left.\left.\frac{4B_1C_1T}{3}+8B_1^2-\frac{2A_1C_1}{3}\right)+\frac{1}{4}\left(\frac{C_1^2T}{9}+\frac{8B_1C_1}{3}\right)+\frac{2C_1^2}{27}\right]-$$

$$-E\alpha^2 \frac{b}{a}\left(\frac{3}{4m^2\pi^2}+\frac{m^2\pi^2}{60}\right)\Biggl[-\frac{\mathcal{X}}{576}+\frac{1}{11}\left(\frac{S}{48}+\frac{A_1\mathcal{X}}{8}\right)+\frac{1}{8}\Biggl(-\frac{A_1^2\mathcal{X}}{6}$$

$$-\frac{7B_1\mathcal{X}}{12}-\frac{A_1S}{8}+\frac{T}{48}\Biggr)+\frac{1}{9}\Biggl(-\frac{C_1\mathcal{X}}{6}+\frac{4A_1B_1\mathcal{X}}{3}+\frac{A_1^2S}{6}+\frac{7B_1S}{12}$$

$$-\frac{A_1T}{8}+\frac{1}{24}\Biggr)+\frac{1}{8}\Biggl(-2B_1^2\mathcal{X}+\frac{A_1C_1\mathcal{X}}{3}+\frac{C_1S}{6}-\frac{4A_1B_1S}{3}+\frac{A_1^2T}{6}$$

$$+\frac{7B_1T}{12}-\frac{A}{4}\Biggr)+\frac{1}{7}\Biggl(-\frac{2B_1C_1\mathcal{X}}{3}+2B_1^2S-\frac{A_1C_1S}{3}+\frac{C_1T}{6}-\frac{4A_1B_1T}{3}$$

$$+\frac{A_1^2}{3}+\frac{7B_1}{6}\Biggr)+\frac{1}{6}\left(\frac{2B_1C_1S}{3}+2B_1^2T-\frac{A_1C_1T}{3}+\frac{C_1}{3}-\frac{8A_1B_1}{3}\right)$$

$$+\frac{1}{5}\left(\frac{2B_1C_1T}{3}+4B_1^2-\frac{2A_1C_1}{3}\right)+\frac{B_1C_1}{3}\Biggr]=0 \quad\text{———} \quad 2.03a$$

and

$$\alpha\frac{m^2\pi^2}{2}\left(\frac{bN_x b^2}{aD}+\frac{m^2\pi^2b^3}{a^3}\right)\Biggl[\frac{1}{5184}-\frac{A_1}{576}+\left(B_1+\frac{A_1^2}{3}\right)\frac{1}{84}+\Biggl(\frac{C}{12}$$

$$-A_1B_1\Biggr)\frac{1}{18}+\left(B_1^2-\frac{A_1C_1}{9}\right)\frac{1}{5}+\frac{B_1C_1}{6}+\frac{C_1^2}{27}\Biggr]+\alpha\frac{a}{6b}\Biggl[\frac{1}{40}-\frac{A_1}{8}+B_1$$

$$+\frac{C_1}{2}\Biggr]-\alpha\frac{m^2\pi^2b}{a}\Biggl[\frac{1}{336}-\frac{A_1}{48}+\left(\frac{7B_1}{12}+\frac{A_1^2}{6}\right)\frac{1}{5}-\left(\frac{4A_1B_1}{3}-\frac{C_1}{6}\right)\frac{1}{4}+$$

$$\left(2B_1^2-\frac{A_1C_1}{3}\right)\frac{1}{3}+\frac{B_1C_1}{3}\Biggr]+\alpha\beta\frac{m^2hb}{Da}\left(\frac{\pi^2}{60}+\frac{3}{4m^4\pi^2}\right)\Biggl[-\frac{5\mathcal{X}}{1728}+\Biggl(\frac{5A_1\mathcal{X}}{18}+$$

$$\frac{S}{48}\Biggr)\frac{1}{11}+\left(-\frac{5B_1\mathcal{X}}{3}-\frac{5A_1^2\mathcal{X}}{9}-\frac{A_1S}{6}+\frac{T}{96}\right)\frac{1}{10}+\Biggl(-\frac{5C_1\mathcal{X}}{9}+\frac{20A_1B_1\mathcal{X}}{3}+$$

$$B_1 S + \frac{A_1^2 S}{3} - \frac{A_1 T}{12} + \frac{1}{144}) \frac{1}{9} + (-20B_1^2\mathcal{H} + \frac{20A_1C_1\mathcal{H}}{9}$$

$$+ \frac{C_1S}{3} - 4A_1B_1S + \frac{B_1T}{2} + \frac{A_1^2T}{6} - \frac{A}{18}) \frac{1}{8} + (\frac{-40B_1C_1\mathcal{H}}{3}$$

$$+12B_1^2S - \frac{4A_1C_1S}{3} + \frac{C_1T}{6} - 2A_1B_1T + \frac{B_1}{3} + \frac{A_1^2}{9}) \frac{1}{7}$$

$$+ (-\frac{20C_1^2\mathcal{H}}{9} + 8B_1C_1S + 6B_1^2T - \frac{2A_1C_1T}{3} + \frac{C_1}{9} - \frac{4A_1B_1}{3}$$

$$+ \frac{24C_1^2}{27}) \frac{1}{6} + (4B_1C_1T + 4B_1^2 - \frac{4A_1C_1}{9} + \frac{4C_1^2}{3}) \frac{1}{5}$$

$$+ (\frac{2C_1^2T}{3} + \frac{8B_1C_1}{3}) \frac{1}{4}] + 3\alpha\beta \frac{hb}{Dam^2\pi^2} [-\frac{\mathcal{H}}{216} + (\frac{7S}{144}$$

$$+ \frac{53A_1\mathcal{H}}{144}) \frac{1}{11} + (\frac{T}{24} - \frac{23A_1S}{72} - \frac{11B_1\mathcal{H}}{6} - \frac{7A_1^2\mathcal{H}}{12})$$

$$\frac{T}{10} + (\frac{5}{72} - \frac{13A_1T}{48} + \frac{19B_1S}{12} + \frac{11B_1A_1\mathcal{H}}{2} + \frac{A_1^2S}{2} -$$

$$\frac{37C_1\mathcal{H}}{72}) \frac{1}{9} + (-\frac{4A_1}{9} + \frac{4B_1T}{3} + \frac{5A_1^2T}{12} - \frac{14A_1B_1S}{3}$$

$$-12\mathcal{H}B_1^2 + \frac{4C_1S}{9} + \frac{13A_1C_1\mathcal{H}}{9}) \frac{1}{8} + (\frac{13B_1}{6} + \frac{2A_1^2}{3} - \frac{23A_1B_1T}{6}$$

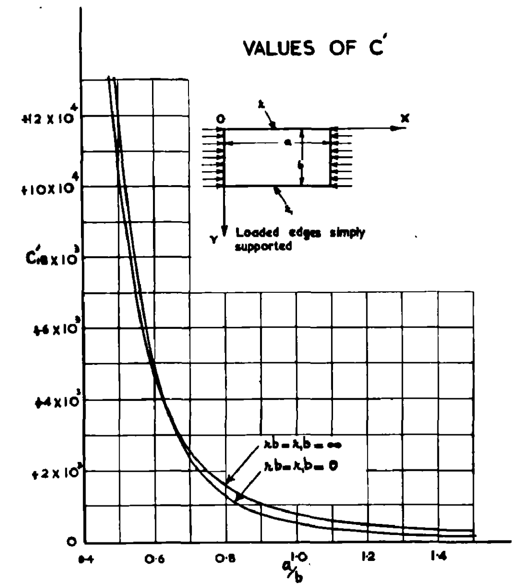

Fig.(15)

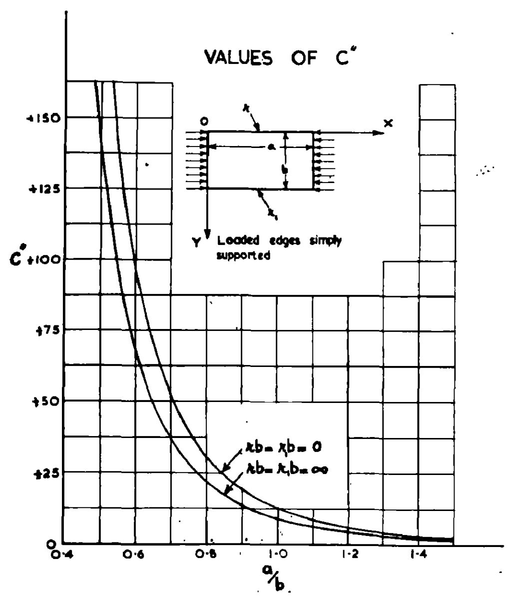

Fig.(16)

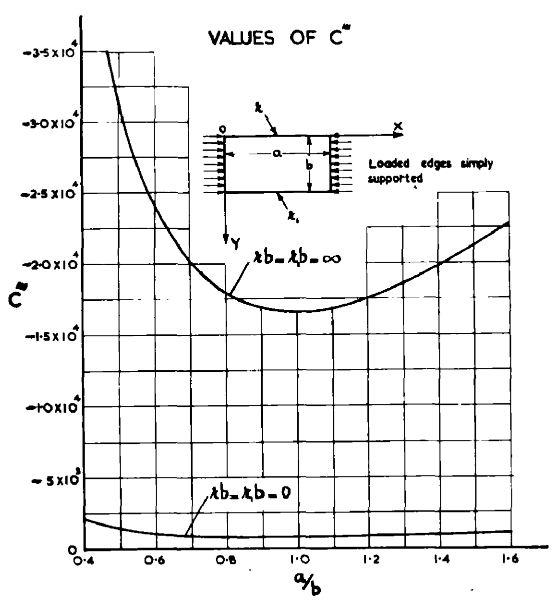

Fig.(17)

$$+10B_1^2S + \frac{3C_1T}{8} - \frac{11A_1C_1S}{9} - \frac{17B_1C_1\gamma}{3} + \frac{28B_1C_1}{3}\Big)\frac{1}{7} +$$

$$\left(-6A_1B_1 + 8B_1^2T + \frac{11C_1}{18} - A_1C_1T + \frac{14B_1C_1}{3} - \frac{5\gamma C_1^2}{9} + \frac{24C_1^2}{27}\right)\frac{1}{6}$$

$$+\left(12B_1^2 - \frac{14A_1C_1}{9} + \frac{11B_1C_1T}{3} + \frac{4C_1^2S}{9}\right)\frac{1}{5} + \frac{TC_1^2}{12}\Big] = 0 \qquad \text{2.04a}$$

Solving these euqations for β and α and noting that the latter cannot be zero the following expressions result:

$$\beta = C'\frac{Da^4}{hb^4} + C''\frac{N_x a^4}{h\,b^2} \qquad \text{2.05a}$$

and

$$\alpha = \sqrt{\frac{C'''\beta}{b^2E}} \qquad \text{2.06a}$$

where C', C'' and C''' are constants: their values depending upon a/b, m, rb and r_1b. Plotted values of C', C'' and C''' against the aspect ratio a/b for selected rb and r_1b values are shown in Figs.(15, 16) and (17) respectively.

For buckling under small deflection conditions $\sigma_x =$ constant hence $\beta = 0$, and equation 2.05a becomes:

$$\frac{N_x}{h} = -\frac{C'\,D}{C''\,h\,b^2}$$

or $N_{x_{crit}} = -\frac{KD}{b^2}$ where $K = \frac{C'}{C''}$

The numerical calculations of equations 2.03a and 2.04a were performed on a DEUCE computer.

Plotted results of $N_{x_{crit}}$ for various cases are given

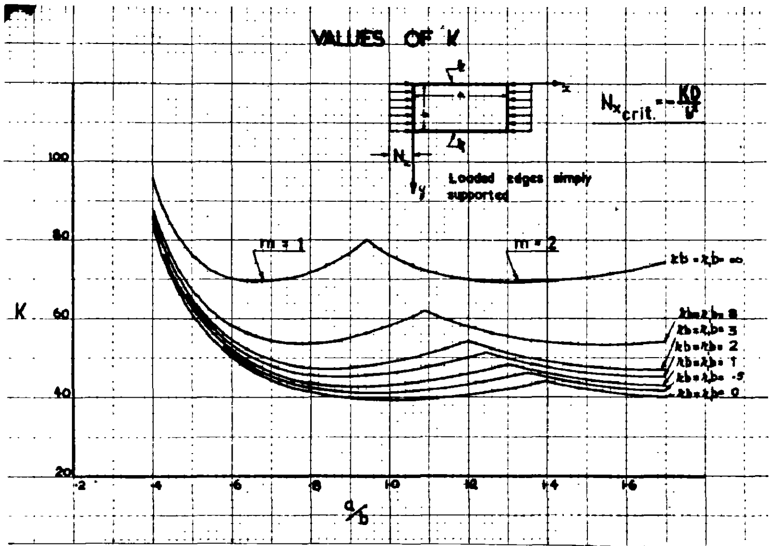

Fig.(18)

Fig.(19)

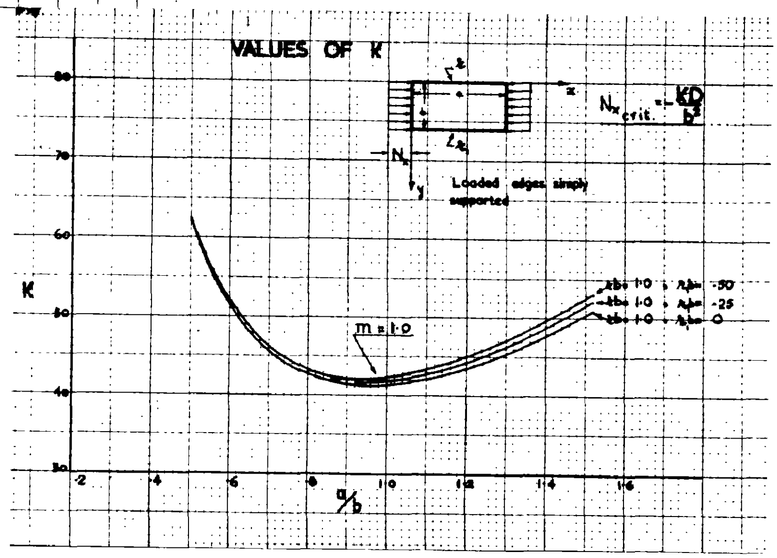

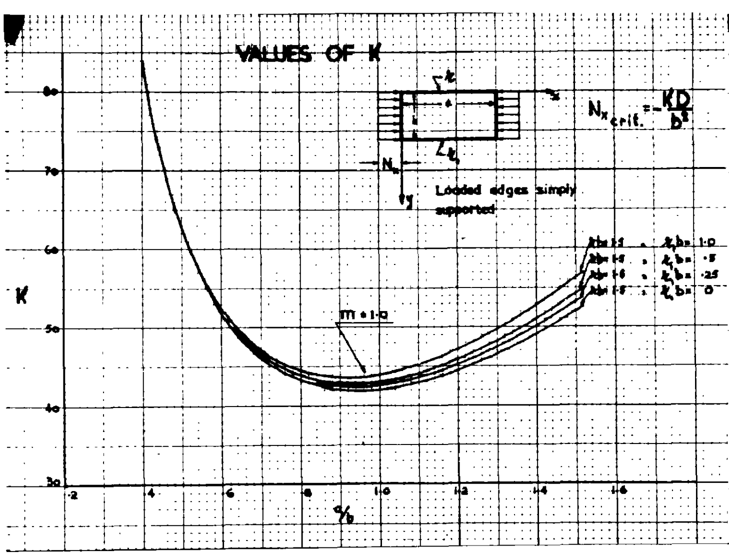

Fig.(20)

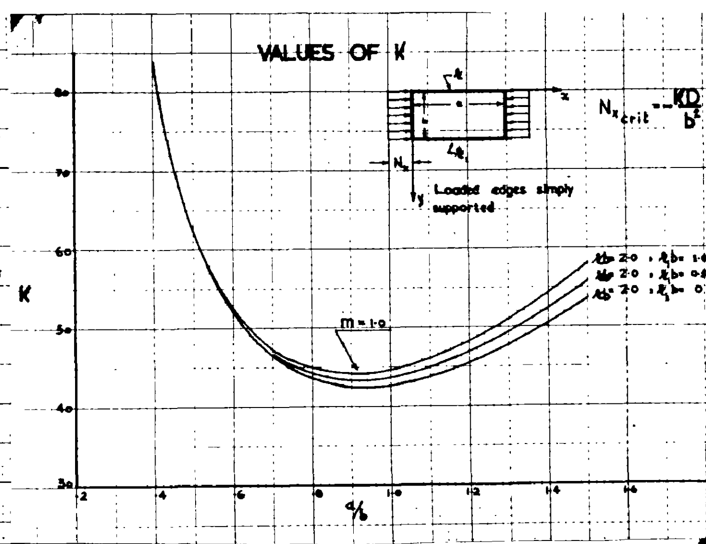

Fig.(21)

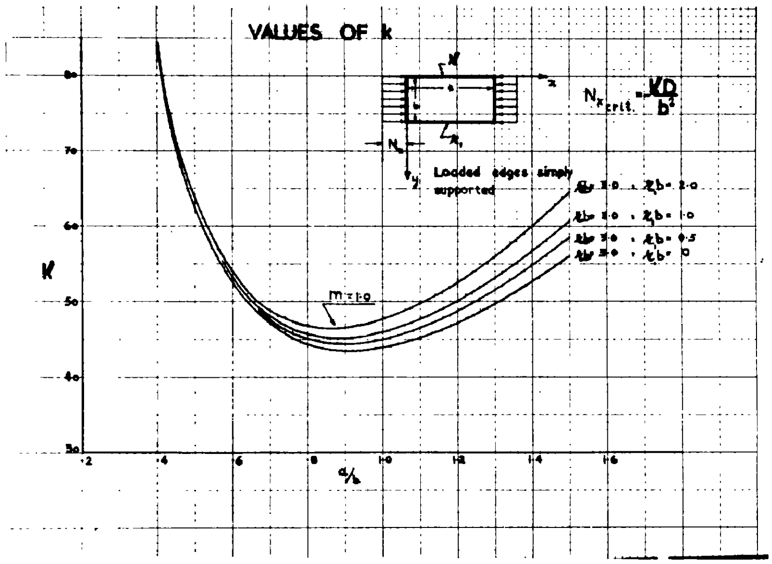

Fig.(22)

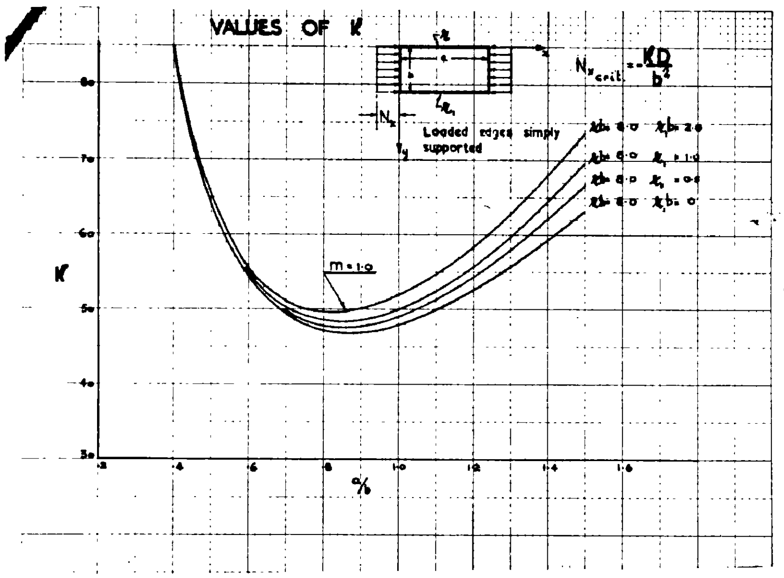

Fig. (23)

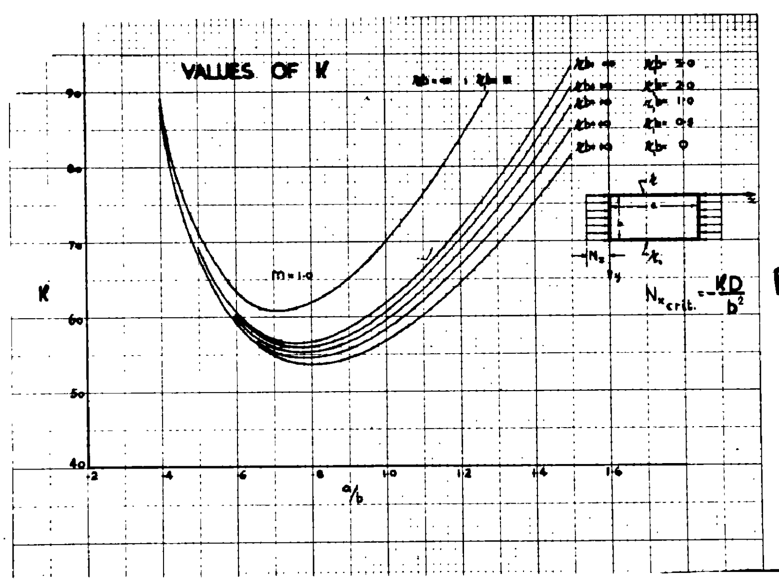

Fig.(24)

in Fig.(18) to (24) inclusive. Additional curves for m = 2, 3, etc. may be obtained by keeping the K ordinate the same but multiplying the corresponding a/b ordinate by the value of m . This construction is indicated in Fig.(18).

Values of K calculated for a simply supported plate by Galerkin's method and the corresponding values given by Timoshenko [1] using the classical equation method are given Table 1. In Tables 2 and 3 values of K for two other cases are compared with those obtained by J.M. Harvey [18, 19].

To observe the effect of the choice of deflection form on the critical stress, Galerkin's equations 2.01a 2.02a were solved by selecting different deflection forms for two of the cases. Results of critical stresses for a simply supported square plate and a built-in rectangular plate are given in Appendix III. It is seen that good agreement is obtained. It is permissible to conclude, therefore, that the accuracy of Galerkin's method is very largely independent of the form assumed, provided the boundary conditions are satisfied.

<u>Table 1</u> Comparison of Values of 'K' for Uniformly Compressed Simply Supported Rectangular Plate $\kappa b = \kappa_1 b = 0$.

a/b	0.4	0.5	0.6	0.7	0.8	0.9	1.0
$K^{\ddagger}$	83.009	61.692	50.717	44.728	41.490	39.934	39.407
K^{*}	83.003	61.685	50.729	44.709	41.709	38.873	39.478

<u>Table 2</u> Comparison of Values of 'K' for Uniformly Compressed Rectangular Plate Simply Supported Along One Unloaded Edge And Elastically Fixed Along the Other $\kappa b = 1.0, \kappa_1 b = 0.$

a/b	0.6	0.8	0.9	1.0	1.1	1.3
$K^{\ddagger}$	51.386	42.655	41.399	41.298	42.033	45.309
$K^{\square}$	51.864	42.814	41.360	41.086	41.516	45.446

<u>Table 3</u> Comparison of Values of 'K' for Uniformly Compressed Built-in - Simply Supported Rectangular Plate $\kappa b = \infty, \kappa_1 b = 0.$

a/b	0.6	0.7	0.8	0.9	1.0	1.1
$K^{\ddagger}$	58.875	54.747	53.656	54.534	56.817	60.186
$K^{=}$	59.800	55.165	53.333	54.304	56.742	60.350

‡ Values dreived by Author.

* Values given by Timoshenko.

= Values given by Harvey.

Case (b) Flat Rectangular Plate Uniformly Compressed Along Two Opposite Simply Supported Edges Elastically Fixed Along One And Free Along the Other:

The stress function and the deflection form, in this case, are given by equations 1.41b and 1.42b respectively. Substituting these expressions for F and w in Galerkin's equations 2.01a and 2.02a, and integrating gives:

$$\frac{\beta}{b^2}\left[\frac{128\,b^3}{1575\,a^3}+\frac{128\,b}{11025\,a}+\frac{8\,a}{1575\,b}\right]+E\alpha^2\frac{b}{a}\left(\frac{3}{4m^2\pi^2}-\frac{m^2\pi^2}{60}\right)$$

$$\left[-\frac{8A_2^2}{11}-\frac{6A_2B_2}{5}+\frac{1}{9}\left(16A_2^2-\frac{4A_2\varepsilon b}{(\varepsilon b+2)}-\frac{9B_2^2}{2}\right)+\frac{1}{8}\left(24A_2B_2-\right.\right.$$

$$- \frac{4A_2}{(\kappa b+2)} - \frac{3B_2 \kappa b}{(\kappa b+2)} \Bigg) + \frac{1}{7}\left(\frac{8A_2 \kappa b}{(\kappa b+2)} + 9B_2^2 - \frac{3B_2}{(\kappa b+2)}\right.$$

$$\left. - \frac{\kappa^2 b^2}{2(\kappa b+2)^2} - 8A_2^2\right) + \frac{1}{6}\left(\frac{8A_2}{(\kappa b+2)} + \frac{6B_2 \kappa b}{(\kappa b+2)} - \frac{\kappa b}{(\kappa b+2)^2} - \right.$$

$$\left. 12A_2B_2\right) + \frac{1}{5}\left(\frac{6B_2}{(\kappa b+2)} + \frac{\kappa^2 b^2}{(\kappa b+2)^2} - \frac{1}{2(\kappa b+2)^2} - \frac{4A_2 \kappa b}{(\kappa b+2)}\right.$$

$$\left. - \frac{9B_2^2}{2}\right) + \frac{1}{4}\left(\frac{2\kappa b}{(\kappa b+2)^2} - \frac{4A_2}{(\kappa b+2)} - \frac{3B_2 \kappa b}{(\kappa b+2)}\right) + \frac{1}{3}$$

$$\left(\frac{1}{(\kappa b+2)^2} - \frac{3B_2}{(\kappa b+2)} - \frac{\kappa^2 b^2}{2(\kappa b+2)^2}\right) - \frac{\kappa b}{2(\kappa b+2)^2} - \frac{1}{2(\kappa b+2)^2}\Bigg]$$

$$-E\alpha^2 \frac{b}{a}\left(\frac{3}{4m^2\pi^2} + \frac{m^2\pi^2}{60}\right)\Bigg[-\frac{6A_2^2}{11} - \frac{9A_2B_2}{10} + \frac{1}{9}\Bigg(12A_2^2$$

$$\left. - \frac{7A_2 \kappa b}{2(\kappa b+2)} - 3B_2^2\right) + \frac{1}{8}\left(18A_2B_2 - \frac{6A_2}{(\kappa b+2)} - \frac{2B_2 \kappa b}{(\kappa b+2)}\right)$$

$$+ \frac{1}{7}\left(\frac{7A_2 \kappa b}{(\kappa b+2)} + 6B_2^2 - \frac{3B_2}{(\kappa b+2)} - \frac{\kappa^2 b^2}{4(\kappa b+2)^2} - 6A_2^2\right)$$

$$+ \frac{1}{6}\left(\frac{12A_2}{(\kappa b+2)} + \frac{4B_2 \kappa b}{(\kappa b+2)} - \frac{\kappa b}{2(\kappa b+2)^2} - 9A_2B_2\right) + \frac{1}{5}$$

$$\left(\frac{6B_2}{(\kappa b+2)} + \frac{\kappa^2 b^2}{2(\kappa b+2)^2} - \frac{7A_2 \kappa b}{2(\kappa b+2)} - 3B_2^2\right) + \frac{1}{4}\left(\frac{\kappa b}{(\kappa b+2)^2}\right.$$

$$-\frac{6A_2}{(\kappa b+2)} - \frac{2B_2\kappa b}{(\kappa b+2)}\Bigg) - \frac{1}{3}\left(\frac{3B_2}{(\kappa b+2)} + \frac{\kappa^2 b^2}{4(\kappa b+2)^2}\right) -$$

$$\frac{\kappa b}{4(\kappa b+2)^2}\Bigg] = 0. \qquad\qquad 2.01b$$

and

$$\alpha\left(\frac{m^4\pi^4 b^3}{2a^3} + \frac{m^2\pi^2 b N_x b^2}{2aD}\right)\left[\frac{A_2^2}{9} + \frac{B_2^2}{7} + \frac{\kappa^2 b^2}{20(\kappa b+2)^2} +\right.$$

$$\frac{1}{3(\kappa b+2)^2} + \frac{12A_2B_2}{8} + \frac{A_2\kappa b}{7(\kappa b+2)} + \frac{A_2}{3(\kappa b+2)} + \frac{B\kappa b}{6(\kappa b+2)} +$$

$$\left.\frac{2B_2}{5(\kappa b+2)} + \frac{\kappa b}{4(\kappa b+2)}\right] - \alpha\frac{m^2\pi^2 b}{a}\left[\frac{12A_2^2}{7} + 3A_2B_2 +\right.$$

$$+\frac{7A_2\kappa b}{5(\kappa b+2)} + \frac{3A_2}{(\kappa b+2)} + \frac{6B_2^2}{5} + \frac{B_2\kappa b}{(\kappa b+2)} + \frac{2B_2}{(\kappa b+2)} +$$

$$\left.\frac{\kappa^2 b^2}{6(\kappa b+2)^2} + \frac{\kappa b}{2(\kappa b+2)^2}\right] + \frac{12\alpha a}{b}\left[\frac{A_2^2}{5} + \frac{A_2B_2}{4} + \frac{A_2\kappa b}{6(\kappa b+2)}\right.$$

$$\left.+\frac{A_2}{2(\kappa b+2)}\right] + \alpha\beta\,\frac{hb}{Da}\left(\frac{m^2\pi^2}{60} + \frac{3}{4m^2\pi^2}\right)\left[A_2^2\left(\frac{2}{9} - \frac{6}{11}\right) +\right.$$

$$\left(B_2^2 + \frac{\kappa A_2 b}{(\kappa b+2)}\right)\left(\frac{2}{7} - \frac{6}{9}\right) + \left(\frac{\kappa^2 b^2}{4(\kappa b+2)^2} + \frac{2B_2}{(\kappa b+2)}\right)\left(\frac{2}{5} - \frac{6}{7}\right)$$

$$+\frac{1}{(\kappa b+2)^2}\left(\frac{2}{3} - \frac{6}{5}\right) + 2A_2B_2\left(\frac{2}{8} - \frac{6}{10}\right) + \left(\frac{2A_2}{(\kappa b+2)} + \frac{\kappa b B_2}{(\kappa b+2)}\right)$$

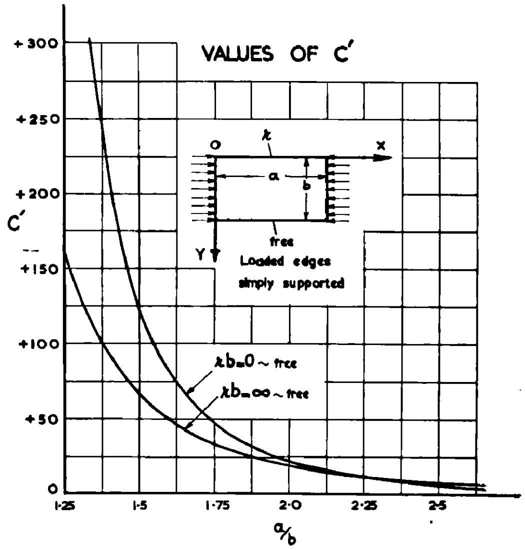

Fig.(25)

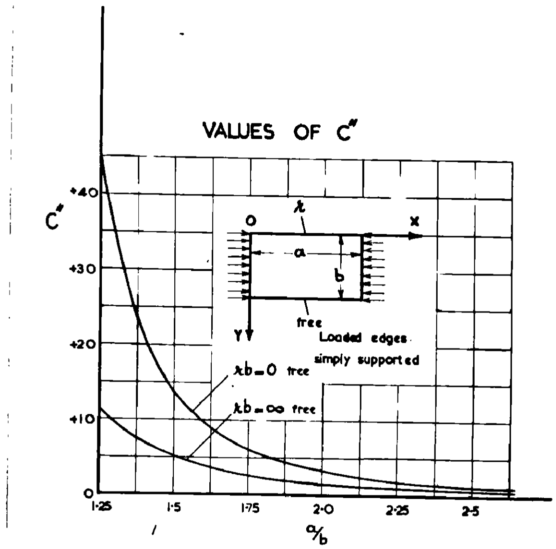

Fig.(26)

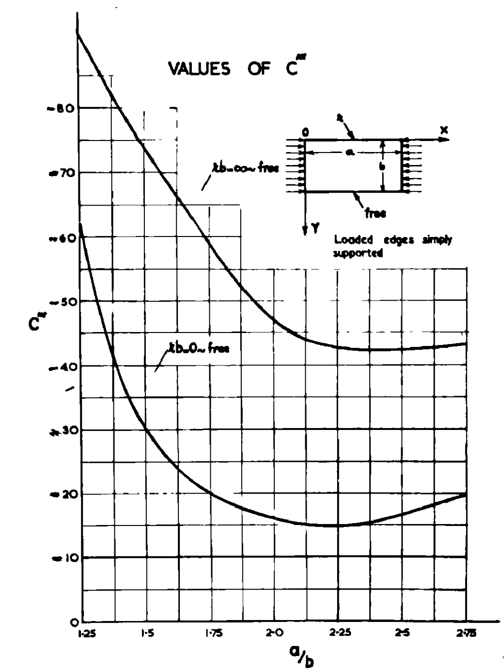

Fig.(27)

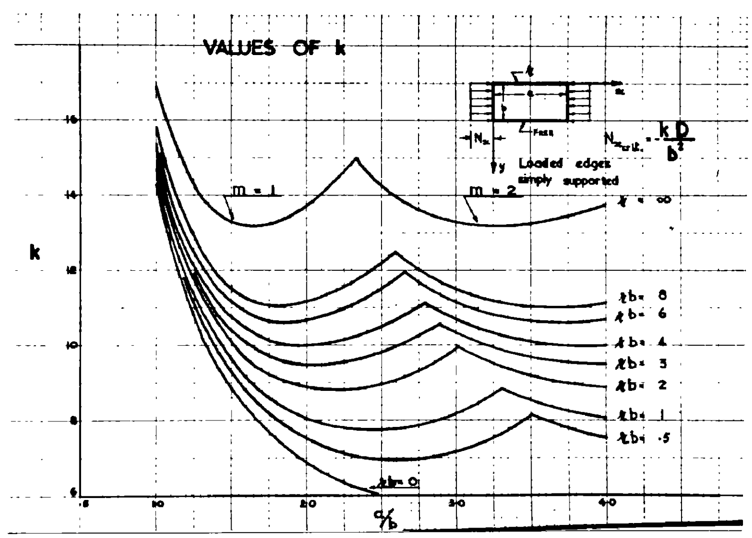

Fig.(28)

$$\left(\frac{2}{6}-\frac{6}{8}\right)+\frac{kb}{(kb+2)^2}\left(\frac{2}{4}-\frac{6}{6}\right)\Bigg]+\alpha\beta\frac{3hb}{m^2\pi^2Da}\Bigg[12A_2^2\left(\frac{1}{9}-\frac{1}{22}\right.$$

$$\left.-\frac{1}{14}\right)+18A_2B_2\left(\frac{1}{8}-\frac{1}{20}-\frac{1}{12}\right)+\left(\frac{7A_2kb}{(kb+2)}+6B_2^2\right)\left(\frac{1}{7}-\frac{1}{18}-\frac{1}{10}\right)$$

$$+\left(\frac{12A_2}{(kb+2)}+\frac{4B_2kb}{(kb+2)}\right)\left(\frac{1}{6}-\frac{1}{16}-\frac{1}{8}\right)+\left(\frac{6B_2}{(kb+2)}+\frac{k^2b^2}{2(kb+2)^2}\right)\left(\frac{1}{5}-\frac{1}{14}-\frac{1}{6}\right)$$

$$+\frac{kb}{(kb+2)^2}\left(\frac{1}{4}-\frac{1}{12}-\frac{1}{4}\right)\Bigg]+\alpha\beta\frac{3hb}{m^2\pi^2Da}\Bigg[4A_2^2\left(\frac{2}{9}-\frac{2}{11}\right)+7A_2B_2\left(\frac{2}{8}-\frac{2}{10}\right)$$

$$+\left(\frac{3A_2kb}{(kb+2)}+3B_2^2\right)\left(\frac{2}{7}-\frac{2}{9}\right)+\left(\frac{5A_2}{(kb+2)}+\frac{5B_2kb}{2(kb+2)}\right)\left(\frac{2}{6}-\frac{2}{8}\right)+\Bigg($$

$$\left(\frac{4B_2}{(kb+2)}+\frac{k^2b^2}{2(kb+2)^2}\right)\left(\frac{2}{5}-\frac{2}{7}\right)+\frac{3kb}{2(kb+2)^2}\left(\frac{2}{4}-\frac{2}{6}\right)+\frac{1}{(kb+2)^2}\left(\frac{2}{3}-\frac{2}{5}\right)\Bigg]=0 \qquad 2.02b$$

In this case also the values of β and α obtained by solving equations 2.01b and 2.02b, are of the forms 2.05a and 2.06a respectively. Plotted values of C', C'' and C''' for two limiting cases are given in Fig. (25, 26) and (27) respectively.

As before $\beta = 0$ gives the critical conditions and $N_{x_{crit}} = \frac{-KD}{b^2}$ where the value of K depends upon a/b, kb and m.

Plotted results of values of K for various values of a/b, kb and m are shown in Fig. (28).

Values of K for various cases, obtained by this method are compared in Tables 4, 5, 6 and 7 with the corresponding values given by Timoshenka [1].

Table 4 Comparison of Values of 'K' for a Uniformly

Compressed Simply Supported $(\kappa b = 0)$ ~ Free Plate.

a/b	1.0	2.0	2.5
$K^{\ddagger}$	14.515	6.944	6.057
K^{*}	14.222	6.889	6.020

Table 5. Comparison of Values of 'K' for a Uniformly Compressed Built-in $(\kappa b = \infty)$ and Free Plate.

a/b	1.0	1.5	2.0
$K^{\ddagger}$	16.910	13.285	13.747
K^{*}	16.679	13.230	13.620

Table 6. Comparison of Values of 'K' for a Uniformly Compressed Elastically Fixed $(\kappa b = 2\cdot0)$ and Free Plate.

a/b	1.0	1.5	2.0	2.5
$K^{\ddagger}$	15.000	10.040	8.896	8.976
K^{*}	14.710	9.968	8.883	8.883

Table 7. Comparison of Values of 'K' for a Uniformly Compressed Elastically Fixed $(\kappa b = 8\cdot0)$ and Free Plate.

a/b	1.0	1.5	2.0	2.5
$K^{\ddagger}$	15.756	11.4822	11.154	12.228
K^{*}	15.596	11.448	11.054	12.139

‡ Values derived by author

* Values given by Timoshenko

It is evident from the comparison of results that the method of analysis presented gives satisfactory results, as far as the critical stress is concerned. The maximum deviation shown by the figures compared is not more than 2%. Thus the approximate solutions obtained provide the required degree of accuracy.

The method as outlined has the further advantage that it is directly suitable for programming for the digital computer which permits the evaluation of a much greater variety of cases than would otherwise be feasible.

SECTION: 3

POST - CRITICAL CARRYING CAPACITY.

POST - CRITICAL CARRYING CAPACITY.

It is a well known feature of thin walled construction that longitudinally compressed thin plates have a considerable reservoir of post-elastic buckling strength associated with "large deflections." The maximum load of such plates can be many times the load at which elastic buckling occurs. To date only the relatively simple case of a simply supported and free edge plate has been treated theoretically [4]. Effective semi-empirical treatments exist [2, 5 - 9, 11, 12] which form the basis of design specifications in this country and abroad. Obviously, however, the need exists for a basic analytical treatment and such a treatment is presented in the following pages.

It should be noted that the post buckling collapse strength is intimately dependent on the stress-strain relations of the material. It is evident that if this relation is linear at all stress values, no maximum load as such is obtainable; increase in the load beyond the elastic critical load resulting only in increasing deformation. It is essential therefore, before embarking on a post-buckling analysis, to specify a basic stress-strain relationship for the material.

Essentially, the method presented, to assess the maximum strength of thin plate elements, consists of applying the stress-strain relationships postulated by the deformation theory of plasticity to plates analysed by means of the large deflection concept.

STRESS — STRAIN
CURVE

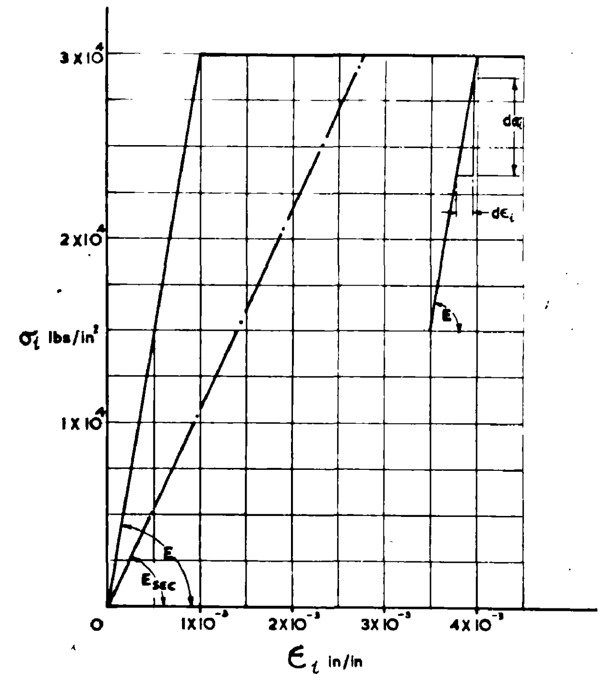

Fig. (29)

In the analysis the stress-strain curve for the material has been assumed to be a "flat top" type shown in Fig.(29). It is emphasised, however, that the method presented is not exclusively dependent on this. Any stress-strain curve derived experimentally may be incorporated in the computations, since the method presented is one of general application to any structural material.

3.0 DEFORMATION THEORY OF PLASTICITY.

The deformation theory of Plasticity as presented below, is restricted to initially isotropic materials with all time dependent effects (e.g. creep) ignored. It is also assumed that the material is incompressible so that Poisson's ratio $\nu = \frac{1}{2}$.

Beyond the critical buckling state, additional stresses are introduced into the stress system becuase of the deformations in the middle plane of the plate. These additional stresses together with the original stress that caused buckling combine to form a "stress intensity" σ_i. For a plane stress the stress intensity is given by [20]:

$$\sigma_i = \sqrt{\sigma_x^2 + \sigma_y^2 - \sigma_x\sigma_y + 3\tau_{xy}^2} \qquad 3.01$$

and the strain intensity by:

$$\epsilon_i = \frac{2}{\sqrt{3}}\sqrt{\epsilon_x^2 + \epsilon_y^2 + \epsilon_x\epsilon_y + \gamma_{xy}^2/4} \qquad 3.02$$

According to the fundamental hypothesis of the deformation theory of plasticity, the stress intensity σ_i is a single valued function of the intensity of strain ϵ_i for the loading condition, i.e.

$$\sigma_i = E_{sec}\epsilon_i \qquad 3.03$$

where E_{sec} is the secant modulus of the material, the value of which depends upon the state of stress.

For unloading condition, however, the relation between σ_i and ϵ_i becomes linear, viz.

$$d\sigma_i = E\, d\epsilon_i \qquad 3.04$$

The stress-strain relations compatible with equations 3.01 and 3.02 are:-

$$\left.\begin{aligned} \epsilon_x &= \frac{\sigma_x + \frac{1}{2}\sigma_y}{E_{sec}} \\ \epsilon_y &= \frac{\sigma_y - \frac{1}{2}\sigma_x}{E_{sec}} \\ \gamma_{xy} &= \frac{3\tau_{xy}}{E_{sec}} \end{aligned}\right] \qquad 3.05$$

The use of this deformation theory of plasticity in the cases attempted is fully justified because "proportional loading" type of stress history, i.e. the one in which the components of stress increase in constant ratio to each other is considered. It is of interest to note that deformation theories of plasticity may be used for a range of loading paths other then the proportional loading without violation of the requirements of the physical soundness of the theory [21].

3.1 EVALUATION OF MAXIMUM LOAD:

The maximum compressive load, for a plate, applied in its plane is computed from the dimensions of the plate, strain distributions across the width of the plate and the stress-strain curve for the material.

It is assumed in the determination of the maximum load that the form of the strain distributions remains unchanged even after yielding has commenced.

The method of evaluation, in general, is outlined below.

The strain intensity ϵ_i at various points across the plate is determined from the strain distributions of the large deflection plate theory by means of equation 3.02. Values of E_{sec} at these points are then read off the $\sigma_i \sim \epsilon_i$ stress-strain curve. For increasing strain intensity the stress at any point across the plate is then obtained from relations 3.05. At the points where strain intensity is decreasing (unloading condition), the elastic modulus E is used to compute the reduction in stress. The average stress $\sigma_{x\,av.}$ is computed from the stress distribution thus obtained. This procedure is repeated for various deformations till the maximum value of is found.

3.2. STRAIN DISTRIBUTIONS.

In accordance with the assumptions made:

$$\left.\begin{aligned} \epsilon_x &= \frac{1}{E_{sec}}\left[\frac{\partial^2 F}{\partial y^2} - \frac{1}{2}\frac{\partial^2 F}{\partial x^2}\right] \\ \epsilon_y &= \frac{1}{E_{sec}}\left[\frac{\partial^2 F}{\partial x^2} - \frac{1}{2}\frac{\partial^2 F}{\partial y^2}\right] \end{aligned}\right\} \qquad 3.21$$

$$\gamma_{xy} = \frac{-3}{E_{sec}} \frac{\partial^2 F}{\partial x \partial y}$$

As shown in the previous sections the general form of the stress function F, for any plate, can be written as:

$$F = \frac{N_x y^2}{2h} + \beta \left[Y \right] \left[X \right] \qquad 3.22$$

where Y and X are, respectively, functions of y and x only, and β is a constant determined by Galerkin's Method.

Substitution from 3.22 in 3.21 gives:

$$\left.\begin{aligned}
\epsilon_x &= \frac{N_x}{E_{sec} h} + \frac{\beta}{E_{sec}} \left[X \frac{d^2 Y}{d y^2} - \frac{Y}{2} \frac{d^2 X}{d x^2} \right] \\
\epsilon_y &= \frac{-N_x}{2 E_{sec} h} + \frac{\beta}{E_{sec}} \left[Y \frac{d^2 X}{d x^2} - \frac{X}{2} \frac{d^2 Y}{d y^2} \right] \\
\gamma_{xy} &= \frac{-3\beta}{E_{sec}} \left[\frac{dX}{dx} \cdot \frac{dY}{dy} \right]
\end{aligned}\right] \qquad 3.23$$

It is seen that the values of various strains, E_{sec} and N_x are inter-dependent. To simplify the relations 3.23 a factor n is introduced such that

$$\frac{N_x}{E_{sec}} = n \frac{N_{x\,crit}}{E} \qquad 3.24$$

and it is assumed that (i) $N_{x\,crit.}$ is restricted to lie within the elastic limit, and (ii) the plate stiffness D' varies with E_{sec} in the post-critical region.

It has been shown in Section 2 that β as obtained from Galerkin's Method, is of the form:

$$\beta = C' \frac{a^4 D}{b^4 h} + C'' \frac{a^4 N_x}{b^2 h} \qquad \text{———} \quad 3.25$$

and $N_{x_{crit}} = \dfrac{-C' D}{C'' b^2}$

now $\dfrac{N_{x_{crit}}}{E} = \dfrac{-C' h^3}{12 C'' b^2 (1 - \nu_e^2)}$

therefore $$\frac{N_x}{E_{sec} h} = -n \frac{C' h^2}{12 C'' b^2 (1 - \nu_e^2)} \qquad \text{———} \quad 3.26$$

where ν_e is the elastic Poisson's ratio.

Again $\dfrac{\beta}{E_{sec}} = \left(\dfrac{C' D'}{E_{sec} h} + \dfrac{C'' N_x b^2}{E_{sec} h} \right) \dfrac{a^4}{b^4}$

where $D' = \dfrac{E_{sec} h^3}{12 (1 - \nu_e^2)}$

Substitution from 3.26 gives:

$$\frac{\beta}{E_{sec}} = \frac{C' h^2 a^4}{12 b^4 (1 - \nu_e^2)} (1 - n) \qquad \text{———} \quad 3.27$$

Substitution from 3.26 and 3.27 into 3.23 yields

$$\epsilon_x = \frac{-C' h^2}{12 C'' (1 - \nu_e^2) b^2} n - \frac{C' h^2 a^4}{12 (1 - \nu_e^2) b^4} (n-1) \left[X \frac{d^2 Y}{dy^2} - \frac{Y}{2} \frac{d^2 X}{dx^2} \right]$$

$$\epsilon_y = \frac{+C' h^2}{24 C'' (1 - \nu_e^2) b^2} n - \frac{C' h^2 a^4}{12 (1 - \nu_e^2) b^4} (n-1) \left[Y \frac{d^2 X}{dx^2} - \frac{X}{2} \frac{d^2 Y}{dy^2} \right]$$

$$\gamma_{xy} = \frac{+3 C' h^2 a^4}{12 (1 - \nu_e^2) b^4} (n-1) \left[\frac{dX}{dx} \cdot \frac{dY}{dy} \right]$$

$$\text{———————}\quad 3.28$$

From equations 3.28, the various distributions, across any section of a given plate, corresponding to any specified value of n may be evaluated.

It follows that the strain intensity

$$\epsilon_i = \frac{2}{\sqrt{3}} \sqrt{\epsilon_x^2 + \epsilon_y^2 + \epsilon_x \epsilon_y + \gamma_{xy}^2/4}$$

is completely determined as soon as a value of the factor $n(\geqslant 1)$ is selected.

3.3 EVALUATION OF DEFLECTION:

The maximum load is associated with large finite deflections and in the following the method of evaluation of deflections is outlined.

As shown in Sections 1 and 2 the general form of deflection w can be written as:

$$w = \alpha . \sin \frac{m\pi x}{a} . f(y) \qquad \text{———} \quad 3.31$$

where $f(y)$ is a function of y only, and α is a constant determined by Galerkin's Method.

α as given by Galerkin's Method is of the form 2.06a viz:

$$\alpha = \sqrt{\frac{C'''\beta}{E\, b^2}} \qquad \text{———} \quad 3.32$$

Since the maximum load occurs when the plate has partially yielded, the deflection at this load is assessed on the basis similar to the strain computations. Thus in accordance with the laws of plasticity and elasticity 3.32 can be written as:

$$\alpha = \sqrt{\frac{C'''\beta}{E_{sec}\, b^2}} \qquad \text{———————} \quad 3.33$$

Now from 3.27

$$\frac{\beta}{E_{sec}} = \frac{C' h^2 a^4}{12(1-\nu_e^2)\, b^4}(1-n)$$

$$\therefore\ \alpha = \frac{h}{b}\sqrt{\frac{C'''C' a^4(1-n)}{12(1-\nu_e^2)\, b^4}} \qquad \text{———————} \quad 3.34$$

Substituting from 3.34 into 3.31 gives:

$$w = \frac{h}{b}\sqrt{\frac{C''' C' a^4 (1-n)}{12(1-\nu_e^2)\, b^4}}\ f(y)\ \sin\frac{m\pi x}{a}$$

from which the deflection at any point of a given plate may be computed for any specific value of n corresponding to any load.

3.4 ILLUSTRATIVE NUMERICAL ANALYSIS:

(a) Maximum Load:

In the actual computations the values of ϵ_x, ϵ_y and γ_{xy} were found from equations 3.28 for a particular value of n at eleven equally spaced points across the central section of a given plate. As an example, a square plate $(a/b = 1{\cdot}0)$ simply supported along all four sides and uniformly compressed in the x- direction will now be considered. The general form of the stress function F for plates supported along all sides as given by 1.41a, is:

$$F = \frac{N_x y^2}{2h} + \beta\left(\frac{x^2}{a^2} - \frac{x}{a}\right)^2\left(-\frac{\gamma y^5}{b^5} + \frac{S y^4}{b^4} + \frac{T y^3}{b^3} + \frac{2y^2}{b^2}\right)$$

where:

$$\mathcal{K} = \sin\left(\frac{\lambda - 1}{\lambda + 1}\right)\frac{\pi}{2}$$

$$\lambda = \left(\frac{\kappa b + 1}{\kappa_1 b + 1}\right)$$

$$S = \left(2 + 2\mathcal{K}\right)$$

$$T = \left(-\mathcal{K} - 4\right)$$

Since, in this case, $\kappa b = \kappa_1 b = 0$ therefore $\lambda = 1$ and $\mathcal{K}$ becomes zero, giving $S = 2$ and $T = -4$.

Thus the stress function becomes:

$$F = \frac{N_x y^2}{2h} + \beta\left(\frac{x^4}{a^4} - \frac{2x^3}{a^3} + \frac{x^2}{a^2}\right)\left(\frac{2y^4}{b^4} - \frac{4y^3}{b^3} + \frac{2y^2}{b^2}\right) \quad \text{—3.41a}$$

Comparing 3.41a and 3.22 and substituting in 3.28 gives:

$$\epsilon_x = \frac{-c'h^2 n}{12(1-\nu_e^2)C'' b^2} - \frac{c'h^2(n-1)}{12(1-\nu_e^2)\,b^2}\left[\frac{a^4}{b^4}\left(\frac{x^2}{a^2} - \frac{x}{a}\right)^2\left(\frac{24y^2}{b^2} - \frac{24y}{b} + 4\right) - \frac{a^2}{b^2}\left(\frac{12x^2}{a^2} - \frac{12x}{a} + 2\right)\left(\frac{y^4}{b^4} - \frac{2y^3}{b^3} + \frac{y^2}{b^2}\right)\right]$$

$$\epsilon_y = \frac{+c'h^2 n}{24(1-\nu_e^2)C'' b^2} - \frac{c'h^2(n-1)}{12(1-\nu_e^2)\,b^2}\left[\left(\frac{12x^2}{a^2} - \frac{12x}{a} + 2\right)\frac{a^2}{b^2}\left(\frac{2y^4}{b^4}\right.\right.$$

$$-\frac{4y^3}{b^3}+\frac{2y^2}{b^2}\Big)-\frac{a^4}{b^4}\left(\frac{x^2}{a^2}-\frac{x}{a}\right)^2\left(\frac{12y^2}{b^2}-\frac{12y}{b}+2\right)\Bigg]$$

$$\gamma_{xy}=\frac{3C'h^2(n-1)}{12(1-\nu_e^2)\,b^2}\left[\left(\frac{4x^3}{a^3}-\frac{6x^2}{a^2}+\frac{2x}{a}\right)\left(\frac{8y^3}{b^3}-\frac{12y^2}{b^2}+\frac{4y}{b}\right)\frac{a^3}{b^3}\right]$$

For a square plate $a/b = 1{\cdot}0$, $C' = 492{\cdot}4902$, $C'' = 12{\cdot}469$ and taking $b/h = 80$ and $\nu_e = \frac{1}{4}$, the strain expressions at the central section $x/a = \frac{1}{2}$ become:

$$\epsilon_x = -0{\cdot}0005483n - 0{\cdot}0068401(n-1)\left[\left(\frac{3y^2}{2b^2}-\frac{3y}{2b}+\frac{1}{4}+\frac{y^4}{b^4}-\frac{2y^3}{b^3}+\frac{y^2}{b^2}\right)\right] \qquad 3.42a$$

$$\epsilon_y = 0{\cdot}00027465n + 0{\cdot}0068401(n-1)\left[\left(\frac{2y^4}{b^4}-\frac{4y^3}{b^3}+\frac{2y^2}{b^2}+\frac{3y^2}{4b^2}-\frac{3y}{4b}+2\right)\right] \qquad 3.43a$$

$$\gamma_{xy} = 0 \qquad 3.44a$$

Considering a point such that $\frac{y}{b} = \frac{1}{10}$ and taking $n = 1{\cdot}5$ gives:

$$\epsilon_x = -0{\cdot}00124386 \quad , \quad \epsilon_y = +0{\cdot}000663485$$

and therefore $\epsilon_i = \frac{2}{\sqrt{3}}\sqrt{\epsilon_x^2+\epsilon_y^2+\epsilon_x\epsilon_y}$ becomes $= -0{\cdot}001244787$ and $\frac{d\epsilon_i}{dn}$ a –ve. quantity: specifying a loading condition because ϵ_i is compressive if negative. The value of E_{sec} can now be determined from the given stress-strain curve of the material. In this analysis this has been assumed to be a "flat top" type (Fig.(29)) with a yield stress of 30×10^3 lbs/in^2 , the corresponding yield strain and the elastic modulus being $0{\cdot}001$ inch/inch and 30×10^6 lbs/in^2 respectively.

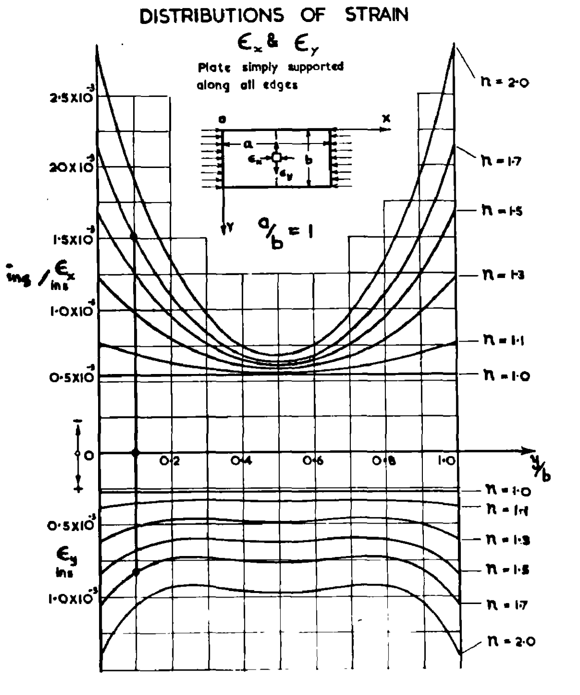

Fig.(30)

Fig.(31)

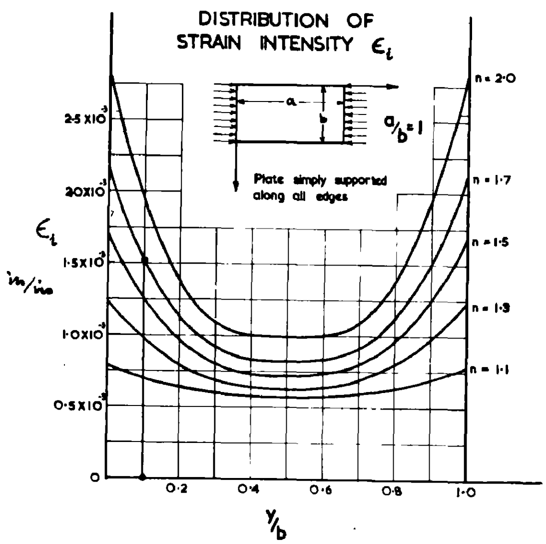

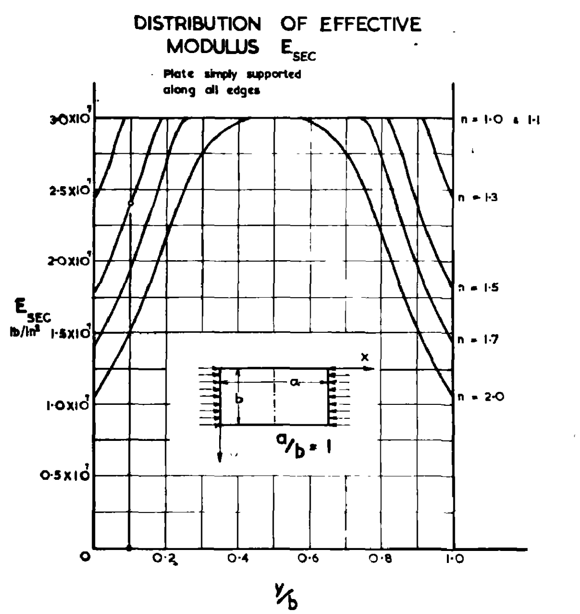

Fig.(32)

It is emphasised, however, that the method presented is not exclusively dependent on this and any stress-strain relation postulated may be incorporated in the numerical calculations.

Now, from Fig.(29) σ_i corresponding to $\epsilon_i = -0.001244787$ is -30×10^3 lbs/in^2.

$$\therefore\ E_{sec} = \frac{-30\times10^3}{-1.244787\times10^{-3}} = 2.41005\times10^7 \text{ lbs/in}^2$$

The stress σ_x at any point is given by

$$\sigma_x = \frac{4}{3}E_{sec}\left(\epsilon_x + \frac{1}{2}\epsilon_y\right)$$

$$\therefore\ \sigma_x = \frac{4}{3}\times 2.41005\times10^7\times 9.1212\times10^{-4} = 2.931\times10^4 \text{ lbs/in}^2$$

For points where $\frac{d\epsilon_i}{dn}$ is positive (unloading condition) the value of the elastic modulus E is used to calculate the corresponding stress reduction.

Similar calculations are performed for each of the eleven points and the distributions of stress σ_x are plotted from which the average stress $\sigma_{x\,av.}$ determined.

The above procedure is repeated for different values of n and curves of $\sigma_{x\,av}$ against n are obtained. The maximum value of $\sigma_{x\,av}$ is then read off these curves.

To illustrate the procedure a sample sequence of plotted results for a simply supported square plate is now presented.

Fig.(30) shows the curves of ϵ_x and ϵ_y for various values of n, across the central section of the plate. Fig.(31) and (32) give the corresponding distributions of the strain intensity ϵ_i and the effective modulus E_{sec} respectively.

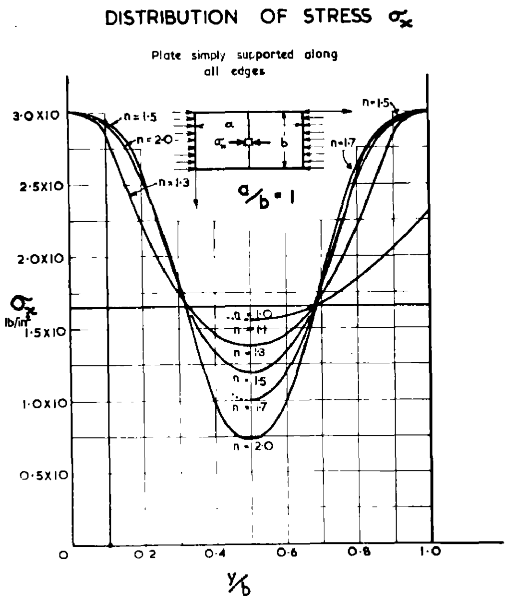

Fig. (33)

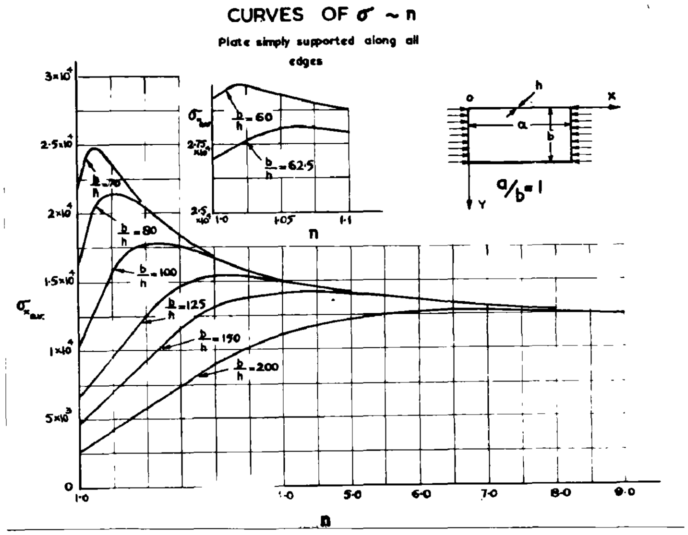

Fig. (34)

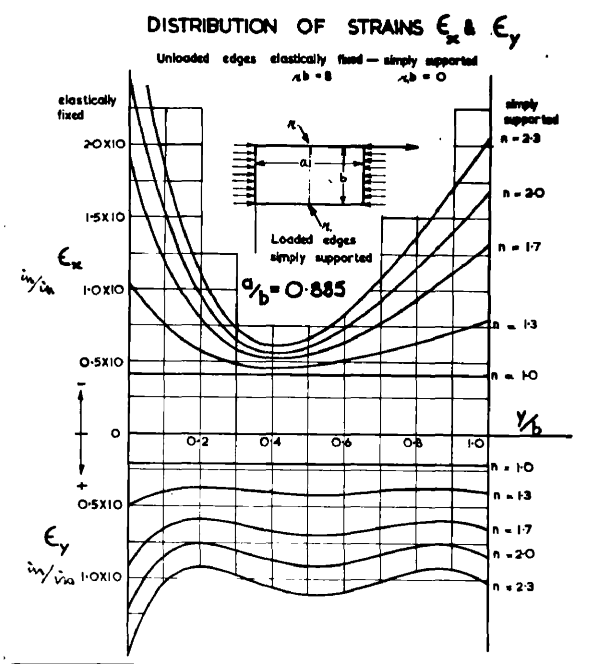

Fig. (36)

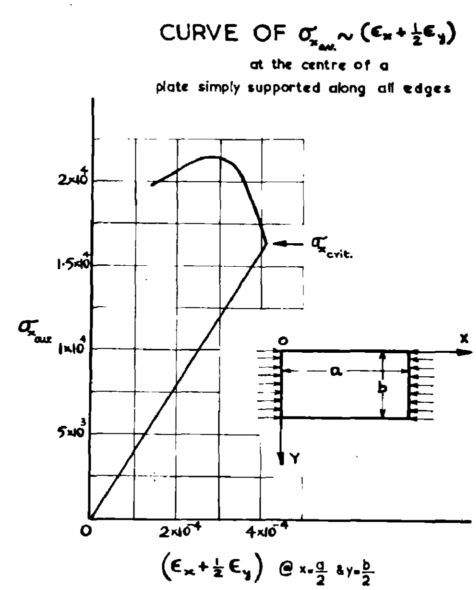

Fig. (35)

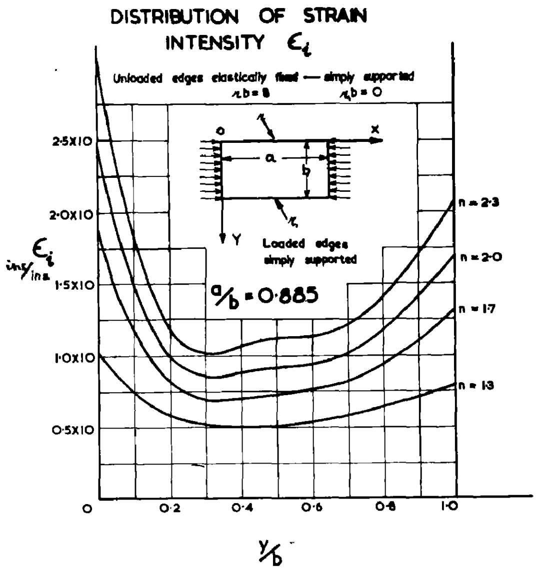

Fig.(37)

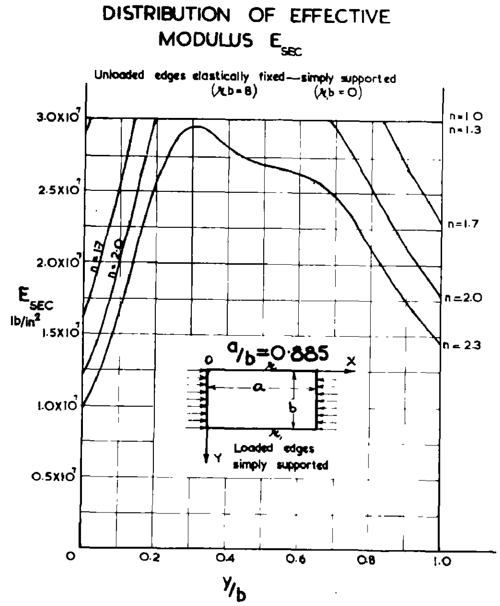

Fig.(38)

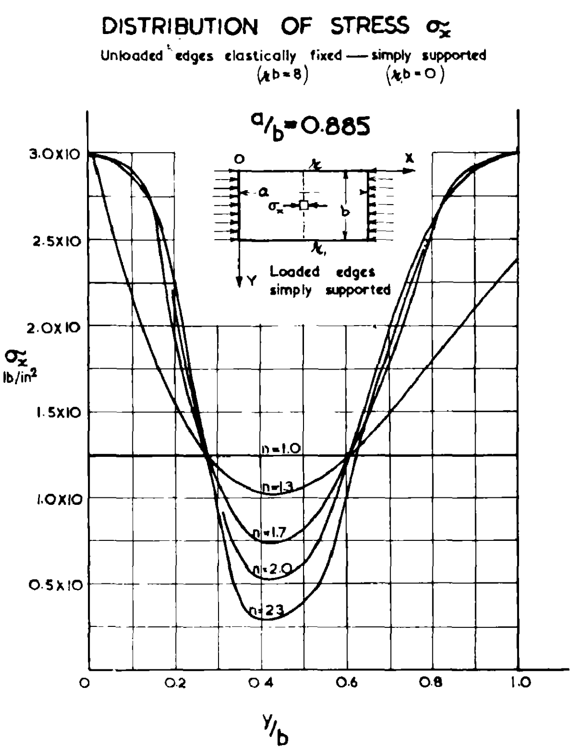

Fig.(39)

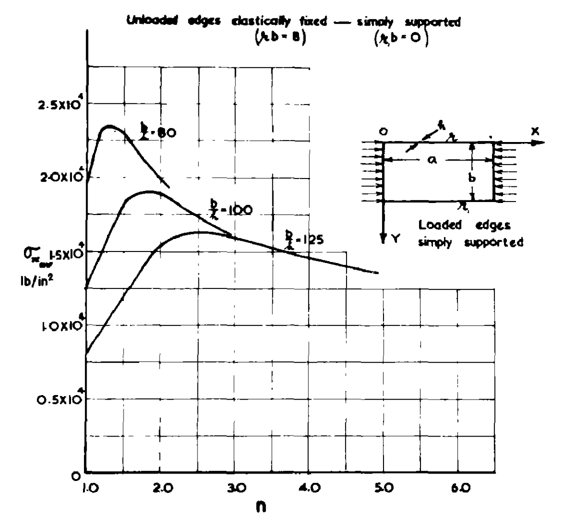

Fig.(40)

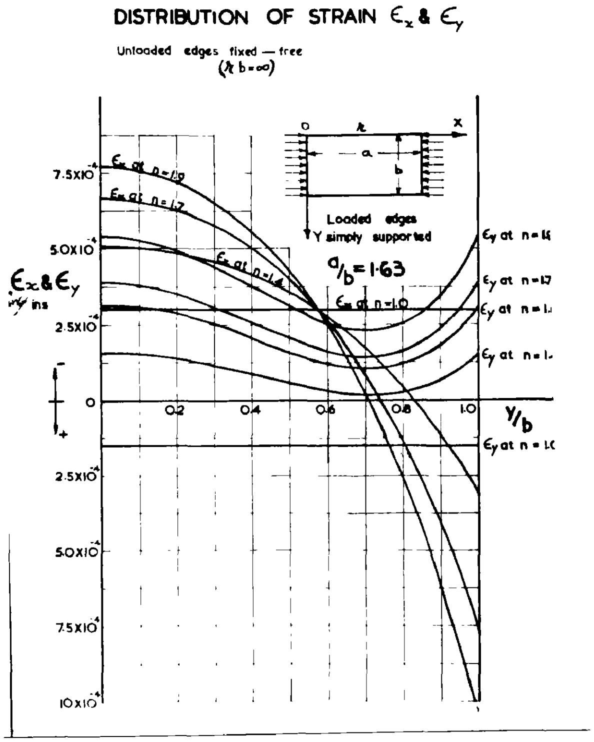

Fig. (41)

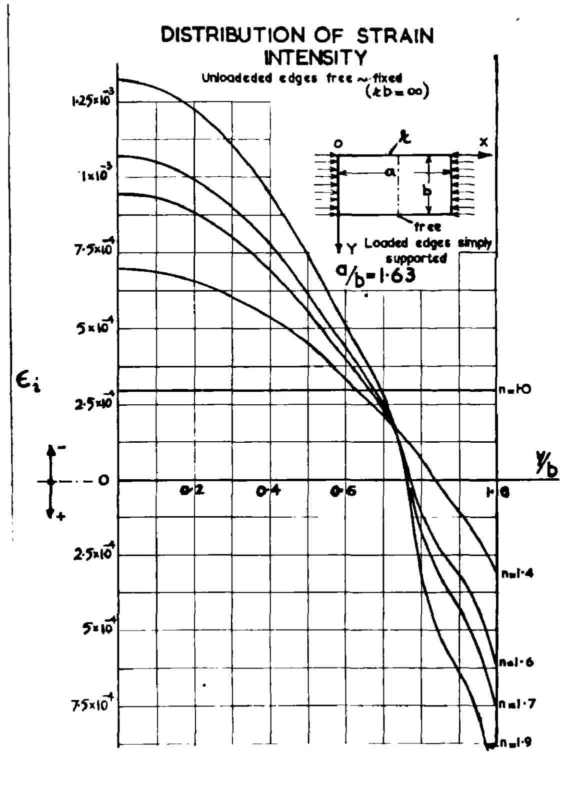

Fig. (42)

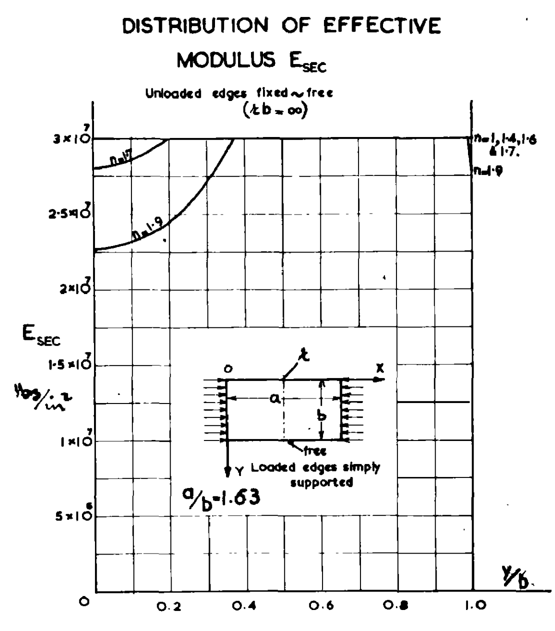

Fig. (43)

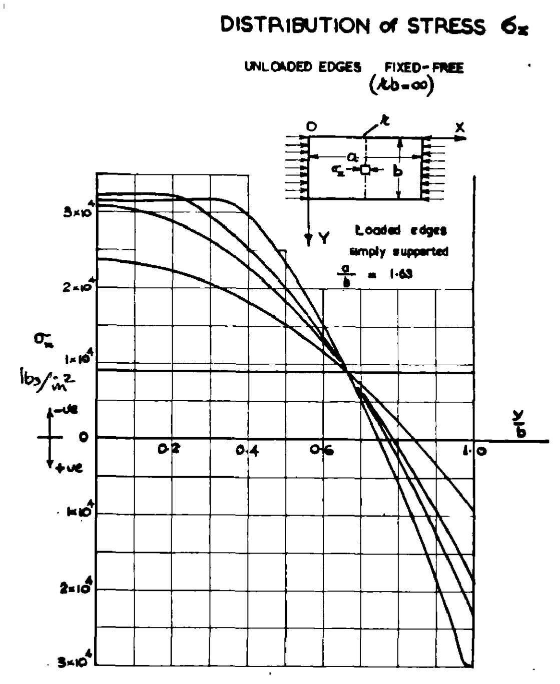

Fig. (44)

Maximum load occurs because the natural tendency for the stress to grow with the increasing strain is counteracted by the decrease in the effective modulus. To illustrate this, curves of σ_x corresponding to the strain distributions shown in Fig.(30) are given in Fig.(33).

Fig.(34) gives the curves of $\sigma_{x_{av}}$ against n obtained in the above manner for various width to thickness ratios of a simply supported square plate. In Fig.(35) curve of $\sigma_{x_{av}}$ against $(\epsilon_x + \frac{1}{2}\epsilon_y)$ at the centre of the plate derived from previous results is shown.

To demonstrate the effect of edge support conditions on the strain, effective modulus and stress distributions; results for two other cases are shown in Fig.(36) to (44) inclusive.

Fig.(36) gives the strains ϵ_x and ϵ_y distributions, for various n values, across the central section of a rectangular plate $(a/b = 0.885,\ b/h = 100)$ elastically fixed $(kb = 8)$ along one unloaded edge and simply supported along the other. The corresponding strain intensity ϵ_i, effective modulus E_{sec} and stress σ_x distributions are given in Figs.(37, 38) and (39). In Figs.(41) to (44) a similar sequence of graphs is given for a plate $(\frac{a}{b} = 1.63, \frac{b}{h} = 62.5)$ fixed along one unloaded edge and free along the other. It may be noted here that the uniformly loaded edges in both the cases are simply supported.

Fig. (40) and (45) give the plots of $\sigma_{x_{av}}$ against n for various width to thickness ratios of the two plates

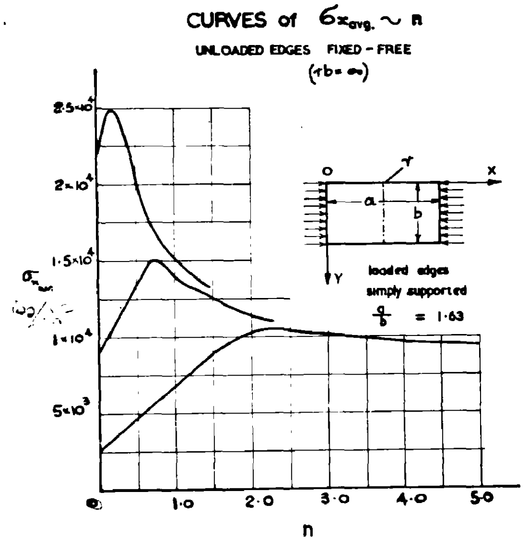
CURVES of $\sigma_{x_{avg.}} \sim n$
UNLOADED EDGES FIXED - FREE
($\tau b = \infty$)
2.5×10^4
2×10^4
1.5×10^4
1×10^4
5×10^3
1.0
2.0
3.0
4.0
5.0
n
loaded edges
simply supported
$\frac{a}{b} = 1.63$

Fig.(45)

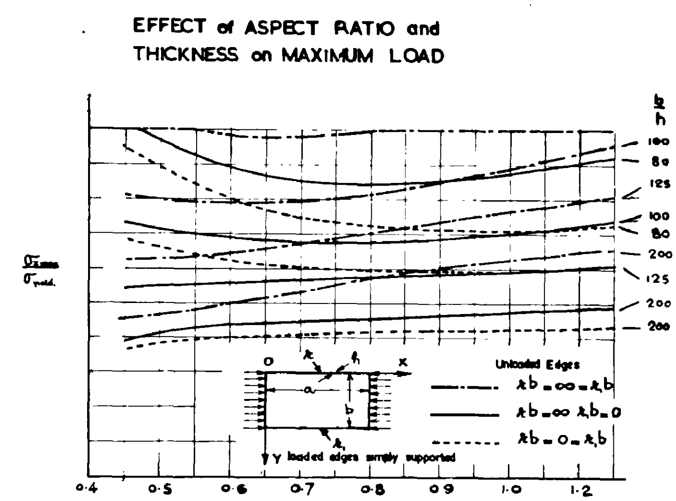
EFFECT of ASPECT RATIO and
THICKNESS on MAXIMUM LOAD
$\frac{\sigma_{x_{max}}}{\sigma_{yield}}$
$\frac{b}{h}$
100
80
125
100
80
200
125
200
200
Unloaded Edges
loaded edges simply supported
0.4
0.5
0.6
0.7
0.8
0.9
1.0
1.2

Fig.(46)

contemplated above.

The effect of the aspect ratio and the thickness on the maximum load for various plates is illustrated in Fig. (46).

(b) Maximum Deflection:

Consider a rectangular plate $(a/b = 0.8)$ simply supported along two uniformly loaded edges and one unloaded edge and built-in along the fourth. The deflection w as given by 1.42a is:

$$w = \alpha \sin \frac{m\pi x}{a}\left(\frac{y^4}{24b^3} - \frac{A_1 y^3}{6b^2} + \frac{B_1 y^2}{b} + \frac{C_1 y}{3}\right)$$

where A_1, B_1 and C_1 are given by 1.43a and 1.44a.

In this case $kb = \infty$ and $k_1 b = 0$ substituting these values in 1.44a and 1.43a gives:

$$A_1 = 0.625$$

$$B_1 = 0.0625$$

$$C_1 = 0$$

Thus the deflection becomes:

$$w = \alpha \sin \frac{m\pi x}{a}\left(\frac{y^4}{24b^3} - \frac{0.625\, y^3}{6b^2} + \frac{0.0625\, y^2}{b}\right) \quad \text{——— } 3.41b$$

Substituting for α from 3.34 in 3.41b gives:

$$w = \sqrt{\frac{C'''C'h^2(n-1)a^4}{12(1-\nu_e^2)\, b^2 \cdot b^4}} \sin \frac{m\pi x}{a}\left(\frac{y^4}{24b^3} - \frac{0.625\, y^3}{6b^2} + \frac{0.0625\, y^2}{b}\right)$$

For this plate $C' = 1997.66$ and $C''' = -4823.96$ and taking $\frac{b}{h} = 100$ and $\nu_e = \frac{1}{4}$ gives:

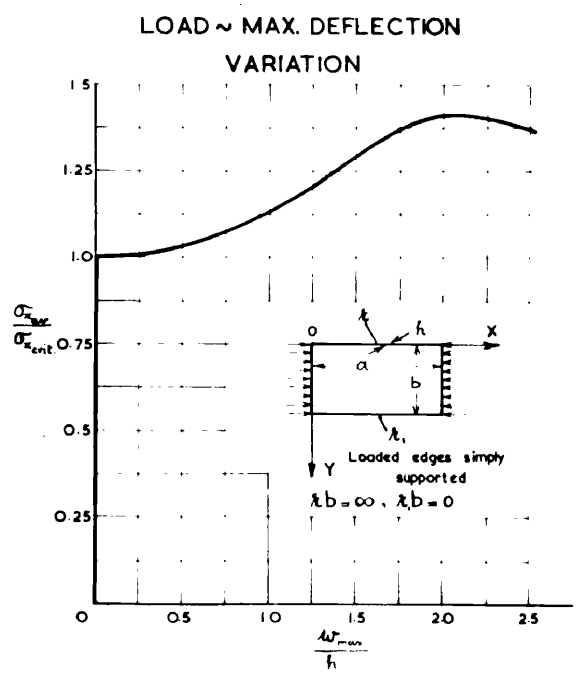
LOAD ~ MAX. DEFLECTION
VARIATION
1.5
1.25
1.0
0.75
0.5
0.25
0
0.5
1.0
1.5
2.0
2.5
$\frac{\sigma_{x_{av}}}{\sigma_{x_{crit}}}$
$\frac{w_{max}}{h}$
o
x
Y
a
b
h
Loaded edges simply supported
$k b = \infty$, $k_1 b = 0$

Fig.(47)

$$w = \sqrt{\frac{-4823.96 \times 1997.66(1-n)(0.8)^4}{11.25 \times 10^4}} \cdot \sin\frac{m\pi x}{a}\left(\frac{y^4}{24b^3} - \frac{0.625y^3}{6b^2} + \frac{0.0625y^2}{b}\right)$$

The value of n corresponding to maximum load of this plate is 1.56.

$$\therefore\ w = 4.076 \sin\frac{m\pi x}{a}\left(\frac{y^4}{24b^3} - \frac{0.625y^3}{6b^2} + \frac{0.0625y^2}{b}\right)$$

For maximum deflection $x = \frac{a}{2}$ and $\frac{\partial w}{\partial y} = 0$

$$\therefore \left|\frac{\partial w}{\partial y}\right|_{x=a/2} = 4.076\left(\frac{y^3}{6b^2} - \frac{0.625y^2}{2b^2} + \frac{0.125y}{b}\right)$$
$$= 0$$

or $\quad y^2 - 1.875yb + 0.75b^2 = 0$

which gives $y = 0.6775b$ and w_{max} at max. load

$$= 4.076\left[\frac{(0.6775)^2}{24} - \frac{0.625(0.6775)^3}{6} + 0.0625\,(0.6775)^2\right] b$$

or

$$w_{max} = 0.02073\,b$$

$$\therefore\ \frac{w_{max}}{h} = \frac{0.02073b}{0.01b} = 2.073$$

As an illustration w_{max}/h against $\sigma_{xav}/\sigma_{crit}$ graph for the plate considered above is given in Fig.(47).

SECTION: 4

APPLICATION OF SINGLE PLATE RESULTS TO COMPOSITE FORMS.

APPLICATION OF SINGLE PLATE RESULTS TO COMPOSITE FORMS.

In Section 2 elastic critical loads calculated by Galerkin's Method for single plates simply supported along the loaded edges with the unloaded edges elastically fixed - elastically fixed and elastically fixed - free are given. If such plates form a part of structural sections regarded as an assembly of plates, the elastic fixity is provided by the adjoining plates. In this Section the value of the elastic fixity provided by the supporting plate to the buckling plate of a composite structural section is determined and the elastic critical loads for the local instability of various structural forms are calculated.

A method similar to that employed by J.M. Harvey [18] is used in computing the elastic fixities of the buckling plate components. As an illustration elastic critical stresses in local instability of box sections and inwardly lipped channels is worked out in detail. A similar method is used for plain channel sections and the results for all these are summarised in the form of graphs.

In the fourth part of this Section the maximum loads of composite structural forms is computed utilizing the single plate results presented in Section 3.

4.0 LOCAL INSTABILITY OF THE PLATE COMPONENTS OF BOX SECTIONS.

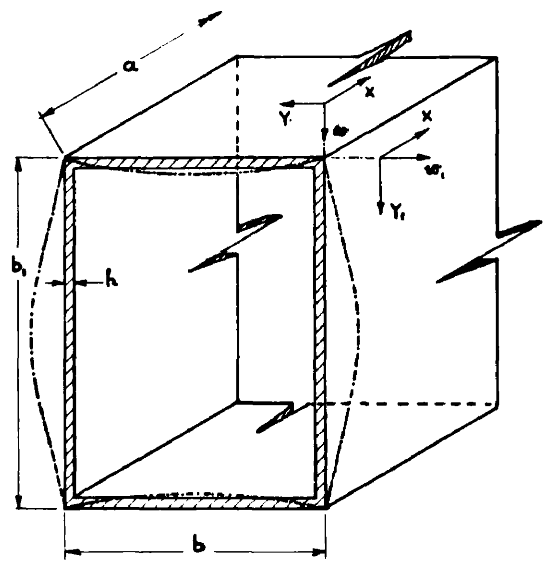

Fig.(48)

Consider a box section with the cross-section shown in Fig.(48).

Assuming the axial load to be uniformly compressive, each flat plate component is subjected to constant compressive stress N_x/h. In a box section two opposite plates support the other two buckling plates. Thus the problem of computing the elastic critical load for the box section reduces to determining the elastic fixity k provided by the supporting plate to the buckling plate and then determining the critical stress by Galerkin's Method.

To determine the elastic fixity for the buckling plate, it is assumed that the slopes and the moments along the common edge are equal and opposite .

Deflected Form Of The Supporting Plates:

Consider first of all the supporting plate; assuming that it has uniform stress distribution when it is supporting the buckling plate, the stress function F can be written as:

$$F = \frac{N_x y^2}{2h}$$

and the large deflection equations reduce to

$$\frac{\partial^4 w}{\partial x^4} + \frac{2\,\partial^4 w}{\partial x^2 \partial y^2} + \frac{\partial^4 w}{\partial y^4} = \frac{N_x}{D}\frac{\partial^2 w}{\partial x^2} \qquad 4.01$$

The solution of this equation for the supporting plate can be written in the form:

$$w = Y \sin\frac{m\pi x}{a} \qquad 4.02$$

where Y is a function of y only. Thus w satisfies the boundary conditions:

$$w = 0$$

$$\frac{\partial^2 w}{\partial x^2} + \nu \frac{\partial^2 w}{\partial y^2} = 0$$

for the simply supported loaded edges $x = 0$ and $x = a$.

Substituting from 4.02 in 4.01 gives:

$$\frac{d^4 Y}{d y^4} - 2\,\frac{m^2\pi^2}{a^2}\,\frac{d^2 Y}{d y^2} + \left(\frac{m^4\pi^4}{a^4} + \frac{m^2\pi^2 N_x}{a^2 D}\right) Y = 0 \quad \text{———— } 4.03$$

The general solution of this equation is:

$$Y = \left(C_1 \cosh \bar{\alpha} y + C_2 \sinh \bar{\alpha} y + C_3 \cos \bar{\beta} y + C_4 \sin \bar{\beta} y\right)$$

where $\bar{\alpha} = \sqrt{\frac{m^2\pi^2}{a^2} + \sqrt{-\frac{N_x}{D}\frac{m^2\pi^2}{a^2}}}$

$$\bar{\beta} = \sqrt{-\frac{m^2\pi^2}{a^2} + \sqrt{-\frac{N_x}{D}\frac{m^2\pi^2}{a^2}}}$$

and C_1, C_2, C_3 and C_4 are constants of integration.

Therefore:

$$w = \left(C_1 \cosh \bar{\alpha} y + C_2 \sinh \bar{\alpha} y + C_3 \cos \bar{\beta} y + C_4 \sin \bar{\beta} y\right) \sin \frac{m\pi x}{a} \quad \text{———— } 4.04$$

Now consider the boundary conditions of the supporting plate at the connecting edges $y = 0$ and $y = b$.

Assuming the connecting edges to remain straight during loading the first set of boundary conditions is:

$$w = 0 \quad \text{at} \quad y = 0 \quad \text{and} \quad y = b \quad \text{———— } 4.05$$

The second set of boundary conditions is obtained

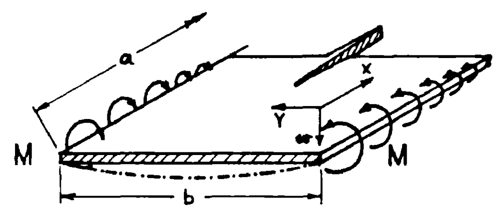

Fig. (49)

by assuming that the bending moment at the connecting edge of the supporting plate varies sinusoidally along the length of the plate.

$$\therefore \quad \frac{\partial^2 w}{\partial y^2} = \frac{M_y}{D} \sin\frac{m\pi x}{a} \qquad \text{at} \quad y=0 \text{ and } y=b \qquad \text{4.06}$$

It may be noted here that M_y is taken positive if it produces compression on the top surface (See Fig.(49)).

Substituting 4.05 and 4.06 in equation 4.04, the constants C_1, C_2, C_3 and C_4 are obtained as:

$$C_1 = \frac{+M_y}{D(\bar{\alpha}^2+\bar{\beta}^2)}$$

$$C_2 = \frac{+M_y}{D(\bar{\alpha}^2+\bar{\beta}^2)}\left[\frac{1-\cosh\bar{\alpha}b}{\sinh\bar{\alpha}b}\right]$$

$$C_3 = \frac{-M_y}{D(\bar{\alpha}^2+\bar{\beta}^2)}$$

$$C_4 = \frac{-M_y}{D(\bar{\alpha}^2+\bar{\beta}^2)}\left[\frac{1-\cos\bar{\beta}b}{\sin\bar{\beta}b}\right]$$

and the deflection form for the supporting plate is completely determined.

By substituting the values of the constants C_1, C_2, C_3 and C_4 in 4.04 and differentiating, the slope at the connecting edge $y=0$ is:

$$\frac{\partial w}{\partial y} = \frac{M_y \sin\frac{m\pi x}{a}}{D(\bar{\alpha}^2+\bar{\beta}^2)}\left[\frac{\bar{\alpha}-\bar{\alpha}\cosh\bar{\alpha}b}{\sinh\bar{\alpha}b} + \frac{\bar{\beta}\cos\bar{\beta}b-\bar{\beta}}{\sin\bar{\beta}b}\right] \qquad \text{4.07}$$

Boundary Conditions For The Buckling Plate:

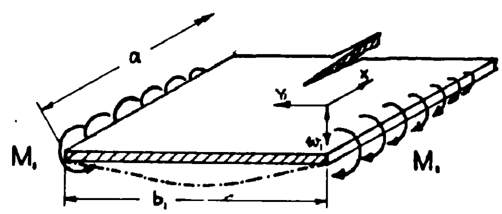

Fig.(50)

For the buckling plate, let the boundary conditions at the connecting edges be:

$$\left.\begin{aligned} & w_1 = 0 \quad \text{at} \quad y_1 = 0, b_1 \\ & \frac{\partial^2 w_1}{\partial y_1^2} = k \frac{\partial w_1}{\partial y_1} \quad \text{at} \quad y_1 = 0 ; \qquad \frac{\partial^2 w_1}{\partial y_1^2} = -k \frac{\partial w_1}{\partial y_1} \quad \text{at} \quad y_1 = b_1 \end{aligned}\right] \text{——— 4.08}$$

Once the value of k is defined in terms of the section dimensions, the boundary conditions for the buckling condition are completely determined and the critical stress can be evaluated by means of Galerkin's Method as shown in Section 2.

From the assumptions made, allowance for the interaction of the plate components at the connected edge requires that:

$M_y \sin\frac{m\pi x}{a} = -M_{y_1} \sin\frac{m\pi x}{a}$ where $M_{y_1} \sin\frac{m\pi x}{a}$ is the fixing moment acting on the buckling plate (Fig.(50)),

and $\dfrac{\partial w}{\partial y} = -\dfrac{\partial w_1}{\partial y_1}$

Now $D_1 \dfrac{\partial^2 w_1}{\partial y_1^2} = -M_{y_1} \sin\dfrac{m\pi x}{a} = M_y \sin\dfrac{m\pi x}{a}$

Also $\dfrac{\partial^2 w_1}{\partial y_1^2} = k \dfrac{\partial w_1}{\partial y_1} = -k \dfrac{\partial w}{\partial y}$

$$\therefore \; k \frac{\partial w}{\partial y} = -\frac{M_y}{D_1} \sin\frac{m\pi x}{a}$$

For the same thickness h for both the plates: $D = D_1$

$$\therefore \; k = \frac{-M_y \sin\frac{m\pi x}{a}}{D \; \partial w / \partial y} \qquad \text{———————— 4.09}$$

Therefore from 4.07 and 4.09

$$k = \frac{(\bar{\alpha}^2 + \bar{\beta}^2) \sinh \bar{\alpha} b \sin \bar{\beta} b}{\bar{\alpha} \sin \bar{\beta} b (\cosh \bar{\alpha} b - 1) + \bar{\beta} \sinh \bar{\alpha} b (1 - \cos \bar{\beta} b)}$$

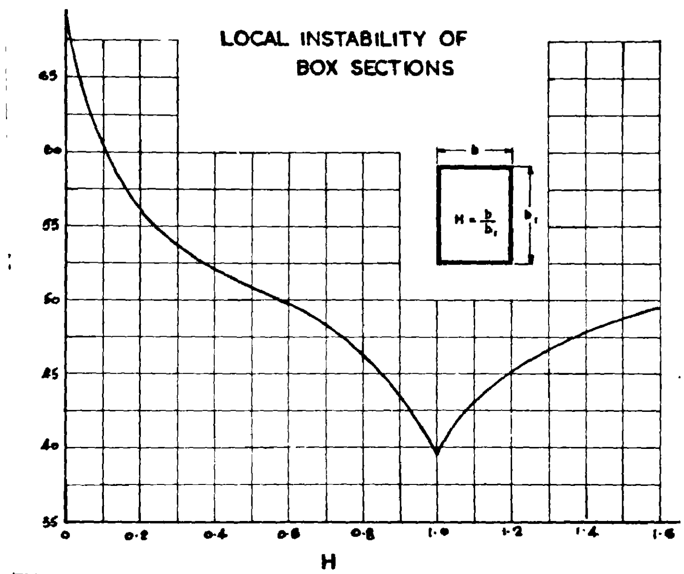

Fig. (51)

For the same uniform stress N_x/h carried by the supporting and the buckling plate, $\bar{\alpha} = \bar{\alpha}_1$ and $\bar{\beta} = \bar{\beta}_1$ and also substituting $b = Hb_1$ where $H = b/b_1$, the elastic fixity for the buckling plate at the connected edges becomes:

$$k = \frac{(\bar{\alpha}_1^2 + \bar{\beta}_1^2)\sinh\bar{\alpha}_1 Hb_1 \sin\bar{\beta}_1 Hb_1}{\bar{\alpha}_1 \sin\bar{\beta}_1 Hb_1 (\cosh\bar{\alpha}_1 Hb_1 - 1) + \bar{\beta}_1 \sinh\bar{\alpha}_1 Hb_1 (1 - \cos\bar{\beta}_1 Hb_1)} \qquad 4.010$$

Critical Stress For The Box Section:

The values of elastic critical loads $N_{x_{crit}}$ for uniformly compressed plates assumed simply supported along the loaded edges and having boundary condition 4.08 along the unloaded edges are obtained as indicated previously by Galerkin's Method for various kb_1 values. The results are shown in Fig.(18) Section 2. Thus from Fig.(18) the value of kb_1 the smallest value of $N_{x_{crit}} = \frac{-KD}{b_1^2}$, which is obtained by assuming the plate to buckle in one half sine wave; $m = 1$ and the corresponding ratio a/b_1 can be obtained from equation 4.010. The results of these calculations are shown in Fig.(51) and a typical calculations is presented in Appendix 4.

From Fig.(51) the value of K for any value of can be obtained and the minimum critical compressive load for the box section is given by:

$$P_{x_{crit}} = \frac{-KE\,h^2}{12(1-\nu^2)\,b_1^2} \times A$$

where A is the area of cross-section.

4.1 LOCAL INSTABILITY OF THE PLATE COMPONENTS OF INWARDLY LIPPED CHANNELS:

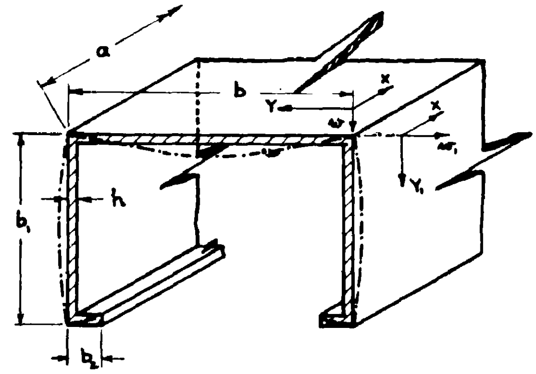

Fig.(52)

Consider the lipped channel shown in Fig.(52). In this case if the web buckles first the elastic fixities at the connecting edges are provided by two identical flanges. However, in the case when the flanges buckle first the elastic fixities at the two connecting edges may be unequal, one provided by the web plate and the other by the lip. In the following analysis it is assumed that the connecting edge of the flange and the lip is simply supported.

(a) **Instability Of Flange Plate:-**

Deflection Form Of The Supporting Plate:

The connecting edge $y_1 = b_1$ of the flange which is supported by the lip is assumed to be simply supported and therefore the deflection form of the lip need not be determined.

Now consider the other supporting plate; the web in this case.

Assuming the web to carry uniform stress, the differential equation for the deflection form of the web is exactly the same as for the supporting plate of a box section, viz: 4.01.

The boundary condition in this case are also similar and hence the deflection form of the web is:

$$w = \left(C_1 \cosh \bar{\alpha} y + C_2 \sinh \bar{\alpha} y + C_3 \cos \bar{\beta} y + C_4 \sin \bar{\beta} y\right) \sin \frac{m\pi x}{a} \qquad \text{4.11a}$$

where

$$C_1 = \frac{M_y}{D(\bar{\alpha}^2+\bar{\beta}^2)}$$

$$C_2 = \frac{M_y}{D(\bar{\alpha}^2+\bar{\beta}^2)}\left[\frac{1-\cosh\bar{\alpha}b}{\sinh\bar{\alpha}b}\right]$$

$$C_3 = \frac{-M_y}{D(\bar{\alpha}^2+\bar{\beta}^2)}$$

$$C_4 = \frac{-M_y}{D(\bar{\alpha}^2+\bar{\beta}^2)}\left[\frac{1-\cos\bar{\beta}b}{\sin\bar{\beta}b}\right]$$

And the slope at the connecting edge $y=0$ is:

$$\frac{\partial w}{\partial y} = \frac{M_y \sin\frac{m\pi x}{a}}{D(\bar{\alpha}^2+\bar{\beta}^2)}\left[\frac{\bar{\alpha}-\bar{\alpha}\cosh\bar{\alpha}b}{\sinh\bar{\alpha}b}+\frac{\bar{\beta}\cos\bar{\beta}b-\bar{\beta}}{\sin\bar{\beta}b}\right] \quad \text{——— 4.12a}$$

Boundary Conditions For The Flange Plate:

In accordance with the assumption made the boundary conditions for the edge $y_1 = b_1$ of the flange are:

$$\left.\begin{aligned} & w_1 = 0 \\ & \frac{\partial^2 w_1}{\partial y_1^2} + \nu\frac{\partial^2 w_1}{\partial x^2} = 0 \end{aligned}\right] \quad \text{——— 4.13a}$$

Let the boundary conditions for the flange along the connecting edge of the flange and the web, i.e. $y_1=0$ be:

$$\left.\begin{aligned} w_1 &= 0 \\ \frac{\partial^2 w_1}{\partial y_1^2} &= k \frac{\partial w_1}{\partial y_1} \end{aligned}\right] \quad \text{———} \; 4.14a$$

Let the fixing moment on the edge $y_1 = 0$ be M_{y_1}. From the assumptions made to incorporate the interaction of the plate components at the connected edges:

$$M_y \sin\frac{m\pi x}{a} = -M_{y_1}\sin\frac{m\pi x}{a}$$

Now $\dfrac{\partial^2 w_1}{\partial y_1^2} = -\dfrac{M_{y_1}}{D_1}\sin\dfrac{m\pi x}{a}$ at $y_1 = 0$

$$\therefore \frac{\partial^2 w_1}{\partial y_1^2} = \frac{M_y}{D_1}\sin\frac{m\pi x}{a} = \frac{M_y}{D}\sin\frac{m\pi x}{a}$$

for constant thickness of the channel.

Also

$$\frac{\partial^2 w_1}{\partial y_1^2} = k\frac{\partial w_1}{\partial y_1} = -k\frac{\partial w}{\partial y}$$

$$\therefore k = \frac{-M_y \sin\frac{m\pi x}{a}}{D\;\partial w/\partial y} \quad \text{———} \; 4.15a$$

From equation 4.12a and 4.15a.

$$k = \frac{(\bar{\alpha}^2+\bar{\beta}^2)\sinh\bar{\alpha}b\,\sin\bar{\beta}b}{\bar{\alpha}\sin\bar{\beta}b\,(\cosh\bar{\alpha}b-1)+\bar{\beta}\sinh\bar{\alpha}b\,(1-\cos\bar{\beta}b)}$$

For the same stress carried by the web flange and the lip $\bar{\alpha} = \bar{\alpha}_1$ and $\bar{\beta} = \bar{\beta}_1$. Also substituting $b = Hb_1$; elastic fixity provided by the web becomes:

$$k = \frac{(\bar{\alpha}_1^2+\bar{\beta}_1^2)\sinh\bar{\alpha}_1 Hb_1\,\sin\bar{\beta}_1 Hb_1}{\alpha_1\sin\bar{\beta}_1 Hb_1(\cosh\bar{\alpha}_1 Hb_1-1)+\bar{\beta}_1\sinh\bar{\alpha}_1 Hb_1(1-\cos\bar{\beta}_1 Hb_1)} \quad \text{———} \; 4.16a$$

Critical Stress For The Lipped Channel.

(Flange Failure):

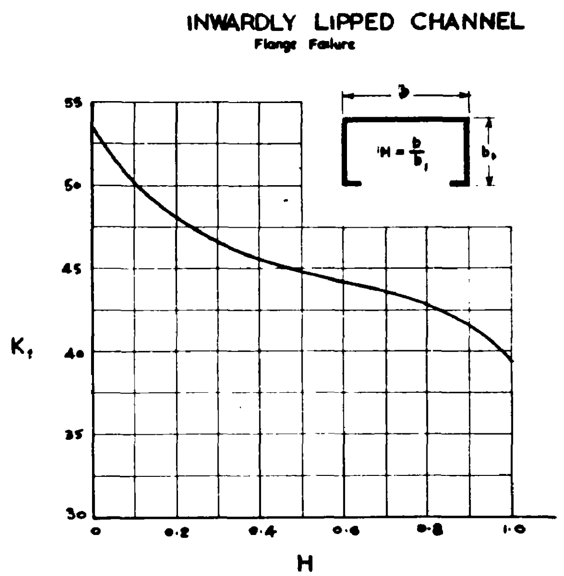

INWARDLY LIPPED CHANNEL
Flange Failure
b
H = b/b1
b1
K1
55
50
45
40
35
30
0
0.2
0.4
0.6
0.8
1.0
H

Fig. (53)

The values of elastic critical loads $N_{x_{crit}}$ for uniformly compressed plates assumed simply supported along the loaded edges and having boundary conditions 4.13a and 4.14a along the unloaded edges are obtained by Galerkin's Method for various $k b_1$ and $k_1 b_1$ values. These results are shown in Figs.(19) to (24) inclusive. Thus from these figures the values of $k b_1$, taking $k_1 b_1 = 0$ for the simply supported edge, the smallest value of K_f where $N_{x_{crit}} = -\frac{K_f D}{b_1^2}$ and the corresponding ratio a/b_1 can be obtained. Using these values the corresponding value of H is then obtained from equation 4.15a.

The results are shown plotted in Fig.(53). The value of K_f for any value of H can be obtained from Fig.(53) and the critical load for the lipped channel when the flange buckles is given by:

$$P_{x_{crit}} = \frac{-K_f \; E \; h^2}{12(1-\nu_e^2)\; b_1^2} \times A$$

where A is the area of cross-section of the inwardly lipped channel.

(b) Instability Of Web Plate:

Deflection Form Of The Supporting Plate:

In this case the supporting plate is the flange. Assuming the flange to carry uniform stress N_x/h the differential equation for the flange is:

$$\frac{\partial^4 w_1}{\partial x^4} + 2\,\frac{\partial^4 w_1}{\partial x^2 \partial y_1^2} + \frac{\partial^4 w_1}{\partial y_1^2} = \frac{N_x}{D_1}\,\frac{\partial^2 w_1}{\partial x^2} \qquad \text{4.11b}$$

and the general solution of 4.11b is:

$$w_1 = \left(C_1 \cosh \bar{\alpha}_1 y_1 + C_2 \sinh \bar{\alpha}_1 y_1 + C_3 \cos \bar{\beta}_1 y_1 + C_4 \sin \bar{\beta}_1 y_1\right) \sin \frac{m\pi x}{a}$$

where

$$\bar{\alpha}_1 = \sqrt{\frac{m^2\pi^2}{a^2} + \sqrt{-\frac{N_x}{D_1}\,\frac{m^2\pi^2}{a^2}}}$$

$$\bar{\beta}_1 = \sqrt{-\frac{m^2\pi^2}{a^2} + \sqrt{-\frac{N_x}{D_1}\,\frac{m^2\pi^2}{a^2}}}$$

and C_1, C_2, C_3 and C_4 are constant of integration.

It is again assumed that the connecting edge of the lip and flange is simply supported, and bending moment at the connecting edge of web and flange varies sinusoidally.

Thus the boundary conditions for the supporting plate become:

$$\left.\begin{aligned} & w_1 = 0 \quad \text{at} \quad y_1 = 0,\ b_1 \\ & \frac{\partial^2 w_1}{\partial y_1^2} = \frac{M_{y_1}}{D_1} \sin \frac{m\pi x}{a} \quad \text{at} \quad y_1 = 0 \\ & \frac{\partial^2 w_1}{\partial y_1^2} = 0 \quad \text{at} \quad y_1 = b_1 \end{aligned}\right] \qquad \text{4.12b}$$

Using these boundary conditions the values of the constants of integration are obtained as:

$$C_1 = \frac{M_{y_1}}{D_1\left(\bar{\alpha}_1^2 + \bar{\beta}_1^2\right)}$$

$$C_2 = \frac{-M_{y_1}}{D_1(\bar{\alpha}_1^2+\bar{\beta}_1^2)\tanh\bar{\alpha}_1 b_1}$$

$$C_3 = \frac{-M_{y_1}}{D_1(\bar{\alpha}_1^2+\bar{\beta}_1^2)}$$

$$C_4 = \frac{+M_{y_1}}{D_1(\bar{\alpha}_1^2+\bar{\beta}_1^2)\tan\bar{\beta}_1 b_1}$$

and the slope of the supporting flange at the connecting edge of the web and flange becomes:

$$\frac{\partial w_1}{\partial y_1} = \frac{M_{y_1}}{D_1(\bar{\alpha}_1^2+\bar{\beta}_1^2)}\left[\frac{\bar{\beta}_1}{\tan\bar{\beta}_1 b_1} - \frac{\bar{\alpha}_1}{\tanh\bar{\alpha}_1 b_1}\right]\sin\frac{m\pi x}{a} \qquad \text{———— 4.13b}$$

Boundary Conditions For the Web Plate:

Let the boundary conditions for the buckling web be:

$$\left.\begin{array}{l} \left.\begin{array}{l} w = 0 \\[2ex] \dfrac{\partial^2 w}{\partial y^2} = k\dfrac{\partial w}{\partial y} \end{array}\right\} \text{at } y=0 \\[6ex] \left.\begin{array}{l} w = 0 \\[2ex] \dfrac{\partial^2 w}{\partial y^2} = -k\dfrac{\partial w}{\partial y} \end{array}\right\} \text{at } y=b \end{array}\right] \qquad \text{———— 4.14b}$$

From the assumptions made, the fixing moment M_y on the edges $y=0$ and $y=b$ is given by:

$$M_y \sin\frac{m\pi x}{a} = -M_{y_1}\sin\frac{m\pi x}{a}$$

Now $\dfrac{\partial^2 w}{\partial y^2} = -\dfrac{M_y}{D}\sin\dfrac{m\pi x}{a}$

$$\therefore \frac{\partial^2 w}{\partial y^2} = \frac{M_{y_1}}{D_1}\sin\frac{m\pi x}{a}$$

for same thickness of flange and web.

Also

$$\frac{\partial^2 w}{\partial y^2} = r\frac{\partial w}{\partial y} = -r\frac{\partial w_1}{\partial y_1} \quad \text{at } y = 0$$

$$\left.\begin{array}{l} \therefore\ r = \dfrac{-M_{y_1}\sin\frac{m\pi x}{a}}{D_1\ \partial w_1/\partial y_1} \quad \text{at } y = 0 \\ \\ \text{and similarly} \\ r = \dfrac{+M_{y_1}\sin\frac{m\pi x}{a}}{D_1\ \partial w_1/\partial y_1} \quad \text{at } y = b \end{array}\right] \text{———— 4.15b}$$

Thus from equations 4.13b and 4.15b

$$r = \frac{(\bar{\alpha}_1^2 + \bar{\beta}_1^2)\tanh\bar{\alpha}_1 b_1 \tan\bar{\beta}_1 b_1}{\bar{\alpha}_1\tan\bar{\beta}_1 b_1 - \bar{\beta}_1\tanh\bar{\alpha}_1 b_1} \qquad \text{———— 4.16b}$$

For the same stress carried by the web and flange $\bar{\alpha} = \bar{\alpha}_1$, $\bar{\beta} = \bar{\beta}_1$. Also substituting $b = Hb_1$ in 4.16b gives:

$$r = \frac{(\bar{\alpha}^2 + \bar{\beta}^2)\tanh\bar{\alpha}b/H \tan\bar{\beta}b/H}{\bar{\alpha}\tan\bar{\beta}b/H - \bar{\beta}\tanh\bar{\alpha}b/H} \qquad \text{———— 4.17b}$$

Critical Load For The Lipped Channel.

(Web Failure)

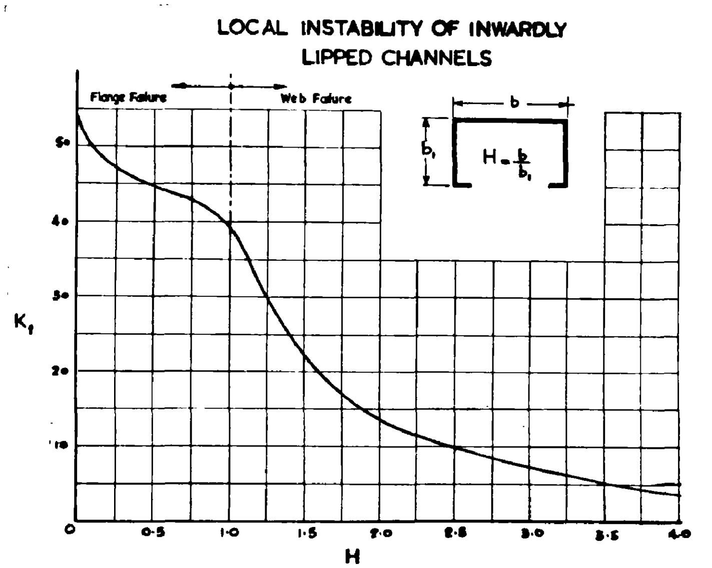
LOCAL INSTABILITY OF INWARDLY
LIPPED CHANNELS
Flange Failure
Web Failure
b
b_1
$H = \frac{b}{b_1}$
K_f
H
0
0·5
1·0
1·5
2·0
2·5
3·0
3·5
4·0

Fig. (54)

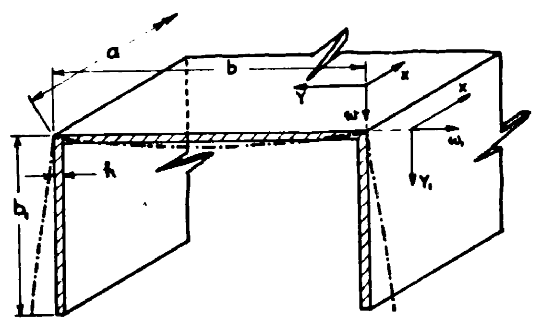
a
b
x
Y
x
w
w_1
Y_1
h
b_1

Fig. (55)

The values of elastic critical loads $N_{x_{crit}}$ for uniformly compressed plates having boundary conditions 4.14b along the unloaded edges are given in Fig.(18).

From this figure values of kb, the smallest value of K_w where $N_{x_{crit}} = \frac{-K_w D}{b^2}$ and the corresponding ratio a/b can be obtained. Using these values, the corresponding value of H is then obtained from equation 4.17b.

In order to simplify the presentation of buckling stress results, values of K_f equivalent to web failure are determined from the relation:

$$K_f = \frac{K_w}{H^2}$$

and the results are incorporated in a combined curve for flange and web failure as shown in Fig.(54).

4.2 LOCAL INSTABILITY OF THE PLATE COMPONENTS OF PLAIN CHANNELS:

Consider first the instability of the web of a plain channel shown in Fig.(55).

(a) Instability of Web:

In this case the flange which is assumed to be uniformly compressed, is the supporting plate. Assuming the bending moment along the edge $y_1 = 0$ of the flange to be M_{y_1} the boundary conditions along the unloaded edges of the flange become:

$$\left.\begin{aligned} w_1 &= 0 \\ \frac{\partial^2 w_1}{\partial y_1^2} &= \frac{M_{y_1}}{D_1} \sin \frac{m\pi x}{a} \end{aligned}\right\} \text{ at } \underline{\qquad\qquad\qquad} \quad 4.21b$$

$$\left.\begin{aligned}&\frac{\partial^2 w_1}{\partial y_1^2} + \nu\,\frac{\partial^2 w_1}{\partial x^2} = 0\\ &\frac{\partial^3 w_1}{\partial y_1^3} + (2-\nu)\frac{\partial^3 w_1}{\partial x^2 \partial y_1} = 0\end{aligned}\right\}\ \text{at}\quad y_1 = b_1 \qquad \text{———} \ 4.22\text{a}$$

Solving the differential equation for the deflection in a manner similar to the one described in the previous cases the slope at the connecting edge of the supporting flange obtains as:

$$\frac{\partial w_1}{\partial y_1} = \frac{-M_{y_1}\sin\frac{m\pi x}{a}}{D_1(\bar{\alpha}_1^2+\bar{\beta}_1^2)}\left[\frac{2\bar{\alpha}_1\bar{\beta}_1 s_1 p_1 + \bar{\alpha}_1\bar{\beta}_1(s_1^2+p_1^2)\cosh\bar{\alpha}_1 b_1\cos\bar{\beta}_1 b_1 + (\bar{\beta}_1^2 s_1^2 - \bar{\alpha}_1^2 p_1^2)\sinh\bar{\alpha}_1 b_1\sin\bar{\beta}_1 b_1}{s_1^2\bar{\beta}_1\cos\bar{\beta}_1 b_1\sinh\bar{\alpha}_1 b_1 - p_1^2\bar{\alpha}_1\sin\bar{\beta}_1 b_1\cosh\bar{\alpha}_1 b_1}\right] \qquad \text{———} \ 4.23\text{a}$$

where: $p_1 = \bar{\alpha}_1^2 - (2-\nu)\dfrac{m^2\pi^2}{a^2} = \bar{\beta}_1^2 + \nu\dfrac{m^2\pi^2}{a^2}$

$$s_1 = \bar{\beta}_1^2 + (2-\nu)\frac{m^2\pi^2}{a^2} = \bar{\alpha}_1^2 - \nu\frac{m^2\pi^2}{a^2}$$

Now, assuming that the boundary conditions for the buckling web along the edge $y = 0$ are:

$$\left.\begin{aligned}&w = 0\\ &\frac{\partial^2 w}{\partial y^2} = k\,\frac{\partial w}{\partial y}\end{aligned}\right\} \qquad \text{———} \ 4.24\text{a}$$

From the assumptions made for the connecting edges:

$$\left.\begin{aligned}&\frac{\partial^2 w}{\partial y^2} = -\frac{M_y}{D}\sin\frac{m\pi x}{a} = \frac{M_{y_1}}{D_1}\sin\frac{m\pi x}{a}\\ &\text{and}\ \frac{\partial w}{\partial y} = -\frac{\partial w_1}{\partial y_1}\end{aligned}\right\} \qquad \text{———} \ 4.25\text{a}$$

Therefore from 4.24a and 4.25a:

$$k = \frac{-M_{y_1}\sin m\pi x/a}{D_1\ \partial w_1/\partial y_1}$$

Substituting from 4.23a and taking $\bar{\alpha}=\bar{\alpha}_1$, $\bar{\beta}=\bar{\beta}_1$ and $b=Hb_1$ gives:

$$r=\frac{(\bar{\alpha}^2+\bar{\beta}^2)\left(s^2\bar{\beta}\sinh\bar{\alpha}b/_H\cos\bar{\beta}b/_H-p^2\bar{\alpha}\cosh\bar{\alpha}b/_H\sin\bar{\beta}b/_H\right)}{\bar{\alpha}\left\{2\bar{\beta}sp+\bar{\beta}(s^2+p^2)\cos\bar{\beta}b/_H\cosh\bar{\alpha}b/_H\right\}+(\bar{\beta}^2s^2-\bar{\alpha}^2p^2)\sinh\bar{\alpha}b/_H\sin\bar{\beta}b/_H} \qquad 4.24a$$

For any value of rb the ratio a/b at which K_w is a minimum can be obtained from Fig.(18). Using these values the corresponding value of H is then obtained from equation 4.24a. The results of these calculations are incorporated in Fig.(56).

(b) Instability of Flange:

Assuming the bending moment at the connecting edge of the supporting plate: in this case the web, to be M_y. The boundary conditions along the unloaded edges of the web are identical with those for the supporting web of a lipped channel, therefore the deflection form is also similar and the slope at the connecting edge is given by:

$$\frac{\partial w}{\partial y}=\frac{M_y\sin\frac{m\pi x}{a}}{D(\bar{\alpha}^2+\bar{\beta}^2)}\left[\frac{\bar{\alpha}\sin\bar{\beta}b(1-\cosh\bar{\alpha}b)+\bar{\beta}\sinh\bar{\alpha}b(\cos\bar{\beta}b-1)}{\sinh\bar{\alpha}b\sin\bar{\beta}b}\right] \qquad 4.21b$$

Let the boundary conditions for the buckling flange along the connecting edge $y_1=0$ be:

$$w_1=0$$

$$\frac{\partial^2 w_1}{\partial y_1^2}=r\frac{\partial w_1}{\partial y_1}$$

Now $\frac{\partial^2 w_1}{\partial y_1^2}=-\frac{M_{y_1}}{D_1}\sin\frac{m\pi x}{a}=\frac{M_y}{D}\sin\frac{m\pi x}{a}$

$\frac{\partial w_1}{\partial y_1}=-\frac{\partial w}{\partial y}$, $\bar{\alpha}=\bar{\alpha}_1$, $\bar{\beta}=\bar{\beta}_1$ and $b=Hb_1$. Therefore from 4.21b and 4.22b. $r=\frac{(\bar{\alpha}_1^2+\bar{\beta}_1^2)\sinh\bar{\alpha}_1Hb_1\sin\bar{\beta}_1Hb_1}{\bar{\alpha}_1\sin\bar{\beta}_1Hb_1(1-\cosh\bar{\alpha}_1Hb_1)+\bar{\beta}_1\sinh\bar{\alpha}_1Hb_1(\cos\bar{\beta}_1Hb_1-1)}$ 4.22b

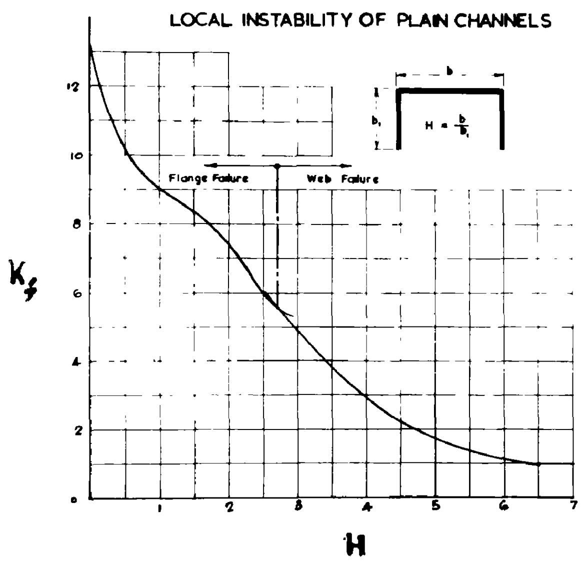
LOCAL INSTABILITY OF PLAIN CHANNELS
b
b_1
$H = \frac{b}{b_1}$
Flange Failure
Web Failure
K_f
H
0
2
4
6
8
10
12
1
3
5
7

Fig. (56)

The values of elastic critical loads for uniformly compressed plates simply supported along the loaded edges and having boundary conditions 4.22a and 4.22b along the unloaded edge have been evaluated in Section 2 for the various values of kb_1 and shown in Fig.(28). From Fig.(28) the value of kb_1 the smallest value of K_f where $N_{x\,crit} = \frac{K_f D_1}{b_1^2}$ and the corresponding ratio a/b_1 can be obtained. Using these values the corresponding value of H is then obtained from equation 4.23b. The results are shown plotted in Fig.(56) which is a combined curve for the flange and web instability. The values of K_f in the web failure range are equivalent values given by $K_f = K_w/H$.

4.3 APPROXIMATE METHOD OF COMPUTING MAXIMUM LOADS OF COMPOSITE STRUCTURAL FORMS:

The curves of average stress $\sigma_{x\,av}$ against n where $n = \frac{N_x\, E}{E_{sec}\, N_{x\,crit}}$ for single plates are computed by the method described in Section 3. In composite structural sections if the boundary conditions of different plates are known the curves of $\sigma_{x\,av}$ against $\epsilon_{x\,av} = \frac{N_x}{h\, E_{sec}}$ can be plotted for each plate. Boundary conditions, along the unloaded connected edges, (at the load at which instability initiates) of the plate component which buckles first can be evaluated for various structural forms by the method described in previous sections. In the present analysis it is assumed that these boundary conditions along these edges of the buckling plate component remain constant during the period following the initiation of instability. It is also assumed that the unloaded

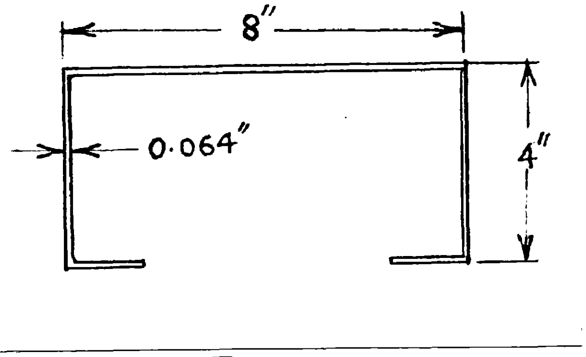

Fig. (57)

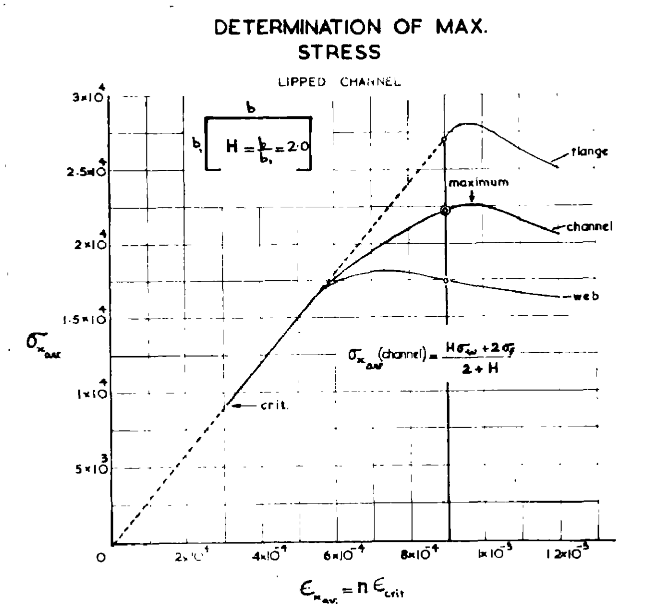

Fig. (58)

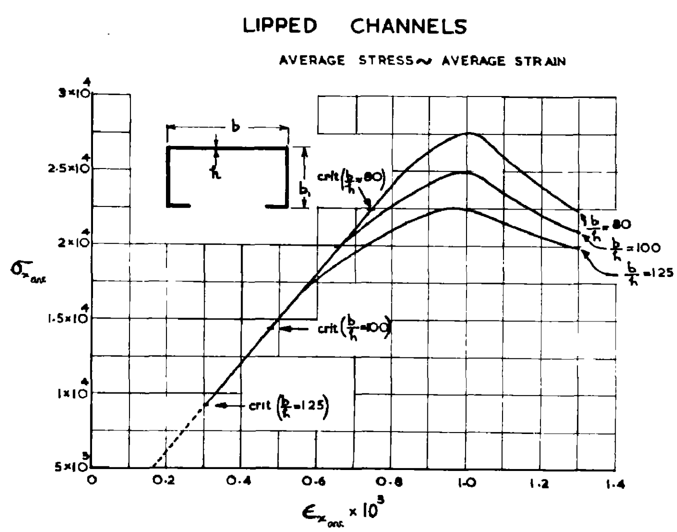

Fig. (59)

edges of the supporting plate component in the post buckling range become simply supported along the connected edges. With these assumption it is possible to plot curves of $\sigma_{x_{av}} \sim \epsilon_{x_{av}}$ for all the plate components. Assuming that the average strains for the various plate components are equal, the sum of the loads carried by the plate components are evaluated, giving the average stress $\sigma_{x_{av}}$ carried by the structural section as $\frac{\text{Total load}}{\text{Area of x section}}$.

From the curve of $\sigma_{x_{av}} \sim \epsilon_{x_{av}}$ the maximum value of this average stress σ_{max} can be evaluated.

As an illustration consider a lipped channel of the dimensions shown in the Fig. (57). For $H = 2.0$ it can be seen from Fig. (54) that the web buckles first and $K_f = 13.25$ and $\therefore K_w = 53$. From Fig (18) corresponding to this minimum value of K_w, λb can be found by interpolation to be 7.9. Thus the elastic fixity for the web is known. The flange is assumed to be simply supported along both the unloaded edges. The curves of $\sigma_{x_{av}} \sim \epsilon_{x_{av}}$ for both the plate components are shown plotted in Fig. (58). The average stress carried by the lipped channel at an average strain of 0.0009 inch/inch is then:

$$\sigma_{x_{av}} = \frac{(1.74 + 2 \times 0.05 \times 2.7) \times 10^4}{2} = 2.22 \times 10^4 \text{ lbs/in}^2$$

Thus the curve of $\sigma_{x_{av}} \sim \epsilon_{x_{av}}$ for the lipped channel can be drawn by means of similar calculations and the maximum stress value can be determined. Curves of $\sigma_{x_{av}} \sim \epsilon_{x_{av}}$ for lipped channels with $H = 2.0$ and various thicknesses are shown in Fig. (59). Curves of

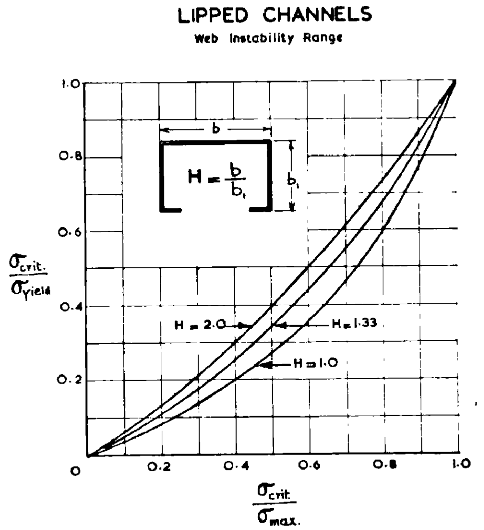

Fig.(60)

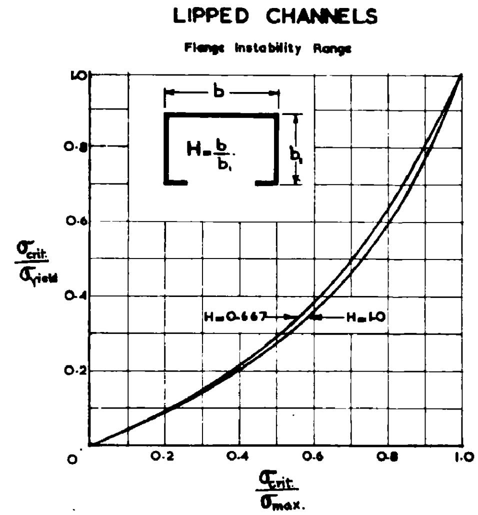

Fig.(61)

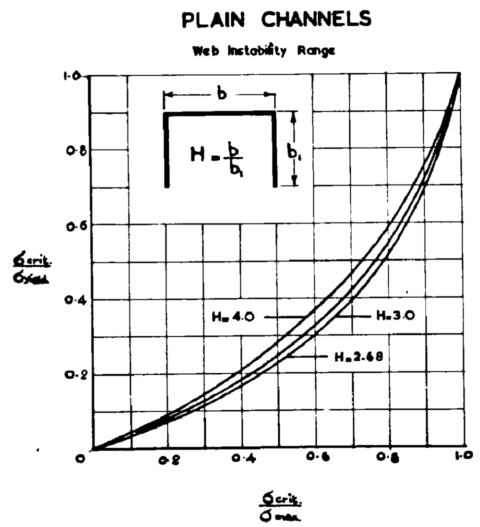

Fig.(62)

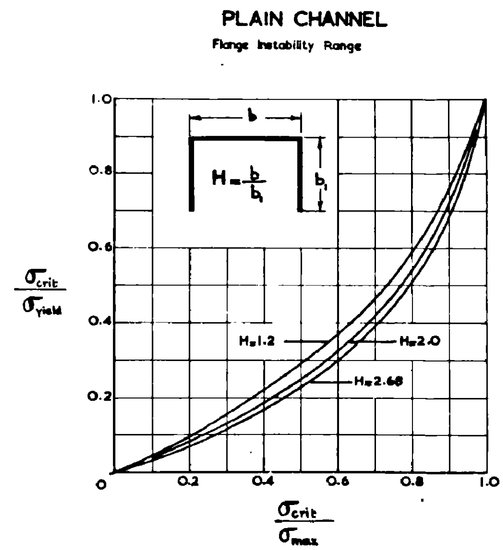

Fig.(63)

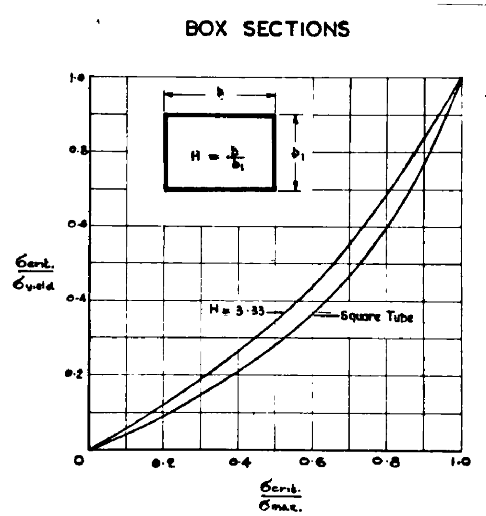

Fig.(64)

$\sigma_{crit}/\sigma_{max} \sim \sigma_{crit}/\sigma_{yield}$ obtained in this manner are shown in Figs. (60) to (64) inclusive for various H values of lipped and plain channel sections, and box sections.

It was seen in Section 3 that the distributions of strains and deflections can be evaluated for plates if the value of $n = \frac{\epsilon_{x\,av}}{\epsilon_{x\,crit}}$ corresponding to a certaih load is known. In the case of composite structural sections, the value of n corresponding to any load; given by $\epsilon_{x\,av}/\epsilon_{x\,crit}$ can be obtained from $\sigma_{x\,av} \sim \epsilon_{x\,av}$ curve for that structural section, and the distributions of strains, etc. obtained for the particular load, in a manner similar to the one described in Section 3.

SECTION 5

EXPERIMENTAL INVESTIGATIONS.

EXPERIMENTAL INVESTIGATIONS.

The experimental work undertaken was planned (a) to determine the effect of dimension variations on the elastic critical and maximum load carrying capacity, of thin walled short struts, and (b) to obtain the strain distributions and deformation characteristics of various plate components.

Experiments under (a) were carried out essentially to determine the critical load and maximum load under local instability conditions and therefore comparatively short lengths were used to ensure that plate buckling would occur with the edges remaining straight.

Experiments under (b) were performed for a comparison of experimental and theoretical strain distributions and deflected forms of various plate components of short structural sections loaded in compression.

The results of a large number of tests on cold pressed plain channels, lipped channels and angle sections and hot drawn box sections are presented. The range of specimens tested is described in detail for each experimental series.

5.0 EXPERIMENTAL APPLIANCES.

End Plattens:

Special end plattens were designed to fit in a 50 ton hydraulically operated Denison Testing Machine

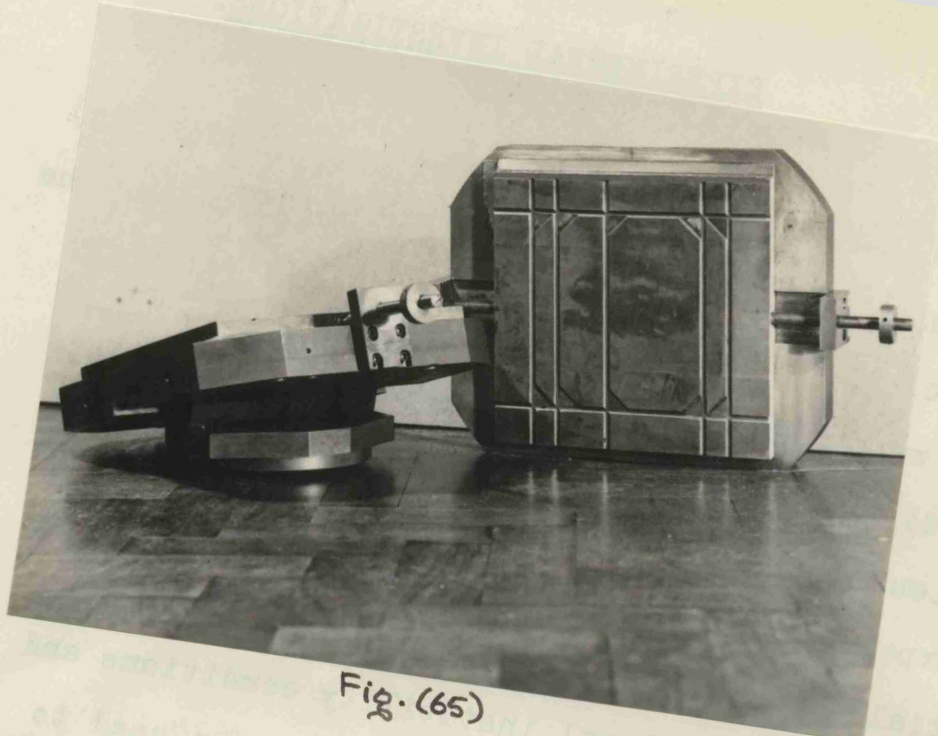

Fig. (65)

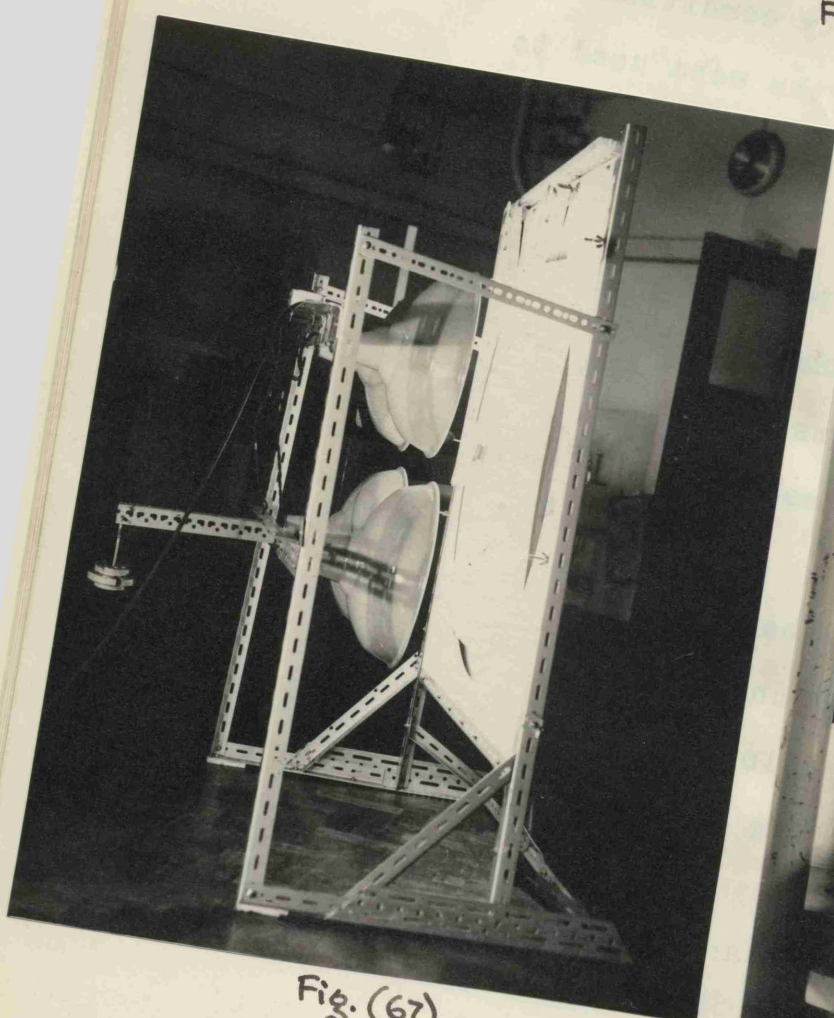

Fig. (67)

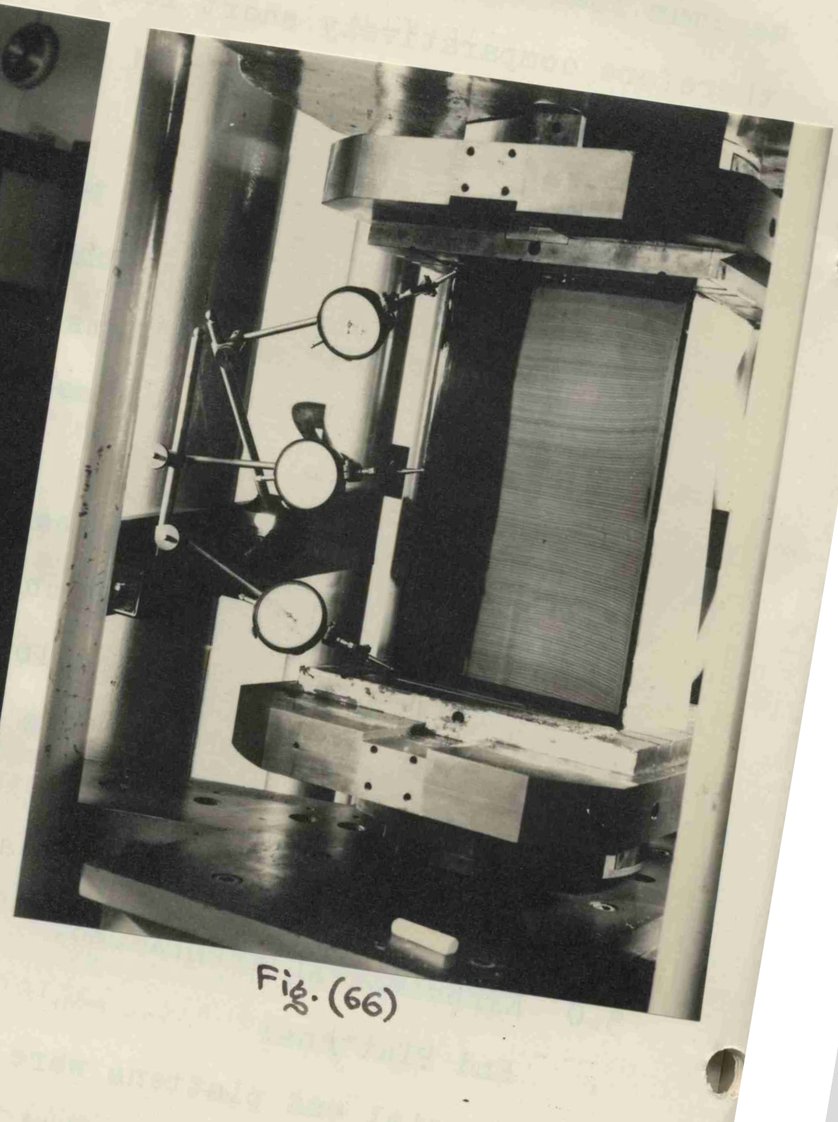

Fig. (66)

which was used for loading all the specimens.
A knife edge was provided at each end of the block parallel to the axis of least moment of inertia of the structural section, thus providing hinged end conditions for the strut as a whole about this axis. In order to realise as nearly as possible simply supported edge conditions for each plate component end supports with semi-circular grooves, as shown in Fig.(65) and (66) were used for accommodating the specimens.

Strain Measuring Gear:

$\frac{1}{2}$ inch gauge length foil type electrical resistance strain gauges were used for measuring the strain distribution. A Baldwin Lima-Hamilton type strain bridge was used for the measurement of strains.

Deflection Measuring Gear:

Dial gauges and Moire fruige apparatus shown in Fig.(67) . were used for the measurement of deflections. The theoretical background and the development of the Moire fruige apparatus is given in Appendix 6 .

5.1 TESTING TECHNIQUES AND EXPERIMENTAL RESULTS.

Determination Of Critical Instability Condition:

Two different methods were used for ascertaining the experimental critical load and the corresponding stress. The first method is based on the strain variation characteristics and the second on the corresponding deflection variation.

In the first method electrical resistance strain gauges were placed - (at the centre of the webs, at

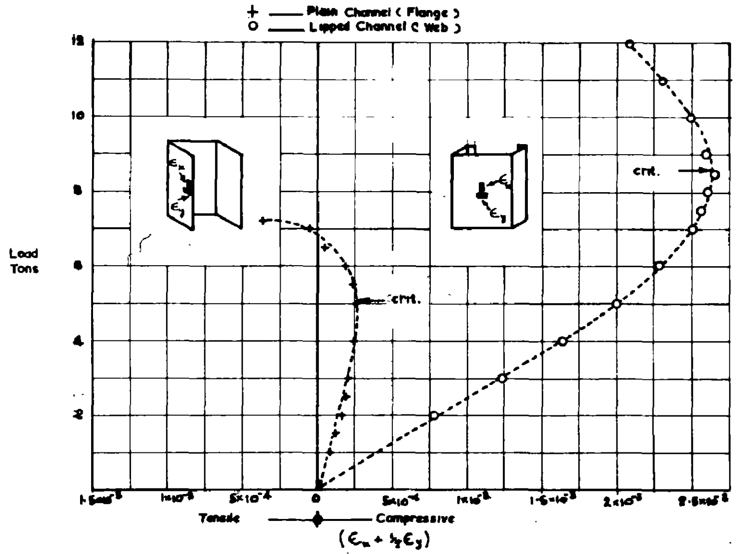

Fig. (68)

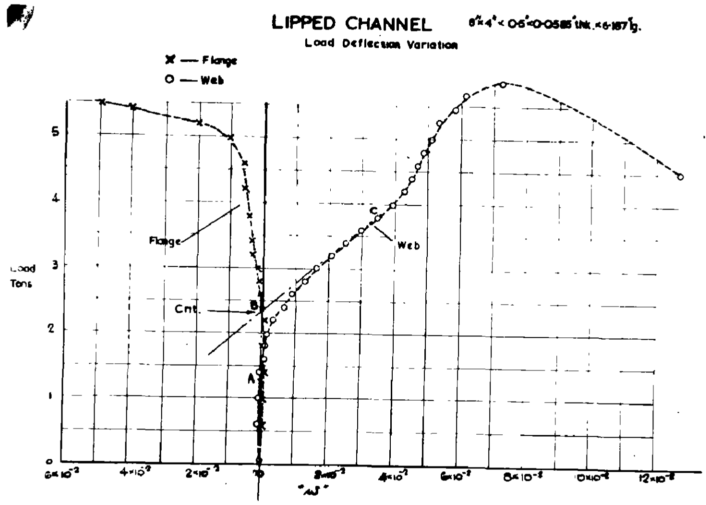

Fig. (69)

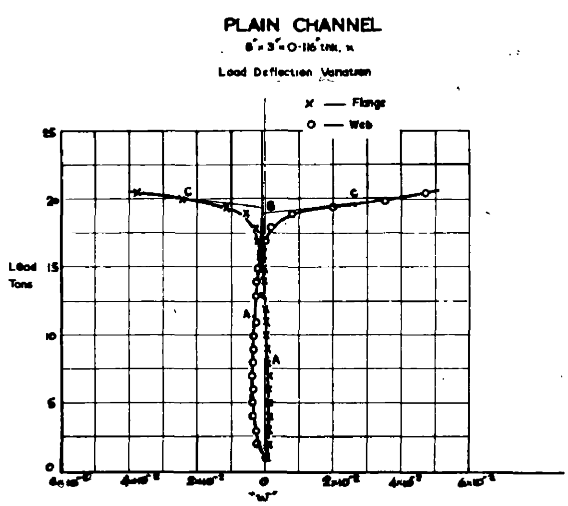

Fig. (70)

the centre of the flanges of lipped channels and near the centre of the outer edge of flanges of plain channels and angle sections) - in the direction of the applied compression for measuring the middle plane strains ϵ_x, and normal to the direction of the applied load for the corresponding middle plain strain ϵ_y. Curves of load P against $(\epsilon_x + \frac{1}{2}\epsilon_y)$ were plotted (Fig(68)); the load corresponding to the maximum value of $(\epsilon_x + \frac{1}{2}\epsilon_y)$ being taken as the critical load. This was in accordance with the theoretical relationships presented in Section III (See Fig(35)).

The second method was suggested by the theoretically derived result shown in Fig.(47). Owing to the initial imperfections present in the plate components flexure of plates occurs before the critical load is reached and the experimentally derived curves obtained are of the form shown in Fig.(69) and (70). In the case of short struts these curves do not have hyperbolic characteristics and therefore the Southwell - Lundquist plots tend to predict values of the critical load higher than the theoretical. It was found, however, that the load corresponding to the "top of knee" of the $P \sim w_{max}$ curve gives a better approximation.

The "top of knee" was observed to be best approximated to by the point of intersection B of the line such as AB drawn through the pre-critical region and the tangent CB drawn through the point of inflexion in the post-critical region.

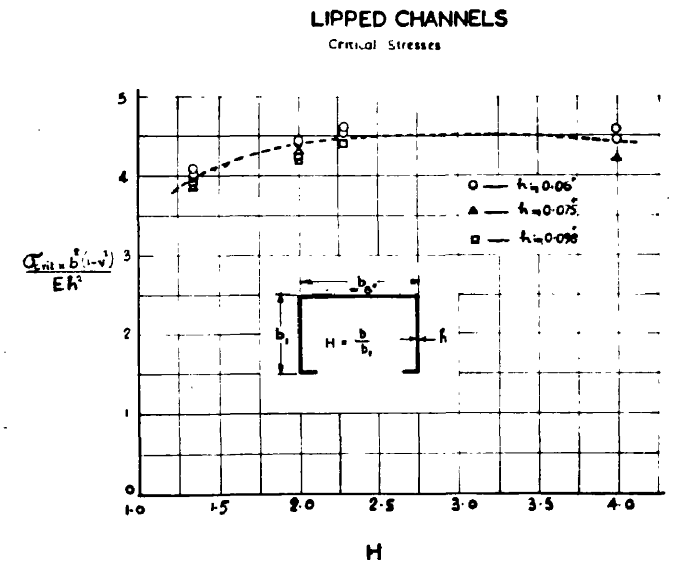
LIPPED CHANNELS
Critical Stresses
H = b/b₁
H

Fig. (71)

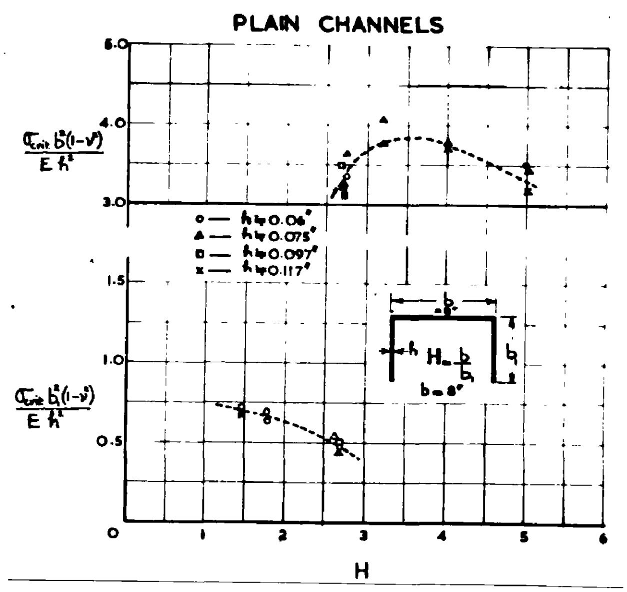
PLAIN CHANNELS
H = b/b₁
b = 8"
H

Fig. (72)

Test Series (a)

The first series of tests were carried out to asses the effect of dimension variations on the elastic critical and maximum load carrying capacity of various structural sections, and also to determine the co-relation between the critical and maximum stresses.

The following groups of experiments were performed in Test Series (a).

Group 1. The first group of tests covered a wide range of lipped and plain channel sections and was intended primarily as a means of studying experimentally the variation of critical stress in local instability with the change in the web to flange width ratio H.

Tests were carried out on lipped channels with constant outside web size of 8", length of 6·4" and lip size of $\frac{3}{4}$" to $1\frac{1}{2}$". Sets of 3 to 4 specimens for three different thicknesses with the flange size varying from 2" to 6" were tested. Twenty two plain channels of various thicknesses and of constant web size of 8", and length of 12·7" with the flange size varying from 1·6" to 5·5" were also tested.

The variation of the critical stresses with H for lipped and plain channels are shown plotted in a non-dimehsional form in Fig. (71) and (72).

The values of E and ν used in Fig. (71) and (72) are average values obtained from extensive material characteristic tests performed on flat specimen machined from the structural sections. These tests

EQUAL ANGLE SECTIONS

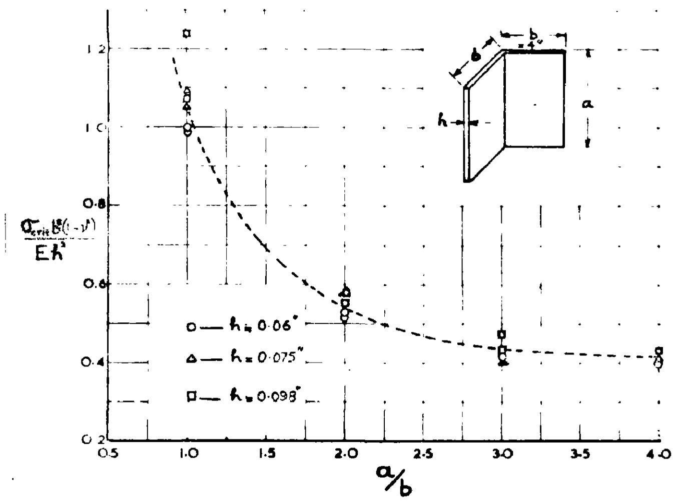

Fig.(73)

LIPPED CHANNEL

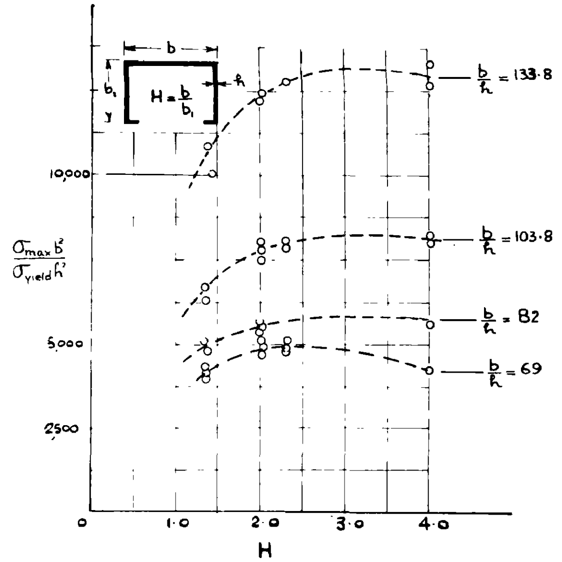

Fig.(74)

PLAIN CHANNELS

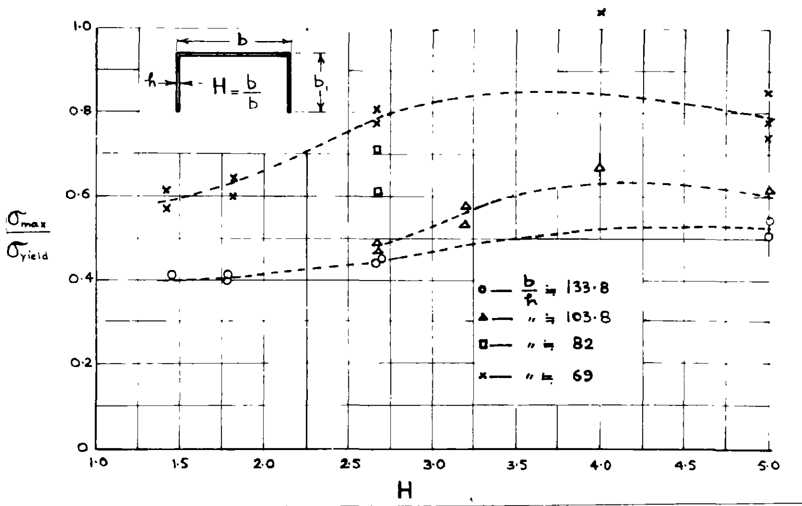

Fig.(75)

EQUAL ANGLES

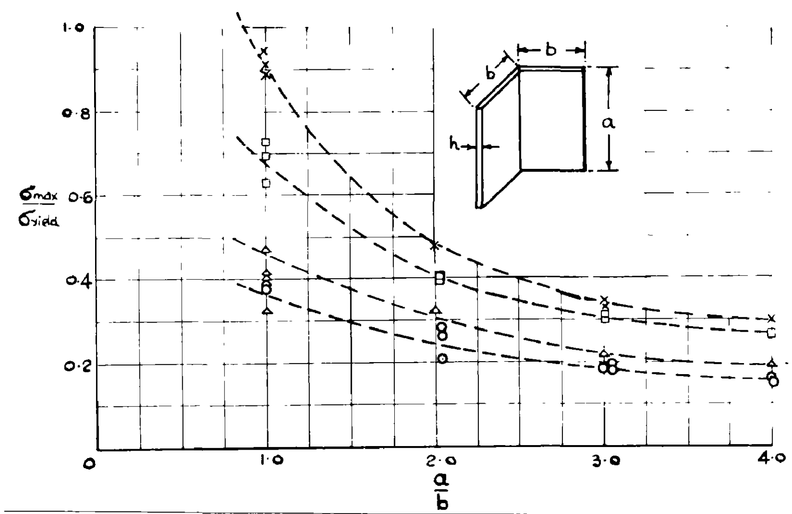

Fig.(76)

are discussed in detail in Appendix 5 .

Group 2. The second group of tests were carried out to determine the variation of critical stress of equal angle sections with the change in length. Thirty-eight equal angle sections of 4" leg size and four different thicknesses and the lengths varying from 4" to 16" were tested. Results obtained are shown in Fig. (73) .

Group 3. Although the first and second group of tests in this series were concerned primarily with the critical stresses, the maximum loads supported by the specimens were also recorded and the maximum stress evaluated. It was found (See Appendix 5) that the yield stresses of mild steel used for these structural sections varied considerably from one thickness to another, and since the maximum stress depends upon the yield strength of the material, therefore curves of $\sigma_{max}/\sigma_{yield} \sim H$ were plotted for lipped and plane channels and are shown in Figs. (74) and (75) . The results of $\sigma_{max}/\sigma_{yield} \sim a/b$ for angle sections are shown in Fig. (76).

Group 4. This group of tests was carried out to determine experimentally the co-relation between the critical and maximum stresses, in local instability, carried by various structural sections. Critical stresses and maximum stress of about 160 lipped channels, plain channels, equal angle sections and box sections were recorded.

Plotted results of $\sigma_{crit}/\sigma_{yield}$ against $\sigma_{crit}/\sigma_{max}$

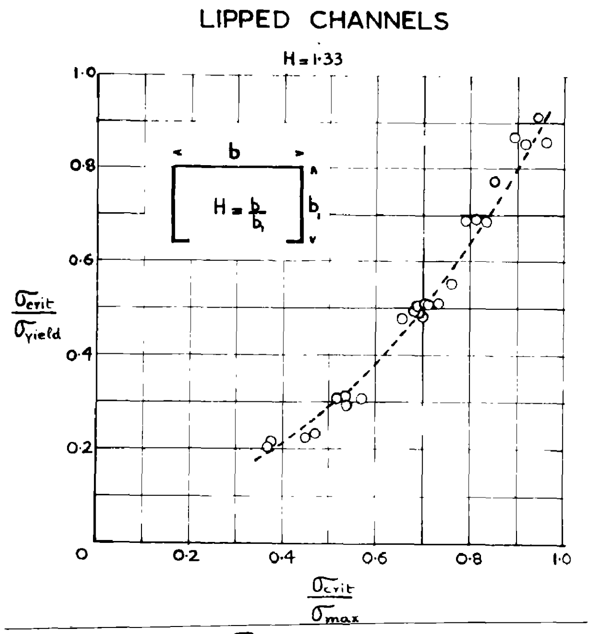

Fig. (77)

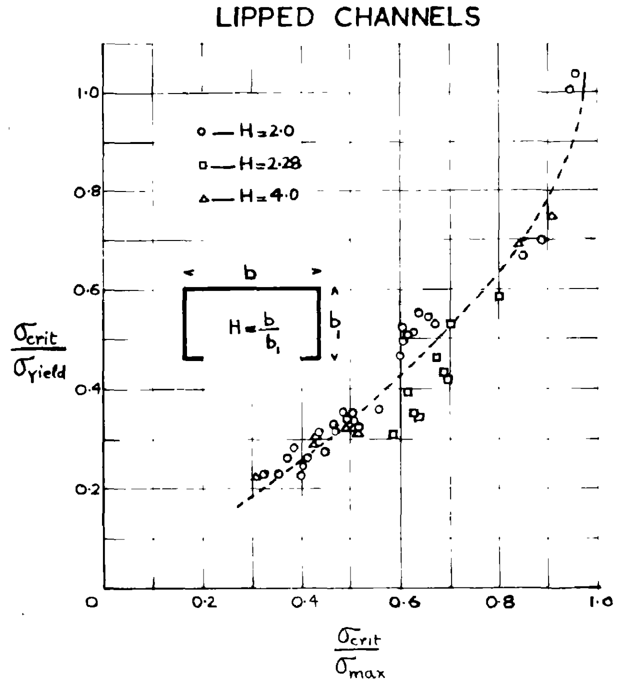

Fig. (78)

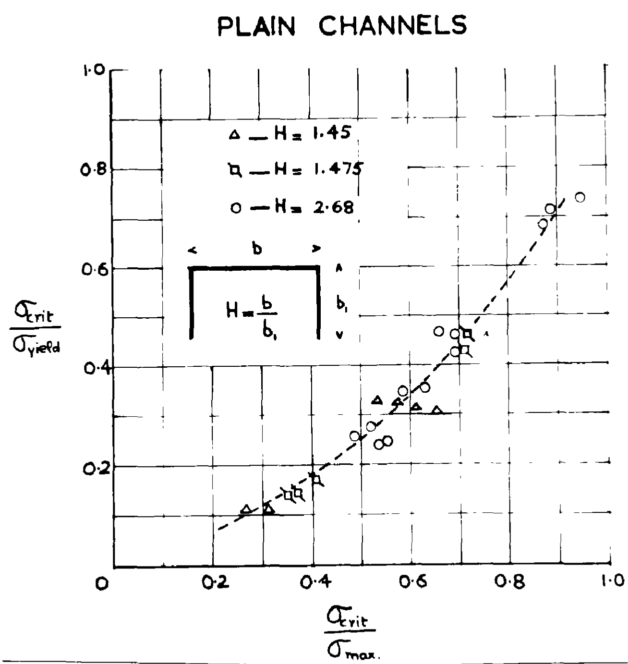

Fig. (79)

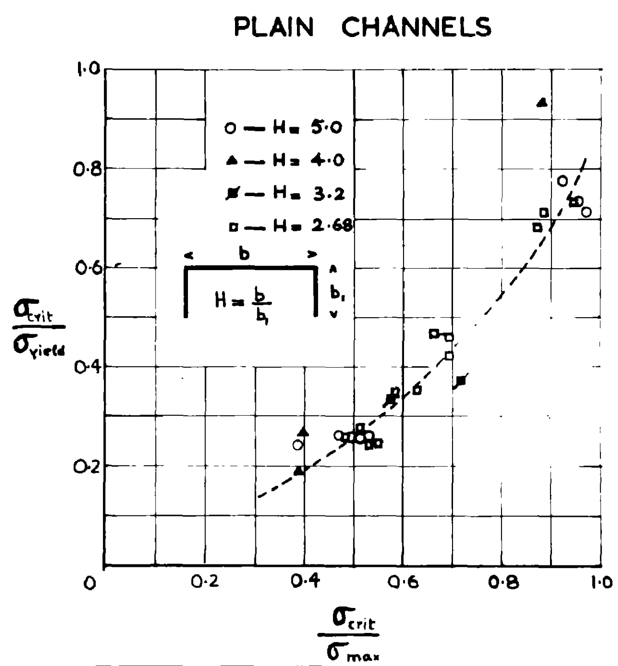

Fig. (80)

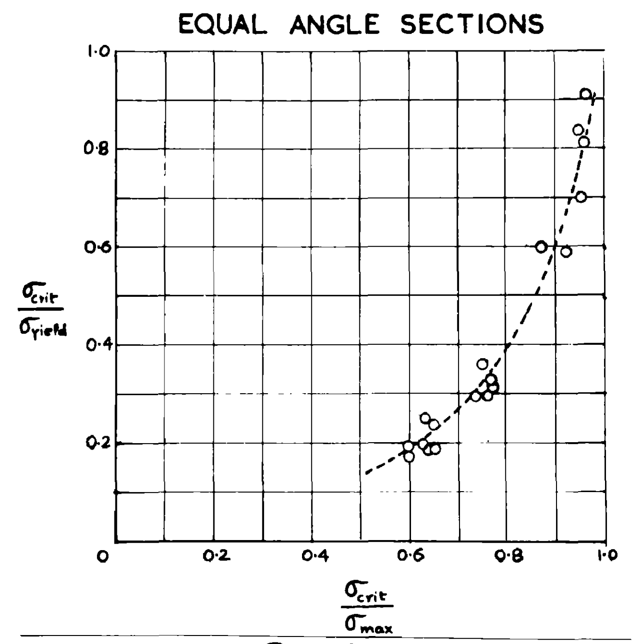
EQUAL ANGLE SECTIONS
1·0
0·8
0·6
0·4
0·2
0
0·2
0·4
0·6
0·8
1·0
$\frac{\sigma_{crit}}{\sigma_{yield}}$
$\frac{\sigma_{crit}}{\sigma_{max}}$

Fig.(81)

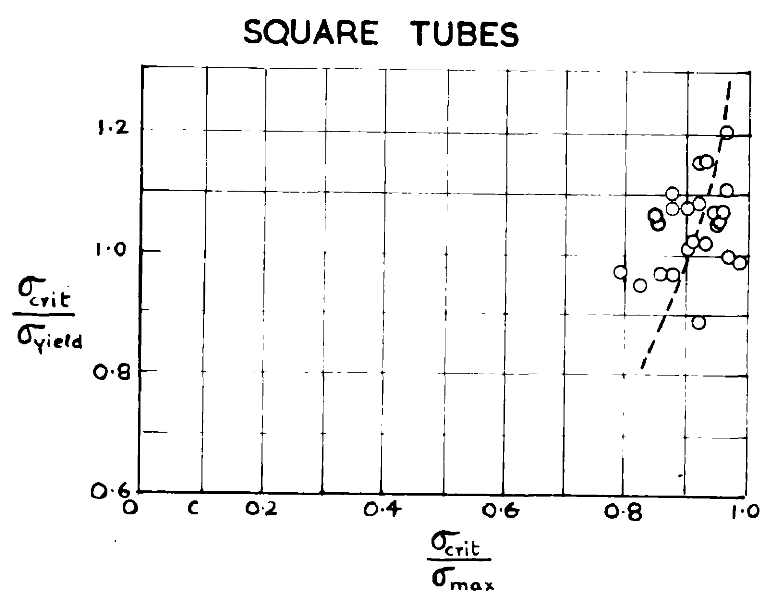
SQUARE TUBES
1·2
1·0
0·8
0·6
0
0·2
0·4
0·6
0·8
1·0
$\frac{\sigma_{crit}}{\sigma_{yield}}$
$\frac{\sigma_{crit}}{\sigma_{max}}$

Fig.(82)

for various μ values of lipped channels are shown in Figs. (77) and (78). Similar results for plain channel sections and equal angle sections are shown in Figs. (79), (80) and (81).

The square tube sections tested were all in the range of material failure and the results for these are shown in Fig. (82).

Test Series (b):

In this series tests were carried out to determine the strain distributions and deflection forms across the plate components of various structural forms. The tests have been devided up into two groups and the techniques of testing is described for each group.

Group 1. In the first group of tests strain distributions across the central section of lipped channels, plain channels and angle sections were determined experimentally.

Electrical resistance strain gauges were placed in the direction and normal to the direction of the load on both faces of the plate components of structural sections. The corresponding strain gauges were connected in series to compensate for the bending strains and thus make it possible to ascertain the middle plane strains. To make sure that the applied load was uniformly distributed across the loaded edges, strain readings, in the direction of the applied load, ϵ_x were measured at a small load and the position of the specimen relative to the knife edge of the loading

LIPPED CHANNEL

8" x 6" x 1½" x 0·0748" thk. x 6·39" lg.

DISTRIBUTION OF STRAIN ϵ_x ACROSS THE CENTRAL X-SECTION

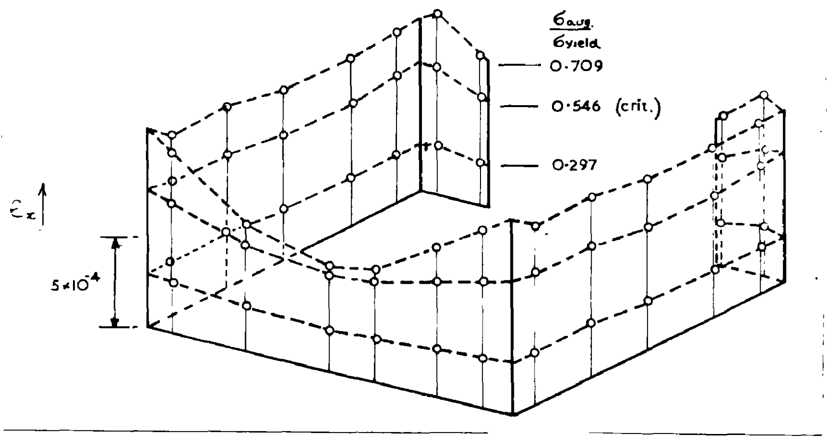

Fig. (83)

LIPPED CHANNEL

8" x 6" x 1½" x 0·0748" thk x 6·39" lg.

DISTRIBUTION OF STRAINS ϵ_x AND ϵ_y ACROSS THE CENTRAL X-SECTION

Fig. (84)

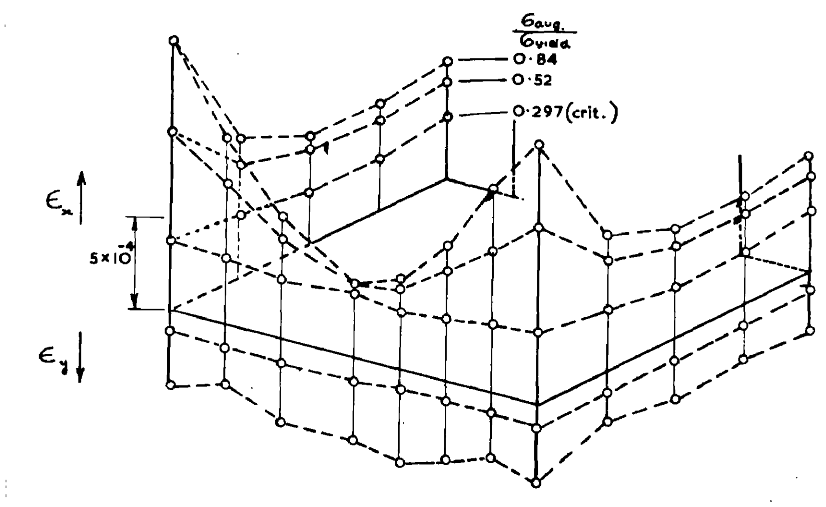

PLAIN CHANNEL

8" x 2·95" x 0 075" thk x 12·78" lg.

Distributions of Strains ϵ_x and ϵ_y Across the Central X-Section

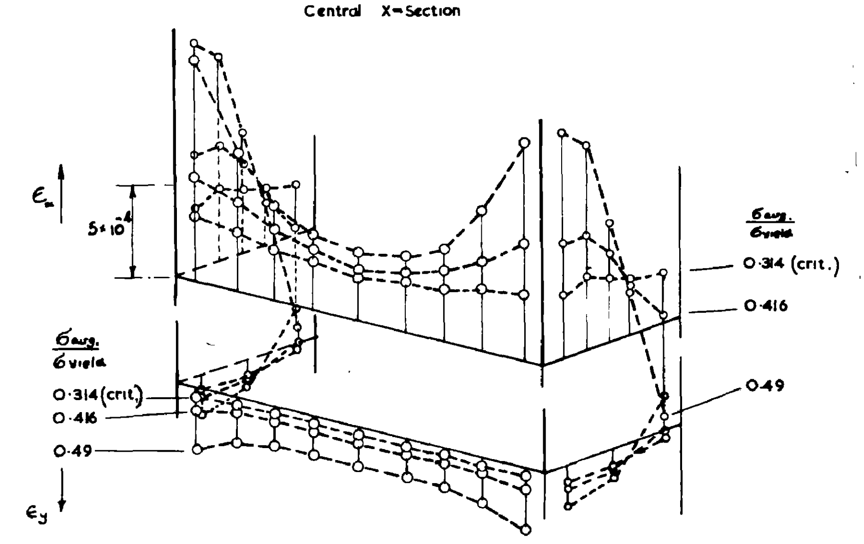

Fig. (85)

EQUAL ANGLE

$4'' \times 4'' \times 0{\cdot}117''$ thk. $\times 8''$ lg.

Distribution of Strains ϵ_x and ϵ_y Across the Central X-Section

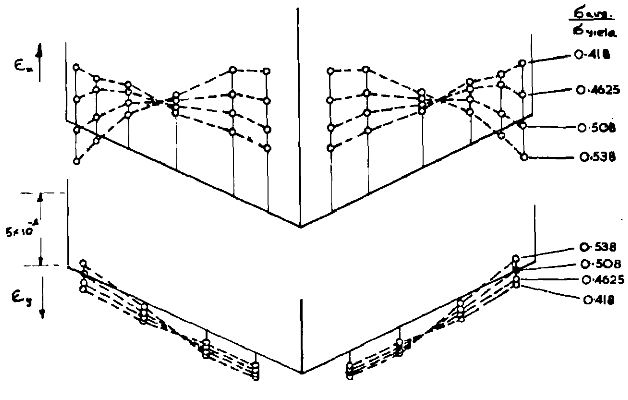

Fig.(86)

SQUARE TUBE

$3.5'' \times 3.5'' \times 0.1435''$ thk. $\times 5.25''$ lgth.

DISTRIBUTION OF STRAIN ACROSS THE CENTRAL X-SECTION

Fig.(87)

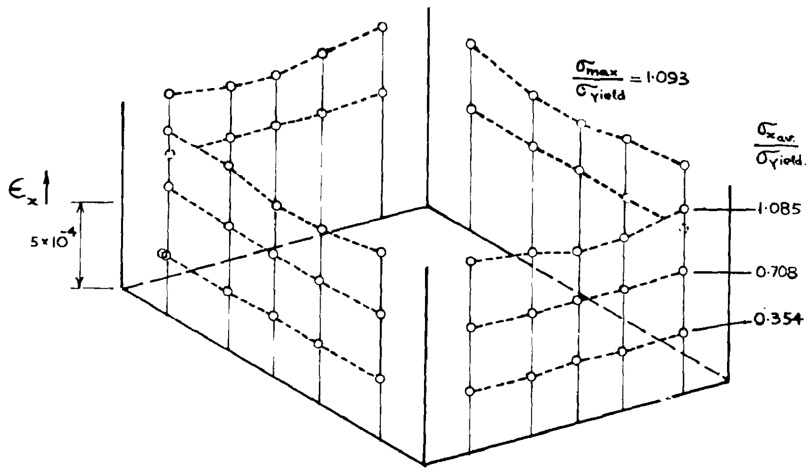

LIPPED CHANNEL

$8'' \times 6'' \times 1.5'' \times 0.0748''$ thk. $\times 6.39''$ lgth.

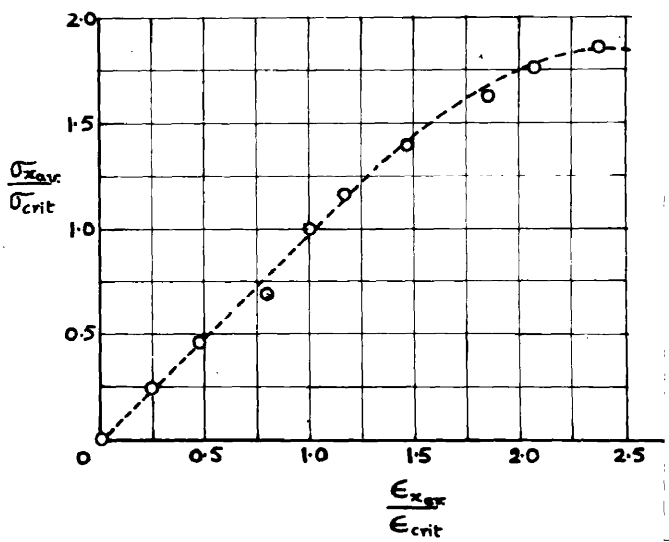

Fig.(88)

PLAIN CHANNEL

$8'' \times 2.95'' \times 0.075''$ thk. $\times 12.78''$ lgth.

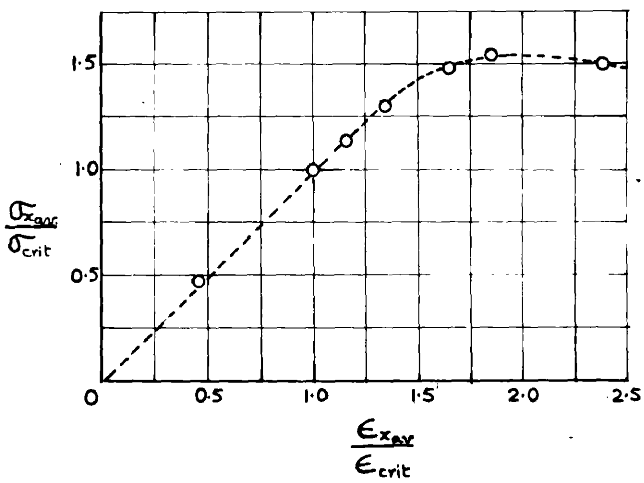

Fig.(89)

plattens adjusted to give approximately equal ϵ_x values. After the specimen was set ϵ_x and ϵ_y strains were measured at a large number of loads. Each of the strain readings were plotted against the ratio average stress/yield stress and "best" curves drawn, readings at selected values of $\sigma_{x\,av.}/\sigma_{yield}$ being then obtained from these curves. Some of the typical results are shown. Figs. (83) and (84) give the distributions of strain across the web and flange of two lipped channels at selected $\sigma_{x\,av.}/\sigma_{yield}$ values. The strains in the case of the flange are averages of the two flanges. Fig. (85) shows the strain distributions across the centre of a plain channel obtained in a similar manner as for the lipped channel. In Fig. (86) and (87) are shown strain distributions across the centre line of an equal angle section and a square tube respectively.

The total average strain $\epsilon_{x\,av.}$ was also evaluated at various loads for the above cases considered and curves of $\sigma_{x\,av.}/\sigma_{crit} \sim \epsilon_{x\,av.}/\epsilon_{crit}$ are shown plotted in Figs. (88) and (89).

Group 2. The second group of tests in this series was carried out on lipped channels for determining the deflected surfaces of various plate components. A Moiré method was developed for determining the slope contours on the actual structural sections. The theoretical background and the development of this technique are discussed in detail in Appendix 6 .

Flange

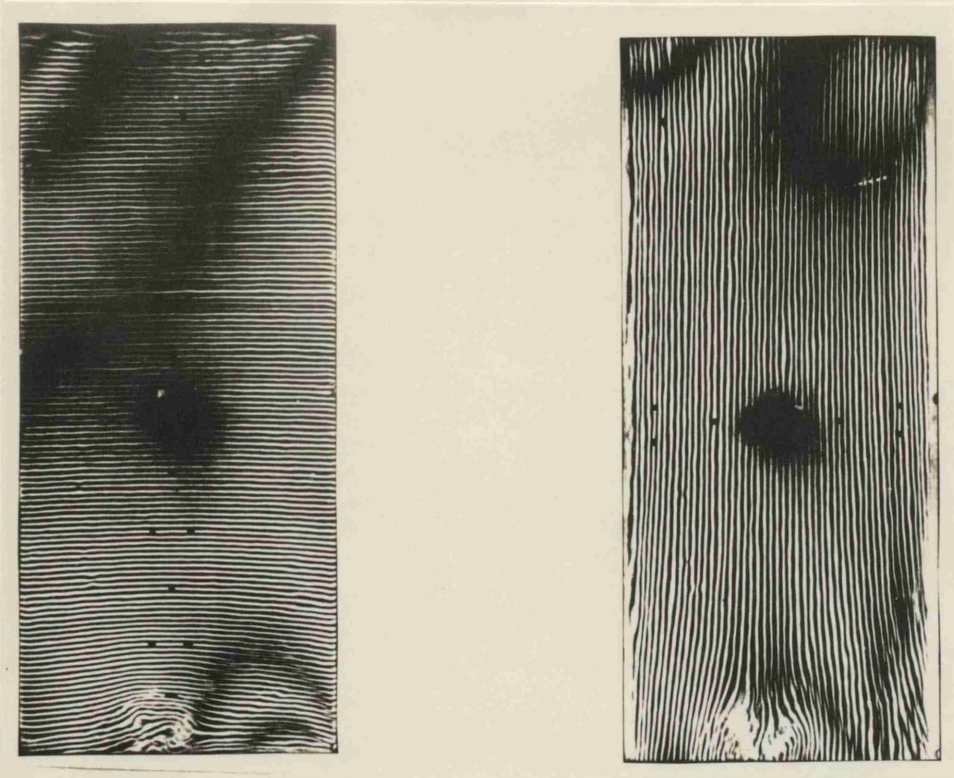

Fig. (90)

Web.

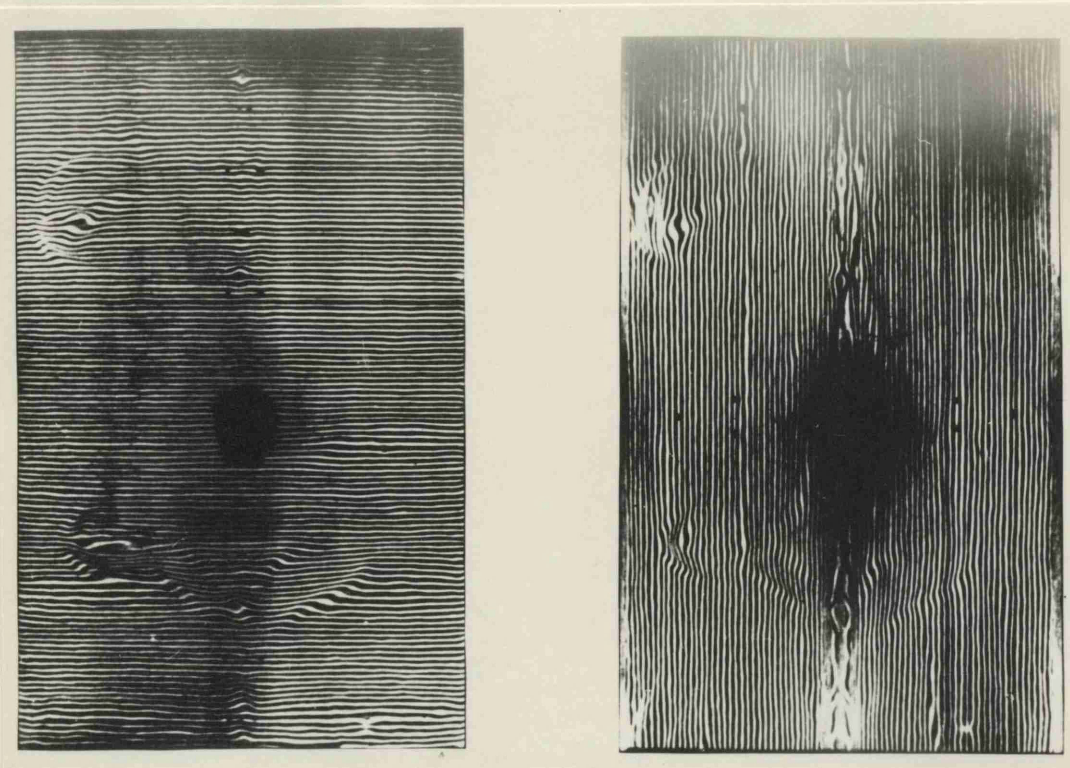

Fig. (91)

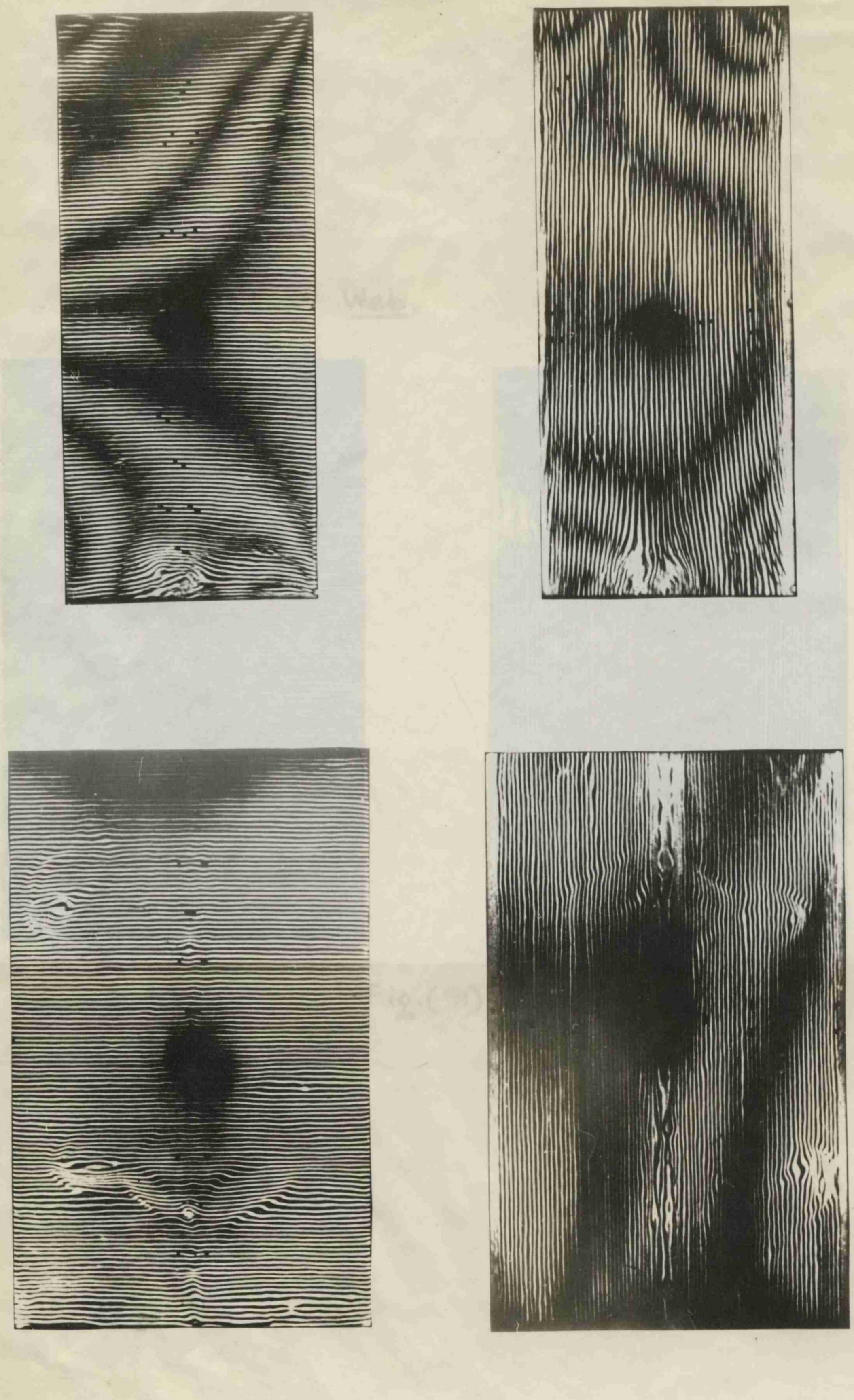

Fig. (92)

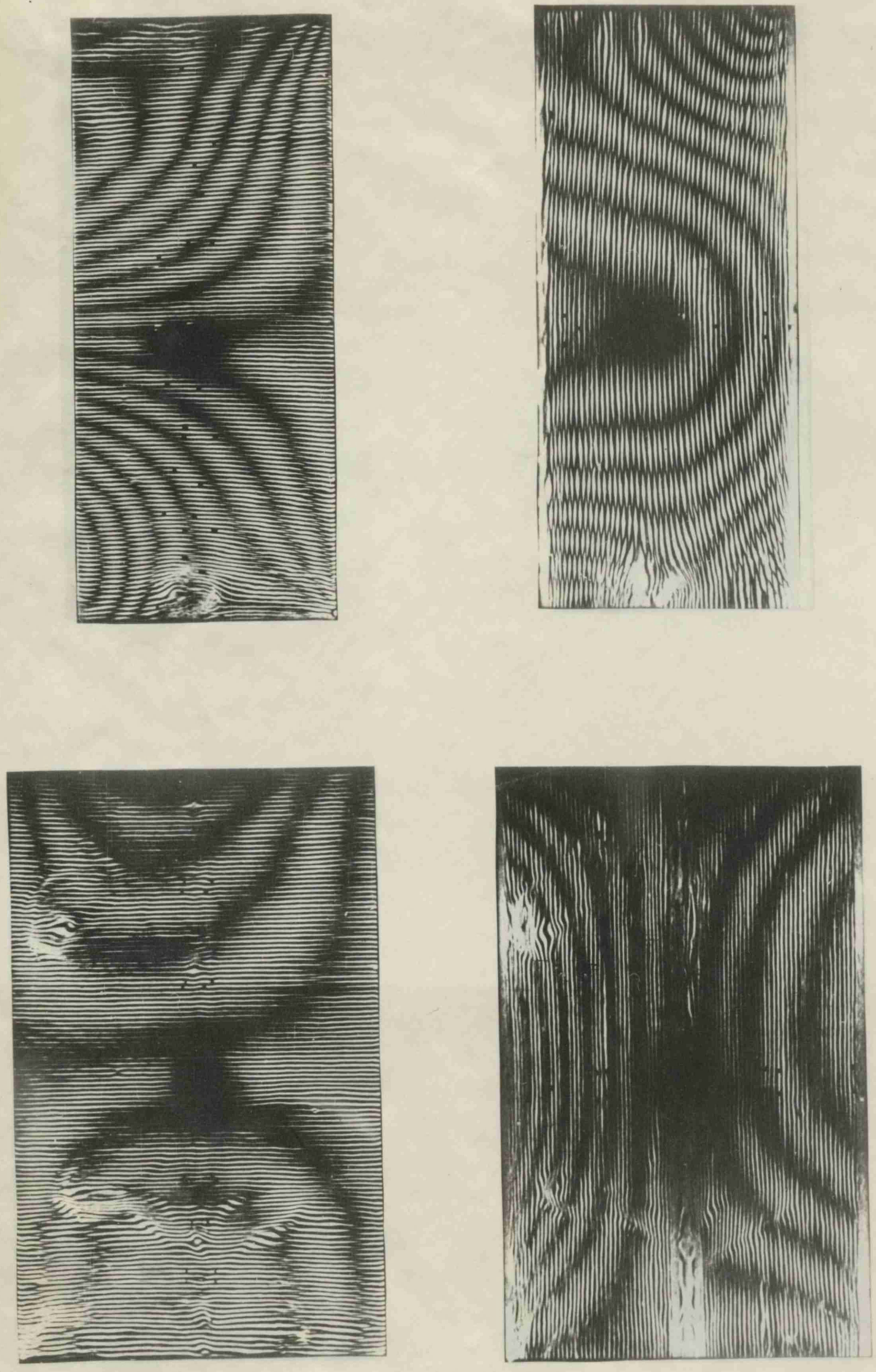

Fig. (93)

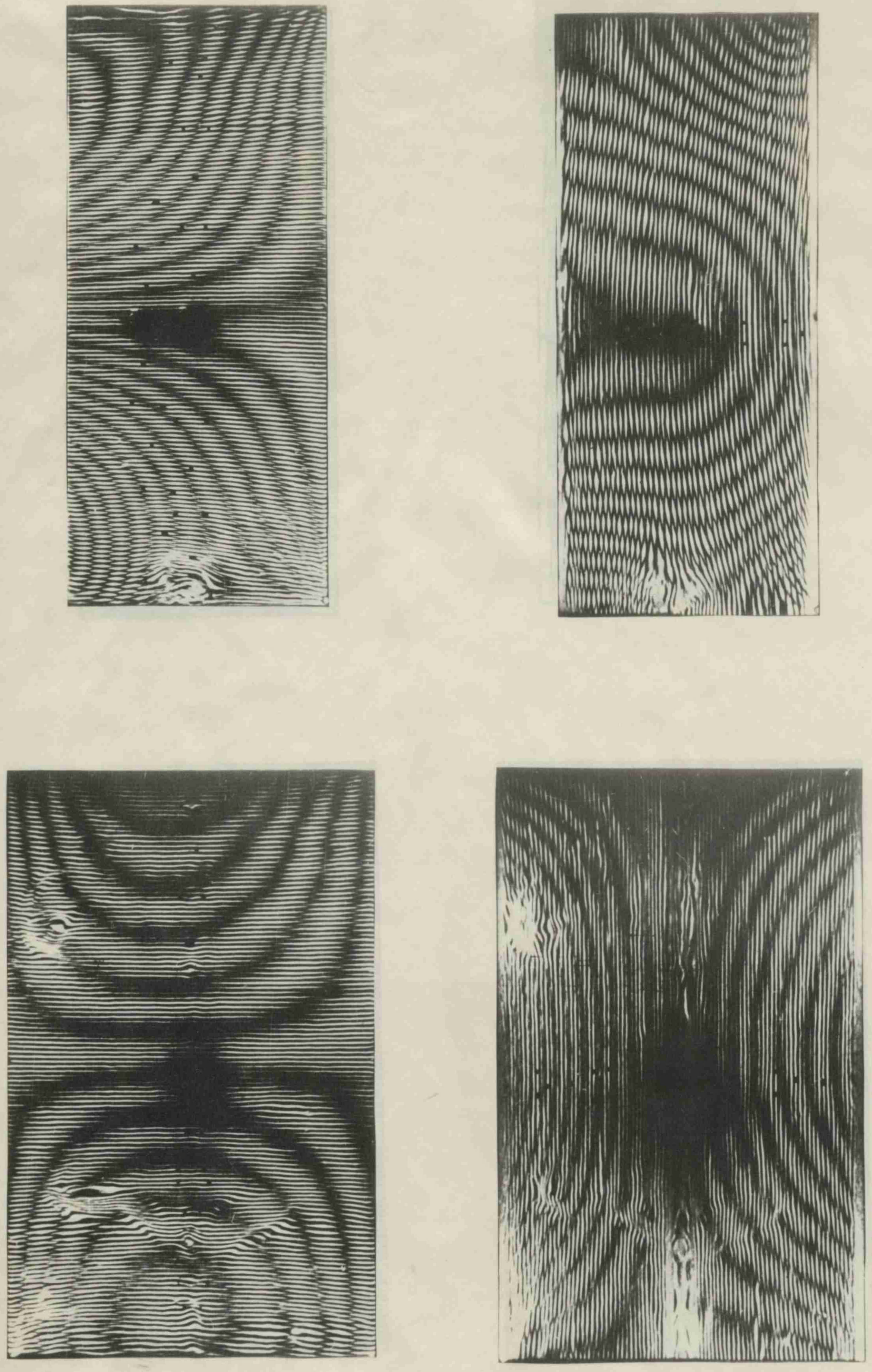

Fig. (94)

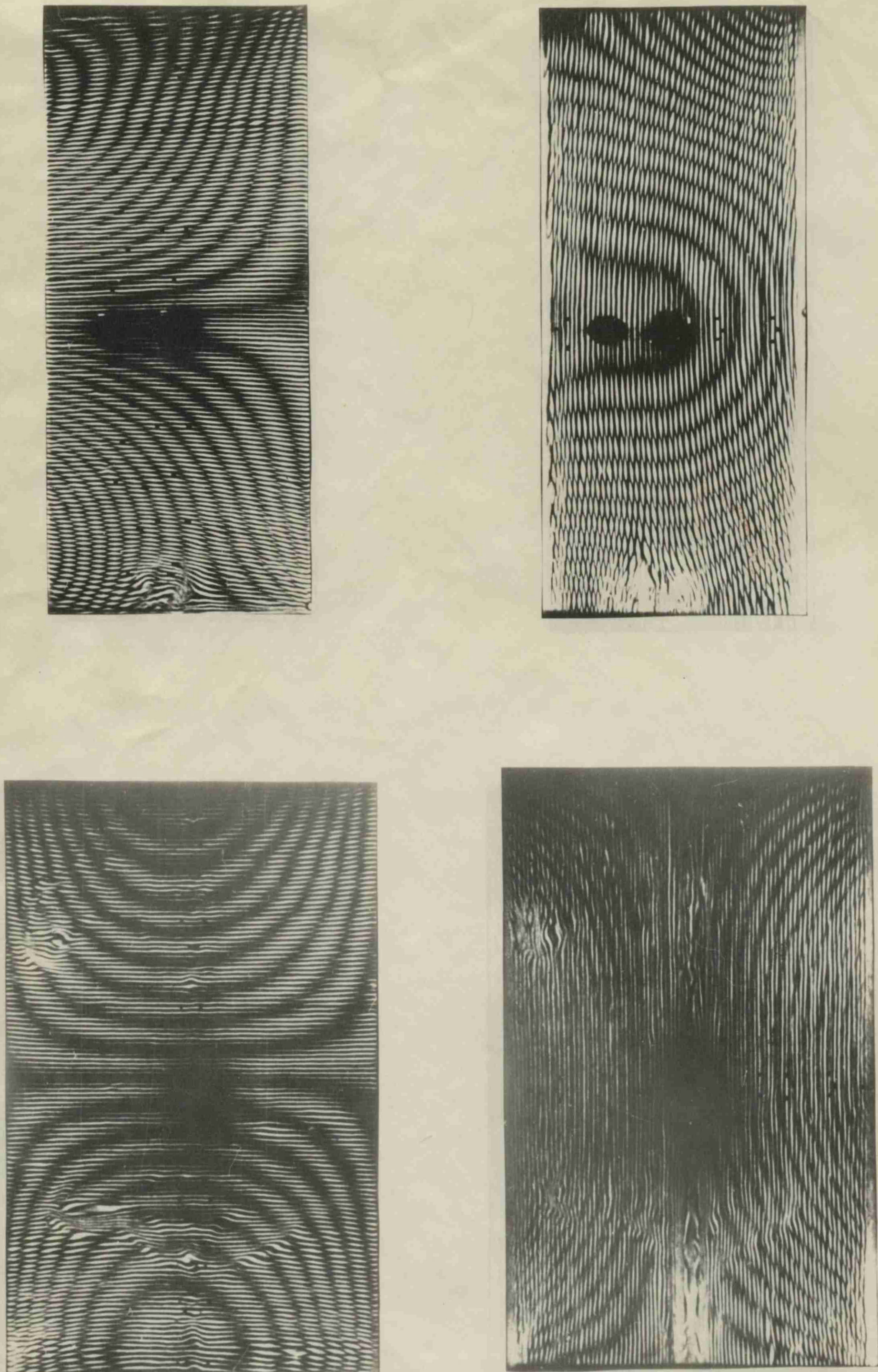

Fig. (95)

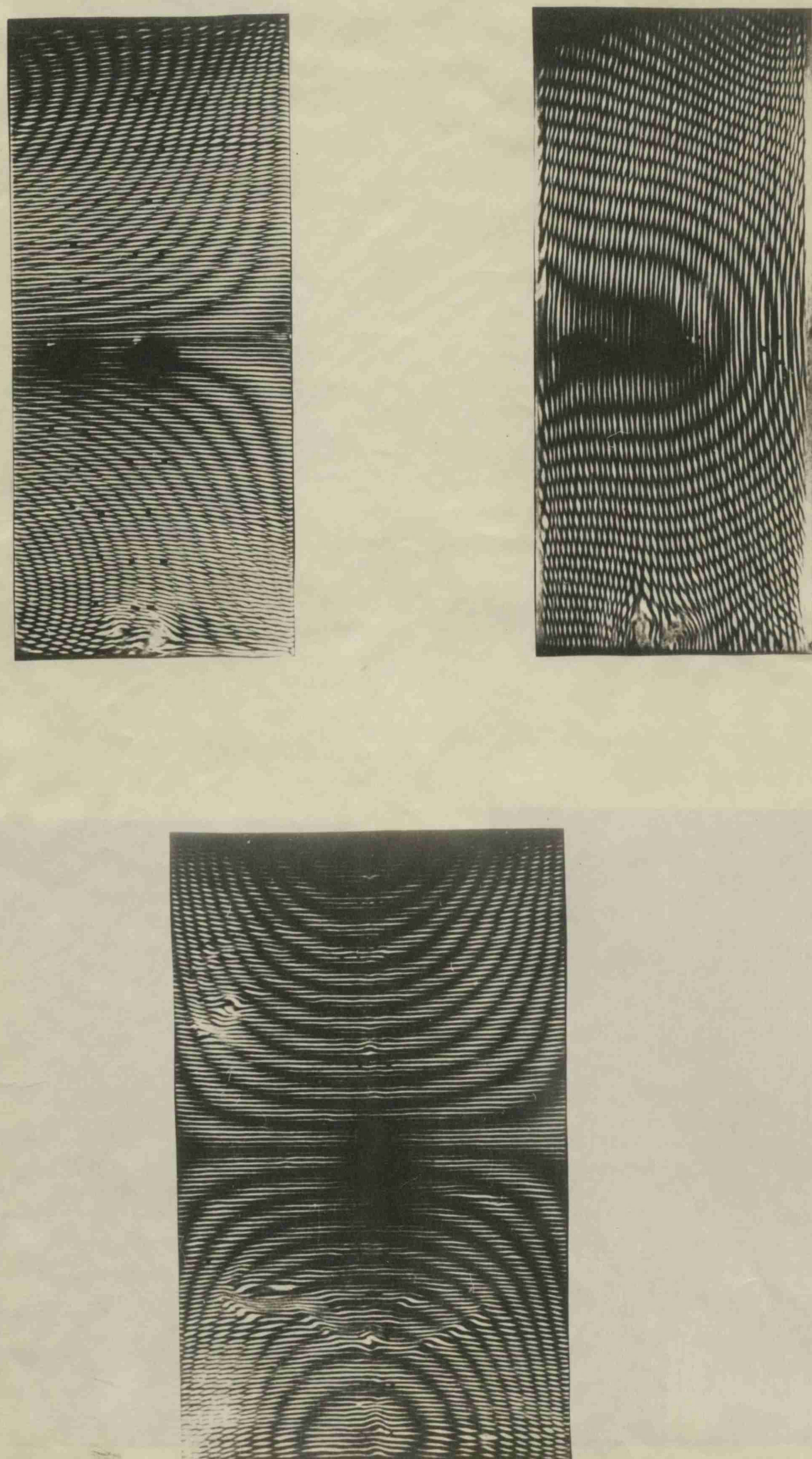

Fig.(96)

Briefly, the method consists in taking photographs of a grid or ruled screen reflected from the polished surface of the unloaded specimen plate and superimposing on this a photograph of the screen reflected from the same surface in the loaded specimen. If the specimen deflects during loading Moiré fruiges, i.e. contours of constant slope are obtained. The ruled screen consisted of parallel straight black and white lines of equal thickness $d/2$. If the vertical axis of the specimen is denoted by x, then if the ruling on the screen is horizontal the Moiré fruiges are equivalent to contours of $\partial w/\partial x$. If, however, the ruling of the screen is vertical, $\partial w/\partial y$ contours are obtained. It has been shown in the Appendix 6 that these slope contours have an interval $d/2c$ where c is the distance between the screen and the specimen.

A typical set of photographs at various loads obtained by this method for a plain channel web and flange are shown in Fig.(90) to(96) inclusive.

A method of marking the ruling on the screen was employed (See Appendix 6) so that the absolute value of the slope contours could be obtained. Once the absolute values of the contours are known the distributions of slopes across any section can be obtained and by means of graphical integration the deflected form evaluated.

The method of obtaining the deflections is illustrated in the Appendix.

Some typical results obtained by this method are ( )

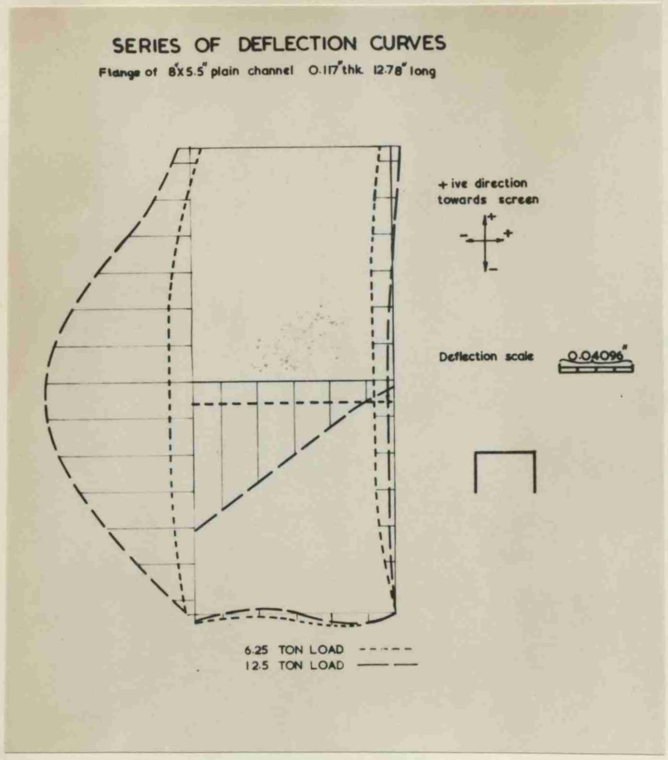

Fig.(97)

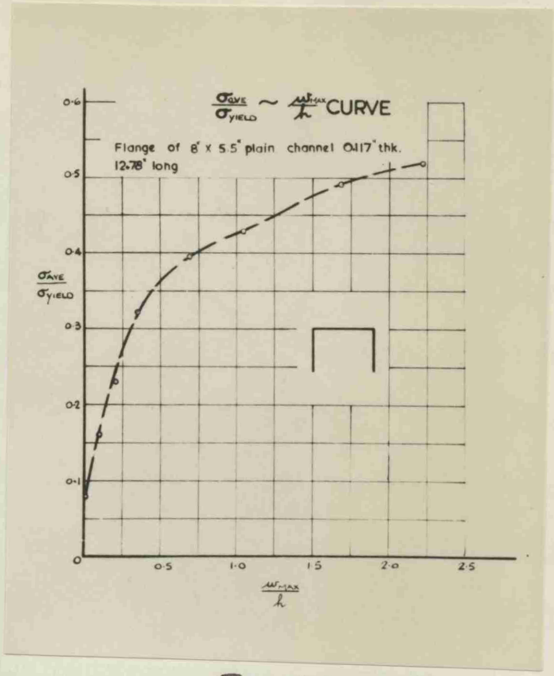

Fig.(98)

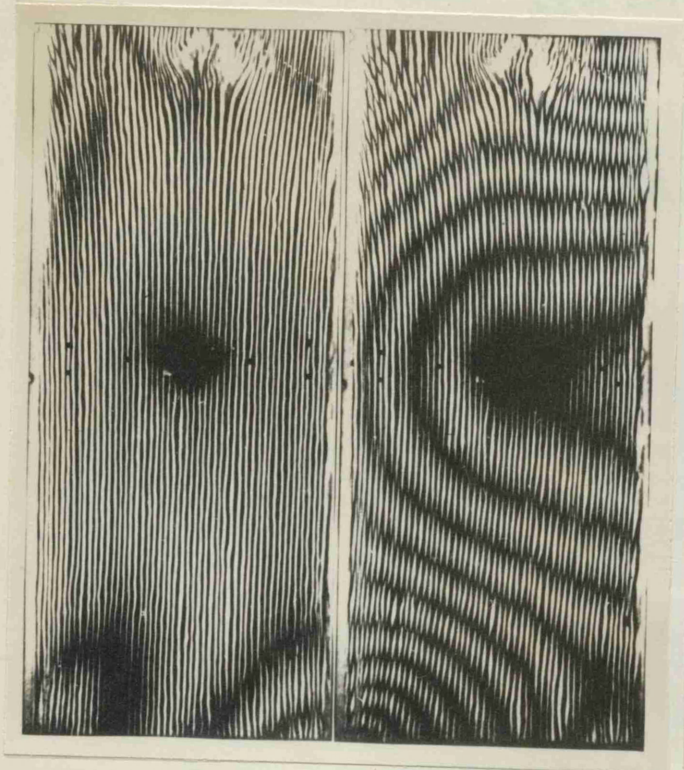

6·25 Tons 12·5 Tons

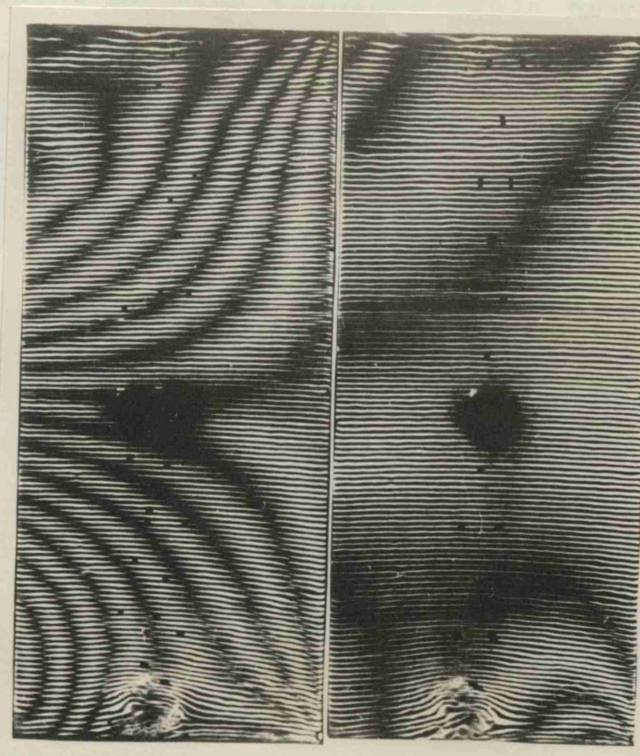

12·5 Tons 6·25 Tons.

Fig.(97)

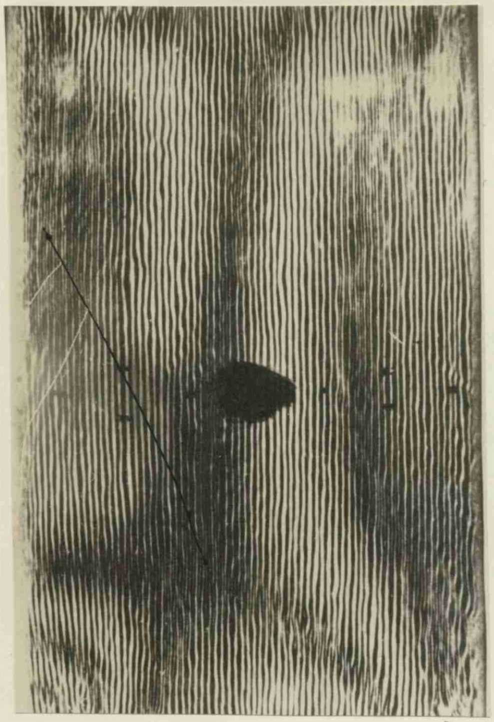

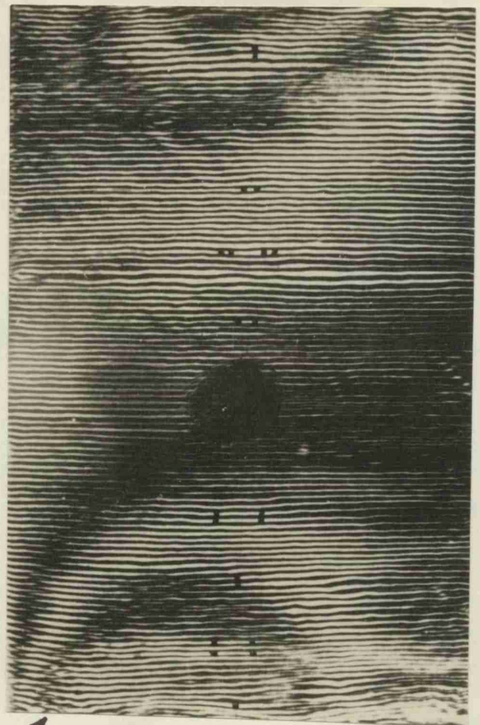

10 Tons.

21·5 Tons

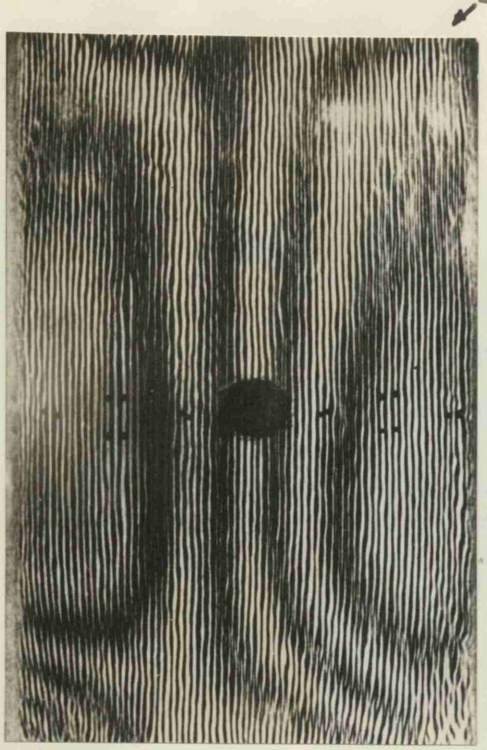

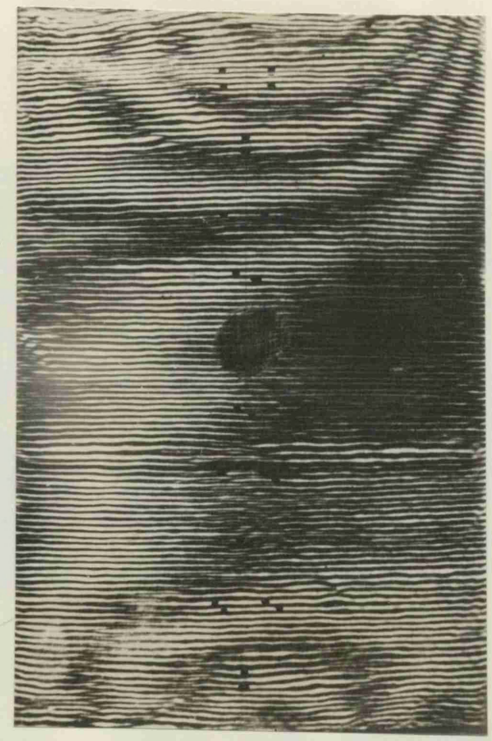

Fig. (99)

shown in Fig.(97) to (99) . Fig. (97) gives the distribution of deflection along various sections of the flange of a plain channel corresponding to a load P values of 6·25 & 12·5 T. In Fig. (98) is shown the plot of $\sigma_{x_{av}}/\sigma_{yield}$ against the maximum deflection of the same flange and Fig. (99) gives the deflection distributions, in the post-buckling range, along various sections of the web of a lipped channel; the corresponding Moiré fringe photographs are also shown in these figures. Further similar results are presented in the Appendix 6 .

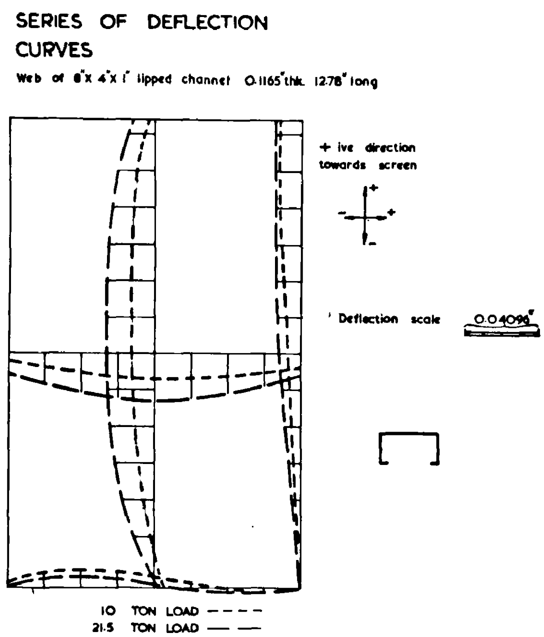

Fig.(99)

SECTION 6

ANALYSIS AND DISCUSSION OF RESULTS.

ANALYSIS AND DISCUSSION OF RESULTS.

6.0 CRITICAL STRESS INITIATING ELASTIC INSTABILITY:

As a preliminary to the major portion of the work undertaken; that dealing with the collapse as opposed to the initiation of buckling conditions it was considered necessary to assess the reliability of the theory concerned with the elastic critical stresses presented in Section 2. Further the determination of the elastic critical stress is a necessary preliminary to the evaluation of the maximum stress as indicated in the theoretical work.

Some one hundred and thirty specimens of lipped and plain channels, and equal angle sections were experimentally tested providing as far as elastic critical conditions were concerned examples of flat components under a variety of edge conditions. In every case the specimen lengths were so chosen that purely local failure un-influenced by overall instability was achieved.

Fig.(100, 101)and (102) present a comparison of some typical experimental and corresponding theoretical critical stress results for a representative range of specimen. The results are presented in a non-dimensional form allowing for the effect of the modulus of elasticity which was determined from tests on several specimens (four to six) from each length of the thickness tested and

LIPPED CHANNELS

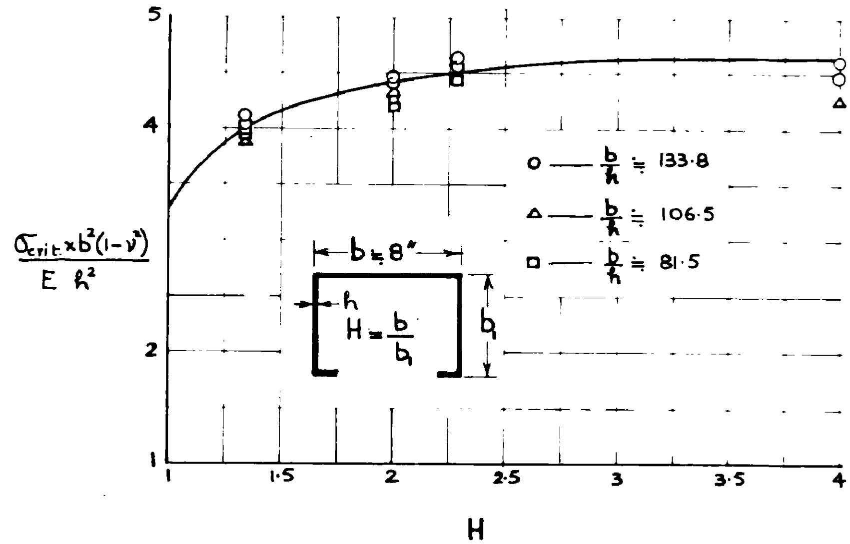

Fig. (100)

PLAIN CHANNELS

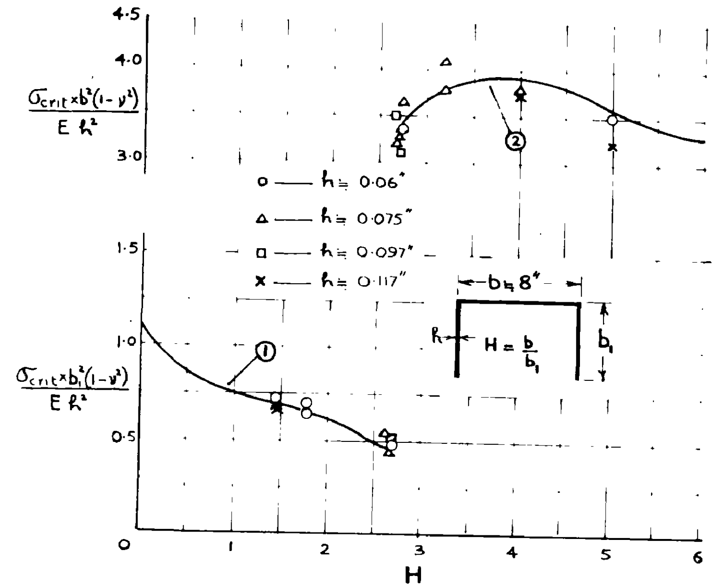

Fig. (101)

EQUAL ANGLE SECTIONS

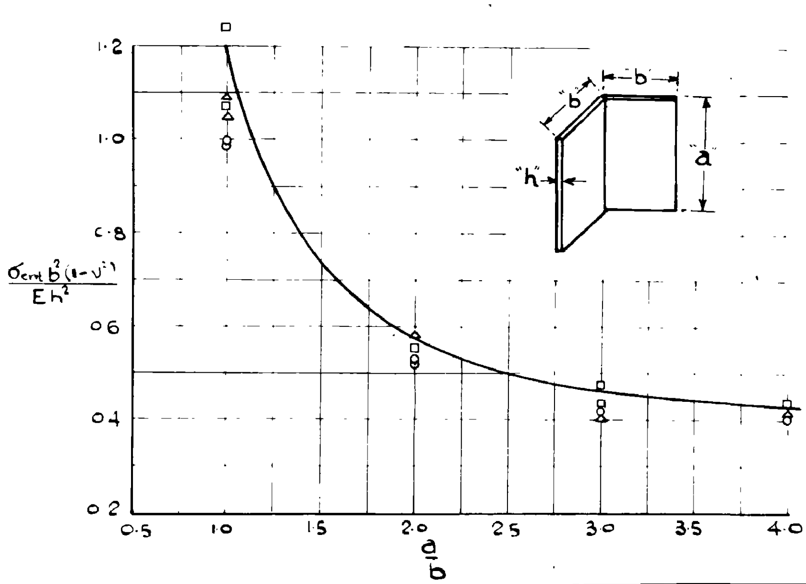

Fig. (102)

which varied from $2{\cdot}8\times10^7$ lbs./in^2 to $3{\cdot}16\times10^7$ lbs./in^2. The results of material characteristic tests are reported fully in Appendix 5.

The theoretical curves are based on the results obtained in sub-section 4.1, 4.2 and 2.0. It may be noted that the theoretical results shown in Fig.(100), (101) and (102) represent the elastic critical stress variation for plates with various edge support conditions along the unloaded edges. In Fig.(100) the web of the lipped channel is equivalent to a plate with symmetrical elastic fixity conditions: $\kappa b = \kappa_1 b$ varying from 0 to 13.5 for the range of H values shown. Similarly curve 1 in Fig.(101) for the flange of a plain channel corresponds to a plate with free conditions for one unloaded edge and elastically fixed along the other; the κb values varying from 0 to ∞. Curve 2 in the same figure for the web of a plain channel is a similar case to that of Fig.(100) with the $\kappa b = \kappa_1 b$ values varying from 0 to 3.0. Finally the theoretical curve in Fig.(102) corresponds to simply supported and free conditions along the unloaded edges.

The experimental critical stresses were determined by using the "top of the knee" method described in Section 5.0. The first was based on load against deflection variation corresponding to the plate component first exhibiting the onset of elastic instability. The deflections were measured by dial gauges at or near the point of maximum

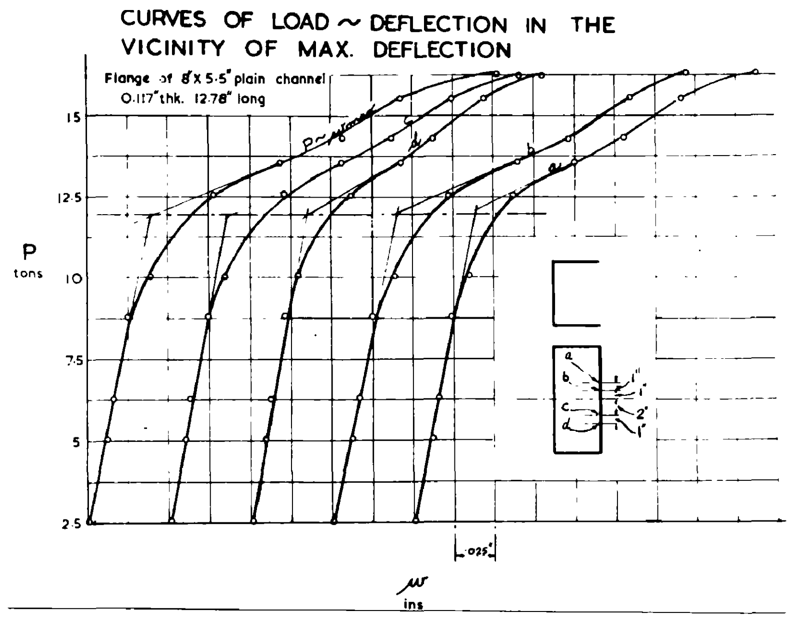

CURVES OF LOAD ~ DEFLECTION IN THE VICINITY OF MAX. DEFLECTION
Flange of 8"x 5·5" plain channel
0·117" thk. 12·78" long
P
tons
15
12·5
10
7·5
5
2·5
·025"
w
ins
a
b
c
d
1"
1"
2"
1"

Fig.(103)

deflection and/or by the Moiré fringe pattern: from which the actual maximum deflection can be deducted. The second method was based on the load-relevant equivalent principal strain $(\epsilon_x + \frac{1}{2}\epsilon_y)$ variation deduced from strain rosette readings placed at the points corresponding to maximum deflection of the particular plate component.

For one fourth of the specimen sizes tested the experimental critical stress was determined using both of the procedures mentioned above. For the same material and specimen dimensions good agreement was invariably obtained by all techniques and in consequence for the remaining three quarters of the tests dial gauges, being simpler in experimental technique, were utilized. It is relevant to comment here, as will be discussed later in detail that the Moiré fringe technique extablishes the complete deflected form of the whole surface making it possible thereby to obtain deflection at any point and to pin-point the maximum deflection. It was shown by the Moire fringe technique that using the "top of the knee" method the deflection in the vicinity of the maximum deflection gives the same critical stress (See Fig.(103)). Hence it should be noted that precise positioning of the dial gauges with respect to the point of actual maximum deflection, is not critical.

Turning now to the the comparison of experimental and theoretical results presented in Figs.(100) to (102) it is seen that good agreement obtains. Fig.(102) shows that some of the experimental results particularly at $a/b = 1{\cdot}0$ tend to be somewhat lower than the theoretical

LIPPED CHANNEL (8"×6"×1")
(WEB)

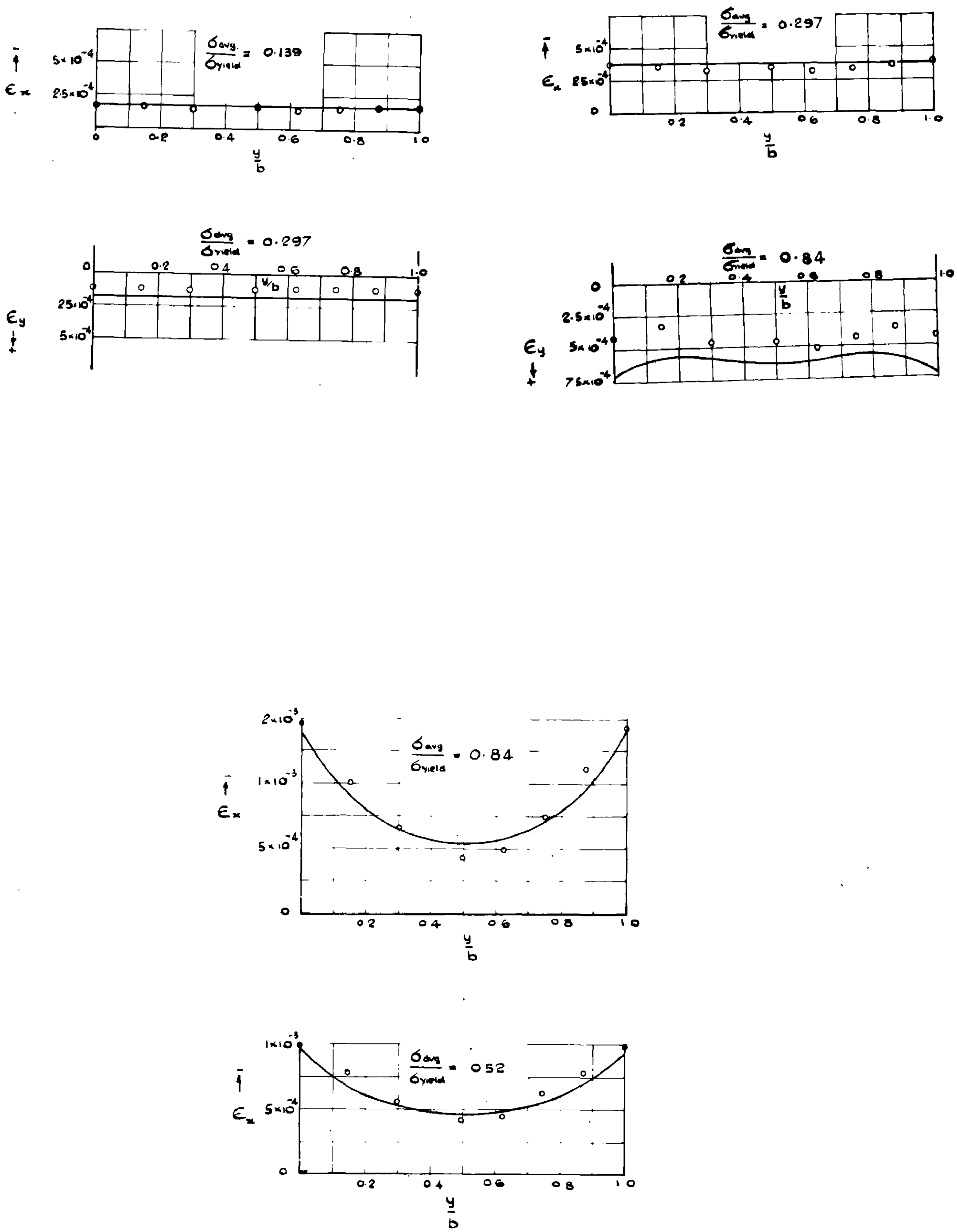

Fig.(104)

PLAIN CHANNEL
(8"×2.97")

WEB

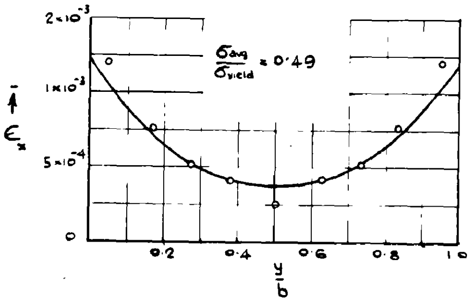

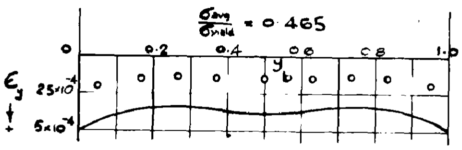

FLANGE

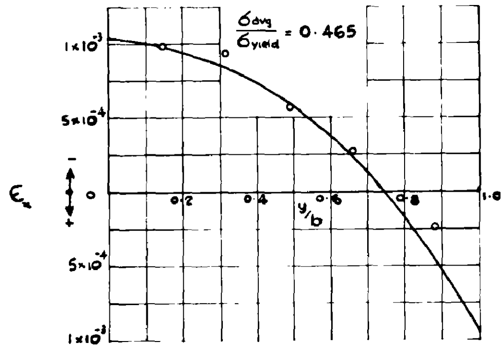

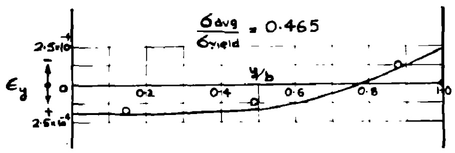

FLANGE

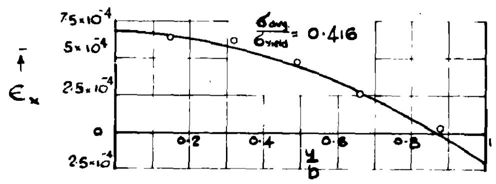

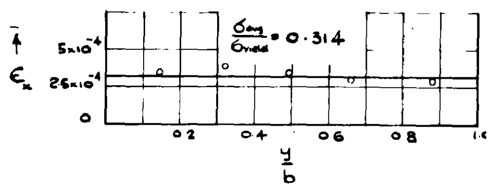

Fig.(105)

EQUAL ANGLE.

(4"x4")

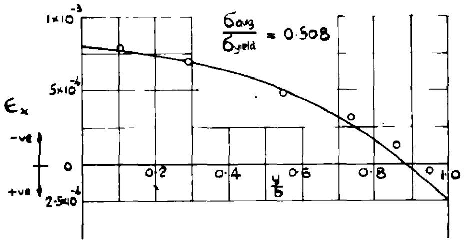

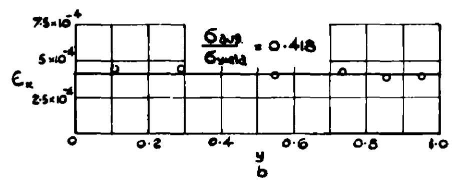

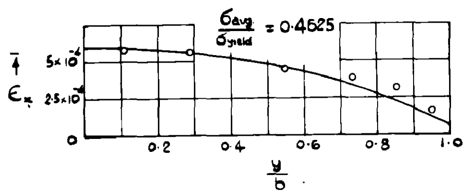

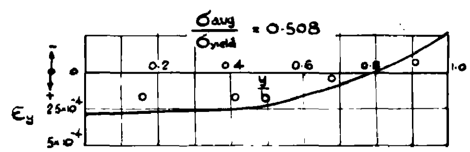

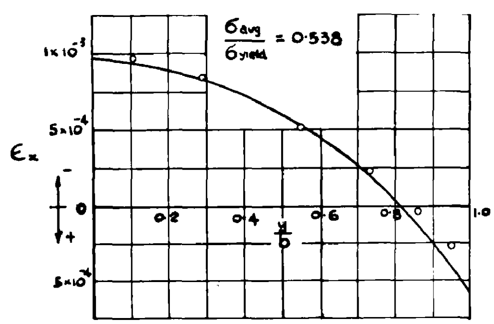

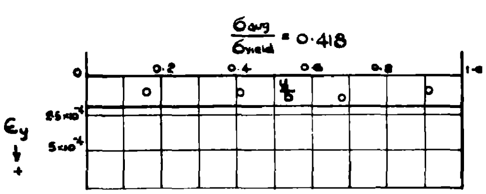

Fig. (106)

results, the deviation present apparently increasing for the smaller thicknesses tested. This is attributed to the effect of initial irregularities and the slight deformation of the "straight" connected edge, during loading, which influence the boundary conditions. In all the other results the scatter of the experimental values in general is evenly distributed about the theoretical curve.

6.1 MAXIMUM STRESS CORRESPONDING TO COLLAPSE:

The theoretical assesement of collapse conditions of plates is presented in Section 3 and their application to structural forms in Section 4.

Comparison of these results is discussed in the following, broadly on two bases. First, strain distributions were determined in a number of typical cases with the purpose to test the rationality of the theoretical treatment by comparing the experimental results with their theoretical counterparts. Secondly, the actual maximum stresses at collapse measured experimentally are compared with the theoretically predicted values.

Fig.(104) to (106) show comparison of the theoretically predicted and the experimentally measured strain distributions across the central cross-section of the plate components (of lipped and plain channel, and equal angle sections) in which elastic instability was initiated first. Graphs presented show values of the longitudinal and lateral strains ϵ_x and ϵ_y respectively up to as near the collapse as was possible to measure. It must be clearly noted that the experimental measurements of strains, as has already been indicated, were carried out on plate components of structural sections. The theoretical analysis presented in Section 3 was developed for individual plates with precisely defined edge conditions along the unloaded edges with the loaded edges simply supported. This theory is then applied in Section 4 to the failure of the plate components of structural sections introducing the assumption of constancy of the edge support condition along the unloaded edges during the period defined by the initiation of elastic instability and collapse. The comparisons that follow test both this assumption of constancy and the theory developed for single plates. The agreement between the experimental and the theoretical forms of distribution may be looked upon as a measure of the reliability of the theory as a whole, while that of the deviation in magnitude of the relevant values may be taken to be indicative of the extent to which the assumption of constancy of edge support applies.

It will be noticed from the comparisons that, although, in magnitude the experimental values of ϵ_x are slightly smaller than the theoretical near the points of maximum deflection and tend to be larger near the edges, the form of distributions in every case corresponds to the theoretically predicted ones. The agreement obtained is considered both good and rational, keeping in mind this assumption of constancy of the elastic

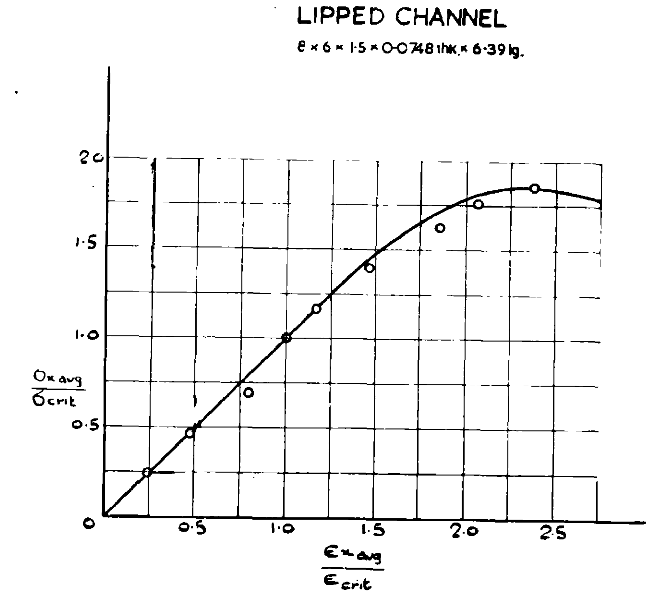

Fig. (107)

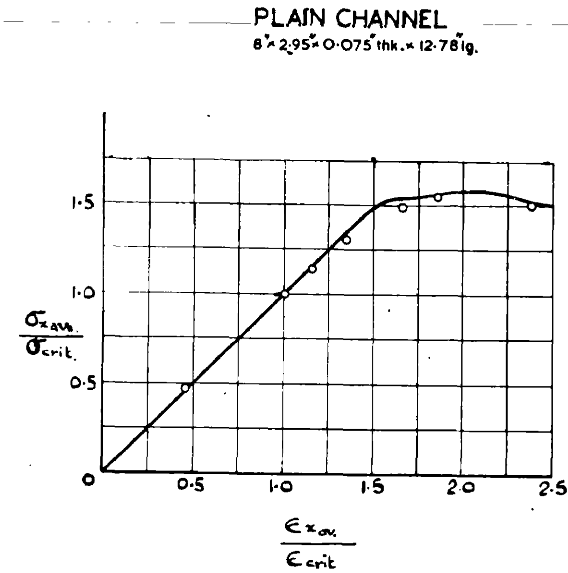

Fig. (108)

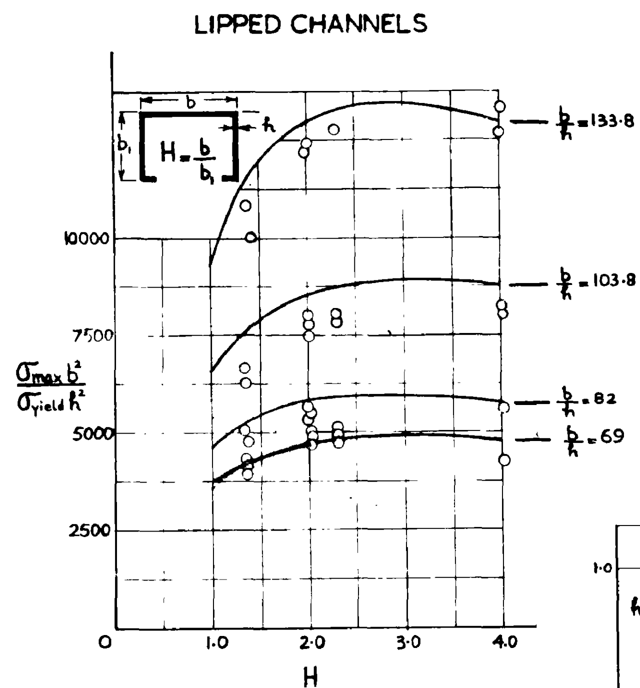

Fig. (109)

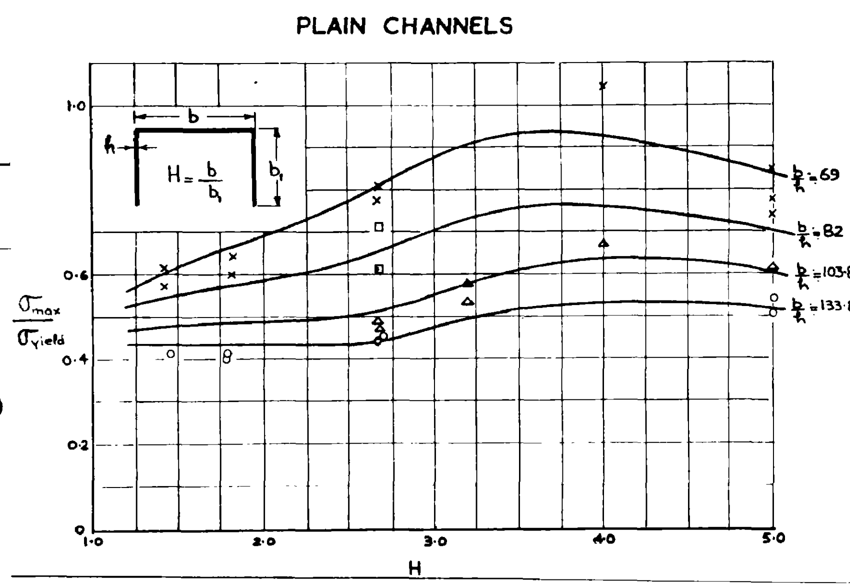

Fig. (110)

edge support fixity and the existence of slight non-uniformity of the applied stress. From the results it would appear that the edge support constancy is not wholy maintained. From the maximum stress results discussed later the effect of this does not appear to be significant; consequently considering strain results in conjunction with the maximum stress results, the assumption of constancy of the edge fixity is seen to be permissible. This reasoning applies to all the results presented in these figures which as a whole confirm the above conclusion.

To asses the relative correctness of the average stress-strain relation developed in the theory, the averages of the longitudinal strain readings across all the plate components of the structural sections obtained by direct measurements at various loads were calculated and plotted in terms of the parameters $\sigma_{x\,av}/\sigma_{x\,crit}$ against $\epsilon_{x\,av.}/\epsilon_{x\,crit}$ and compared with the relevant theoretical curves in Fig. (107) and (108). It is seen that excellent agreement obtains indicative of the reliability in applying single plate theory to structural sections regarded as an assembly of interacting plates.

Fig. (109) and (110) present the comparison of the theoretical and experimental variation of maximum stress with the web to flange ratio H and thickness h of lipped and plain channels. These results are again presented in a non-dimensional form which allows for the effect of yield stress. The yield stress

LIPPED CHANNEL

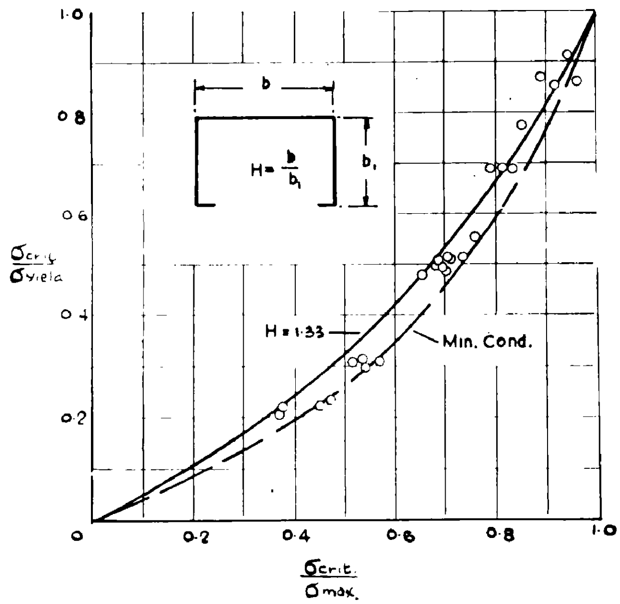

Fig. (111)

LIPPED CHANNEL

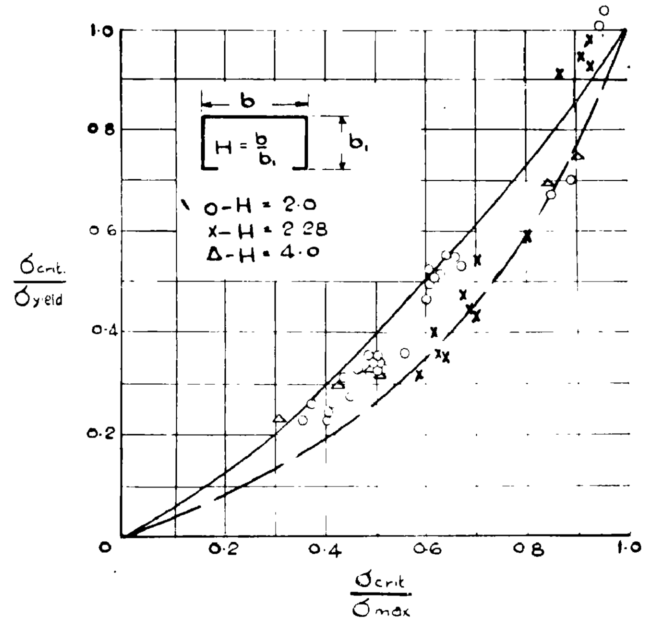

Fig. (112)

PLAIN CHANNEL

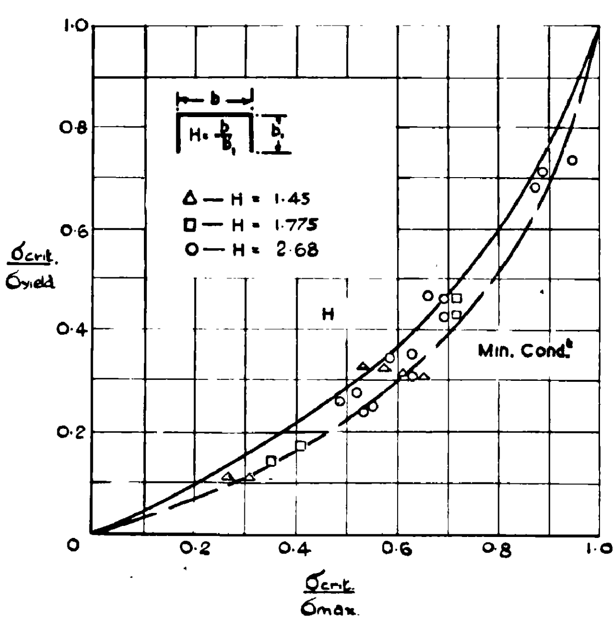

Fig. (113)

PLAIN CHANNEL

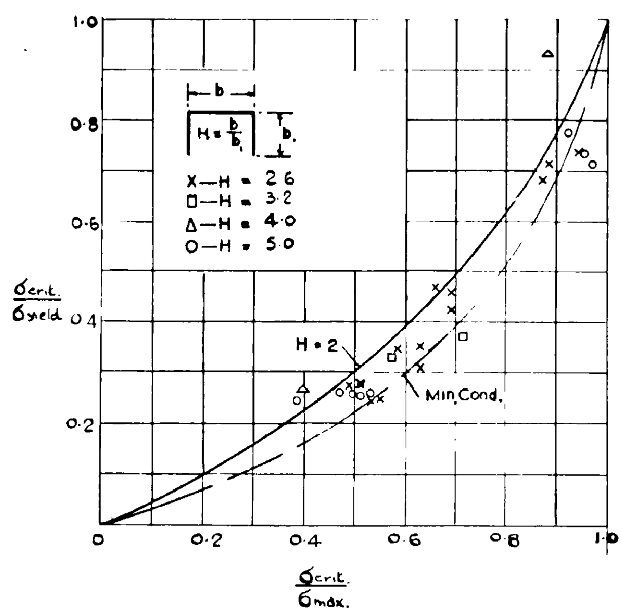

Fig. (114)

was determined for several specimens from each length of different thicknesses tested (Appendix 5) and was found to be considerably different for different thicknesses. It can be seen that the agreement between the theory and experiments is again good.

In Fig.(111) to (115) the value of maximum stress obtained experimentally and those predicted theoretically as described in Section 4 are compared. The structural sections considered are plain and lipped channels and equal angle sections. The method of presentation is the usual non-dimensional form in which the parameters $\sigma_{crit}/\sigma_{Yield}$ and $\sigma_{crit}/\sigma_{max}$ are regarded as the controlling ones.

Fig.(111) shows the results obtained for lipped channels of web to flange ratio H = 1.33 and the web to lip ratio varying from a maximum of 8 (normally considered in practice to provide minimum edge support condition equivalent to a simple support) down to a value of 6. The theoretical curve shown in full is the one corresponding to the structural section where the collapse is initiated by the web instability and corresponding to the appropriate web to flange ratio. The second curve shown by broken line corresponds to the minimum edge support at all connected edges i.e. simple support. It is seen that the distribution of the experimental points is sensibly contained between these two curves. The distribution further indicates that the edge support conditions corresponding to the interaction of the plate components is not fully developed in every case

EQUAL ANGLES

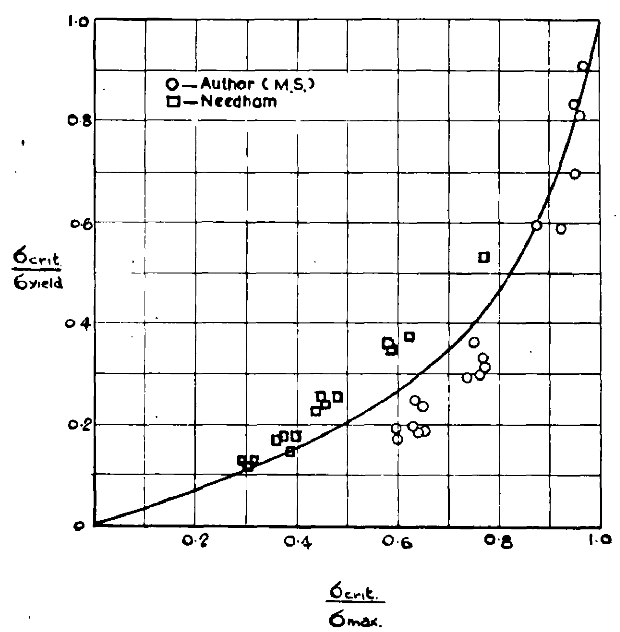

Fig. (115)

due presumably to random initial irregularities present in the various specimens. Fig.(112) presents the experimental results for various lipped channels with H = 2.0, 2.28 and 4.0 and the web to lip ratios varying from 6 to 16. The full line shows the theoretically predicted values for web to flange ratio H = 2.0; the broken line again represents the minimum possible edge conditions. Comments similar to those made for Fig.(111) apply.

Fig.(113) and (114) present the experimental and the theoretical results in an exactly similar manner for plain channels where the collapse is initiated by the buckling of the flange and the web, respectively.

Fig.(115) gives the comparison of the theoretical results for a simply supported - free plate with the experimental results obtained by Needham [41] on Aluminium Alloy angles and steel angle specimens tested by the author. It is seen that a certain degree of scatter obtains.

Taking account of the various factors mentioned above, the comparisons presented generally indicate that the predicted results obtained by the method put forward in the analytical part of the thesis show good agreement with the experiments implying that the theoretical analysis developed by the author is rational and reliable.

6.2 MOIRE FRINGE METHOD:

Before concluding this discussion it is considered

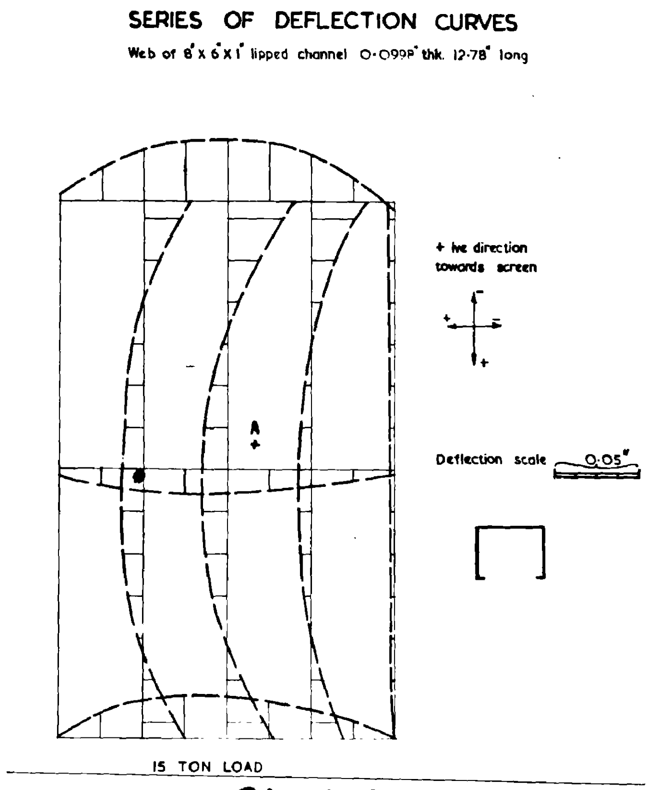

Fig. (116)

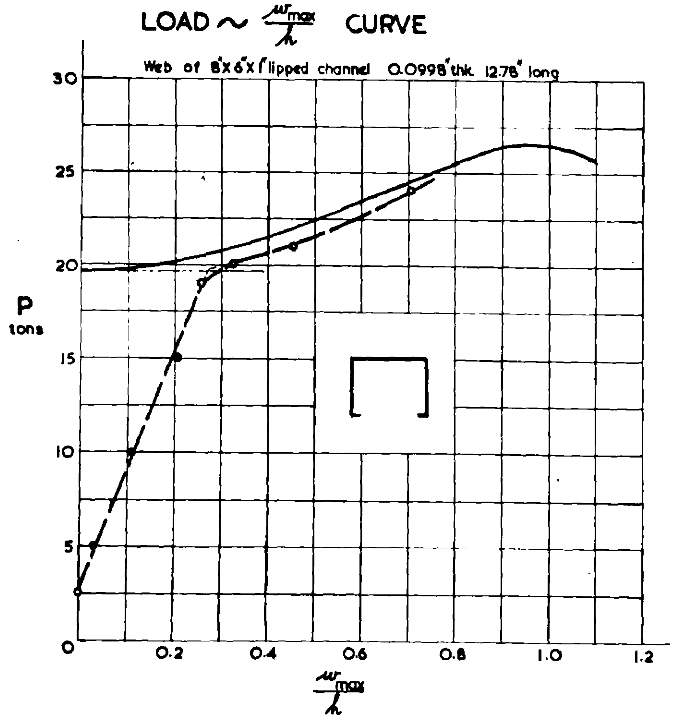

Fig. (117)

of interest to comment on the use of the Moiré technique for the determination of deflections right up to collapse, developed for this application by the author. Fig.(116) shows a typical deflected surface of a web of a lipped channel for a load of 15 tons. It is seen that the loaded edges have a tendency to shift in the semi-circular grooves of the loading plattens. Fig.(117) shows the load against maximum deflection variation for the same lipped channel deduced from the experimental Moire results at point A. This is compared with the theoretical variation computed as described in Section 4. Two points are of interest. First, the theoretical variation assumes zero deflection up to the initiation of elastic instability while the experimental readings indicate gradually increasing deflection due to the presence of initial irregularities. Despite this the experimental "top of the knee" method of prediction of the load initiating elastic instability gives, for all practical purposes, a value close to that forecast by the theory. The second point is the correspondance of the experimental variation in the post critical region with that predicted by the theory. The distributions are similar in form, with the experimental values slightly larger than the theoretical due to the presence of initial irregularities. This naturally has a bearing on the "top of the knee" prediction of the experimental critical load.

A typical series of curves of load against deflection at points other than the point of maximum

LOAD ~ DEFLECTION CURVES IN THE VICINITY OF MAX. DEFLECTION

Web of 8"X6"X1" lipped channel 0.0998" thk. 12.78" long

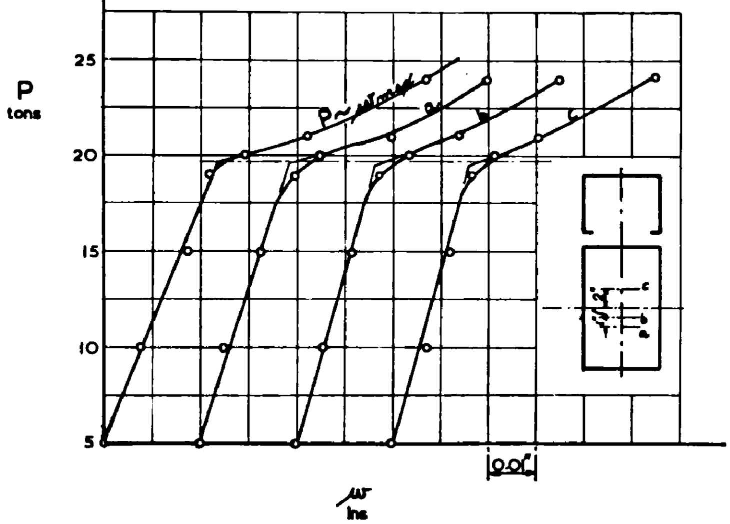

Fig.(118)

SERIES OF DEFLECTION CURVES

Flange of 8"X5.5" plain channel 0.117" thk. 12.78" long

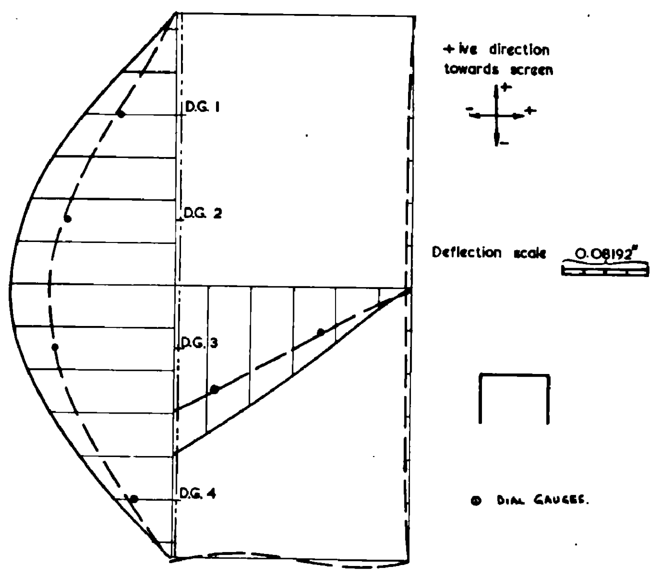

13.5 TON LOAD

Fig.(119)

LOAD ~ MAX. DEFLECTION CURVE

8"X5.5" plain channel 0.117" thk. 12.78" long

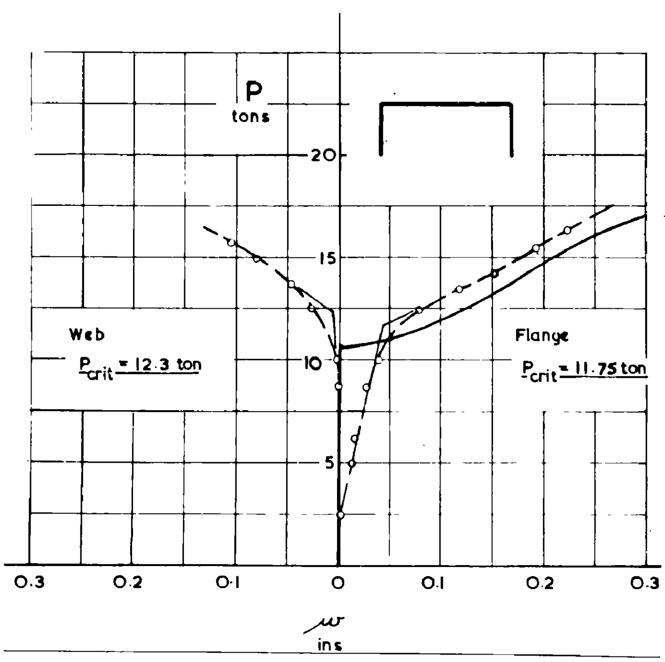

Fig(120)

deflection are shown in Fig.(118) for the web of this lipped channel. As indicated previously the "top of the knee" technique applied to the curve of load deflection in the vicinity of the maximum deflection also give nearly the same critical load as the load ~ absolute maximum deflection curve.

Moiré fringe distributions were taken in a selected number of cases. The experimental procedure involved, however, is relatively complex and consequently the deflection measurements in the majority of cases were carried out by means of dial gauges. Fig.(119) compares the distributions of deflection in the longitudinal and transverse directions obtained by the Moiré fringes for the flange of a plain channel and by direct dial gauge measurements. It is seen that these, for all practical purposes, coincide indicating that the Moiré method may, reliably, be used in determining the deflected surfaces. For this plain channel curves of maximum deflection for the flange and web obtained by Moiré method are shown in Fig.(120) together with the corresponding theoretical curve for the flange.

SUMMARY AND CONCLUSIONS.

1. The derivation of the basic large deflection equations effected by the use of Euler's equations for minimizing the energy integrals has been presented. Galerkin's method was applied to these equations to determine the approximate solutions of two general cases. ((a) both unloaded elastically fixed; symmetrical and unsymmetrical combinations, and (b) one unloaded edge elastically fixed and the other free) of rectangular plates loaded in uniform lengthwise compression.

2. These approximate solutions were then utilized to obtain:

(i) The load initiating elastic instability of plates with a variety of edge conditions. These ranged from elastically fixed and free to symmetrical and unsymmetrical combinations of elastic fixity along the unloaded edges.

(ii) The maximum strength in compression of the flat plates by using the solutions of the large deflection equations in conjunction with the deformation theory of plasticity.

3. The results obtained for single plates were then applied to various structural forms to obtain the critical loads initiating local instability and the maximum loads at collapse.

4. The experimental work consisted of compression tests to failure of concentrically loaded steel plain channel, lipped channel, equal angle and

square tube sections under conditions ensuring failure initiated by local instability. Application of the Moiré fringe method to the measurements of deflected surfaces of the plate components of plain and lipped channel sections concentrically loaded in compression, is also presented.

5. Good agreement is obtained between the theoretical results predicted and the experiments and the following points have come to light.

(i) The experimental determination of the load initiating elastic instability by the technique of the "top of the knee" of the load against deflection variation is relatively independent of the position of the point at which the "maximum" deflections are measured. Results showing good agreement with the theory are obtained as long as this point is in the near vicinity of the point of actual maximum deflection.

(ii) The forms chosen for the deflection and the stress function to obtain the solution of the large deflection equations for plates, at and beyond elastic instability, have been shown to be rational and give results in agreement with the experiments.

(iii) The analysis of critical and maximum strength of structural sections regarded as an assembly of interacting single plates is rational and gives results in agreement with the experiments.

(iv) The assumption of constancy of elastic edge fixity during the period following the initiation of instability upto collapse is permissible.

APPENDICES.

APPENDIX I

MINIMIZATION OF THE ENERGY INTEGRALS.

(GENERAL PROOF OF EULER'S EQUATIONS):

The general form of the energy integral of two functions w and F can be written as:

$$I = \iint_R \phi\Big(x, y, w, w_x, w_y, w_{xx}, w_{yy}, w_{xy}, \ldots\ldots\ldots, w_{x^s}, w_{y^s}, w_{x^p y^q}, \ldots\ldots\ldots, F, F_x, F_y, F_{xx}, F_{yy}, F_{xy}, \ldots\ldots \ldots\ldots, F_{x^s}, F_{y^s}, F_{x^p y^q}, \ldots\ldots\ldots\Big)\, dx\, dy \quad \text{——— AI.00}$$

Here, a single subscript in a function denotes its partial derivatives with respect to the subscript e.g. $w_y = \dfrac{\partial w}{\partial y}$, and double subscripts denote the partial derivatives of the second order with respect to the subscripts. Similarly subscripts of higher order, say s denote the partial derivatives of the sth order:

e.g. $$F_{xx} = \frac{\partial^2 F}{\partial x^2} \quad ; \quad w_{xy} = \frac{\partial^2 w}{\partial x \partial y}.$$

$$F_{y^s} = \frac{\partial^s F}{\partial y^s} \quad \text{and} \quad w_{x^p y^q} = \frac{\partial^s w}{\partial x^p \partial y^q}.$$

Note that $p+q=s$ and p and q are integers.

If the highest order derivative in the integral I is of the order t then it is assumed that ϕ, the integrand given as the function of the arguments $(x, y, w, w_x, \ldots F, F_x, \ldots)$ and its partial derivatives up to and including the order $2t$ are continuous.

Likewise $w(x,y)$ and $F(x,y)$ are continuous and have continuous partial derivatives with respect to x and y upto and including those of order $2t$. It is also assumed that these functions and their derivatives upto order $(t-1)$ have values prescribed on the boundary C of the simply connected region R, (viz. the boundary conditions are of the form:

$$B_s[w] = g_s, \qquad s = 1, 2, 3, \ldots\ldots, (t-1)$$

$$B_s[F] = l_s, \qquad s = 1, 2, 3, \ldots\ldots, (t-1)$$

where $B_s[w]$ etc. stand for expressions containing w and its derivatives normal to the boundary, and symbols g_s and l_s stand for prescribed values known at every boundary point). That is $w(x,y)$ and $F(x,y)$ satisfy all the essential boundary conditions [25] and are termed admissible functions. (In the principle of minimum potential energy the essential boundary conditions are the requirements of geometric compatibility).

For given functions $\bar{w}(x,y)$ and $\bar{F}(x,y)$ having the same respective boundary values as $w(x,y)$ and $F(x,y)$, the integral I yields a definite numerical value. It is required to determine the particular functions $w(x,y)$ and $F(x,y)$ which make the integral I a minimum.

Assume the correct compatible solutions of the problem which minimize the integral to be $w(x,y)$ and $F(x,y)$. This minimum value of the integral will now be compared with the value of the integral obtained for other functions $\bar{w}(x,y)$ and $\bar{F}(x,y)$. This is achieved by adopting the standard procedure of the calculus of variations. [17,22,23,25].

Represent, respectively, the functions $\bar{w}(x,y)$ and $\bar{F}(x,y)$ by $w(x,y)+\varepsilon\eta(x,y)$ and $F(x,y)+\varepsilon\psi(x,y)$ where $\varepsilon\eta(x,y)$ and $\varepsilon\psi(x,y)$ are variations from the respective minimizing functions $w(x,y)$ and $F(x,y)$.

For the requirement that $\bar{w}(x,y)$ and $\bar{F}(x,y)$ satisfy the boundary conditions imposed on $w(x,y)$ and $F(x,y)$ the variational functions $\eta(x,y)$ and $\psi(x,y)$ should be such that they meet all the requirements of admissible functions except that they satisfy homogeneous essential boundary conditions:

$$B_s[\eta] = 0 \quad , \quad s = 1,2,3,\ldots\ldots,(t-1)$$

$$B_s[\psi] = 0 \quad , \quad s = 1,2,3,\ldots\ldots,(t-1)$$

That is $\eta(x,y)$ and $\psi(x,y)$ and their partial derivatives upto the order $(t-1)$ have prescribed values equivalent to zero at every boundary point. In the region R however, $\eta(x,y)$ and $\psi(x,y)$ are arbitrary. (If, however, in a particular problem there are no essential boundary conditions then the

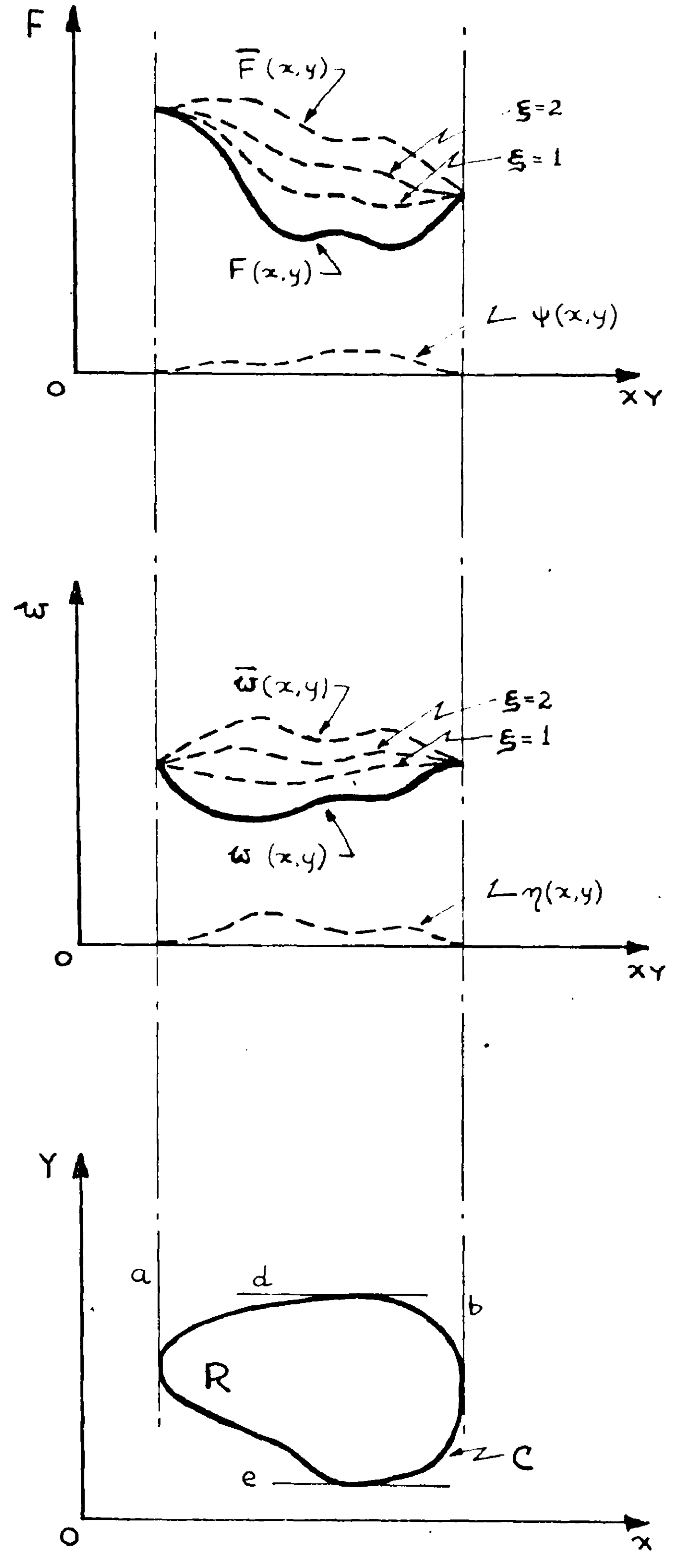

F
$\overline{F}(x,y)$
$\xi=2$
$\xi=1$
$F(x,y)$
$\psi(x,y)$
O
XY
w
$\overline{w}(x,y)$
$\xi=2$
$\xi=1$
$w(x,y)$
$\eta(x,y)$
O
XY
Y
a
d
b
R
C
e
O
x

Fig. (121)

variational functions $\eta(x,y)$ and $\psi(x,y)$ may be entirely arbitrary and in the analysis additional boundary conditions result. Hence for the minimization of the integral the minimizing functions will be the functions which satisfy the additional conditions also. In the principle of minimum energy these additional conditions are the requirements of force balance.) The multiplying factor ξ is a small parameter. Thus by varying ξ and keeping $\eta(x,y)$ and $\psi(x,y)$ the same, $\bar{w}(x,y)$ and $\bar{F}(x,y)$ can be made to vary about the neighbourhood of the true values $w(x,y)$ and $F(x,y)$. This procedure reduces the variation of all these functions to the variation of a single parameter ξ i.e. I now becomes a function of ξ. By choice of w and F, I is a minimum for $\xi = 0$, hence:

$$\left| \frac{dI}{d\xi} \right|_{\xi=0} = 0$$

Now

$$I(\xi) = \iint_R \phi \Big(x, y, w+\xi\eta, w_x+\xi\eta_x, w_y+\xi\eta_y,$$

$$w_{xx}+\xi\eta_{xx}, w_{yy}+\xi\eta_{yy}, w_{xy}+\xi\eta_{xy}, \ldots$$

$$\ldots, w_{x^s}+\xi\eta_{x^s}, w_{y^s}+\xi\eta_{y^s}, w_{x^p y^q}+$$

$$\xi\eta_{x^p y^q}, \ldots, F+\xi\psi, F_x+\xi\psi_x,$$

$$F_y + \xi\psi_y\,,\ F_{xx} + \xi\psi_{xx}\,,\ F_{yy} + \xi\psi_{yy}\,,\ F_{xy} + \xi\psi_{xy}\,,$$

$$\ldots\ldots\ldots\ldots,\ F_{x^s} + \xi\psi_{x^s}\,,\ F_{y^s} + \xi\psi_{y^s}\,,\ F_{x^p y^q} +$$

$$\xi\psi_{x^p y^q}\,,\ldots\ldots\ldots\ldots\Big)\,dx\,dy.$$

Again $\frac{dI(\xi)}{d\xi} = \iint_R \frac{d\phi}{d\xi}\,dx\,dy$ and note that if $\phi = f(\bar{w}, \bar{F}, \ldots \ldots\ldots)$ where $\bar{w}, \bar{F}, \ldots$ are all functions of ξ .

$$\frac{d\phi}{d\xi} = \frac{\partial f}{\partial \bar{w}} \times \frac{d\bar{w}}{d\xi} + \frac{\partial f}{\partial \bar{F}} \times \frac{d\bar{F}}{d\xi} + \ldots\ldots\ldots$$

Setting $\xi = 0$, is equivalent to replacing $\bar{w}$, $\bar{w}_x$, etc., and $\bar{F}$, $\bar{F}_x$, etc., by w, w_x, etc., and F, F_x, etc., respectively. Hence, w and F are now the minimizing functions and $\left|\frac{dI(\xi)}{d\xi}\right|_{\xi=0}$ gives:

$$\iint_R \Big(\phi_w \eta + \phi_{w_x} \eta_x + \phi_{w_y} \eta_y + \phi_{w_{xx}} \eta_{xx}$$

$$+ \phi_{w_{yy}} \eta_{yy} + \phi_{w_{xy}} \eta_{xy} + \ldots\ldots\ldots\ldots + \phi_{w_{x^s}} \eta_{x^s}$$

$$+ \phi_{w_{y^s}} \eta_{y^s} + \phi_{w_{x^p y^q}} \eta_{x^p y^q} + \ldots\ldots + \phi_F \psi$$

$$+ \phi_{F_x} \psi_x + \phi_{F_y} \psi_y + \phi_{F_{xx}} \psi_{xx} +$$

$$+ \phi_{F_{yy}} \psi_{yy} + \phi_{F_{xy}} \psi_{xy} + \ldots\ldots\ldots\ldots +$$

$$\phi_{F_{x^s}}\psi_{x^s}+\phi_{F_{y^s}}\psi_{y^s}+\phi_{F_{x^p y^q}}\psi_{x^p y^q}+\cdots\cdots\Big)\,dx\,dy \qquad \text{A1.01}$$

where $\phi_w=\frac{\partial\phi}{\partial w}$, $\phi_{w_x}=\frac{\partial\phi}{\partial\left(\frac{\partial w}{\partial x}\right)}$ etc. Integrating by parts, gives:

$$\iint_R \phi_{w_x}\eta_x\,dx\,dy=\int_e^d\left[\left|\eta\frac{\partial\phi}{\partial w_x}\right|_a^b-\int_a^b\eta\frac{\partial}{\partial x}(\phi_{w_x})\,dx\right]dy.$$

Now, since it is assumed that η vanishes on the boundary, $\left|\eta\frac{\partial\phi}{\partial w_x}\right|_a^b=0$ and therefore

$$\iint_R \phi_{w_x}\eta_x\,dx\,dy=-\iint_R\eta\frac{\partial}{\partial x}(\phi_{w_x})\,dx\,dy$$

Also

$$\iint_R \phi_{w_{xx}}\eta_{xx}\,dx\,dy=\int_e^d\left[\left|\frac{\partial\eta}{\partial x}\phi_{w_{xx}}\right|_a^b+\left|\eta\frac{\partial}{\partial x}\phi_{w_{xx}}\right|_a^b+\int_a^b\eta\frac{\partial^2}{\partial x^2}\phi_{w_{xx}}\,dx\right]dy.$$

Again, since η and $\frac{\partial\eta}{\partial x}$ are assumed to vanish on the boundary, $\left|\eta\frac{\partial\eta}{\partial x}\phi_{w_{xx}}\right|_a^b$ and $\left|\frac{\partial\eta}{\partial x}\phi_{w_{xx}}\right|_a^b$ are both zero.

therefore

$$\iint_R \phi_{w_{xx}}\eta_{xx}\,dx\,dy=+\iint_R\eta\frac{\partial^2}{\partial x^2}(\phi_{w_{xx}})\,dx\,dy$$

Similarly:

$$\iint_R \phi_{w_{xy}}\eta_{xy}\,dx\,dy=\int_e^d\left[\left|\frac{\partial\eta}{\partial y}\phi_{w_{xy}}\right|_a^b-\int_a^b\frac{\partial\eta}{\partial y}\cdot\frac{\partial}{\partial x}\phi_{w_{xy}}\,dx\right]dy$$

$$= -\int_a^b \int_e^d \frac{\partial \eta}{\partial y} \cdot \frac{\partial}{\partial x} \cdot \phi_{w_{xy}} \, dy \, dx$$

$$= -\int_a^b \left[\left| \eta \frac{\partial}{\partial x} \phi_{w_{xy}} \right|_e^d - \int_e^d \eta \frac{\partial^2}{\partial x \partial y} \phi_{w_{xy}} \, dy \right] dx$$

$$= + \iint_R \eta \frac{\partial^2}{\partial x \partial y} \phi_{w_{xy}} \, dx \, dy.$$

for $\left| \frac{\partial \eta}{\partial y} \phi_{w_{xy}} \right|_a^b = \left| \eta \frac{\partial}{\partial x} \phi_{w_{xy}} \right|_e^d = 0$

In the same manner, it may be shown that:

(In the formal procedure of calculus of variations actual evaluation of the integrals for a given I may be required and then conclusions drawn from considerations that η can be an arbitrary variational function.)

$$\iint_R \phi_{w_{x^s}} \eta_{x^s} \, dx \, dy = (-1)^s \iint_R \eta \frac{\partial^s}{\partial x^s} \phi_{w_{x^s}} \, dx \, dy$$

$$\iint_R \phi_{w_{y^s}} \eta_{y^s} \, dx \, dy = (-1)^s \iint_R \eta \frac{\partial^s}{\partial y^s} \cdot \phi_{w_{y^s}} \, dx \, dy$$

$$\iint_R \phi_{w_{x^p y^q}} \eta_{x^p y^q} \, dx \, dy = (-1)^s \iint_R \eta \frac{\partial^s}{\partial x^p \partial y^q} \phi_{w_{x^p y^q}} \, dx \, dy.$$

Equation A1.01 now becomes:

$$\iint_R \Big\{ \eta \Big(\phi_w - \frac{\partial}{\partial x} \phi_{w_x} - \frac{\partial}{\partial y} \phi_{w_y} + \frac{\partial^2}{\partial x^2} \phi_{w_{xx}} + \frac{\partial^2}{\partial y^2} \phi_{w_{yy}}$$

$$+ \frac{\partial^2}{\partial x \partial y} \phi_{w_{xy}} - \cdots\cdots + (-1)^s \frac{\partial^s}{\partial x^s} \phi_{w_{x^s}} + (-1)^s \frac{\partial^s}{\partial y^s} \phi_{w_{y^s}}$$

$$+(-1)^{s}\frac{\partial^{s}}{\partial x^{p}\partial y^{q}}\phi_{w_{x^{p}y^{q}}}+\Big)+\psi\Big(\phi_{F}-\frac{\partial}{\partial x}\phi_{F_{x}}-\frac{\partial}{\partial y}\phi_{F_{y}}+$$

$$\frac{\partial^{2}}{\partial x^{2}}\phi_{F_{xx}}+\frac{\partial^{2}}{\partial y^{2}}\phi_{F_{yy}}+\frac{\partial^{2}}{\partial x\partial y}\phi_{F_{xy}}-\cdots\cdots+(-1)^{s}\frac{\partial^{s}}{\partial x^{s}}\phi_{F_{x^{s}}}$$

$$+(-1)^{s}\frac{\partial^{s}}{\partial y^{s}}\phi_{F_{y^{s}}}+(-1)^{s}\frac{\partial^{s}}{\partial x^{p}\partial y^{q}}\phi_{F_{x^{p}y^{q}}}+\Big)\Big\}\,dx\,dy=0 \qquad \text{A1.02}$$

The two integrals in A1.02 will be individually zero.

$$\therefore \iint_{R}\eta\Big(\phi_{w}-\frac{\partial}{\partial x}\phi_{w_{x}}-\frac{\partial}{\partial y}\phi_{w_{y}}+\frac{\partial^{2}}{\partial x^{2}}\phi_{w_{xx}}+\frac{\partial^{2}}{\partial y^{2}}\phi_{w_{yy}}$$

$$+\frac{\partial^{2}}{\partial x\partial y}\phi_{w_{xy}}-\cdots\cdots+(-1)^{s}\frac{\partial^{s}}{\partial x^{s}}\phi_{w_{x^{s}}}+$$

$$(-1)^{s}\frac{\partial^{s}}{\partial y^{s}}\phi_{w_{y^{s}}}+(-1)^{s}\frac{\partial^{s}}{\partial x^{p}\partial y^{p}}\phi_{w_{x^{p}y^{q}}}+\cdots\Big)\,dx\,dy=0$$

$$\text{and}\ \iint_{R}\psi\Big(\phi_{F}-\frac{\partial}{\partial x}\phi_{F_{x}}-\frac{\partial}{\partial y}\phi_{F_{y}}+\frac{\partial^{2}}{\partial x^{2}}\phi_{F_{xx}}+\frac{\partial^{2}}{\partial y^{2}}\phi_{F_{yy}}$$

$$+\frac{\partial^{2}}{\partial x\partial y}\phi_{F_{xy}}-\cdots\cdots+(-1)^{s}\frac{\partial^{s}}{\partial x^{s}}\phi_{F_{x^{s}}}+$$

$$(-1)^{s}\frac{\partial^{s}}{\partial y^{s}}\phi_{F_{y^{s}}}+(-1)^{s}\frac{\partial^{s}}{\partial x^{p}\partial y^{q}}\phi_{F_{x^{p}y^{q}}}+\cdots\cdots\Big)\,dx\,dy=0$$

Since the variations η and ψ are arbitrary functions, the following are obtained:

$$\phi_w - \frac{\partial}{\partial x}\phi_{w_x} - \frac{\partial}{\partial y}\phi_{w_y} + \frac{\partial^2}{\partial x^2}\phi_{w_{xx}} + \frac{\partial^2}{\partial y^2}\phi_{w_{yy}}$$

$$+ \frac{\partial^2}{\partial x \partial y}\phi_{w_{xy}} - \cdots\cdots + (-1)^s \frac{\partial^s}{\partial x^s}\phi_{w_{x^s}} + (-1)^s \frac{\partial^s}{\partial y^s}\phi_{w_{y^s}}$$

$$+ (-1)^s \frac{\partial^s}{\partial x^p \partial y^q}\phi_{w_{x^p y^q}} + \cdots\cdots = 0 \qquad \text{A1.03}$$

and

$$\phi_F - \frac{\partial}{\partial x}\phi_{F_x} - \frac{\partial}{\partial y}\phi_{F_y} + \frac{\partial^2}{\partial x^2}\phi_{F_{xx}} + \frac{\partial^2}{\partial y^2}\phi_{F_{yy}}$$

$$+ \frac{\partial^2}{\partial x \partial y}\phi_{F_{xy}} - \cdots\cdots + (-1)^s \frac{\partial^s}{\partial x^s}\phi_{F_{x^s}} + (-1)^s \frac{\partial^s}{\partial y^s}\phi_{F_{y^s}}$$

$$+ (-1)^s \frac{\partial^s}{\partial x^p \partial y^q}\phi_{F_{x^p y^q}} + \cdots\cdots = 0 \qquad \text{A1.04}$$

Thus, the condition of minimizing the integral I reduces to the solution of two differential equations A1.03 and A1.04 called Euler's Equations.

Strictly speaking it has been proved only that if w and F satisfy the Euler's Equations the energy is an extremum: either maximum or minimum. However, it is physically evident that the energy in the true state cannot be a maximum because it is always possible to make the energy greater by locking some extra internal stresses. Therefore Euler's Equations are in fact the conditions of minimizing the energy integral and not maximizing it.

In the problem considered in the text the relevant boundary conditions considered for the governing functions w and F may be regarded as special cases of the boundary conditions assumed in this proof and Euler's Equations can be directly applied to the energy integral to give the differential equations for determining the minimizing functions.

APPENDIX 2

(i) Formulation Of The General Form Of The Stress Function F:

The boundary conditions to be satisfied by the stress function F are:

$$\left|\frac{\partial^2 F}{\partial y^2}\right|_{\substack{x=0\\x=a}} = \frac{N_x}{h} \qquad \text{——— A2.10}$$

$$\left|\frac{\partial^2 F}{\partial x^2}\right|_{\substack{y=0\\y=b}} = 0 \qquad \text{——— A2.11}$$

$$\left|\frac{\partial^2 F}{\partial x \partial y}\right|_{\substack{x=0\\x=a}} = 0 \qquad \text{——— A2.12}$$

$$\left|\frac{\partial^2 F}{\partial x \partial y}\right|_{\substack{y=0\\y=b}} = 0 \qquad \text{——— A2.13}$$

Let the stress function be

$$F = A y^2 + f(x) \cdot g(y)$$

where

A is a constant

$f(x)$ is a function of x only.

$g(y)$ is a function of y only.

Now condition A2.10 gives:

$2A + f(x) g(y) = \frac{N_x}{h}$ at $x=0$ and $x=a$; equating the terms of the same order on both sides:

$$2A = \frac{N_x}{h} \quad ; \quad \left| f(x)\, g''(y) \right|_{\substack{x=0\\x=a}} = 0 \qquad \text{———— (a)}$$

Conditions A2.11 gives: $\left|f''(x)\,g(y)\right|_{\substack{y=0\\ =b}} = 0$ ———(b)

Conditions A2.12 gives: $\left|f'(x)\,g'(y)\right|_{\substack{x=0\\ =a}} = 0$ ———(c)

and condition A2.13 gives: $\left|f'(x)\,g'(y)\right|_{\substack{y=0\\ =b}} = 0$ ———(d)

Considering equations (a), (b), (c) and (d) it is easily verified that:

In (a) $g''(y) \neq 0 \therefore \left|f(x)\right|_{\substack{x=0\\ =a}} = 0$ ——— A2.14

In (b) $f''(x) \neq 0 \therefore \left|g(x)\right|_{\substack{y=0\\ =b}} = 0$ ——— A2.15

In (c) $g'(y) \neq 0 \therefore \left|f'(x)\right|_{\substack{x=0\\ =a}} = 0$ ——— A2.16

In (d) $f'(x) \neq 0 \therefore \left|g'(y)\right|_{\substack{y=0\\ =a}} = 0$ ——— A2.17

Now, let $f(x) = \bar{B}_0 + \frac{\bar{B}_1 x}{a} + \frac{\bar{B}_2 x^2}{a^2} + \frac{\bar{B}_3 x^3}{a^3} + \frac{\bar{B}_4 x^4}{a^4}$ where $\bar{B}_0, \bar{B}_1, \bar{B}_2, \bar{B}_3$ and $\bar{B}_4$ are constants.

At $x=0$ equation A2.14 gives $f(x)=0$

$\therefore \bar{B}_0 = 0$

At $x=a$ equation A2.14 gives $f(x)=0$

$\therefore \bar{B}_1 + \bar{B}_2 + \bar{B}_3 + \bar{B}_4 = 0$ ——— I

Now, $f'(x) = \frac{\bar{B}_1}{a} + \frac{2\bar{B}_2 x}{a^2} + \frac{3\bar{B}_3 x^2}{a^3} + \frac{4\bar{B}_4 x^3}{a^4}$

At $x=0$ equation A2.16 gives $f'(x)=0$

$\therefore \bar{B}_1 = 0$

At $x=a$ equation A2.16 gives $f'(x)=0$

$\therefore 4\bar{B}_4 + 3\bar{B}_3 + 2\bar{B}_2 = 0$ ——— II

Dividing equations I and II by $\bar{B}_2$ throughout and taking $\frac{\bar{B}_4}{\bar{B}_2} = \bar{H}_1$ and $\frac{\bar{B}_3}{\bar{B}_2} = \bar{H}_2$ gives:

$\bar{H}_1 + \bar{H}_2 + 1 = 0$ ——— III

$4\bar{H}_1 + 3\bar{H}_2 + 2 = 0$ ——— IV

Solving III and IV simultaneously for $\overline{H}_1$ and $\overline{H}_2$ the following is obtained: $\overline{H}_1 = 1$ and $\overline{H}_2 = -2$

$$\therefore f(x) = \left(\frac{x^4}{a^4} - \frac{2x^3}{a^3} + \frac{x^2}{a^2}\right)\overline{B}_2$$

Working in exactly the same way as above it is found that:

$$g(y) = \left(\frac{y^2}{b^2} - \frac{y}{b}\right)^2 \overline{C}_2$$

therefore the general form of the stress function becomes:

$$F = \frac{N_x y^2}{2h} + \beta\left(\frac{x^2}{a^2} - \frac{x}{a}\right)^2\left(\frac{y^2}{b^2} - \frac{y}{b}\right)^2$$

where β is an arbitrary constant.

It is easily verified that the boundary conditions continue to be satisfied if β is replaced by a factor ρ in the second term of the stress function F. ρ may be constant, a function of x and/or a function of y.

Thus:

$$F = \frac{N_x y^2}{2h} + \rho\left(\frac{x^2}{a^2} - \frac{x}{a}\right)^2\left(\frac{y^2}{b^2} - \frac{y}{b}\right)^2 \qquad \text{A2.18}$$

(ii) METHOD USED TO OBTAIN THE DEFLECTION FORM FOR THE ELASTICALLY FIXED - ELASTICALLY FIXED PLATE:

The boundary conditions:

$$\left.\begin{aligned} w &= 0 \\ \frac{\partial^2 w}{\partial x^2} + \nu\frac{\partial^2 w}{\partial y^2} &= 0 \end{aligned}\right\} \text{at } x = 0, a \qquad \text{A2.20}$$

are satisfied by assuming that the plate deflects in

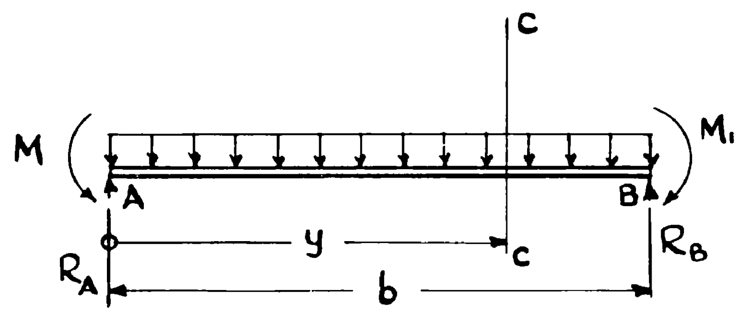

Fig. (122)

m sinusoidal half waves, i.e. the deflection surface can be written in the form:

$$w = Y \sin \frac{m\pi x}{a} \qquad \text{A2.21}$$

in which Y is a function of y only and determines the deflection form in the y- direction.

To obtain Y consider the analogy between a beam and a thin strip of the plate cut parallel to the x-axis at the centre of the plate.

Let a beam of span 'b' carry a uniformly distributed load p along its entire length. To make the boundary conditions of the beam analogous to that of the plate consider end moments M and M_1 acting at A and B respectively (Fig.(122)), such that if Y is the deflection of the beam:

$$M = EIk\left|\frac{dY}{dy}\right|_{y=0}; \quad M_1 = EIk_1\left|\frac{dY}{dy}\right|_{y=b}$$

where k and k_1 are constants equivalent to the coefficients of edge fixity of the plate and EI is the flexural rigidity of beam.

Taking a section CC at distance y from the left hand side and applying Macaulay's Method:

$$EI\frac{d^2Y}{dy^2} = M + \frac{py^2}{2} - R_A y$$

$$EI\frac{dY}{dy} = My + \frac{py^3}{6} - \frac{R_A y^2}{2} + \bar{C}_1$$

$$EI\,Y = \frac{My^2}{2} + \frac{py^4}{24} - \frac{R_A y^3}{6} + \bar{C}_1 y + \bar{C}_2$$

Boundary condition:

$w \equiv Y = 0$ at $y = 0$ gives $\bar{C}_2 = 0$ and $w \equiv Y = 0$ at $y = b$

gives:

$$\bar{C} = \frac{-Mb}{2} - \frac{pb^3}{24} + \frac{R_A b^2}{6} \qquad \text{———— (a)}$$

Taking moments about B :

$$R_A = \frac{M}{b} + \frac{pb}{2} - \frac{M_1}{b} \qquad \text{———— (b)}$$

(a) and (b) give:

$$\bar{C}_1 = -\frac{Mb}{3} - \frac{M_1 b}{6} + \frac{pb^3}{24}$$

$$\therefore EI\,Y = \frac{My^2}{2} + \frac{py^4}{24} - \frac{My^3}{6b} - \frac{pby^3}{12} + \frac{M_1 y^3}{6b} - \frac{Mby}{3} - \frac{M_1 by}{6} + \frac{pb^3 y}{24}.$$

Dividing throughout by p and denoting $\frac{M}{p}$ by $\bar{p}$ and $\frac{M_1}{p}$ by $\bar{q}$

$$\frac{EI\,Y}{p} = \frac{\bar{p}y^2}{2} + \frac{y^4}{24} - \frac{\bar{p}y^3}{6b} - \frac{by^3}{12} + \frac{\bar{q}y^3}{6b} - \frac{\bar{p}by}{3} - \frac{\bar{q}by}{6} + \frac{b^3 y}{24} \qquad \text{———— A2.22}$$

$$\therefore \frac{EI}{p}\frac{dY}{dy} = \frac{y^3}{6} + \bar{p}y - \frac{\bar{p}y^2}{2b} - \frac{by^2}{4} + \frac{\bar{q}y^2}{2b} - \frac{\bar{p}b}{3} - \frac{\bar{q}b}{3} + \frac{b^3}{24} \qquad \text{———— A2.23}$$

Now, at $y = 0$ $\frac{EI}{p}\frac{dY}{dy} = \frac{\bar{p}}{r}$

$$\therefore \frac{\bar{p}}{r} = -\frac{\bar{p}b}{3} - \frac{\bar{q}b}{6} + \frac{b^3}{24} \qquad \text{———— (c)}$$

Also at $y = 0$ $\frac{EI}{p}\frac{dY}{dy} = \frac{-\bar{q}}{r_1}$

$$\therefore -\frac{\bar{q}}{r_1} = \frac{b^3}{24} - \frac{\bar{p}b}{3} - \frac{\bar{q}b}{3} \qquad \text{———— (d)}$$

Equations (c) and (d) give:

$$\bar{q} = \frac{(6k_1 b + k k_1 b^2)\, b^2}{144 + 48 k_1 b + 48 k b + 12 k k_1 b} \quad \text{———} \quad A2.24$$

and $$\bar{p} = \frac{k b^3}{28 + 8 k b} - \bar{q}\, \frac{k b}{6 + 2 k b} \quad \text{———} \quad A2.25$$

Hence, from A2.22

$$Y = \frac{p}{EI}\left[\frac{y^4}{24} - \frac{b\, y^3}{12} + \frac{b^3 y}{24} - \bar{p}\left(\frac{y^3}{6b} - \frac{y^2}{2} + \frac{b y}{3}\right) + \bar{q}\left(\frac{y^3}{6b} - \frac{b y}{6}\right)\right] \quad \text{———} \quad A2.26$$

Thus for the plate the deflection form can be written as:

$$w = \frac{\alpha}{b^3} \sin\frac{m\pi x}{a}\left[\frac{y^4}{24} - \frac{b\, y^3}{12} + \frac{b^3 y}{24} - \bar{p}\left(\frac{y^3}{6b} - \frac{y^2}{2} + \frac{b y}{3}\right) + \bar{q}\left(\frac{y^3}{6b} - \frac{b y}{6}\right)\right]$$

$$w = \alpha \sin\frac{m\pi x}{a}\left[\frac{y^4}{24 b^3} - \frac{A_1 y^3}{6 b^2} + \frac{B_1 y^2}{b} + \frac{C_1 y}{3}\right] \quad \text{———} \quad A2.27$$

where α is an unknown constant and

$$A_1 = \left(\frac{1}{2} + \frac{\bar{p}}{b^2} - \frac{\bar{q}}{b^2}\right)$$

$$B_1 = \frac{\bar{p}}{2 b^2}$$

$$C_1 = \left(\frac{1}{8} - \frac{\bar{p}}{b^2} - \frac{\bar{q}}{2 b^2}\right)$$

and $\bar{q}$ and $\bar{p}$ are given by equations A2.24 and A2.25.

(iii) FORMULATION OF THE STRESS FUNCTION F FOR THE ELASTICALLY BUILT-IN-FREE PLATE.

Let the stress function be:

$$F = Ay^2 + f(x)\,g(y) \qquad \text{A2.30}$$

where A is a constant.

$f(x)$ is a function of x only and $g(y)$ is a function of y only.

The boundary conditions to be satisfied are:

$$\left|\frac{\partial^2 F}{\partial y^2}\right|_{\substack{x=0\\x=a}} = \frac{N_x}{h} \qquad \text{A2.31}$$

$$\left|\frac{\partial^2 F}{\partial x^2}\right|_{\substack{y=0\\y=b}} = 0 \qquad \text{A2.32}$$

$$\left|\frac{\partial^2 F}{\partial x\,\partial y}\right|_{\substack{x=0,\ y=0\\x=a,\ y=b}} = 0 \qquad \text{A2.33}$$

Along with the above mentioned boundary conditions one more condition required to be satisfied, is that the variable part of σ_x. i.e. $\left|\partial^2 F/\partial y^2\right|$ excluding the constant portion, at $x = \frac{a}{2}$ should have a parabolic distribution of the form:

$$(\bar{J} - \bar{H}y^2) \qquad \text{A2.34}$$

where $\bar{J}$ and $\bar{H}$ are constants.

Condition A2.34 represents a physically admissible form.

It can be verified that this condition together with the two conditions A2.32 cannot all be satisfied simultaneously. To permit a solution, it is assumed that σ_y stress is of relatively little significance and hence the condition $\frac{\partial^2 F}{\partial x^2} = 0$ at the elastically built-in edge $y=0$ need not be satisfied.

Condition A2.31 gives:

$2A + f(x) g''(y) = \frac{N_x}{h}$ at $x=0$ and $x=a$

Equating the terms of the same order on both sides:

$$2A = \frac{N_x}{h} \quad \text{and} \quad \left| f(x)\, g''(y) \right|_{\substack{x=0\\x=a}} = 0 \quad \text{———— (a)}$$

Condition A2.32 gives:

$$\left| f'(x)\, g'(y) \right|_{\substack{x=0\\x=a}} \Big|_{\substack{y=0\\y=b}} = 0 \quad \text{———— (b)}$$

and condition A2.34, excluding the constant portion from $\left| \partial^2 F / \partial y^2 \right|_{x=\frac{a}{2}}$ gives:

$$\left| f(x)\, g''(y) \right|_{x=a/2} = \bar{J} - \bar{H} y^2 \quad \text{———— (c)}$$

It is concluded from (a), (b), and (c) that the conditions reduce to:

$$\left| f(x) \right|_{\substack{x=0\\x=a}} = 0 \quad \text{———— I}$$

$$\left| g(y) \right|_{y=b} = 0 \quad \text{———— II}$$

$$\left| f'(x) \right|_{\substack{x=0\\x=a}} = 0 \quad \text{———— III}$$

$$\left| g'(y) \right|_{\substack{y=0\\y=b}} = 0 \quad \text{———— IV}$$

$$\left| g''(y) \right|_{x=a/2} \equiv \bar{J}_1 - \bar{H}_1 y^2 \qquad \text{V}$$

where $\bar{J}_1$ and $\bar{H}_1$ are constants different from $\bar{J}$ and $\bar{H}$.

Let $f(x) = \bar{B}_0 + \frac{\bar{B}_1 x}{a} + \frac{\bar{B}_2 x^2}{a^2} + \frac{\bar{B}_3 x^3}{a^3} + \frac{\bar{B}_4 x^4}{a^4}$ where $\bar{B}_0, \bar{B}_1, \bar{B}_2, \bar{B}_3$ and $\bar{B}_4$ are constant.

Working in exactly the same manner as in part (1) of Appendix 2 the following is obtained:

$$f(x) = \left(\frac{x^2}{a^2} - \frac{x}{a}\right)^2 \bar{B}_2$$

Again let $g(y) = \bar{C}_0 + \frac{\bar{C}_1 y}{b} + \frac{\bar{C}_2 y^2}{b^2} + \frac{\bar{C}_3 y^3}{b^3} + \frac{\bar{C}_4 y^4}{b^4}$ where $\bar{C}_0, \bar{C}_1, \bar{C}_2, \bar{C}_3$ and $\bar{C}_4$ are constants.

Condition II gives:

$$\bar{C}_0 + \bar{C}_1 + \bar{C}_2 + \bar{C}_3 + \bar{C}_4 = 0 \qquad \text{A2.35}$$

Now, $g'(y) = \frac{\bar{C}_1}{b} + \frac{2\bar{C}_2 y}{b^2} + \frac{3\bar{C}_3 y^2}{b^3} + \frac{4\bar{C}_4 y^3}{b^4}$ and

$$g''(y) = \frac{2\bar{C}_2}{b^2} + \frac{6\bar{C}_3 y}{b^3} + \frac{12\bar{C}_4 y^2}{b^4}$$

At $y = 0$ $\quad g'(y) = 0$

$$\therefore \bar{C}_1 = 0 \qquad \text{A2.36}$$

At $y = b$ $\quad g'(y) = 0$

$$\therefore 2\bar{C}_2 + 3\bar{C}_3 + 4\bar{C}_4 = 0 \qquad \text{A2.37}$$

At $x = \frac{a}{2}$, $\quad g''(y) \equiv \bar{J}_1 - \bar{H}_1 y^2$

$$\therefore \frac{2\bar{C}_2}{b^2} + \frac{6\bar{C}_3 y}{b^3} + \frac{12\bar{C}_4 y^2}{b^4} \equiv \bar{J}_1 - \bar{H}_1 y^2 \qquad \text{A2.38}$$

Equivalence A2.38 will only be satisfied if

$$\bar{C}_3 = 0 \qquad \text{A2.39}$$

Now dividing A2.35 and A2.36 by $\overline{C}_4$ and taking $\frac{\overline{C}_2}{\overline{C}_4} = \overline{L}_1$ and $\frac{\overline{C}_0}{\overline{C}_4} = \overline{L}_2$, the following is found:

$$1 + \overline{L}_1 + \overline{L}_2 = 0 \qquad \text{—— VI}$$

$$4 + 2\overline{L}_1 = 0 \qquad \text{—— VII}$$

Solving VI and VII simultaneously for $\overline{L}_1$ and $\overline{L}_2$ gives: $\overline{L}_1 = -2$ and $\overline{L}_2 = 1$

$$\therefore g(y) = -2\,\overline{C}_4\left(\frac{y^2}{b^2} - \frac{y^4}{2b^4} - \frac{1}{2}\right)$$

Hence the form of the stress function becomes:

$$F = \frac{N_x y^2}{2h} + \beta\left(\frac{x^2}{a^2} - \frac{x}{a}\right)^2\left(\frac{y^2}{b^2} - \frac{y^4}{2b^4} - \frac{1}{2}\right).$$

where β is an unknow constant.

(iv) Method Used To Obtain The Deflection Function For The Elastically Fixed Plate:

The boundary conditions to be satisfied by the deflection form are:

$$\left.\begin{aligned} w &= 0 \\ \frac{\partial^2 w}{\partial x^2} + \nu \frac{\partial^2 w}{\partial y^2} &= 0 \end{aligned}\right] \text{ at } x = 0 \text{ and } x = a \qquad \text{—— A2.40}$$

$$w = 0 \quad \text{at} \quad y = 0 \qquad \text{—— A2.41}$$

$$\frac{\partial^2 w}{\partial y^2} - k\frac{\partial w}{\partial y} = 0 \quad \text{at} \quad y = 0 \qquad \text{—— A2.42}$$

$$\frac{\partial^2 w}{\partial y^2} + \nu \frac{\partial^2 w}{\partial x^2} = 0 \quad \text{at} \quad y = b \text{ ——————— A2.43}$$

$$\frac{\partial^3 w}{\partial y^3} + (2-\nu)\frac{\partial^3 w}{\partial x^2 \partial y} = 0 \quad \text{at} \quad y = b \text{ ——————— A2.44}$$

It is observed that conditions A2.40 are completely satisfied, if

$$w = \alpha \sin \frac{m\pi x}{a} \left[Y \right]$$

where Y is a function of y only and α is an arbitrary constant.

Let $Y = \frac{A_2 y^4}{b^3} + \frac{B_2 y^3}{b^2} + \frac{\bar{C}_2 y^2}{b} + \frac{\bar{C}_1 y}{1} + \bar{C}_0 b$

At $y = 0$, $w = 0$ gives $Y = 0$

$$\therefore \bar{C}_0 = 0 \text{ ——————— A2.45}$$

Now

$$Y' = \frac{4A_2 y^3}{b^3} + \frac{3B_2 y^2}{b^2} + \frac{2\bar{C}_2 y}{b} + \bar{C}_1$$

$$Y'' = \frac{12A_2 y^2}{b^3} + \frac{6B_2 y}{b^2} + \frac{2\bar{C}_2}{b}$$

$$Y''' = \frac{24A_2 y}{b^3} + \frac{6B_2}{b^2}$$

At $y=0$ condition A2.42 is equivalent to $Y''=kY'$.

$\therefore$ Condition A2.42 gives:

$$\frac{2\overline{C_2}}{b} = k\,\overline{C_1}$$

$$\therefore\ \overline{C_2} = \frac{k\,\overline{C_1}\,b}{2} \qquad \text{A2.46}$$

Evidently, for the deflection function to be useful, $\overline{C_1}$ must be so chosen that $\overline{C_2}$ does not tend to infinity when k tends to infinity. It can easily be verified that if: $\overline{C_1}=\frac{1}{(kb+2)}$ a dimensionless ratio then $\overline{C_2}=\frac{kb}{2(kb+2)}$ is not infinite when $k\to\infty$.

Hence the deflection form becomes:

$$w = \alpha \sin\frac{m\pi x}{a}\left[\frac{A_2 y^4}{b^3} + \frac{B_2 y^3}{b^2} + \frac{kby^2}{2(kb+2)b} + \frac{y}{kb+2}\right] \qquad \text{A2.47}$$

The constants A_2 and B_2 are determined from the conditions A2.43 and A2.44

Condition A2.43 gives:

$$12A_2 + 6B_2 + \frac{kb}{(kb+2)} = \nu\frac{m^2\pi^2 b^2}{a^2}\left[A_2 + B_2 + \frac{kb}{2(kb+2)} + \frac{1}{(kb+2)}\right] \qquad \text{(a)}$$

and condition A2.44 gives:

$$24A_2 + 6B_2 = (2-\nu)\frac{m^2\pi^2 b^2}{a^2}\left[4A_2 + 3B_2 + \frac{kb}{(kb+2)} + \frac{1}{(kb+2)}\right] \qquad \text{(b)}$$

Equations (a) and (b) are simple algebraic equations which can be solved simultaneously for A_2 and B_2. The deflection form A2.47 is determined and satisfies all the boundary conditions.

APPENDIX 3

Effect Of Deflection Form On The Critical Stress:-

The critical stresses were evaluated for two cases viz. simply supported and built-in along the unloaded edges, by selecting different deflection forms:

1. Flat square plate simply supported on all edges and uniformly compressed in one direction:

The assumed deflection form in this case is:

$$w = \alpha \sin\frac{m\pi x}{a}\sin\frac{\pi y}{b} \qquad \text{A3.10}$$

This deflection form satisfies all of the following boundary conditions:

$$\left.\begin{aligned} &w = 0 \\ &\frac{\partial^2 w}{\partial x^2} + \nu\frac{\partial^2 w}{\partial y^2} = 0\end{aligned}\right\} \text{ at } x = 0, a \qquad \text{A3.11}$$

$$\left.\begin{aligned} &w = 0 \\ &\frac{\partial^2 w}{\partial y^2} + \nu\frac{\partial^2 w}{\partial x^2} = 0\end{aligned}\right\} \text{ at } y = 0, b \qquad \text{A3.12}$$

The same stress function is used as in case (a) Page and the Galerkin's Equations 2.01a and 2.02a solved for $a/b = 1{\cdot}0$ and $m = 1{\cdot}0$ giving:

$$N_{x_{crit}} = -\frac{40.041 D}{b^2}$$

compared to

$$N_{x_{crit}} = -\frac{39.497 D}{b^2}$$ as calculated before

with $w = \alpha \sin \frac{m\pi x}{a}\left(\frac{y^4}{24b^3} - \frac{y^3}{12b^2} + \frac{y}{24}\right)$

2. Rectangular Plate Uniformly compressed along the simply supported edges, built-in along the unloaded edges:

The deflection form selected in this case is:

$$w = \alpha \sin \frac{m\pi x}{a}\left(1 - \cos\frac{2\pi y}{b}\right) \qquad \text{A3.20}$$

It satisfies all the following boundary conditions:

$$\left.\begin{aligned} w &= 0 \\ \frac{\partial^2 w}{\partial x^2} + \nu \frac{\partial^2 w}{\partial y^2} &= 0 \end{aligned}\right] \quad \text{at} \quad x = 0, a \qquad \text{A3.21}$$

$$\left.\begin{aligned} w &= 0 \\ \frac{\partial w}{\partial y} &= 0 \end{aligned}\right] \quad \text{at} \quad y = 0, b \qquad \text{A3.22}$$

Using the same stress function as in Case(a) in the text and taking $a/b = 2.0$ and $m = 2.0$ the solution of Galerkin's Equations gives:

$$N_{x_{crit}} = \frac{-71.86\,D}{b^2}$$

as compared to:

$N_{x_{crit}} = \dfrac{-69.81\,D}{b^2}$ obtained by taking:

$$w = \alpha \sin \frac{m\pi x}{a} \left(\frac{y^4}{24 b^3} - \frac{y^3}{12 b^2} + \frac{y^2}{24 b} \right)$$

APPENDIX 4.

TYPICAL EVALUATION OF THE SECTION RATIO H CORRESPONDING TO A GIVEN ELASTIC FIXITY FOR PLATE BUCKLING OF A BOX SECTION.

The equation defining the elastic edge fixity r provided by the supporting plate component to the buckling plate component of a box section obtained in Section 4 is:

$$k = \frac{(\bar{\alpha}_1^2+\bar{\beta}_1^2)\sinh\bar{\alpha}_1 H b_1 \sin\bar{\beta}_1 H b_1}{\bar{\alpha}_1 \sin\bar{\beta}_1 H b_1(\cosh\bar{\alpha}_1 H b_1 - 1) + \bar{\beta}_1 \sinh\bar{\alpha}_1 H b_1(1-\cos\bar{\beta}_1 H b_1)} \quad \text{——— A4.00}$$

where

$$\bar{\alpha}_1 = \sqrt{\frac{m^2\pi^2}{a^2} + \sqrt{\frac{-N_x}{D}\frac{m^2\pi^2}{a^2}}}$$

$$\bar{\beta}_1 = \sqrt{-\frac{m^2\pi^2}{a^2} + \sqrt{-\frac{N_x}{D}\frac{m^2\pi^2}{a^2}}}$$

$$H = \frac{b}{b_1}$$

By taking $m = 1{\cdot}0$ and substituting $-K/b^2$ for the smallest value of $\frac{N_x}{D}$, $\bar{\alpha}_1$ and $\bar{\beta}_1$ are obtained as:

$$\bar{\alpha}_1 = \frac{1}{b_1}\sqrt{\frac{\pi^2 b_1^2}{a^2} + \frac{\pi b_1}{a}\sqrt{K}}$$

$$\bar{\beta}_1 = \frac{1}{b_1}\sqrt{-\frac{\pi^2 b_1^2}{a^2} + \frac{\pi b_1}{a}\sqrt{K}}$$

For any value of $k b_1$ the ratio a/b_1 at which K is a minimum for $m = 1{\cdot}0$ can be obtained from Fig. (18), and thus the corresponding value of H can be obtained from equation A4.00 . To illustrate this the solution for $\lambda b_1 = 2{\cdot}0$ is presented.

For $\lambda b_1 = 2{\cdot}0$, the minimum value of $K = 45.23$ for for $m = 1.0$ at $a/b_1 = 0.87$.

$$\bar{\alpha}_1 = \sqrt{\frac{\pi^2}{0{\cdot}757 b_1^2} + \frac{7{\cdot}72\pi}{b_1^2}} = \frac{6{\cdot}11}{b_1}$$

$$\bar{\beta}_1 = \sqrt{-\frac{\pi^2}{0{\cdot}757 b_1^2} + \frac{7{\cdot}72\pi}{b_1^2}} = \frac{3{\cdot}345}{b_1}$$

Inserting these values in equation

$$\frac{2}{b_1} = \frac{\left[(6{\cdot}11/b_1)^2 + (3{\cdot}345/b_1)^2\right] \sinh 6{\cdot}11 H \sin 3{\cdot}345 H}{\frac{6{\cdot}11}{b_1} \sin 3{\cdot}345 H \left(\cosh 6{\cdot}11 H - 1\right) + 3{\cdot}345 \sinh 6{\cdot}11 H \left(1 - \cos 3{\cdot}345 H\right)}$$

Solving by trial and error this gives $H = 0{\cdot}837$
The values of H obtained by this method are shown plotted in Fig. (51).

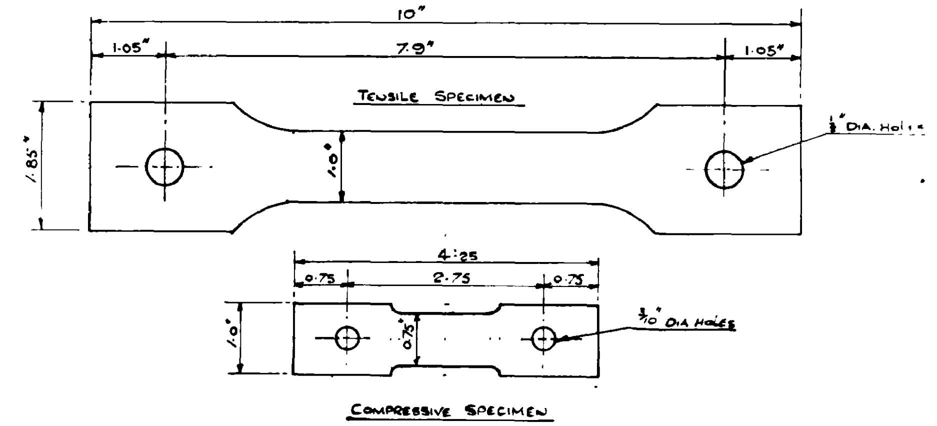

Fig. (123)

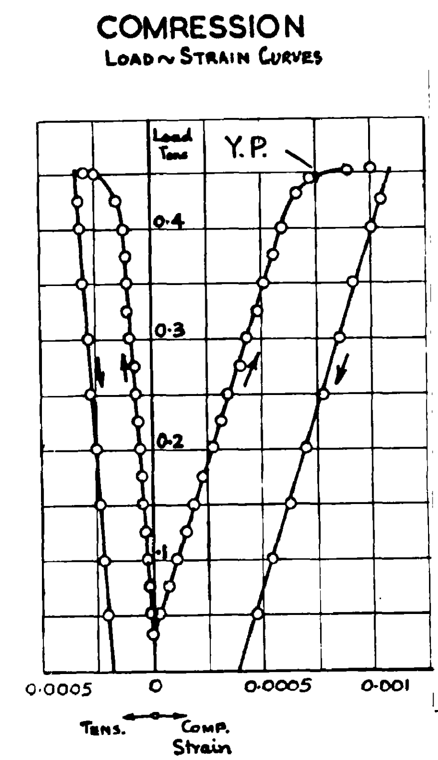

Fig. (125)

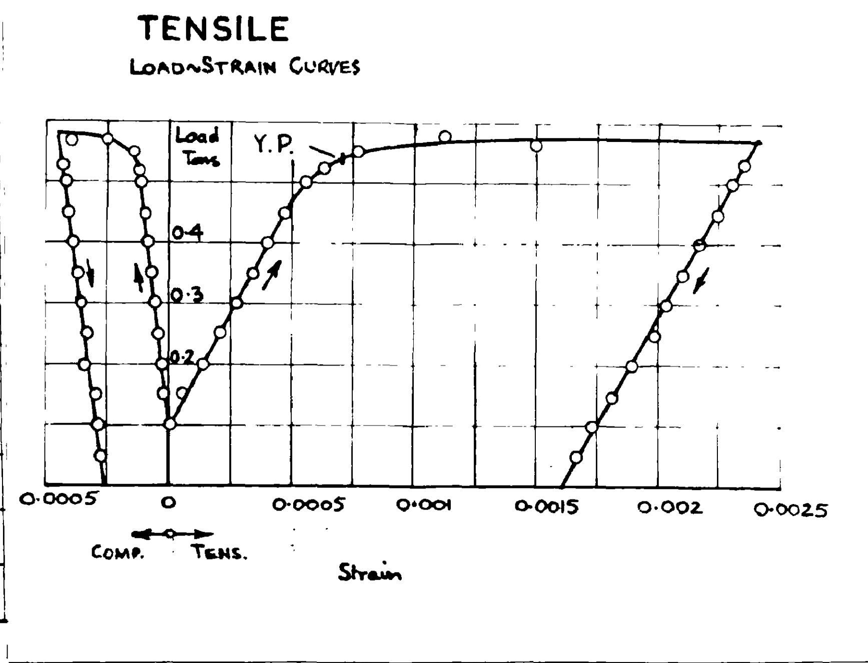

Fig. (124)

APPENDIX 5.

MATERIAL CHARACTERISTICS OF MILD STEEL STRIP.

Tensile And Compression Tests.

All the plain channels, lipped and angle sections used in the experiments were formed by cold pressing from mild steel strip. Preliminary tension tests on flat specimens cut from the same structural section from different places showed some variations in the tension yield stresses and values of Young's Modulus. It was planned to carry out extensive tests for determining the material characteristics, in tension and compression.

Tensile and Compression specimens of the dimensions shown in Fig.(123) were cut at five to seven different places from lipped, and plain channels and angle sections. Tensile and compression load-strain curves Figs.(124) and (125) were determined by the use of electrical resistance strain gauges which were used on both sides of the specimen and connected in series to take account of any bending moment effects that might be present. For compression tests special grips were made (Fig.(126)). These grips realised built-in end conditions for the compression specimen so as to increase the buckling load and thus make the determination of the yield stress in compression possible.

The variations in Modulus of elasticity E and the yield stress σ_{yield} across the cross-section of

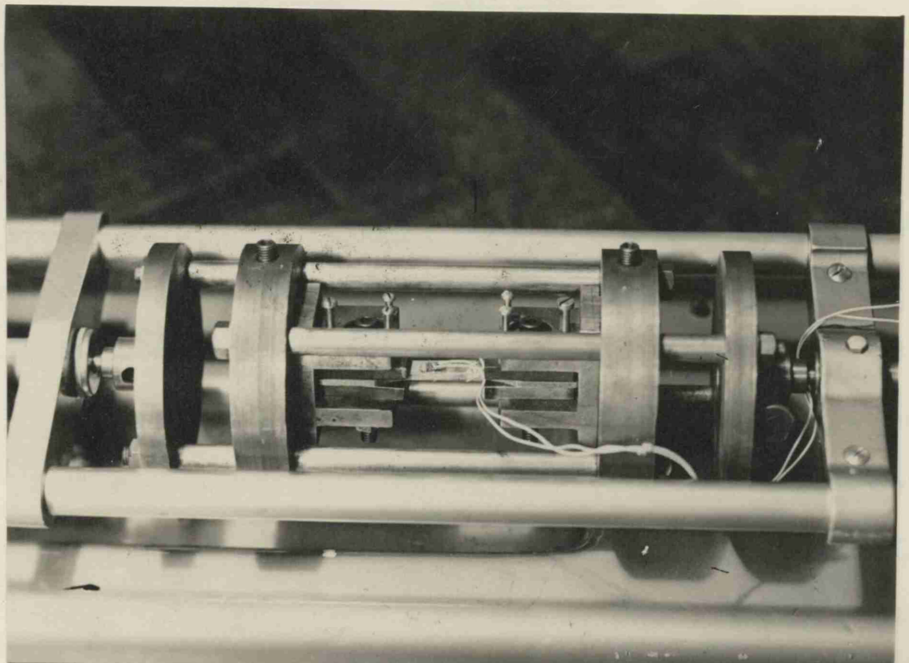

Fig.(126)

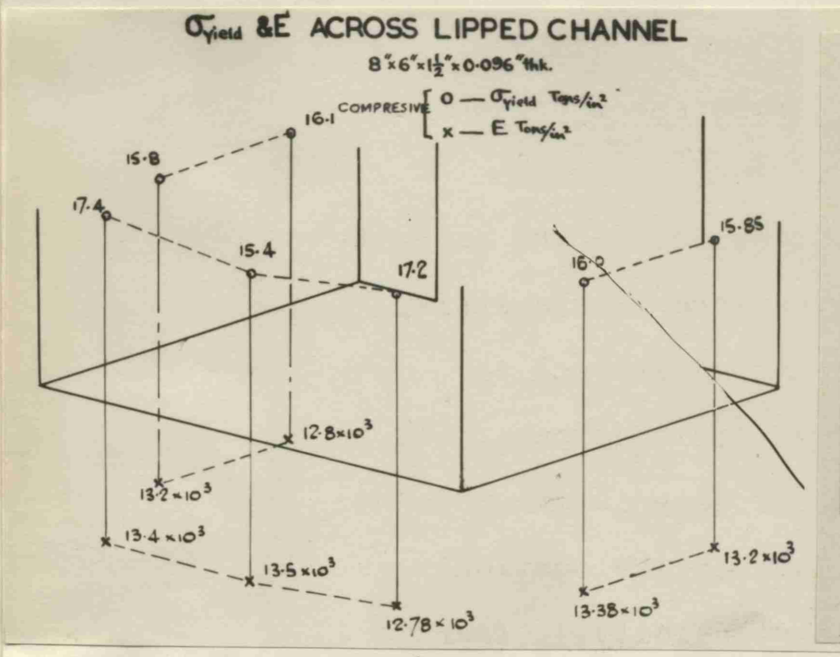

Fig.(127)

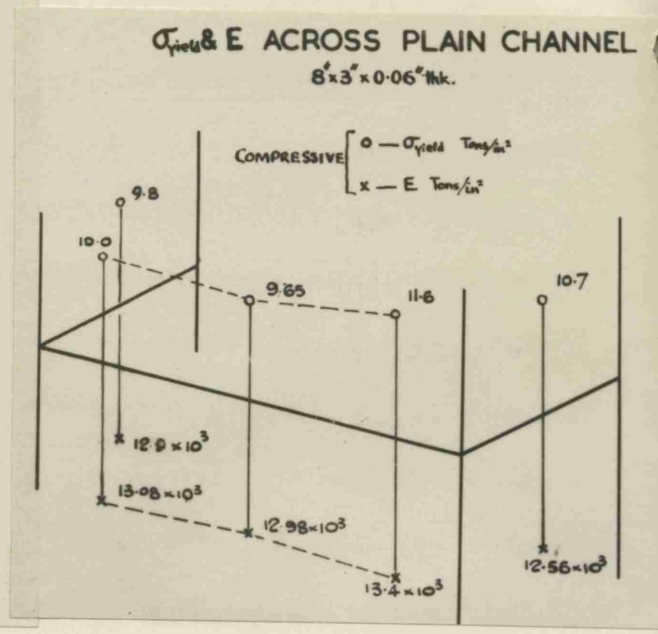

Fig.(128)

lipped channel and a plain channel are illustrated in Fig. (127) and Fig. (128). respectively. Average values of E, σ_{Yield} and ν for various sizes of plain, lipped and angle sections are tabulated.

It might be of interest to note here that it was found that the slope of the unloading portion of the stress curve was greater than that corresponding to the value of Young's Modulus, determined from the loading portion of the graph.

Resonant frequency method was also used for the determination of E. The theoretical background and the experimental details with the results of the experiments are presented in the following.

Resonant Frequency Method of Measurement Of Modulus Of Elasticity.

It is well known that a rise in damping capacity of a vibrating specimen (the measure of the energy dissipated per cycle of alternating stress) is associated with the movement of dislocations. It is also generally believed that stresses in the purely elastic region in metals produce no dislocation movement which is associated with plasticity. Therefore in the determination of the true modulus of elasticity of a material it is necessary to work in a range where a small increase in applied energy of vibration causes no increase in the damping capacity and consequently no dislocation movement.

In the normal methods of determining modulus of

Elasticity very large stresses are involved which may result in dislocation movement.

The technique described below produces extremely small stresses (less than about 0·015 Tons/in^2) in the material and since in mild steel the dislocations are effectively pinned, it can be assumed that the induced vibrations do not produce any dislocation movement and are in the range of pure elasticity.

Theoretical Background:

If a bar is caused to vibrate a certain frequency termed the resonant frequency is found at which the bar absorbs the minimum energy of the applied vibrations. This frequency depends upon the size, density and modulus of elasticity of the bar.

In an exhaustive mathematical analysis of the subject Wood [53] assumes that the bar is uniform in x-section, is subjected to neither tension nor compression, the amplitude of vibration is so small that rotary effects can be neglected and the radius of curvature is small enough to be represented by a second differential.

The formula developed for the resonant frequency of a bar free at both ends and having one peak of maximum amplitude at the midpoint is:

$$N = 1{\cdot}133416 \frac{\bar{s}}{l^2}\sqrt{\frac{E}{\rho}}$$

where $\bar{s}^2 = \frac{h^2}{12}$ for a rectangular bar of thickness h in the vibrating plane, length l and density ρ .

The working formula becomes:

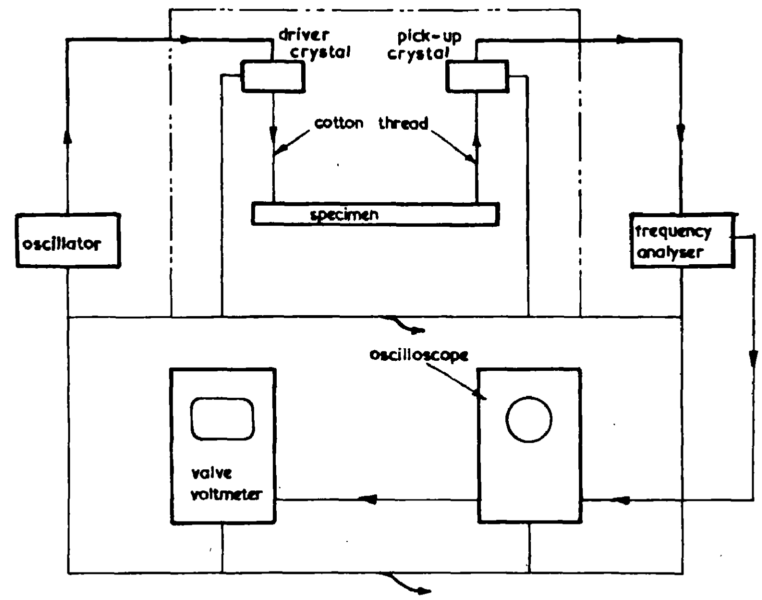

CIRCUIT DIAGRAM

Fig.(129).

$$E = \frac{N^2 \ell^4 \rho}{1{\cdot}05625\, h^2}$$

with E in dynes/cm^2 for the c.g.s. system.

This mode of vibration has two nodes on either side of the centre of the bar at a distance of $0{\cdot}224\,\ell$ from each end.

Experimental Details and Results:

The apparatus used in determining the resonant frequency is essentially that used by O'Hara [54] and similar to ones described in [55, 56].

The vibrations are transmitted to the bar by means of a thread connected to a piezo-electric crystal, the signal to which is supplied by an oscillator. The pick-up crystal receives these vibrations from the thread at the other node point, the resulting alternating voltage is supplied to a frequency analyser which measures the frequency of vibration.

The amplitude of vibration is increased by increasing the power output of the oscillator (from 0 to 50 decibels). Metallic screens are used to prevent feed back from the crystals to the wires from the oscillator and analyser.

The bars (length = 10 c.ms) used were of rectangular X-section with one dimension twice the other; the smaller dimension being the thickness of the lipped channel from which they were cut.

The resonant frequency was measured with the bar

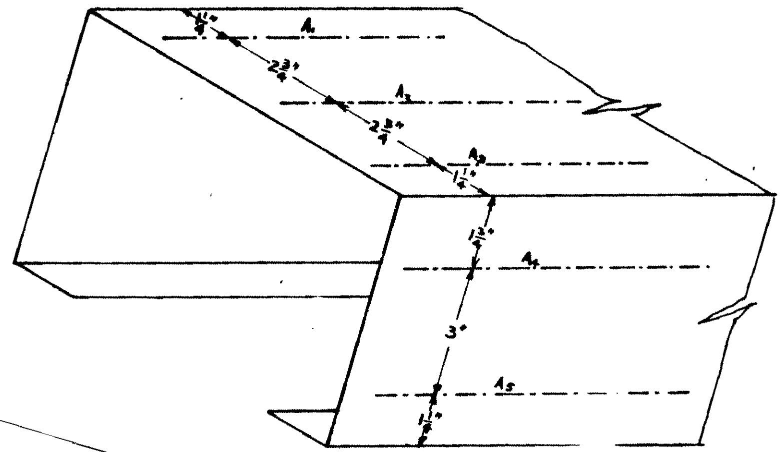

Fig. (130)

vibrating in first one plane, and the other, being referred to as vertical and horizontal positions respectively.

The first run of tests consisted in the determination of the variation of Modulus of Elasticity across the x-section of a cold pressed lipped channel 0·0965″ thick. The specimen were cut length-wise at five different points (shown in Fig. (130)). The results are tabulated below:

Spec.	Dimension	Density gm/cc	$E \times 10^{-3}$ T/in² Vert.	$E \times 10^{-3}$ T/in² Hor.	E mean
A_1	0.096" x 0.194" x 3.952"	7.66	13.2	12.88	13.04
A_2	0.097" x 0.194" x 3.951"	7.734	13.16	13.14	13.14
A_3	0.0965"x 0.194" x 3.949"	7.796	13.48	13.29	13.38
A_4	0.096" x 0.195" x 3.950"	7.71	13.13	13.08	13.11
A_5	0.097" x 0.194" x 3.951"	7.76	13.26	13.21	13.24

The second run of test consisted in determination of the modulus of elasticity of specimens cut from the centre of the web of lipped channels of various thicknesses. The results are tabulated below:

Dimensions of Spec.	Mean E $\times 10^{-3}$ Tons/in²
0.153" x 0.304" x 3.945"	13.01
0.117" x 0.236" x 3.993"	13.15
0.0965"x 0.1925"x 3.986"	13.13
0.0751"x 0.151" x 3.951"	13.18
0.058" x 0.115" x 3.985"	13.16

LIPPED CHANNELS
8" WEB × 4" FLANGE

t	E TENS.	E COMP.	σ YIELD TENS.	σ YIELD COMP.	ν TENS.	ν COMP.
0.06	12.97×10^3	13.02×10^3	9.27	9.58	0.246	0.25
0.075	13.42×10^3	13.61×10^3	15.7	15.97	0.273	0.282
0.096	12.97×10^3	12.715×10^3	16.64	15.49	0.283	0.29
0.117	12.97×10^3	12.81×10^3	13.5	13.59	0.247	0.258

LIPPED CHANNELS
8" WEB × 3.5" FLANGE

t	E TENS.	E COMP.	σ YIELD TENS.	σ YIELD COMP.	ν TENS.	ν COMP.
0.06	12.77 10^3	12.92 10^3	9.98	10.26	0.236	0.248
0.075	13.14 10^3	13.4 10^3	18.2	18.45	0.262	0.253
0.096	13.33 10^3	13.45 10^3	17.0	17.4	0.253	0.247
0.117	13.2 10^3	13.46 10^3	12.22	11.92	0.239	0.25

PLAIN CHANNELS
8" WEB × 4.5" FLANGE

t	E TENS.	E COMP.	σ YIELD TENS.	σ YIELD COMP.	ν TENS.	ν COMP.
0.06	12.6 10^3	12.77 10^3	10.37	10.51	0.248	0.255
0.0785	13.23 10^3	13.3 10^3	15.23	15.1	0.239	0.242
0.117	13.2 10^3	13.03 10^3	13.02	13.22	0.254	0.224
	10^3	10^3				

ANGLE SECTIONS
4" × 4"

t	E TENS.	E COMP.	σ YIELD TENS.	σ YIELD COMP.	ν TENS.	ν COMP.
0.06	12.97 10^3	13.0 10^3	9.66	9.75	0.228	0.23
0.077	13.87 10^3	14.35 10^3	17.52	17.76	0.248	0.247
0.098	13.16 10^3	13.2 10^3	15.9	15.98	0.26	0.252
0.117	13.41 10^3	13.6 10^3	13.6	13.57	0.251	0.249

All values in Tons – Inches.

LIPPED CHANNELS
8" WEB × 2" FLANGE

h	E TENS.	E COMP.	σ YIELD TENS.	σ YIELD COMP.	ν TENS.	ν COMP.
0.058	$2\ 6 \times 10^3$	12.5×10^3	9.9	10.0	0.252	0.247
0.075	13.41×10^3	13.6×10^3	18.49	19.0	0.26	0.239
0.117	13.67×10^3	14.1×10^3	12.65	12.6	0.25	0.256

PLAIN CHANNELS
8" WEB × 3" FLANGE

h	E TENS.	E COMP.	σ YIELD TENS.	σ YIELD COMP.	ν TENS.	ν COMP.
0.06	13.04×10^3	12.98×10^3	10.33	10.51	0.248	0.251
0.0785	13.58×10^3	13.75×10^3	15.82	15.97	0.259	0.265
0.097	13.3×10^3	13.05×10^3	15.52	15.49	0.253	0.247
0.117	12.81×10^3	12.85×10^3	13.48	13.59	0.260	0.235

PLAIN CHANNELS
8" WEB × 1.6" FLANGE

h	E TENS.	E COMP.	σ YIELD TENS.	σ YIELD COMP.	ν TENS.	ν COMP.
0.06	12.62×10^3	12.5×10^3	9.8	10.0	0.239	0.248
0.078	13.58×10^3	13.6×10^3	18.57	19.0	0.260	0.251
0.117	13.81×10^3	14.1×10^3	12.77	12.6	0.263	0.279

LIPPED CHANNELS
8" WEB × 6" FLANGE

h	E TENS.	E COMP.	σ YIELD TENS.	σ YIELD COMP.	ν TENS.	ν COMP.
0.06	12.66×10^3	12.77×10^3	10.17	10.57	0.238	0.234
0.075	13.22×10^3	13.49×10^3	16.88	16.73	0.282	0.271
0.096	12.73×10^3	13.18×10^3	16.48	16.25	0.296	0.28
0.117	13.01×10^3	13.03×10^3	14.1	14.22	0.26	0.264
0.1515	13.5×10^3	13.52×10^3	14.76	14.86	0.26	0.265

All values in Tons– Inches.

APPENDIX 6.

MOIRÉ FRINGE METHOD FOR THE DETERMINATION OF DEFLECTED FORMS OF PLATE COMPONENTS OF STRUCTURAL SECTIONS LOADED IN AXIAL COMPRESSION.

The determination of complete deflected surfaces of buckled plate components of structural sections such as plain and lipped channels by means of large numbers of dial gauges becomes very awkward. Therefore a Moiré Method was developed for this purpose. The Moiré method which determines the changes in slope of a loaded specimen has previously been adopted [46, 47] to determine the distributions of moments and surface stresses in slabs under lateral loads. In this method and some other existing techniques for slope and deflection measurements [48,49,50,51,52] models are used instead of the original specimens. In buckling problems the material characteristics and the initial imperfections in the manufactured specimens are of importance and therefore attempt was made in these experiments to use the actual structural specimens.

The Basic Idea Of the Method And the Theoretical Background:

A mirror surfaced specimen is used to observe the reflection of a ruled screen placed in front of the specimen. These observations are usually made by means of a photographic camera. Consider the image S of a

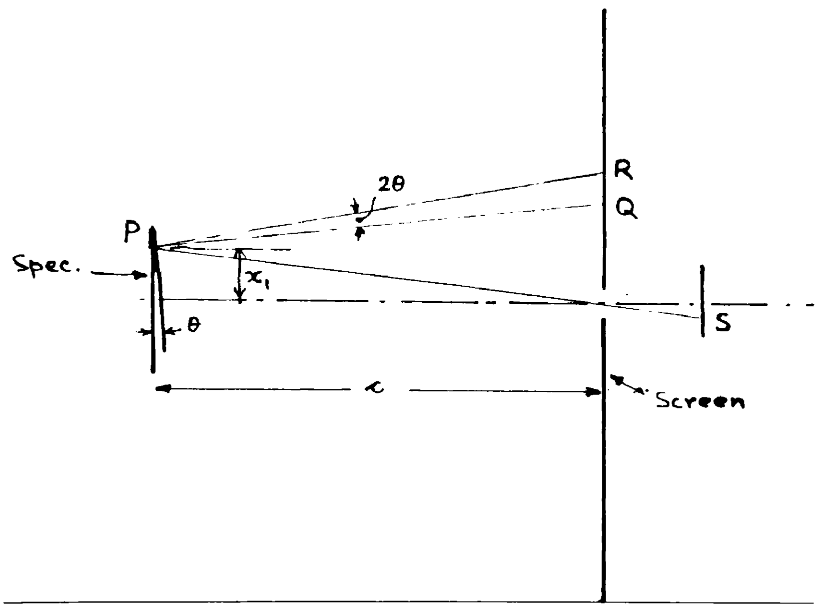

Fig. (131)

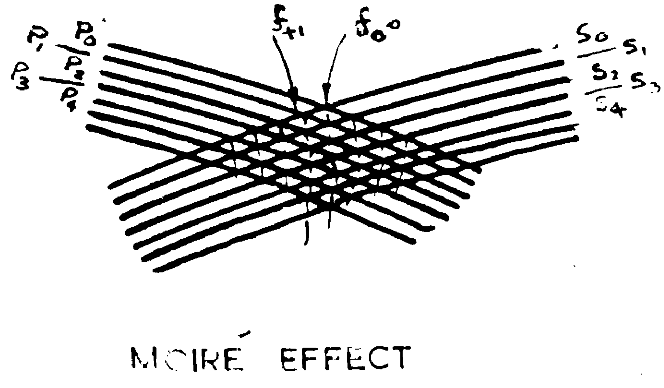

Fig. (132)

certain point P of the specimen plate on the ground glass screen of the camera, it can be seen that in the point S a reflected image of the point Q on a line of the screen appears. If now the specimen is made to deflect, the slope θ makes the reflection of a point R on another line coincide with S on the ground glass. (Fig.(131)). Clearly the distance QR can be used to determine the slope θ. One of the practical ways of observing QR and thus determining the slope is by super-imposing photographs of the reflected images from the initially flat plate and the deflected plate. The ruling of the screen is chosen in such a manner that the super-imposed photographs - if at all different - exhibit Moiré fringes.

If lines on the ruled screen produce reflected images, S_0 S_1, S_2, S_3 etc. on the photograph from the unloaded specimen and the images P_0, P_1, P_2, P_3, etc. after the plate has been deflected, then the line (See Fig.(132)) joining all the points where P_0 and S_0 P_1 and S_1, etc. intersect each other is the locus of all the points where the distance QR has a value = 0. A line f_1 adjacent to f_0 is the locus of the points where P_0 and S_1, P_1 and S_2 etc. intersect. Between f_1 and f_0, QR differs exactly by an amount d where d is the interval on the ruled screen (the lines on the screen are made $\frac{d}{2}$ black and $\frac{d}{2}$ white). In this way it becomes possible to obtain Moiré fringes which may be interpreted as contour lines of QR. Now it remains to compute the slope θ from QR. For a flat screen (See

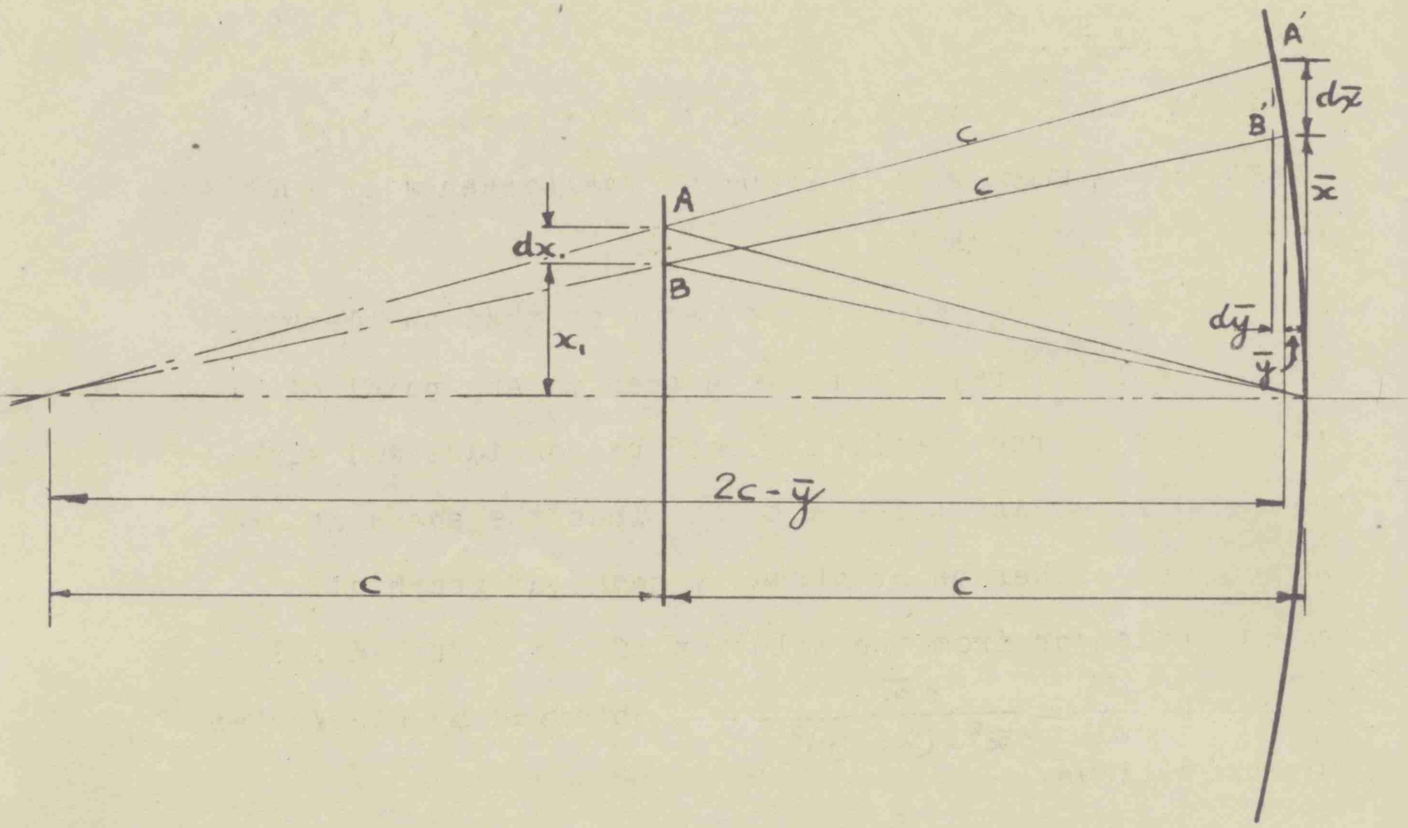

Fig.(133)

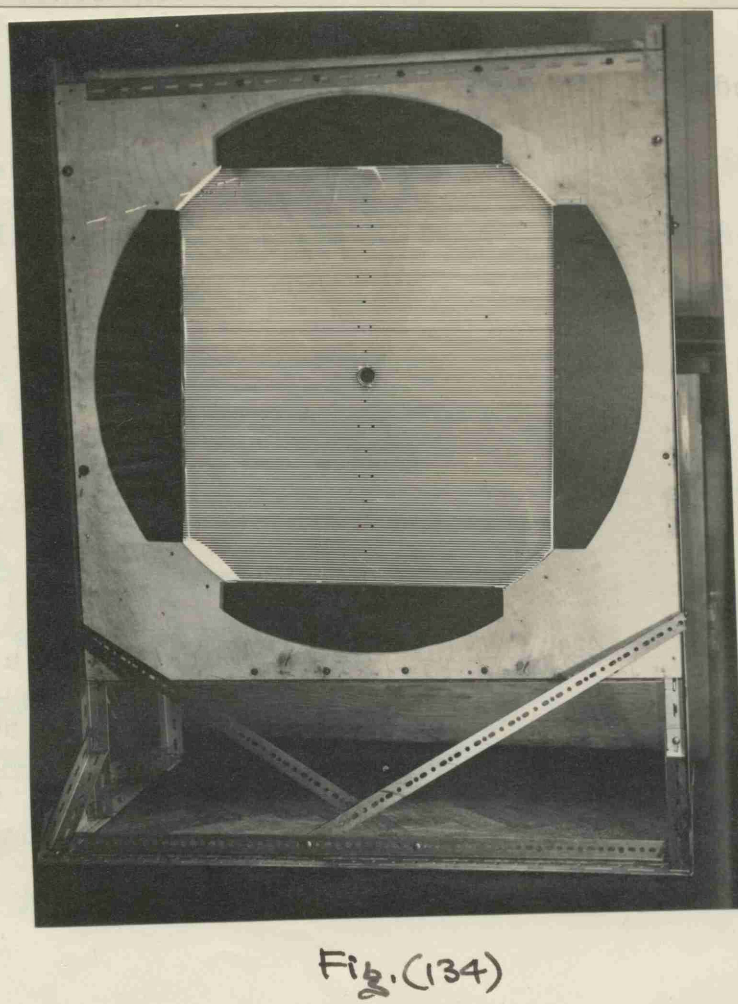
Fig.(134)

Fig.(131) the relation between QR and θ is found to be $QR = \frac{2c\theta + 2c\phi\frac{x_1^2}{c^2}}{(1 - 2x_1/c\,\theta)}$. The small term x_1^2/c^2 is a variable for various points on the specimen. This suggests a choice of the shape of the screen V in such a way that QR = $2c\theta$.

To make QR $\doteqdot 2c\theta$ it is required that the lengths of the incident rays from the screen to any point of reflection on the specimen should be constant and equal to c . i.e. AA' = BB' = c . Thus the shape of the screen can either be obtained by means of graphical construction or from the solution of the differential equation: $\frac{d\bar{y}}{d\bar{x}} = \frac{c\bar{x}}{\bar{x}^2 + (2c - \bar{y})^2}$. obtained by successive approximations.

Apparatus And Experimental Technique:

The screen was made of a photographic film 30" x 36" with black and white parallel lines each 1/10" thick, glued on to a transparent perspex sheet. The black lines on the film were photographic silver deposit and were practically opaque. Two formers were screwed on to the screen to give the required cylindrical shape and the whole screen mounted on a wooden frame so that the screen could be turned about its axis to orient the lines upon it in any desired direction (Figs.(134)). The lines are of-course parallel to the axis of the cylinder. To the back of the screen was attached a sheet of white paper to diffuse the light supplied by four 200 watt lamps mounted behind the screen. A "Leica" camera for 35 m.m. film with a f 3.5 lens was used. A Kodak Panchromatic film was used for photographing

The specimen tends to make the reflected virtual image very irregularly astigmatic by its curvature and therefore the photographs were taken with a small aperture of 1:12.5 and exposures of 5.5 seconds. Enlargements of the photographs were made on translucent paper and the photographs superimposed and printed for analysis.

The specimens had to be prepared with elaborate care. The surface was carefully cleaned and after applying a cellulose primer several coats of a mixture (2 parts of black cellulose paint, 12 parts of fast thinners and 1 part retarder) were sprayed. After the paint had dried the surface was "planed" by means of 600 grit water paper used with soap and water so that no "orange peel" effect was left. This was then polished with metal polishes (Brasso and Silvo in order) and wax, producing an excellent reflecting surface.

Determination Of Deflections And Bending Moments:

To evaluate deflections from the slope contours it is required to know the absolute value of the contours. This could be achieved by numbering the lines on the screen and in fact this was done by marking on the centre line of the screen, normal to the ruled lines on it, a series of reference dots at an interval of every ten lines (See Fig.(134)). In this way the zero contour was determined and hence the value of all the contours obtained. An indication of the deflected form at a convenient place (preferably near the edges)

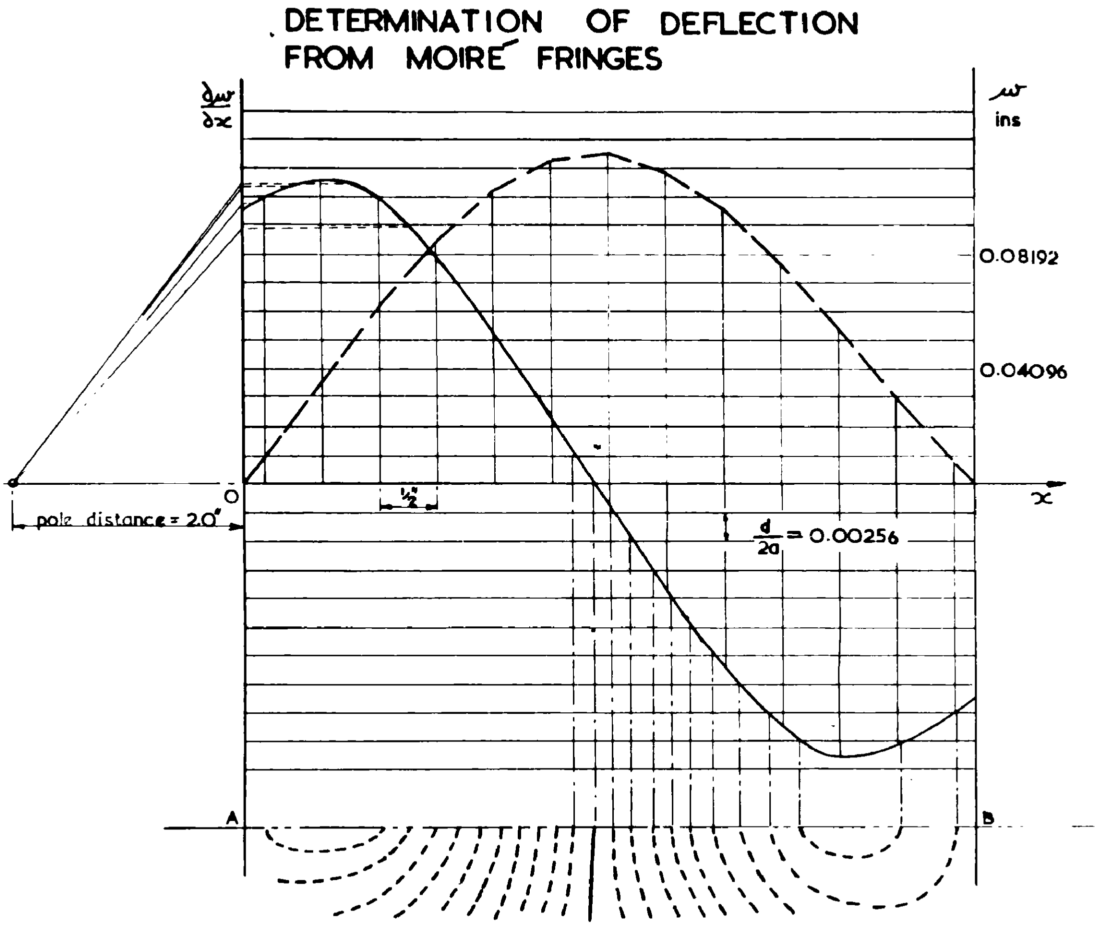

Fig. (135)

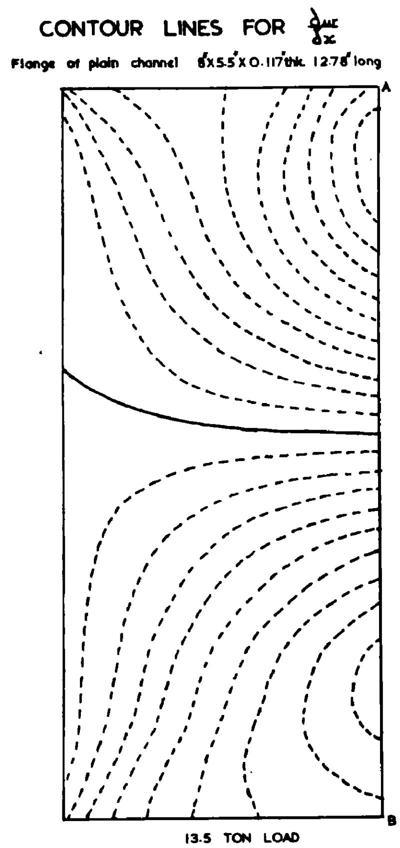

Fig. (136)

SERIES OF DEFLECTION CURVES

Web of 8" x 5.5" plain channel 0.117" thk. 12.78" long

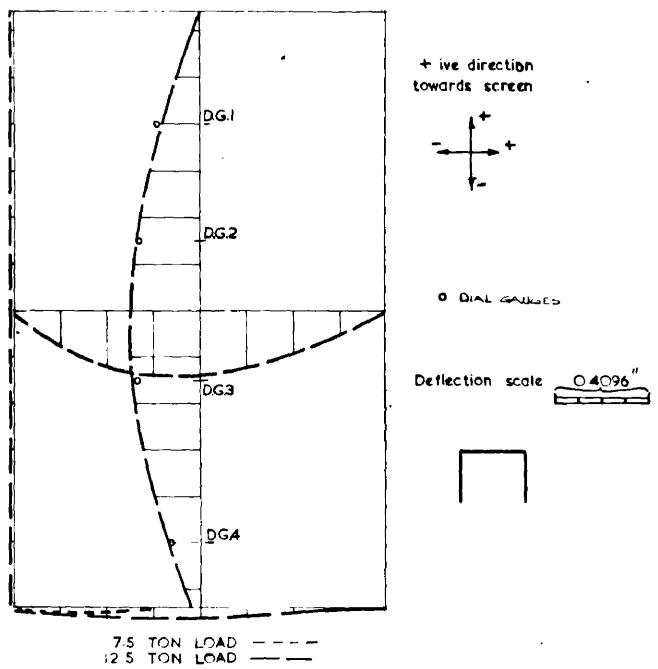

Fig. (137)

SERIES OF DEFLECTION CURVES

Web of 8" x 6" x 1" lipped channel 0.0998" thk. 12.78" long

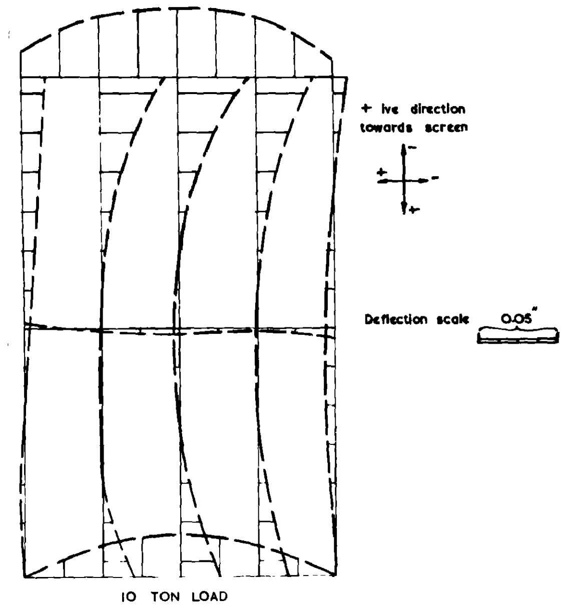

Fig. (138)

RELATIVE DEFLECTION CURVES

Flange of 8" x 5.5" plain channel 0.117" thk. 12.78" long

Fig. (139)

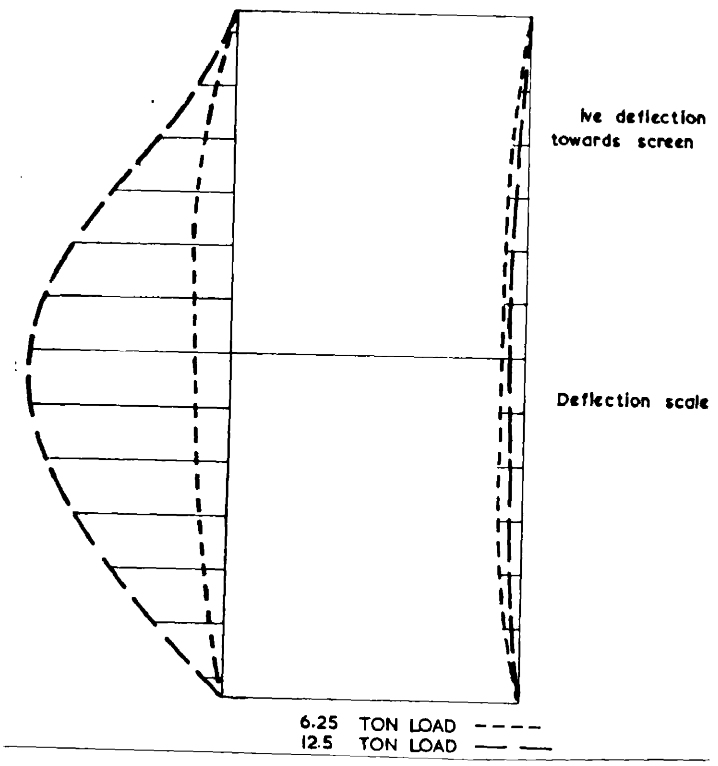

on the specimen was then ascertained from the separate photographs by observing the spread or contraction of the lines (if the lines have spread after the application of load then the specimen has deflected concave away from the screen). Thus knowing the deflected form at a certain place the slope distribution curve was constructed, and the signs of the slope contours about the zero contour, established to give the required deflection form on graphical integration of this curve. These deflections were then used to evaluate critical loads in the manner described in Section 5. The plotting of the slope distribution curves and the graphical method of integration is illustrated in Fig.(135). The corresponding fringe pattern and contour lines are shown in Fig.(136).

Experimental Results:

Results obtained by means of the method described above for uniformly compressed plate components of plain and lipped channels are shown in Figs.(137)to(139)inclusive. The graphs of maximum deflection as a function of the load for the buckling plate components are shown in Figs(117,120).

APPENDIX 7

TABLES OF CRITICAL STRESS, MAXIMUM STRESS AND YIELD STRESS FOR LIPPED AND PLAIN CHANNEL, AND EQUAL ANGLE SECTIONS.

LIPPED CHANNEL

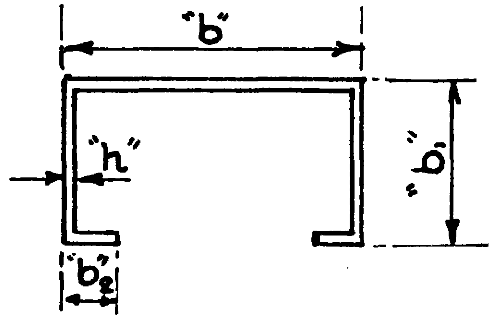

X-SECTION SIZE INS. $b \times b_1 \times b_2$	THICKNESS INS. h	LENGTH INS. a	$\sigma_{CRIT.}$ Tons/in^2	$\sigma_{MAX.}$ Tons/in^2	σ_{YIELD} Tons/in^2
8 × 4 × 0·5	0·0587	9·22	2·5	6·12	9·58
8 × 4 × 0·5	0·075	9·22	4·38	11·65	15·97
8 × 4 × 0·5	0·077	9·22	5·32	10·4	15·97
8 × 4 × 0·5	0·075	9·22	5·4	11·65	15·97
8 × 4 × 0·5	0·077	9·22	5·26	10·3	15·97
8 × 4 × 0·5	0·075	9·22	5·75	11·8	15·97
8 × 4 × 0·5	0·075	9·22	5·75	10·25	15·97
8 × 4 × 0·5	0·076	6·1875	5·18	11·25	15·97
7·975 × 4 × 1	0·076	9·25	5·05	11·55	15·97
8 × 4 × 1	0·096	9·22	7·95	12·9	15·49
8 × 4 × 1	0·096	9·22	8·43	13·69	15·49
8 × 4 × 1	0·0955	9·22	8·15	13·45	15·49
8 × 4 × 1	0·0955	9·22	7·7	12·7	15·49
8 × 4 × 0·5	0·0965	12·25	7·2	11·95	15·49
8 × 4 × 1	0·094	12·4	8·28	12·35	15·49
8 × 4 × 0·5	0·0771	9·22	5·2	10·38	15·97
8 × 6 × 1	0·06	6·39	2·23	5·97	10·57

LIPPED CHANNEL

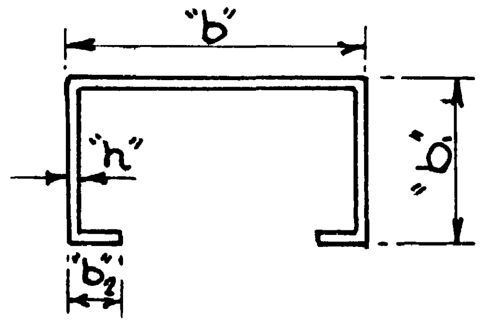

X-SECTION SIZE INS. "b"×"b₁"×"b₂"	THICKNESS INS. "h"	LENGTH INS. "a"	$\sigma_{crit.}$ Tons/in²	$\sigma_{max.}$ Tons/in²	σ_{yield} Tons/in²
8×3.5×0.5	0.0585	12.3	3.18	5.48	10.26
7.95×3.5×0.5	0.059	12.3	3.5	5.5	10.26
8×3.5×0.5	0.0945	12.3	7.38	10.6	17.4
7.95×3.5×0.5	0.095	12.3	6.95	11.3	17.4
8×3.46×0.5	0.116	12.3	10.98	11.82	11.92
8×4×0.5	0.0585	6.1875	2.36	5.83	9.58
8×4×0.5	0.0585	6.1875	2.21	6.21	9.58
8×4×1	0.075	6.1875	5.33	10.9	15.97
8×4×0.5	0.076	6.1875	5.44	10.88	15.97
8×4×0.5	0.096	6.1875	8.6	12.86	15.49
8×4×0.5	0.097	6.1875	8.0	12.74	15.49
8×4×1	0.0963	6.1875	10.32	12.12	15.49
8×4×1	0.0963	6.1875	10.86	12.2	15.49
7.97×3.98×1	0.116	6.1875	13.65	14.45	13.59
8×3.98×1	0.117	6.1875	14.15	14.81	13.59
8×4×0.5	0.0587	6.1875	2.62	5.83	9.58
8×4×0.5	0.076	6.1875	5.10	10.88	15.97

LIPPED CHANNEL

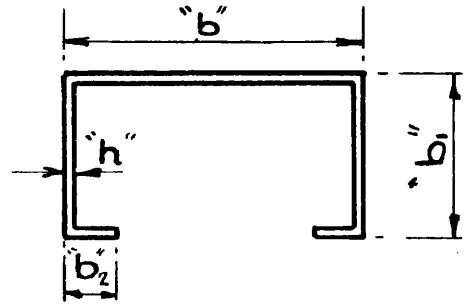

X-SECTION SIZE INS. $b \times b_1 \times b_2$	THICKNESS INS. h	LENGTH INS. a	$\sigma_{CRIT.}$ Tons/in^2	$\sigma_{MAX.}$ Tons/in^2	σ_{YIELD} Tons/in^2
7.97 × 2 × 0.5	0.0585	6.2	2.22	7.2	10.0
8.0 × 1.97 × 0.5	0.073	6.2	5.87	13.68	19.0
7.95 × 2 × 0.5	0.059	9.1	3.27	6.66	10.0
8 × 2 × 0.5	0.0785	9.1	5.52	13.1	19.0
7.97 × 1.95 × 0.5	0.1165	9.1	9.45	10.43	12.6
7.97 × 2 × 0.5	0.1172	9.1	9.96	10.25	12.6
7.93 × 2 × 0.5	0.058	12.2	3.08	6.1	10.0
7.97 × 1.95 × 0.5	0.1165	12.2	8.6	10.26	12.6
7.95 × 3.47 × 0.5	0.0585	6.16	3.56	5.73	10.26
7.95 × 3.46 × 0.5	0.096	6.16	10.2	12.72	17.4
7.98 × 3.45 × 0.5	0.116	6.16	11.58	12.4	11.92
7.9 × 3.47 × 0.5	0.0585	9.22	4.24	5.5	10.26
7.97 × 3.5 × 0.5	0.078	9.22	8.0	11.7	18.45
7.95 × 3.45 × 0.5	0.078	9.22	8.54	12.67	18.45
7.95 × 3.5 × 0.5	0.0968	9.22	9.3	13.3	17.4
7.95 × 3.45 × 0.5	0.116	9.22	10.78	12.5	11.92
7.97 × 3.47 × 0.5	0.117	9.22	11.2	12.28	11.92

LIPPED CHANNEL

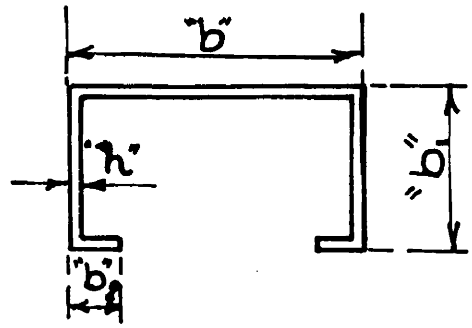

X-SECTION SIZE INS "b"×"b_1"×"b_2"	THICKNESS INS "h"	LENGTH INS. "a"	$\sigma_{CRIT.}$ Tons/in²	$\sigma_{MAX.}$ Tons/in²	σ_{YIELD} Tons/in²
8×6×1·5	0·0595	6·39	2·362	5·26	10·57
8×6×1·5	0·059	6·39	2·5	5·3	10·57
8×6×1·5	0·059	6·39	2·13	5·66	10·57
8×6×1·5	0·075	6·39	4·98	9·27	16·73
8×6×1	0·0752	6·39	5·32	10·0	16·73
8×6×1	0·097	6·39	8·84	11·43	16·25
8×6×1·5	0·0965	6·39	8·33	11·36	16·25
8×6×1	0·0965	6·39	8·01	11·57	16·25
8×6×1·5	0·0996	6·39	7·8	11·91	16·25
8×6×1	0·0997	6·39	7·84	11·18	16·25
8×6×1	0·117	6·39	9·87	12·13	14·22
8×6×1	0·117	6·39	9·83	11·78	14·22
8×6×1	0·117	6·39	11·05	12·96	14·22
8×6×1	0·1515	6·39	13·48	14·22	14·86
8×6×1·5	0·075	12·78	5·08	9·86	16·73
8×6×1·5	0·0765	12·78	5·13	8·98	16·73
8×6×1·485	0·0965	12·78	8·25	11·96	16·25

LIPPED CHANNEL

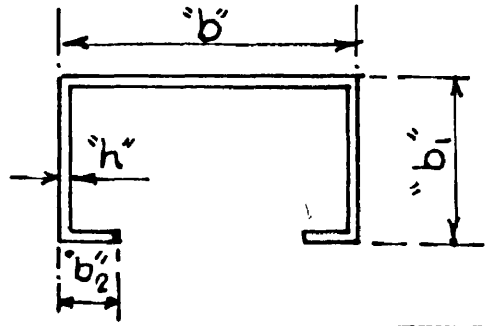

X-SECTION SIZE INS. "b"×"b₁"×"b₂"	THICKNESS INS "h"	LENGTH INS. "a"	$\sigma_{CRIT.}$ Tons/in^2	σ_{MAX} Tons/in^2	σ_{YIELD} Tons/in^2
8×6×1	0·098	12·78	8·28	11·7	16·25
8×6×1·5	0·096	12·78	8·06	11·78	16·25
8×6×1	0·0998	12·78	8·3	11·7	16·25
8×6×1·5	0·117	12·78	9·83	12·43	14·22
8×6×1	0·1515	12·78	12·9	14·42	14·86
8×6×1	0·1515	12·78	12·7	13·82	14·86
8×6×1	0·152	12·78	12·77	13·2	14·86

PLAIN CHANNEL

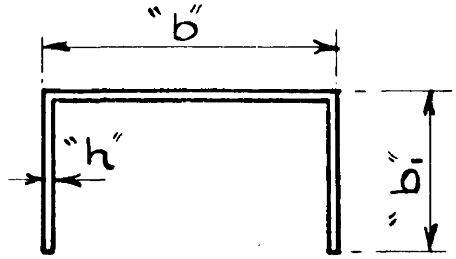

X-SECTION SIZE INS. "b" × "b_1"	THICKNESS INS. "h"	LENGTH INS. "a"	$\sigma_{CRIT.}$ Tons/in^2	$\sigma_{MAX.}$ Tons/in^2	$\sigma_{YIELD.}$ Tons/in^2
8 × 2.97	0.075	12.78	5.5	8.8	15.49
8 × 3	0.0975	6.1	7.25	11.0	15.49
8 × 3	0.0962	9.26	7.12	10.3	15.49
8 × 3	0.0977	12.3	6.56	9.5	15.49
8 × 3	0.1165	6.1	10.0	10.52	13.59
8 × 3	0.116	9.25	9.72	10.9	13.59
8 × 3	0.061	12.3	2.83	5.8	10.51
8 × 3	0.078	6.15	4.91	7.8	15.97
8 × 4.5	0.061	6.1	1.735	4.315	10.51
8 × 4.5	0.0587	12.78	1.475	4.2	10.51
8 × 4.5	0.116	12.7	6.1	8.48	13.22
8 × 4.5	0.116	12.7	5.7	7.92	13.22
8 × 5.5	0.06	6.3	1.14	4.355	10.51
8 × 5.5	0.06	6.3	1.13	3.68	10.51
8 × 5.5	0.117	12.78	4.3	6.55	13.22
8 × 5.5	0.117	12.78	4.33	7.14	13.22
8 × 5.5	0.117	12.78	4.24	7.85	13.22

PLAIN CHANNEL

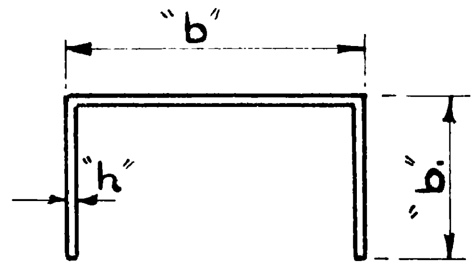

X-SECTION SIZE INS. "b"×"b_1"	THICKNESS INS. "h"	LENGTH INS. "a"	$\sigma_{CRIT.}$ Tons/in²	$\sigma_{MAX.}$ Tons/in²	σ_{YIELD} Tons/in²
8" × 1·6"	0·0593"	6·05	2·61	5·49	10
8" × 1·6"	0·058"	12·4	2·55	4·94	10
8" × 1·6"	0·0785	6·05	4·86	9·77	19
8 × 1·6	0·078	9·14	4·89	9·12	19
8 × 1·6	0·0785	12·4	4·42	11·42	19
8 × 1·6	0·1165	6·05	9·26	9·7	12·6
8 × 1·6	0·1168	6·05	9·82	10·65	12·6
8 × 1·6	0·1168	12·4	9·0	9·26	12·6
8 × 2	0·079	12·35	3·56	9·07	13·57
8 × 2	0·117	12·35	11·07	12·58	11·92
8 × 2·5	0·075	12·35	6·16	10·7	18·45
8 × 2·5	0·077	12·35	7·0	9·81	18·45
8 × 3	0·06	6·1	2·57	4·66	10·51
8 × 2·97	0·0582	9·26	2·47	4·6	9·58
8 × 2·95	0·0602	12·3	2·56	4·77	10·51
8 × 3	0·0785	6·15	5·46	9·4	15·97
8 × 3	0·075	12·3	4·31	8·3	15·57

EQUAL ANGLE

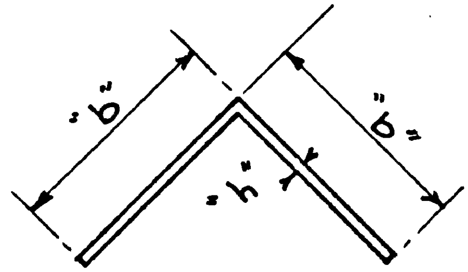

X-SECTION SIZE INS. "b" × "b"	THICKNESS INS. "h"	LENGTH INS. "a"	σ_{crit} Tons/in²	σ_{max} Tons/in²	σ_{yield} Tons/in²
3·97 × 3·97	0·0973	8	4·74	6·45	15·98
4 × 4	0·0784	12	3·53	5·57	17·76
4 × 4	0·098	12	3·87	5·03	15·98
4 × 4	0·0585	16	1·187	1·6	9·7
4 × 4	0·0575	16	1·195	1·52	9·7
4 × 4	0·06	16	1·185	1·52	9·7
4 × 4	0·0784	16	2·42	3·47	17·76
4 × 4	0·078	16	2·41	3·394	17·76
4 × 4	0·0785	16	2·2	3·49	17·76
4 × 4	0·0975	16	3·39	4·31	15·98
4 × 4	0·097	16	3·58	4·25	15·98
4 × 4	0·097	16	3·33	4·22	15·98
4 × 4	0·1172	16	3·85	4·02	13·57
4 × 4	0·1179	16	3·83	4·01	13·57
4 × 4	0·1173	16	3·87	4·01	13·57

EQUAL ANGLE

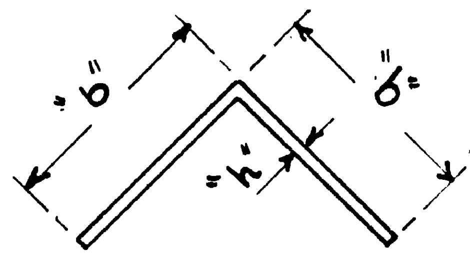

X-SECTION SIZE INS. "b" × "b"	THICKNESS INS. "h"	LENGTH INS. "a"	$\sigma_{CRIT.}$ Tons/in²	$\sigma_{MAX.}$ Tons/in²	σ_{YIELD} Tons/in²
4 × 4	0.061	4	3.18	4.16	9.75
4 × 4	0.0595	4	2.41	3.78	9.75
4 × 4	0.0607	4	2.32	3.58	9.75
4 × 4	0.0785	4	6.36	8.10	17.76
4 × 4	0.0785	4	6.18	7.16	17.76
4 × 4	0.0978	4	11.2	11.73	15.98
4 × 4	0.098	4	9.38	10.02	15.98
4 × 4	0.098	4	9.68	11.05	15.98
4 × 4	0.1171	4	10.9	11.35	13.57
4 × 4	0.1171	4	12.3	12.8	13.57
4 × 4	0.1171	4	11.32	11.94	13.57
4 × 4	0.06	8	1.79	2.75	9.7
3.94 × 3.94	0.06	8	1.67	2.78	9.7
3.94 × 3.94	0.0615	8	1.79	2.784	9.7
4 × 4	0.0784	8	3.46	5.79	17.76
3.96 × 3.96	0.0972	8	4.78	6.25	15.98
4 × 4	0.0973	8	4.85	6.23	15.98

BIBLIOGRAPHY

BIBLIOGRAPHY.

1. Timoshenko S.P. "Theory of Elastic Stability" McGraw-Hill Book Co. Inc., New York, N.Y. 1936

2. Von Karman T., Sechler, E.E. and Donnell L.H., "Strength of Thin Plates in Compression". Trans. Amer. Soc. mech. Engrs. Vol.54 1932.

3. Stowell E.Z. Heimerl G.J. Libone C., and Lundquist E.E. "Buckling Stresses for Flat Plates and Section." Trans. Amer. Soc. civ. Engrs. Separate Vol. 77, 1951.

4. Stowell E.Z. "Compressive Strength of Flanges" nat.adv. Comm. Aero., Wash., Tech. Note 2020, 1950.

5. Kenedi R.M. and Shearer Smith W. "Application of Cold Formed Sections". The West of Scot. Iron and Steel Inst. Paper No. 509, May, 1958.

6. Moir C.H. and Kenedi R.M. "Factors Influencing the Design of Thin Walled Columns" Struct. Engr. Vol. 26, 1948.

7. Chilver A.H. "Maximum Strength of Thin Walled Channel Struts" Civ. Engng. Lond. Vol. 1953.

8. Winter G. "Strength of Thin Steel Compression Flanges" Proc. Amer. Soc. civ. Engrs. February, 1946.

9. Kenedi, R.M., Shearer Smith & Fahmy F.O. "Light Structures - Research and its Applications to Economic Design" Trans. Instn. Engrs. Shipb. Scot. Vol. 99, 1955-56.

10. Wagner H. "Torsion and Buckling of Open Sections" nat. adv. Comm. Aero., Wash. Tech. Memor.807, 1936.

11. Marguerre, Karl "The Apparent Width of Plates in Compression" nat. adv. Comm. Aero., Wash. Tech.Memor. 833, 1942.

12. Levy S. "Bending of Rectangular Plates with Large Deflection" nat. Adv. Comm. Aero., Wash. Tech. Note. 846, 1942.

13. Shearer Smith, W. "Cold Formed Sections in Structural Practice with a Proposed Design Specification" Struct.Engr. June, 1951.

14. Todhunter and Pearsons. "History of The Theory of Elasticity" Vol. 1 Cambridge, 1886.

15. Timoshenko S.P. "Theory of Plates and Shells" McGraw-Hill Book Co. Inc. New York, 1940.

24. Heimerl G.J. "Determination of Plate Compressive Strengths" nat. adv. Comm. Aero., Wash. Tech. Note. 1480, 1947.

25. Crandall S.H. "Engineering Analysis" McGraw-Hill Book Co. Inc., New York, 1956.

26. Duncan W.J. "Galerkin's Method in Mechanics and Differential Equations". Aeronautical Research Committee, Rep. and Memor. 1798, 1937.

27. Duncan W.J. "The Principles of Galerkin's Method" Aeronautical Research Committee, Rep. and Memor. 1848, 1937.

28. Gerard G. " Handbook of Structural Stability" Part IV "Failure of Plates and Composite Elements" nat. adv. Comm. Aero., Wash. Tech. Note 3784, 1957.

29. Mayers J. and Budiansky B. "Analysis of Behaviour of Simply Supported flat plates Compressed Beyond the Buckling Load into the Plastic Range" nat. Adv. Comm. Aero., Wash. Tech. Note 3368, 1955.

30. Bleich F. "Theorie u Berchnung der Eiserner Brucken" Berlin, 1924.

31. Melan E. "Uber die Stabilitat von Staben welche aus eimen Randwinkeln, Verstarkten Blech bestehen" Proc.3rd int. Congress Appl.

Mechanics. page 59, 1930.

32. Chwalla E. "Das allgemeine Stabilitats problem der gedrukten durch Randwinkel verstarkten Platte" Ing. Archiv. Vol. 5, 1934.

33. Parr W.S. and Beakley W.M. "An Investigation of Duralumin Channel Section Struts in Compression" J. aero. Sci. Vol. 3. September, 1935.

34. Lundquist E.E. "Local Instability of Centrally Loaded Columns of Channel and Z Sections" nat. adv. Comm. Aero., Wash. Tech. Note 722, 1939.

35. Lundquist E.E. "Local Instability of Symmetrical Rectangular Tubes Under Axial Compression" nat. adv. Comm. Aero., Wash. Tech. Note 686, 1939.

36. Stowell E.Z. and Lundquist E.E. "Local Instability of Columns with I, Z, Channel and Rectangular Tube Sections" nat. adv. Comm. Aero., Wash. Tech. Note 743, 1939.

37. Chilver A.H. "Thin Walled Structural Members" Engineering Lond., August, 1951.

38. Kroll W.D. "Tables of Stiffness and Carry-over Factors for Flat Rectangular Plates Under Compression" nat. adv. Comm. Aero., Wash. Wartime Rep. L-396, 1943.

39. Kroll W.D., Fisher G.P. and Heimerl G.J. "Charts for Calculation of Critical Stress for Local Instability of Columns with I, Z, Channel and Rectangular Tube Sections" nat. adv. Comm. Aero., Wash. Wartime Rep. L-129, 1943.

40. Sechler E.E. and Dunn L.G. "Airplane Structural Analysis and Design" John Wiley and Sons Inc., 1942.

41. Needham R.A. "The Ultimate Strength of Aluminium Alloy formed Structural Shapes in Compression" J. aero. Sci. Vol. 21, no. 4 April, 1954.

42. Anderson R. A. & Anderson M.S. "Correlation of Cripling Strengths of Plate Structures and Material properties" nat. adv. Comm. Aero. Wash. Tech. Note 3600, January, 1956.

43. Botman M. "De Experimentele bepaling van de Meedragende breedte van vlakke platten in het elastiche en het plastische gebied (Part II) Rep. S.438., National Luchtvaartlaboratorium, January 1954.

44. Besseling J.F. "De Experimentele Bepaling van de Meedragende breedte van vlakke platten in het elastiche en het

plastische gebied" Rep. S.414
National Luchtvaartlaboratorium,
February, 1953.

45. Schuette E.H. "Observations of Maximum Average Stress of Flat Plates Buckled in Edge Comprèssion" nat. adv. Comm. Aero. Wash. Tech. Memor. 1625,1949.

46. Lightenber F.K. "The Moire Method, a New Experimental Method for the Determination of Moments in Small Slab Models" Proc. Soc. of Expt. Stress Analysis Vo. XII, no. 2, 1955.

47. Vreedenburgh C.G.J. and van Wigngaarden H. "New Progress in our Knowledge about the Moment Distributions in Flat Slabs by means of the Moire Method" Proc. Soc. of Expt. Stress Analysis. Vol. XII, no. 2, 1955.

48. Holmberg A. "Tests with Circular Plates" Acta Polytechnica., Civ. Eng. Series 1. Vol. 1 Nr. 1., 1947.

49. Moore A.D. "Soap film and Sand bed Mapper Techniques" J. Appl. Mech. Vol. 17, No. 3, 1950.

50. Salet G. "Nouvelle Methode de Mise en oevre de l'analogie de la Membrane pur l'etude de la Torsion des Poutres Cylindriques" Bul. Ass'n Tech. Maritime et Aeronautique. Vol. 43, 1939.

51. Brown C.J.E. "The Determination of Slope Contours in Plates in Flexure by the Salet-Ikeda Technique" Brit. Institute of Physics - Stress Analysis Group. Annual Conference, Keele, April, 1960.

52. Duncun J.P. "The Study by Interferometry by the Flexure of Multiply Connected Plates. Brit. Institute of Physics - Stress Analysis Group. Annual Conference, Keele, April, 1960.

53. Wood A.B. "Text Book of Sound" London, 1955.

54. O'Hara S. Ph.D. Thesis on "Fracture in Metals" University of Glasgow, 1959.

55. Forster and Korster. Engineer Vol. 166, 1938.

56. Smithells C.J. "Metals Reference Book" Vol. 2, 1955.

ACKNOWLEDGMENTS.

The work presented in the thesis was carried out in the Department of Mechanical Civil and Chemical Engineering, The Royal College of Science and Technology, Glasgow.

The author wishes to acknowledge with gratitude his indebtedness to Professor A.S.T. Thomson, D.Sc., Ph.D., A.R.C.S.T., M.I.Mech.E., and Dr. R.M. Kenedi, B.Sc., Ph.D., A.R.C.S.T., A.M.I. Mech.E., A.F.R.Ac.S., for their continued interest and encouragement.

SUMMARY OF THESIS

ON

ANALYTICAL AND EXPERIMENTAL INVESTIGATIONS OF THE COLLAPSE LOAD CHARACTERISTICS OF THIN WALLED STRUCTURAL FORMS UNDER COMPRESSIVE LOAD ACTIONS

by

Iftikharul Haq Qureshi,

B.Sc.,(Mech.Eng.) Pb., A.R.C.S.T.,

The advent of thin walled structural compression members high-lighted the reservoir of strength which exists beyond the initiation of a state of elastic instability in thin flat rectangular plates loaded in lengthwise compression. The evaluation of this post-critical strength generally called 'maximum' strength has been attempted on a variety of semi-empirical bases and in a few cases on purely theoretical grounds.

The thesis presents a theoretical treatment for flat plates, developed by tho author, using the concepts of the classical large deflection theory of plates and the deformation theory of plasticity. A variety of unloaded edge conditions ranging from free through elastically fixed to built-in conditions and their symmetrical and unsymmetrical combinations are considered.

This theory, developed for single plates is then applied by the introduction of appropriate assumptions to the assessment of the maximum strength of structural sections regarded as an assembly of such plates. Computations connected with the theory were programmed and carried out by the author on a 'DEUCE' digital computer.

To check the results of the theory an extensive experimental programme covering the measurements of strains and deformations corresponding to the initiation of instability and progress to collapse was carried out. In connection with the experimental programme an original application of the Moire fringe technique was developed by the author for the determination of deflection variations.

Following an introductory review of the relevant published literature, the subject matter of the thesis is divided into six Sections.

Section 1 presents the derivation of the basic large deflection equations by minimization of the energy integral effected by the use of Euler's equations, and a procedure for the approximate solution of the large deflection equations by Galerkin's method. This energy approach to the problem considered, and the generalisation of Euler's equations for two variables with higher derivatives put forward in this thesis is, to the author's knowledge, original.

In Section 2 the approximate solutions of the large deflection equations and the results of elastic critical loads obtained thereby for two general cases of plates are presented. These are then compared with other available published results obtained by classical methods. The comparisons show excellent agreement.

Section 3 presents an analytical method for the maximum load carried by compressed plates, based on the application of the deformation theory of plasticity to the plates analysed by means of the large deflection concept. The application of this method of analysis to the evaluation of the maximum load for plates with free and/or elastically supported unloaded edges is to the author's knowledge presented here for the first time.

In Section 4 the results obtained for single plates have been applied to evaluate the local instability and maximum stresses for box sections, lipped channels and plain channels.

The experimental work performed is presented in Section 5. This covers tests in uniform compression of plain and lipped channel, square tube and equal angle sections. In addition to the results of the actual tests, the various auxiliary techniques such as an original application of the Moire fringe method are fully described.

The mechanical properties inclusive of tensile and compressive yield, Young's Modulus E at zero and varying mean stress, have been evaluated for all the specimens used and are presented in full.

Section 6 contains the comparison of the theoretical and experimental results with a relevant critical discussion.

The main text concludes with a Summary indicating that generally good agreement has been obtained between the theory and the experiments, establishing the former as a rational and reliable analysis for the maximum strength in compression of single-plates and structural sections.

This is followed by six Appendices and an extensive Bibliography. The Appendices contain those details of the theoretical and experimental investigations which have been considered too bulky for inclusion in the main text.